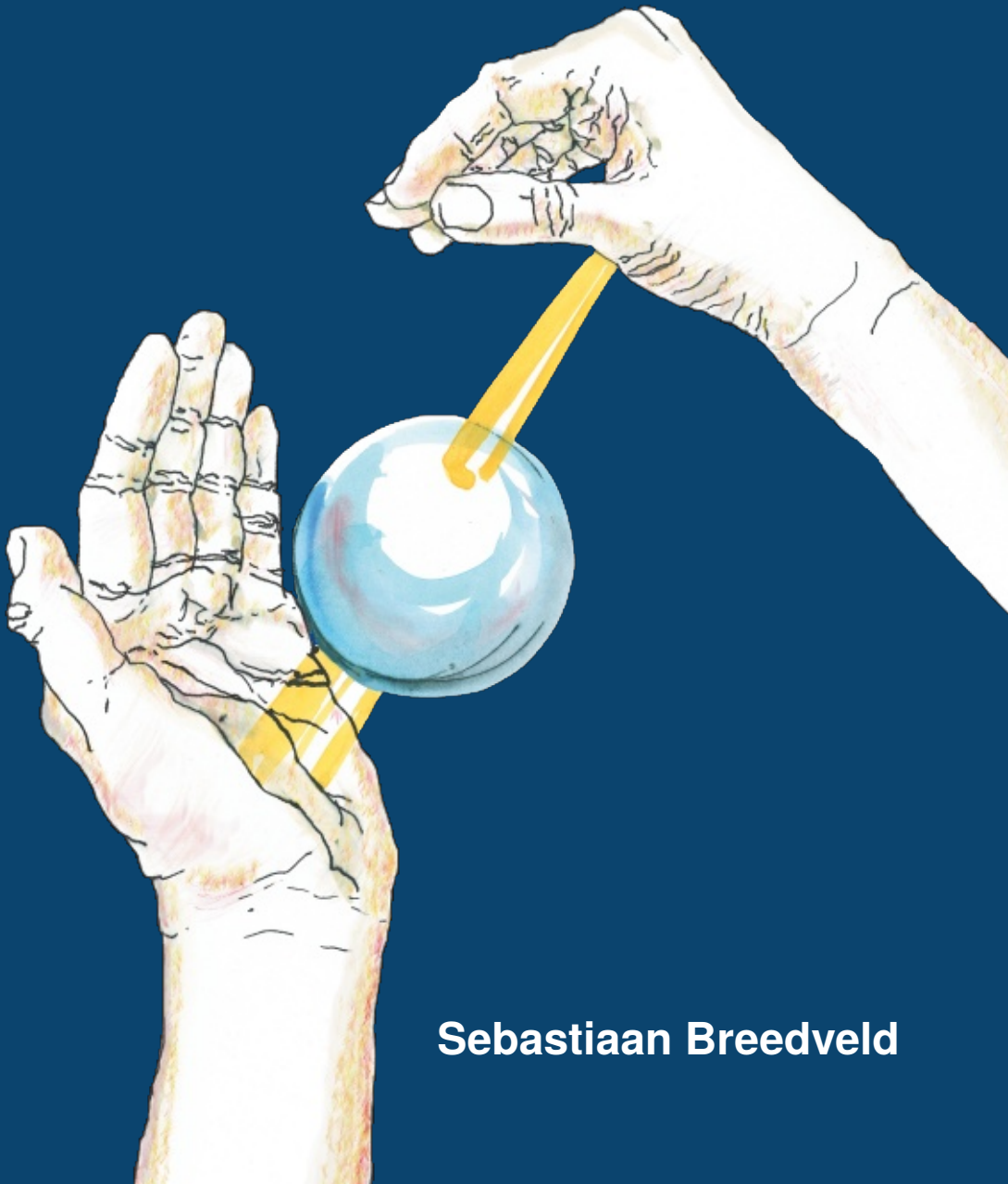


Towards Automated Treatment Planning in Radiotherapy



Sebastian Breedveld

Towards Automated Treatment Planning in Radiotherapy

Cover design: Berry van Oers-Breedveld

Layout: Sebastiaan Breedveld, using L^AT_EX 2_ε with CUED thesis template

Printed by: Gildeprint Drukkerijen

First print: March 2013

Second print: November 2013, updated references

Copyright:

© Sebastiaan Breedveld

© Institute of Physics (chapters 2, 4, 5 and 9)

© American Association of Physicists in Medicine (chapters 6 and 7)

© Elsevier Science Inc. (chapters 8 and 10)

ISBN: 978-94-6108-396-8

Towards Automated Treatment Planning in Radiotherapy

A mathematical approach to automated and integrated multi-criterial optimization of beam angles and IMRT fluence profiles

Op weg naar het automatisch genereren van behandelplannen in de radiotherapie

Een wiskundige aanpak van geautomatiseerde en geïntegreerde multi-criteria optimalisatie van bundelhoeken en IMRT fluentieprofielen

Proefschrift

ter verkrijging van de graad van doctor aan de
Erasmus Universiteit Rotterdam
op gezag van de rector magnificus

Prof.dr. H.G. Schmidt

en volgens besluit van het College voor Promoties

De openbare verdediging zal plaatsvinden op
woensdag 13 maart 2013 om 11:30 uur door

Sebastiaan Breedveld

geboren te Rotterdam



Promotiecommissie

Promotor: Prof.dr. B.J.M. Heijmen

Overige leden: Prof.dr. J.N.M. IJzermans
Prof.dr. H.E. Romeijn
Dr. D. Craft

Copromotor: Dr.ir. P.R.M. Storchi

This thesis has been prepared at the Department of Radiation Oncology, Erasmus Medical Center - Daniel den Hoed Cancer Center, Rotterdam, The Netherlands.

The printing of this thesis was partially funded by Elekta AB.

Cover: light between two hands passing through a sphere, depicting a non-coplanar irradiation.

E-mail for correspondence: s.breedveld@erasmusmc.nl

To my loving family

Berry

Nicolai

Shanne

Ingmar

Contents

Title	i
Contents	v
1 Introduction	1
1.1 Radiation therapy	1
1.2 Treatment plan optimization for external beam treatment with photons .	2
1.3 Outline of the thesis	3
2 Fast, multiple optimizations of quadratic dose objective functions in IMRT	5
2.1 Introduction	7
2.2 Methods and materials	7
2.2.1 Dose calculation algorithm	7
2.2.2 Quadratic objective function	8
2.2.3 Calculation of A and \mathbf{b}	9
2.2.4 Minimization of $s(\mathbf{f})$ with BOXCQP	10
2.2.5 Test setup	11
2.3 Results	11
2.4 Discussion	15
2.5 Conclusions	15
2.A Compressed Row Storage format for sparse matrices	17
2.B Algorithm for calculating $Z = H^T Q$ for sparse matrices	18
3 Automated adjustment of voxel-dependent importance factors in inverse planning	19
3.1 Introduction	21
3.2 Methods and materials	21
3.2.1 Objective function	21

3.2.2	Beam profile optimization	22
3.2.3	Optimization of the voxel-coefficients	23
3.3	Results and discussion	24
3.4	Conclusion	26
4	A novel approach to multi-criteria inverse planning for IMRT	27
4.1	Introduction	29
4.2	Methods and materials	30
4.2.1	Global description of optimization routines	30
4.2.2	Coefficients optimization	32
4.2.2.1	Adaptation of voxel-coefficients for dose-volume constraints.	32
4.2.2.2	Adaptation of voxel-coefficients for maximum-dose con- straints.	34
4.2.3	Constraint optimization	34
4.2.3.1	Stage 1	34
4.2.3.2	Stage 2	34
4.2.3.3	Stages 3 and 4	36
4.2.4	Calculations	36
4.3	Results	36
4.3.1	Rectum	37
4.3.2	Complex head-and-neck case	37
4.3.3	Constraint list sensitivity	40
4.4	Discussion and conclusions	43
5	The equivalence of multi-criteria methods for radiotherapy plan opti- mization	45
5.1	Introduction	47
5.2	Methods	48
5.2.1	Weighted-sum optimization	48
5.2.2	ϵ -constraint optimization	49
5.3	Results	50
5.3.1	From weighted-sum to ϵ -constraint	50
5.3.2	From ϵ -constraint to weighted-sum	51
5.3.3	Simple example	52
5.3.4	Oropharyngeal cancer case	53
5.4	Discussion and conclusions	56

6	iCycle: integrated, multi-criterial beam angle and profile optimization for generation of coplanar and non-coplanar IMRT plans	59
6.1	Introduction	61
6.2	Methods	62
6.2.1	Global description of iCycle	62
6.2.2	Wish-lists	63
6.2.3	Brief overview of the $2pec$ optimization method	65
6.2.4	Selection of optimal beam direction to add to the plan; definition of IMRT optimization problems to be solved	65
6.2.5	Candidate beam directions	67
6.2.6	Target dose prescription for plans with small beam numbers . . .	67
6.2.7	Optimization details	68
6.3	Results	68
6.3.1	Maxillary sinus case - comparison of optimized coplanar and non-coplanar plans with equi-angular plans	68
6.3.2	Maxillary sinus case - convergence with number of beams	71
6.3.3	Maxillary sinus case - alternative problem definitions for selecting the next beam	72
6.3.4	Maxillary sinus case - target dose prescription for plans with small beam numbers	72
6.3.5	Maxillary sinus case - runtimes	73
6.3.6	Cervical cancer case - impact of beam angle optimization for coplanar plans	73
6.3.7	Liver case - impact of optimized non-coplanar beam arrangements	77
6.4	Discussion	80
6.5	Conclusions	84
7	Integrated multi-criterial optimization of beam angles and intensity profiles for coplanar and non-coplanar head-and-neck IMRT and implications for VMAT	85
7.1	Introduction	87
7.2	Methods and materials	88
7.2.1	Study patients and clinical treatment plans	88
7.2.2	iCycle: integrated beam angle and profile optimization	89
7.2.3	iCycle plan generation for the study patients	91
7.2.4	Impact of couch angle on VMAT plans	92
7.2.5	Comparison of treatment plans	92
7.3	Results	92

7.3.1	Comparison of iCycle plans	92
7.3.2	Calculation times for generating iCycle plans	93
7.3.3	Impact of couch optimization on VMAT plans	93
7.4	Discussion	96
7.5	Conclusions	98
8	Toward fully automated multi-criterial plan generation: a prospective clinical study	99
8.1	Introduction	101
8.2	Methods and materials	101
8.2.1	Patients	101
8.2.2	Study design	102
8.2.3	iCycle plan generation	103
8.3	Results	105
8.4	Discussion	108
8.5	Conclusions	110
9	On the beam direction search space in computerized non-coplanar beam angle optimization for IMRT – prostate SBRT	111
9.1	Introduction	113
9.2	Methods and materials	114
9.2.1	Patients	114
9.2.2	iCycle	114
9.2.3	Investigated beam direction input sets (search spaces)	114
9.2.4	iCycle generation of prostate SBRT plans	116
9.2.5	Details on plan evaluation and comparison	118
9.2.6	Treatment time calculation for the CK search space	118
9.3	Results	120
9.3.1	Generated plans	120
9.3.2	Plan quality vs number of beams in plans, PTV and rectum	120
9.3.3	25-beam plans - Coplanar (CP) vs non-coplanar beam direction search spaces	121
9.3.4	25-beam plans - Comparison of non-coplanar search spaces	125
9.3.5	25-beam plans - Distribution of selected beam orientations	125
9.3.6	25-beam plans - Treatment times for the CK search space	126
9.3.7	11 vs 25-beam coplanar plans	126
9.3.8	Calculation times	129
9.4	Discussion	129

9.5	Conclusion	132
10	Adaptive liver stereotactic body radiotherapy: can automated daily plan re-optimization prevent dose delivery degradation caused by anatomy deformation?	133
10.1	Introduction	135
10.2	Methods and materials	135
10.2.1	Patients	135
10.2.2	Study design	137
10.2.3	Optimization of dose distributions	137
10.3	Results	138
10.4	Discussion	140
10.5	Conclusion	142
11	Discussion	143
11.1	Introduction	143
11.2	iCycle automated plan generation and plan quality	143
11.3	iCycle for optimizing beam angles and generation of non-coplanar plans	144
11.4	iCycle automated plan generation to reduce workload and enhance treatment efficiency	144
11.5	iCycle in treatment planning studies	146
11.6	iCycle in clinical practice	146
11.7	Plan quality control	146
11.8	The optimizers	147
11.8.1	Iterative constrained optimizer	147
11.8.2	Interior-point optimizer	148
11.9	The dose-volume problem	149
11.10	Calculation times and online re-planning	151
11.11	Direct aperture optimization	153
11.12	iCycle for other treatment modalities	154
	References	157
	List of publications	175
	Summary	179
	Samenvatting	185
	Acknowledgements	191

PhD Portfolio	193
Curriculum Vitae	195

Chapter 1

Introduction

1.1 Radiation therapy

Around half of the patients diagnosed with cancer is treated with radiation therapy in some stage of the disease. Radiation therapy is a treatment modality that uses ionizing radiation. The goal is to destroy the malignant cells (i.e. the tumour), while saving the healthy tissues as much as possible. This can be done by (temporarily) implanting radioactive sources inside the patient (brachytherapy) or by using an external radiation source. The latter is called *external beam radiation therapy* (EBRT). The focus of this work is on EBRT with X-ray beams (photons).

When a patient is diagnosed with cancer and radiation therapy is a selected treatment, a *computer tomography* (CT) scan is made and all regions of interest, i.e. the *organs at risk* and the tumour (also referenced to as the *target*) are delineated. Then a treatment plan has to be made to specify the settings of the treatment device to deliver enough dose (ionizing radiation) to the target, while keeping the doses to the healthy tissues below acceptable levels.

After the treatment plan has been approved, the patient is treated up to 40 days. Each day, a fraction of the total dose is delivered. This is done to allow repair of healthy tissues in between the fractions.

It is physically impossible to irradiate a tumour while fully sparing the healthy cells around it. Consequently, there is generally a risk for treatment related side effects. Examples of *radiation induced injuries* are reduced saliva production when the patient has a tumour in the head-and-neck area, or pneumonitis when a tumour in the lung has been irradiated. Another type of risk is development of secondary cancer by the applied ionizing radiation, often appearing more than 10 years after initial treatment. To avoid serious treatment complications as much as possible and maintain an optimal quality of life after treatment, it is important to design a treatment plan with a high probability of

cure while optimally minimizing dose delivery to (critical) surrounding healthy structures. The process of designing such a plan is called *treatment plan optimization*.

1.2 Treatment plan optimization for external beam treatment with photons

In external beam radiation therapy, a patient is irradiated from several directions with beams that overlap at the tumour to maximize the tumour dose relative to the surroundings. There are mainly 2 sets of physical parameters to configure the treatment device: 1) the directions from which to irradiate (placement of beams) and 2) the shapes and 2D intensity profiles of the fields. If the intensity profiles are not uniform and optimized for the individual patient, the treatment is called *intensity modulated radiation therapy* (IMRT).

Optimizing both beam directions and intensity profiles is a huge mathematical multi-criteria, non-convex, discrete combinatorial problem that cannot be solved directly. For example, if a discretized beam angle space has 72 possible positions and one wants to use 9 of them, the number of possible combinations is $\binom{72}{9} = 85 \cdot 10^9$. For each possible scenario, a full IMRT optimization has to be performed as well, leading to an impossible problem to solve even on modern computers. The beam angle optimization problem can therefore generally not be solved exactly, and an heuristic approach is required to find an acceptable solution in feasible time. Advanced algorithms for beam angle optimization are still hardly available, and the potential impact on quality of clinical treatments has hardly been investigated.

Additionally, treatment plan optimization is a *multi-criterial* problem, i.e. there are several treatment objectives. Not only should the tumour be irradiated to a high dose, also healthy surrounding tissues should be avoided as much as possible. A head-and-neck case for example may have 10 structures to take into account (tumour, spinal cord, salivary glands, etc). The number of criteria optimized on may even be larger, as often more than one criterion per structure may be involved. In multi-criterial optimization, trade-offs have to be made: some structures are more sensitive to radiation than others, and sometimes one structure has to be sacrificed in order to keep more important (with respect to treatment related morbidity or quality-of-life) structures functional.

In current clinical practice, plans are generated with a software application called *treatment planning system* (TPS), using an iterative trial-and-error process, called forward planning. In this process, based on experience, a human operator makes a first choice of beam angles, weighting factors for the various clinical criteria, and other parameters. A 3D dose calculation algorithm in the TPS is then used to automatically optimize beam profiles and calculate the resulting dose distribution, based on the pa-

tient's planning CT-scan. If the dose distribution is unacceptable or if the operator and treating physician see room for improvement, the operator will change some parameters (again based on experience) to generate a next, hopefully better, dose distribution, and so on. Reasons for stopping the iterative process may be that the dose distribution is considered satisfactory and/or the physician and operator may not see how new parameter adjustments could further improve the patient's dose. With this procedure, the final dose distribution will generally depend on the skills and available time of the operator and the physician. In times with an increased workload in the department, final dose distributions may become less optimal because of lack of available time to do many iterations. Whether or not an adequate number of beams with appropriate directions is used is generally not known. Furthermore, there is no guarantee for an optimal trade-off between objectives, nor is there a guarantee that for the same tumour dose, dose delivery to the most important healthy tissues cannot be further reduced. Apart from these quality issues, the process may be very labour-intensive, taking up to several days for an individual patient.

In this thesis, we have developed and investigated algorithms for treatment plan optimization with strong accents on:

1. Fully automated, multi-criterial plan generation, i.e. avoidance of human interaction.
2. Inclusion of beam angle optimization in IMRT plan generation, both for coplanar and non-coplanar arrangements.
3. Integrated multi-criterial optimization of both beam profiles and angles. Generated plans are Pareto-optimal for beam profiles, i.e. for a selected beam arrangement, changing profiles to improve one of the objectives will always result in plan quality reduction for one or more of the other objectives.
4. Clinically feasible calculation times.

1.3 Outline of the thesis

In chapters 2-4, a new method is presented for automated multi-criterial optimization of IMRT intensity profiles, constraint levels and voxel-dependent importance factors for imposed constraints. Chapter 2 describes the use of a fast mathematical solver for quadratic dose objective functions and a sparse linear algebra implementation dedicated to solving these types of radiation therapy problems. Chapter 3 describes a method to automatically adapt voxel-dependent weights in a quadratic dose objective function to satisfy maximum-dose and dose-volume constraints. Constraints are divided in priority classes, giving highest priority to avoiding violation of the most important constraints. In chapter

4, optimization of the constraints is embedded in a multi-criteria optimization approach that iteratively optimizes imposed constraint levels, again using ascribed constraint priorities.

In chapter 5 a new mathematical optimizer for multi-criterial IMRT optimization, called the *2-phase ϵ -constraint (2pec)* approach, is introduced and compared to the widely applied optimization of weighted-sum objective functions. As in chapter 4, optimization is again driven by a list of hard constraints and prioritized objectives (called a *wish-list*). Steered by the wish-list, a single Pareto-optimal IMRT plan is generated for a preselected beam configuration.

In chapter 6, the developed optimizer is integrated in a new algorithm for multi-criterial beam angle optimization in IMRT, called iCycle. The wish-list is used to iteratively add optimal beam directions to the plan and then optimize profiles to generate a Pareto-optimal plan for the selected configuration. Based on the obtained solution, the Lagrangian (chapter 5) is defined and used for selection of the next beam. As a result, iCycle outputs a list of Pareto-optimal plans, one for each number of beams, without any user-interaction. More specifically, plans are generated without interactive tuning of weights of objectives.

Chapters 7 and 8 describe investigations on the use of iCycle for generating treatment plans for head-and-neck patients. Chapter 7 describes a planning study on the value of integrated beam profile and angle optimization for this patient group. Moreover, iCycle was used to study the importance of nonzero couch angles for VMAT (volumetric arc therapy). Chapter 8 reports on a prospective clinical study in which patients were treated either with an IMRT plan generated by dosimetrists, or with an automatically generated iCycle plan, depending on the physician's preference. In chapter 9, iCycle is used to investigate the importance of the non-coplanar beam search space for treatment of prostate cancer patients with an IMRT plan, mimicking an HDR-brachytherapy dose distribution. Chapter 10 uses iCycle to investigate the effect of daily plan re-optimization for liver stereotactic body radiation therapy, with and without beam angle optimization.

Chapter 11 concludes this thesis with a discussion.

Chapter 2

Fast, multiple optimizations of quadratic dose objective functions in IMRT

Sebastiaan Breedveld¹, Pascal Storchi¹, Marleen Keijzer² and Ben Heijmen¹

¹Department of Radiation Oncology, Erasmus MC Rotterdam, Groene Hilledijk 301, 3075 EA Rotterdam, The Netherlands

²Delft University of Technology, Delft Institute of Applied Mathematics, PO Box 5031, 2600 GA Delft, The Netherlands

E-mail: s.breedveld@erasmusmc.nl

Published 6 July 2006 in *Physics in Medicine and Biology*, volume **51**, pages 3569-3579³

[doi:10.1088/0031-9155/51/14/019](https://doi.org/10.1088/0031-9155/51/14/019)

³In the original publication, there was an error in the algorithm in appendix 2.B.

Abstract

Inverse treatment planning for intensity modulated radiotherapy may include time consuming, multiple minimizations of an objective function. In this paper, methods are presented to speed up the process of (repeated) minimization of the well-known quadratic dose objective function, extended with a smoothing term that ensures generation of clinically acceptable beam profiles. In between two subsequent optimizations, the voxel-dependent importance factors of the quadratic terms will generally be adjusted, based on an intermediate plan evaluation. The objective function has been written in matrix-vector format, facilitating the use of a recently published, fast quadratic minimization algorithm, instead of commonly applied gradient based methods. This format also reduces the calculation time in between subsequent minimizations, related to adjustment of the voxel-dependent importance factors. Sparse matrices are used to limit the required amount of computer memory. For three patients comparisons have been made with a gradient method. Mean speed improvements of up to a factor of 37 have been achieved.

2.1 Introduction

In inverse treatment planning, a quadratic dose objective function with terms $\eta_i(d_i - d_i^p)^2$ (where d_i is the dose in voxel i , d_i^p the prescribed dose in voxel i and η_i the importance factor in voxel i) is often used to optimize the fluence for intensity modulated radiotherapy. Generally, the importance factors η_i are equal for all voxels in an organ (Bortfeld *et al* 1990, Brahme 1995, Spirou & Chui 1998, Wu & Mohan 2000). Another approach uses voxel-dependent importance factors, which are individually optimized in an iterative procedure, requiring repeated minimizations of a modified objective function (Cotrutz & Xing 2002, Wu *et al* 2003, Yang & Xing 2004). The consequence is that the inverse planning may become time consuming.

In our institute, an inverse planning algorithm is being developed which directly accounts for geometrical uncertainties using known distributions of geometrical variations, such as setup errors and internal organ motion (Heijmen *et al* 2003), thereby avoiding the use of PTV margins. Apart from the quadratic terms, the objective function also contains a term that ensures the generation of clinically acceptable, smooth fluence profiles (see section 2.2.2). In an iterative procedure, the voxel-dependent importance factors are adjusted, each time followed by a minimization of the modified dose objective function. This paper describes methods to speed up this process of multiple minimizations. The *smoothing term*, introduced in the objective function to prevent high frequencies in the fluence, also yields a well-conditioned Hessian. This, combined with rewriting the quadratic objective function in canonical form, allows us to use a fast, recently published algorithm (BOXCQP, Voglis & Lagaris (2004)) to minimize the objective function. BOXCQP solves convex quadratic problems with simple bounds, such as fluences $\mathbf{f} \geq 0$, and claims to be up to 30 times faster than other quadratic problem solving algorithms. Also, BOXCQP always finds the exact minimum, while others, especially gradient methods, need a termination criterion, which needs additional work to determine. The algorithm relies on solving linear systems. BOXCQP is compared with a gradient based minimization algorithm.

2.2 Methods and materials

2.2.1 Dose calculation algorithm

Since the dose distribution is a linear combination of fluence elements, the calculation of the dose distribution can be written in matrix-vector form (Cho & Phillips 2001, Thieke *et al* 2002):

$$\mathbf{d} = H\mathbf{f}, \quad (2.1)$$

where \mathbf{d} is the dose distribution vector, with the dose for each voxel in the patient, H is the dose deposition matrix, composed of the distribution vectors of all beamlets, and \mathbf{f}

is the fluence vector, with the beamlet weights.

In this paper, the algorithm to calculate H is from [Storchi & Woudstra \(1996\)](#) with a scatter radius of 3 *cm*.

2.2.2 Quadratic objective function

The quadratic objective function applied consists of two terms:

$$s(\mathbf{f}) = \sum_v \xi_v (H\mathbf{f} - \mathbf{d}_v^p)^T \tilde{\eta}_v (H\mathbf{f} - \mathbf{d}_v^p) + \kappa (M\mathbf{f})^T (M\mathbf{f}). \quad (2.2)$$

The first term is the widely used quadratic dose objective (see the introduction), modified for use with voxel-dependent importance factors. $H\mathbf{f}$ is the dose resulting from the fluence \mathbf{f} , and \mathbf{d}_v^p is the dose objective for voxels in volume v . Each volume v has a volume-wide importance factor ξ_v and a vector of voxel-dependent importance factors $\tilde{\eta}_v$. The tilde denotes a diagonal matrix representation of the coefficient vector $\boldsymbol{\eta}_v$. In this approach, the dimension of the coefficient vector equals the number of patient voxels considered. However, only a subset of the coefficients are unequal to zero, depending on the choice of the adoption of the voxel-dependent importance factors, but the maximum number of nonzero coefficients in $\boldsymbol{\eta}_v$ equals the number of voxels in volume v . This approach also accounts for overlap between volumes, e.g. a PTV with an OAR.

The second term in equation (2.2) is the smoothing term, regulated by a smoothing factor κ . This term encourages the fluence \mathbf{f} to be smooth. Inspired by [Webb et al \(1998\)](#), the second derivative of the fluence was used as an indicator for smoothness. If the second derivative equals zero, the fluence is linear (linearly increasing or decreasing, like a wedge or constant). For a two-dimensional fluence, the Laplacian of the fluence \mathbf{f} can be discretized using standard difference formulae for a fluence element $f_{i,j}$. With resolutions h and k of the fluence in the x - and y direction respectively, we have:

$$\Delta \mathbf{f}|_{(ih,jk)} = \frac{k^2(f_{i-1,j} + f_{i+1,j}) - 2(h^2 + k^2)f_{i,j} + h^2(f_{i,j-1} + f_{i,j+1})}{h^2k^2}. \quad (2.3)$$

The ideal case for a smooth fluence is when $\Delta \mathbf{f} = 0$. We choose to keep the denominator h^2k^2 so the smoothing factor κ is independent of the fluence grid size. The discretization can be written in a matrix M , such that $\Delta \mathbf{f} = M\mathbf{f}$. Figure 2.1 shows an example of the use of the second derivative to generate a smoothing penalty.

Equation (2.2) can be written in canonical form:

$$s(\mathbf{f}) = \frac{1}{2} \mathbf{f}^T A \mathbf{f} + \mathbf{f}^T \mathbf{b} + c, \quad (2.4)$$

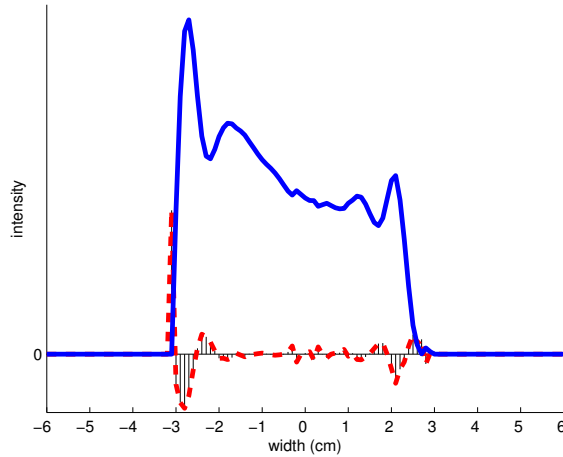


Figure 2.1: Example of the smoothing penalty for a one-dimensional fluence (solid line). The second derivative of the fluence is the dashed line. The square of the area covered by the second derivative equals the penalty.

where:

$$A = H^T Q H + \kappa S, \quad \mathbf{b} = H^T \mathbf{q}, \quad c = \sum_v \xi_v (\mathbf{d}_v^p)^T \tilde{\eta}_v \mathbf{d}_v^p, \quad (2.5)$$

$$Q = 2 \sum_v \xi_v \tilde{\eta}_v, \quad S = 2M^T M, \quad \mathbf{q} = -2 \sum_v \xi_v \tilde{\eta}_v \mathbf{d}_v^p. \quad (2.6)$$

The scalar c in equation (2.4) can be neglected for minimization of $s(\mathbf{f})$. At the start of each new iteration A and \mathbf{b} need to be recalculated based on updated Q and \mathbf{q} (S does not change).

Note that A is symmetric and positive definite. In this form, the Hessian A is given directly and does not need any approximations, or additional calculations. The gradient is provided by computing $A\mathbf{f} + \mathbf{b}$ ($= \nabla \mathbf{f}$).

2.2.3 Calculation of A and \mathbf{b}

The dimensions of H in equation (2.1) are $m \times n = \#\text{voxels} \times \#\text{fluence elements}$, but the matrix is usually filled for only 5% – 20%. A typical patient has $m = \mathcal{O}(10^5)$ voxels and $n = \mathcal{O}(10^3)$ fluence elements. Storage of H in 8 bytes double precision, requires several gigabytes of memory. Therefore *sparse matrices* are used, since this format only stores the nonzero elements of a matrix (appendix 2.A, Cho & Phillips (2001)).

Q is the only matrix that changes with every iteration. The most time consuming

computation then becomes the third order computation $H^T Q H$ when calculating A .

An efficient algorithm has been developed to perform this computation based on the transposition algorithm presented in Pissanetsky (1984) (which is based on Gustavson (1978)). The idea is to multiply the diagonal of Q (which is sparse in our approach) with H^T while transposing H . Details on how to compute $Z = H^T Q$ are presented in appendix 2.B.

This approach has two advantages: it is not necessary to store H^T for a speedup in the multiplication, and only one matrix-matrix (ZH) computation has to be performed later. The time needed for transposition and multiplication with the diagonal of Q is linear in the number of nonzeros in Q (Gustavson 1978).

The computation of the product of two sparse matrices is described by Gustavson (1978). Algorithms for other sparse operations (e.g. addition of two sparse matrices to calculate $A = ZH + \kappa S$ and the matrix-vector multiplication to calculate $\mathbf{b} = H^T \mathbf{q}$) can be found in Pissanetsky (1984) and Duff *et al* (1986).

A is usually a relatively full matrix (70% – 80% nonzeros), so we can refrain from accounting the sparse pointer lists by storing A as a full matrix. This simplifies the algorithms significantly.

2.2.4 Minimization of $s(\mathbf{f})$ with BOXCQP

The implementation of BOXCQP requires relatively few lines of code. However, the way the algorithm works is less trivial to understand than gradient based algorithms.

First, equation (2.4) is extended with the associated Lagrangian for $\mathbf{f} \geq 0$ (i.e. all elements of \mathbf{f} are ≥ 0):

$$L(\mathbf{f}, \boldsymbol{\lambda}) = \frac{1}{2} \mathbf{f}^T A \mathbf{f} + \mathbf{f}^T \mathbf{b} - \mathbf{f}^T \boldsymbol{\lambda}. \quad (2.7)$$

At the minimum $(\mathbf{f}^*, \boldsymbol{\lambda}^*)$, the Karush-Kuhn-Tucker conditions require that:

$$A \mathbf{f}^* + \mathbf{b} - \boldsymbol{\lambda}^* = 0, \quad (2.8)$$

$$\boldsymbol{\lambda}^* \geq 0, \quad (2.9)$$

$$(\mathbf{f}^*)^T \boldsymbol{\lambda}^* = 0, \quad (2.10)$$

$$\mathbf{f}^* \geq 0. \quad (2.11)$$

The steps needed to satisfy these conditions can be found in Voglis & Lagaris (2004).

The BOXCQP algorithm heavily depends on solving linear systems. It is therefore required that the Hessian A has a proper condition (less than $\approx 10^{12}$). The condition is defined as the quotient between the largest and the smallest eigenvalue. Without the smoothing term ($\kappa = 0$), A is usually ill-conditioned because the smallest eigenvalue is

usually close to 0 (Carlsson & Forsgren 2006), making this algorithm unusable for these matrices. A method to improve the condition of A is to add a small identity matrix (κ small, $S = I$), increasing the smallest eigenvalue by κ . This changes the solution minimally, but the condition improves significantly. The same happens when using the smoothing term $S = 2\kappa M^T M$.

The matrix A is symmetric and positive definite, so it is natural to solve the systems using the Cholesky decomposition (Golub & van Loan 1989).

2.2.5 Test setup

The algorithms were tested on an Intel Xeon 3.2 GHz running Linux. The routines to calculate A and \mathbf{b} were written in Fortran according to the ideas presented in section 2.2.3. The BOXCQP algorithm for minimization of $s(\mathbf{f})$ (section 2.2.2) was implemented in Matlab 7.

Matlab's function `quadprog`, which is suitable for minimization of functions such as equation (2.4), was compared with our implementation of the BOXCQP algorithm. The termination tolerance on the function value was set to 10^{-15} for `quadprog`.

To compare the two minimization algorithms, matrices Q and vectors \mathbf{q} are needed to define clinically relevant functions $s(\mathbf{f})$. In our inverse planning algorithm we concentrate on changing the weight of the individual voxels in each iteration. The volume-wide importance factors ξ_v and the planning doses \mathbf{d}_v^p remain constant.

The planning algorithm was run for three patients, while automatically adapting the relevant voxels weights in each iteration, with a maximum of 100 iterations. This results in a unique $\tilde{\eta}_v$ for each iteration. To compare the minimization times of BOXCQP and `quadprog`, every tenth iteration matrix Q and vector \mathbf{q} were recorded. The precise algorithm used for the adoption of the voxel weights is out of scope for this paper but will be discussed in a future paper.

The computation times were recorded for three scenarios: no smoothing ($\kappa = 0$), condition improver ($\kappa = 10^{-6} \max_v \xi_v$ and $S = I$) and with smoothing ($\kappa = 10^{-2} \max_v \xi_v$). To show that the differences between using the condition improver and no smoothing are minimal, DVHs of both solutions are shown.

2.3 Results

Details of the plans used in this study are shown in table 2.1. The head-and-neck patient has three PTVs of which the primary PTV has a higher dose prescription than the other PTVs (elective neck glands). Computation times are presented in table 2.2, showing mean calculation speed enhancements for BOXCQP with factors 5 – 37.

Because of the poor condition of matrix A BOXCQP cannot be used without condition improver or smoothing. As demonstrated in table 2.2, calculation times for the gradient

Table 2.1: Relevant patient information.

	Oesophagus	Prostate	Head-and-neck
Beam resolution (XY (cm))	0.5	0.5	0.5
#Beams	5	5	7
#Voxels	163 053	188 153	100 554
#Beamlets	2342	1701	3116
Nonzeros in H (%)	6.0	11.1	19.3

Table 2.2: Comparison between BOXCQP and the gradient based `quadprog` regarding times to minimize quadratic objective functions. For each clinical case, data are presented for no smoothing, condition improver and with smoothing. The mean times in columns 3 and 4 are averages for ten different combinations of the matrix Q and vector \mathbf{q} . The second column shows the condition of matrix A . The latter three columns are minimization time ratios that demonstrate the speed enhancement obtained with BOXCQP.

	Condition A	Mean minimization time (seconds)		Time ratio		
		quadprog	BOXCQP	Mean	Min	Max
Oesophagus						
No smoothing	$8.9 \cdot 10^{36}$	310.7	—	—	—	—
Condition improver	$3.2 \cdot 10^5$	300.0	12.1	24.3	7.3	36.7
Smoothing	$1.7 \cdot 10^4$	109.8	9.8	22.9	5.2	74.2
Prostate						
No smoothing	$8.7 \cdot 10^{14}$	198.7	—	—	—	—
Condition improver	$4.4 \cdot 10^5$	206.5	5.6	36.7	11.7	44.6
Smoothing	$2.0 \cdot 10^4$	75.5	5.5	19.5	9.2	83.4
Head-and-neck						
No smoothing	∞	617.8	—	—	—	—
Condition improver	$1.4 \cdot 10^8$	597.3	32.0	18.7	9.3	23.0
Smoothing	$1.0 \cdot 10^5$	201.6	39.8	5.3	2.8	7.2

method without smoothing and with condition improver are very similar. Also, both approaches result in similar (clinically non-feasible) peaky fluence profiles. Typical results of using the condition improver and no smoothing are evaluated in DVHs, see figure 2.2. There is no significant difference between the solutions.

The influence of smoothing is shown in figures 2.3 and 2.4. The unsmoothed fluence shows high intensity peaks, which are unrealistic in practice. With the smoothing term enabled, an acceptable fluence is generated. But a too strong smoothing results in parabolic fluences. The amount of smoothing applied influences the solution. No smoothing easily leads to hot spots (up to 500 Gy). Too much smoothing makes it harder to shape the fluence. A good choice for κ is between $10^{-3} \max_v \xi_v$ and $10^{-1} \max_v \xi_v$.

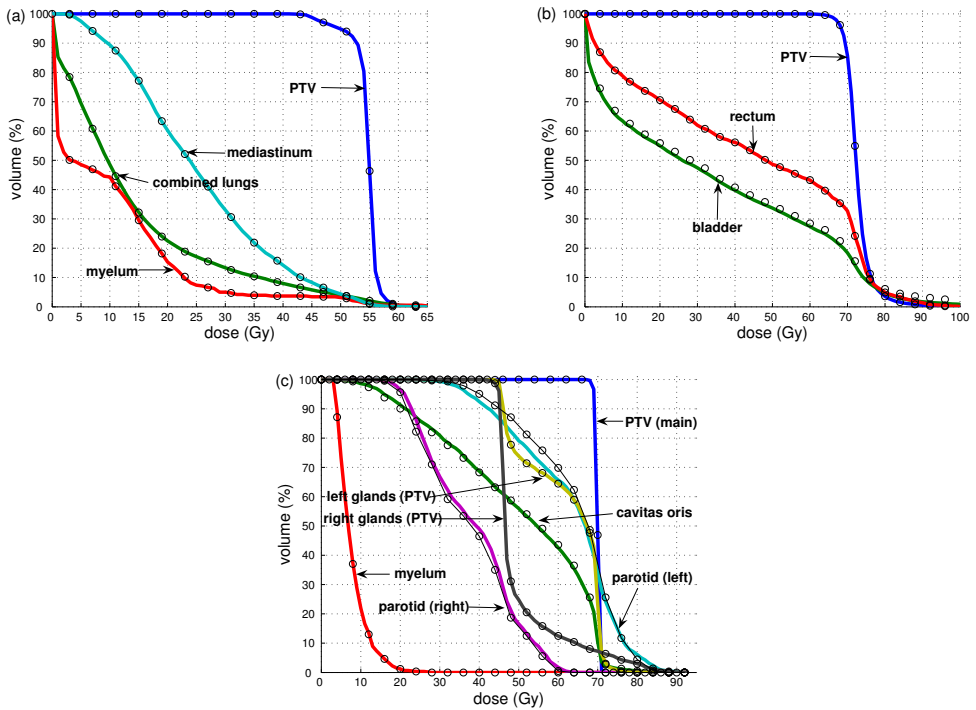


Figure 2.2: DVH comparisons between the solution obtained without smoothing (—) and with condition improver (○) for the oesophagus (a), the prostate (b) and the head-and-neck case (c).

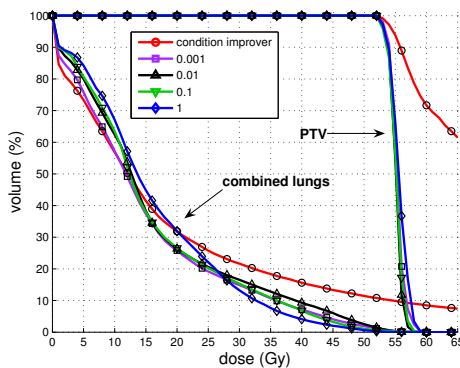


Figure 2.3: Influence of the smoothing factor κ on the solution for the oesophagus case for two volumes. The DVHs for different choices of κ , ranging from no smoothing, $0.001 \max \xi_v$ till $\max \xi_v$, are shown.

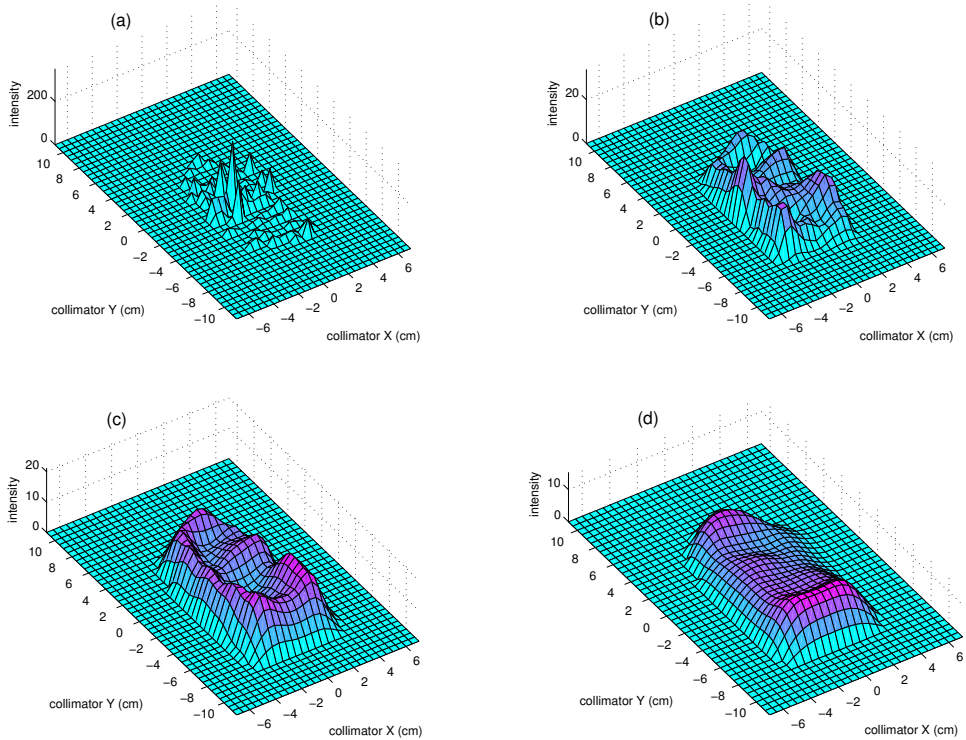


Figure 2.4: Fluence profiles for different smoothing options. (a) is without smoothing, (b) for $\kappa = 10^{-3} \max_v \xi_v$, (c) for $\kappa = 10^{-2} \max_v \xi_v$ and (d) for $\kappa = \max_v \xi_v$. Note the differences in scale on the *intensity* axes.

2.4 Discussion

The minimization times can be significantly reduced by using the BOXCQP minimization algorithm, compared to the gradient algorithm. These times were reduced to the same order that is needed for the calculation of the matrices. Therefore it became interesting to also improve the procedure to calculate the matrices.

When using gradient based methods, one has to provide an initial solution for each minimization. The initial solution used in this paper is the zero vector, but the performance can be increased by roughly a factor of 2 when using the solution \mathbf{f} from the previous Q and \mathbf{q} as the initial solution.

The smoothing term is a powerful tool to embed the generation of smooth fluences in the objective function. A good choice for the smoothing factor κ is between $10^{-3} \max_v \xi_v$ and $10^{-1} \max_v \xi_v$. Our experience is that $\kappa = 10^{-2} \max_v \xi_v$ generally generates the best plans while the fluence is sufficient smooth.

With multi-core processors becoming highly available for workstations in the near future, it is interesting to have a look at the scalability of the algorithms presented in this paper. The BOXCQP algorithm heavily depends on the Cholesky decomposition. This decomposition algorithm is very suitable for parallelization. Most CPU manufacturers offer an optimized and parallelized LAPACK (Anderson *et al* 1999) library, for example in Intel's Math Kernel Library and AMD's Core Math Library, making a parallel implementation easy. A simple test on a dual Xeon showed an improvement close to a factor of 2. In the sparse matrix - sparse matrix algorithm from Gustavson (1978) each row of the resulting matrix is calculated independently from the others, which should be well parallelizable. However, the improvement was less than expected: 1.3 times. Possibly, this is due to our lack of experience in multi-threaded programming. Table 2.3 shows preliminary results of the difference between the use of one or two processors when smoothing is involved.

Because the Cholesky decomposition requires $\mathcal{O}(n^3)$ operations, the time required to minimize the objective function grows polynomial with increasing dimension of the matrix A (i.e. the number of beamlets used), see figure 2.5. The time to set up the matrices grows linearly with the dimensions of H and number of nonzero elements (see section 2.2.3 and Gustavson (1978)).

2.5 Conclusions

The quadratic dose objective function with intrinsic fluence smoothing term can be written in a canonical quadratic form. This allows the use of a broad scala of quadratic minimization algorithms. Apart from the generation of clinically acceptable smooth fluence profiles, the smoothing term also considerably improves the condition of the involved Hessian A , allowing the use of BOXCQP, a recently published algorithm for minimization

Table 2.3: Speed comparisons between the use of one CPU and two CPUs. While the matrix setup times are disappointing, the minimization shows an improvement close to a factor of 2.

	Sparsity η_v	Setup A (seconds)			Minimization (seconds)		
		1 CPU	2 CPUs	Ratio	1 CPU	2 CPUs	Ratio
Oesophagus	1.6%	5.8	4.4	1.3	15.6	8.1	1.9
Prostate	1.4%	5.9	4.4	1.3	8.7	4.6	1.9
Head-and-neck	5.2%	23.6	17.7	1.3	77.9	40.3	1.9

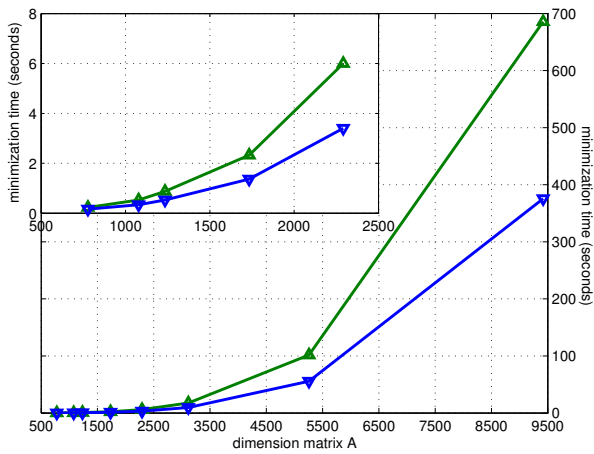


Figure 2.5: Time required to minimize the objective function using BOXCQP for different dimensions of the matrix A by using 1 (Δ) and 2 (∇) processors. The tail is magnified in the top-left part of the figure.

of a quadratic objective function.

For the clinical cases studied in this paper, BOXCQP is 5 – 37 times faster than the gradient method. Parallelization of BOXCQP is relatively easy and very effective in further reducing the minimization times.

Acknowledgements

We want to thank C. Vuik, PhD (Delft Institute of Applied Mathematics at Delft University of Technology) for the communications on sparse matrices and other numerical mathematics.

2.A Compressed Row Storage format for sparse matrices

In this paper we use the 0-indexed *Compressed Row Storage* (CRS) for storing sparse matrices. (0-indexed means that the first element in a vector has index 0.) Consider the 4×6 sparse matrix A given in equation (2.12). This matrix has 8 nonzero elements and is therefore 33% sparse:

$$A = \begin{pmatrix} 0 & 0 & 0 & 5 & 0 & 9 \\ 9 & 0 & 3 & 2 & 0 & 0 \\ 0 & 0 & 0 & 0 & 0 & 0 \\ 0 & 9 & 2 & 0 & 0 & 6 \end{pmatrix}. \quad (2.12)$$

This matrix can be written in CRS using two pointer lists (integer) IA and JA and a value list (real) AN :

$$\begin{aligned} IA &= (0 \ 2 \ 5 \ 5 \ 8), \\ JA &= (3 \ 5 \mid 0 \ 2 \ 3 \parallel 1 \ 2 \ 5), \\ AN &= (5 \ 9 \mid 9 \ 3 \ 2 \parallel 9 \ 2 \ 6). \end{aligned} \quad (2.13)$$

Each entry in IA represents a row of the matrix and points to the starting position for the column indices in JA . AN holds the corresponding values of the nonzero elements. The vertical delimiters indicate the rows in the matrix. For example, the elements for the second row in the matrix A are indexed in JA from index $IA(1) \rightarrow (IA(2) - 1)$. So $JA(2 \rightarrow 4)$ holds the column positions for the elements in the second row (column indices 0, 2 and 3). The corresponding values for these elements are stored in $AN(2 \rightarrow 4)$: 9, 3 and 2 respectively.

Vectors are best stored as row vectors: the row pointer list becomes superfluous.

2.B Algorithm for calculating $Z = H^T Q$ for sparse matrices

% Definitions:

IH, JH, HN pointer lists for matrix H (input)
 JQ, QN pointer lists for vector from the diagonal of Q (input)
 IZ, JZ, ZN pointer lists for matrix Z (output)
 $nzmQ, nzmZ$ number of nonzeros in Q and Z respectively
 N number of rows in Z and columns in H

% determine the number of nonzeros in each column of Z

```
IZ(0 → N) = 0
nzmZ = 0
do IP = 0 → nzmQ - 1
  JP = JQ(IP)
  do I = IH(JP) → IH(JP + 1) - 1
    J = JH(I) + 2
    if J ≠ N then
      IZ(J) = IZ(J) + 1
    endif
    nzmZ = nzmZ + 1
  enddo
enddo
```

% initiate row pointer list

```
IZ(0 → 1) = 0
if N > 1 then
  do I = 2 → N
    IZ(I) = IZ(I) + IZ(I - 1)
  enddo
endif
```

% transpose H and perform the multiplication with Q

```
do IP = 0 → nzmQ - 1
  I = JQ(IP)
  QNV = QN(IP)
  do JP = IH(I) → IH(I + 1) - 1
    J = JH(JP) + 1
    K = IZ(J)
    JK(K) = I ←4
    ZN(K) = HN(JP) * QNV
    IZ(J) = IZ(J) + 1
  enddo
enddo
```

⁴Statement missing in the original publication.

Chapter 3

Automated adjustment of voxel-dependent importance factors in inverse planning

Sebastiaan Breedveld¹, Pascal Storchi¹, Marleen Keijzer² and Ben Heijmen¹

¹Department of Radiation Oncology, Erasmus MC Rotterdam, Groene Hilledijk 301, 3075 EA Rotterdam, The Netherlands

²Delft University of Technology, Delft Institute of Applied Mathematics, PO Box 5031, 2600 GA Delft, The Netherlands

E-mail: s.breedveld@erasmusmc.nl

Published 4 June 2007 in *Proceedings of the XVth International Conference for the Use of Computers in Radiation Therapy (Toronto, Canada)* volume 1, pages 232-236

Abstract

For IMRT, the goal is to generate fluence maps such that the dose distribution satisfies the given constraints. This is achieved by optimizing an objective function, in which the OARs are weighted against each other and the PTV. In clinical planning, the weighting factors are adapted in a lengthy, manual trial-and-error process. This approach, using volume-wide importance factors, can be improved by individual voxel-dependent importance factors. In this paper we present a two-step algorithm that automatically adapts these voxel-dependent importance factors for dose-volume and maximum-dose constraints. The constraints are divided into different sets with different priorities. This allows meeting important constraints prior to meeting less important constraints. The resulting dose distributions are highly conformal.

3.1 Introduction

For IMRT, the goal is to generate fluence maps for each beam such that the dose distribution satisfies certain constraints, usually dose-volume or maximum-dose. Traditionally, volumes of interest are weighted against each other by use of volume-wide importance factors. By assigning the PTV a higher importance than the organs at risk, the objective of giving the PTV its prescribed dose outweighs the desired zero dose in the OARs. However, the solution heavily depends on the choice of these volume-wide importance factors. Generally, manual adaptation is a lengthy trial-and-error process.

A new approach is the use of voxel-dependent importance factors (Cotrutz & Xing 2002). This provides more local control over the dose distribution. In this paper, an inverse planning algorithm is presented that is based on voxel-dependent importance factors that are automatically adapted. The constraints are prioritized to ensure correct PTV dosage and maximum sparing of important OARs, at the expense of less important OARs. With this approach it is also possible to obtain highly conformal dose distributions.

3.2 Methods and materials

To meet the imposed constraints a two-step algorithm is used. In the first step beam profiles are optimized according to a quadratic objective function, with the condition that the fluence is non-negative. In the second step, the result is evaluated and according to violated dose-volume or maximum-dose constraints, the voxel-coefficients for the objective function are adapted, and the first step is run again. This process is repeated until all the constraints are satisfied, or for a maximum number of iterations.

3.2.1 Objective function

The relation between the dose and the fluence (represented as a vector of beamlets) is linear and can be written as a matrix-vector product $\mathbf{d} = H\mathbf{f}$. The matrix H is the dose deposition matrix composed of the distribution vectors of all beamlets and is stored as a sparse matrix to reduce memory usage and increase speed when computing matrix-vector or matrix-matrix products. The quadratic objective function used in the beam profile optimization can be written as follows (Breedveld *et al* 2006):

$$s(\mathbf{f}) = \sum_{v \in \mathcal{V}} \xi_v (H\mathbf{f} - \mathbf{d}_v^p)^T \tilde{\eta}_v (H\mathbf{f} - \mathbf{d}_v^p) + \kappa (M\mathbf{f})^T (M\mathbf{f}), \quad \mathbf{f} \geq 0. \quad (3.1)$$

This function consists of two terms: a dose objective term and a smoothing term. The first term records for each voxel in a volume v the difference between the attainable dose $H\mathbf{f}$ and the prescribed dose \mathbf{d}_v^p , which is kept constant for all voxels in a certain volume, usually the prescribed dose for the PTV, and 0 for the organs at risk. The diagonal

matrix $\tilde{\eta}_v$ contains the voxel-dependent importance factors. The different volumes of interest (representing structures) $v \in \mathcal{V}$ are weighted by volume-wide importance factors ξ_v .

The second term is the smoothing term, regulated by a smoothing factor κ . This term encourages the fluence to be smooth. The product $M\mathbf{f}$ is a discretization of the Laplacian (second derivative) of the fluence \mathbf{f} .

3.2.2 Beam profile optimization

Equation 3.1 can be written in canonical form:

$$s(\mathbf{f}) = \frac{1}{2} \mathbf{f}^T A \mathbf{f} + \mathbf{f}^T \mathbf{b} + c, \quad (3.2)$$

where:

$$A = H^T Q H + \kappa S, \quad \mathbf{b} = H^T \mathbf{q}, \quad c = \sum_v \xi_v (\mathbf{d}_v^p)^T \tilde{\eta}_v \mathbf{d}_v^p, \quad (3.3)$$

$$Q = 2 \sum_v \xi_v \tilde{\eta}_v, \quad S = 2M^T M, \quad \mathbf{q} = -2 \sum_v \xi_v \tilde{\eta}_v \mathbf{d}_v^p. \quad (3.4)$$

The advantage of this formulation is that the calculation of the score requires only a few matrix-vector computations and that there are many methods available for minimizing this function. The most time consuming computation is that of the first term of matrix A. We have developed an efficient sparse matrix algorithm to compute $Z = H^T Q$ by only transposing the rows of H if the corresponding element on the diagonal of Q is nonzero. The number of computations scales linearly with the number of nonzero elements on the diagonal of Q .

An IMRT problem using an objective function similar to equation 3.1 without the smoothing term is usually ill-posed because it is possible to obtain nearly identical dose distributions with different fluence maps (Alber *et al* 2002b). Without precautions the resulting fluence will contain high frequencies due to the numerical noise in the problem. The numerical degeneracy of a matrix depends on the condition number, which is the ratio between the largest and smallest eigenvalue. By adding a well-conditioned matrix (such as the identity matrix or Laplacian) the smallest eigenvalue increases, so the condition decreases, which is favourable.

The Hessian (matrix A in equation 3.2) is positive definite, so minimizing $s(\mathbf{f})$ under the condition that $\mathbf{f} \geq 0$ can be solved by any convex quadratic minimization algorithm. Our algorithm of choice is BOXCQP (Voglis & Lagaris 2004) because this algorithm is easy to implement and faster than most quadratic programming algorithms. Furthermore it uses the Cholesky decomposition which is suitable for parallelization on SMP (symmetric multiprocessors) computers. The average speed-up when using 2 CPUs is

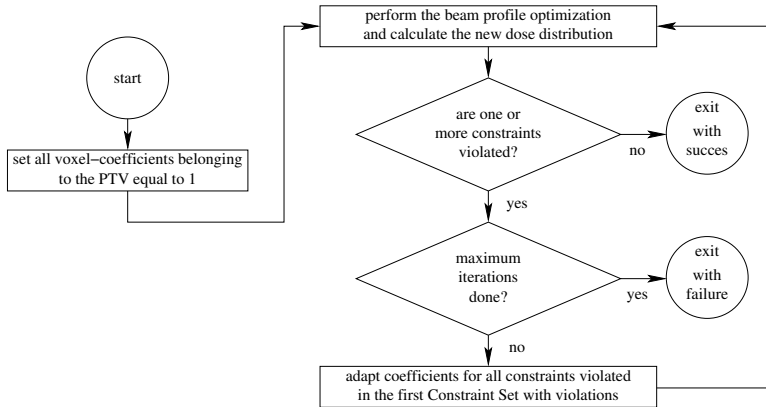


Figure 3.1: Flow diagram of the two-step voxel-coefficients optimization.

over 90%.

3.2.3 Optimization of the voxel-coefficients

After the first beam profile optimization, the result is evaluated and the the voxel-dependent importance factors η_v (the voxel-coefficients) are adapted according to the violated constraints. A flow diagram of this algorithm is depicted in figure 3.1.

The constraints are divided into different constraint sets C_k , where k is a priority index. For example, the minimum PTV dose is usually put into C_1 , because irradiating the PTV is the most important objective. The maximum dose in the PTV will usually be in C_2 , and the organs at risk in C_3 , C_4 , ... (see table 3.1). In the second step of the optimization, the voxel-coefficients η_v are adapted only for the constraints in the first set C_k in which one or more constraints are violated.

Table 3.1: Constraint list for the rectum case with a prescribed dose of 44.65 Gy. Five constraint sets are used. The smaller k , the higher is the importance of meeting that particular constraint.

volume	type	objective	critical	C_k
PTV	DV	100%	42.42 Gy	1
PTV	Max	47.78 Gy		2
Body	Max	47.78 Gy		2
Bowel	DV	25%	35 Gy	3
Bladder	DV	10%	40 Gy	3
Colon	DV	8%	40 Gy	3
Bowel	DV	37%	20 Gy	4
Bladder	DV	26%	20 Gy	4
Colon	DV	14%	20 Gy	4
Body	DV	16%	30 Gy	5

To select the voxels of which the coefficient is adapted (i.e. increased), the dose of the particular volume is sorted in ascending order, see figure 3.2 (Bortfeld *et al* 1997). For a maximum-dose constraint violation, a subset of the voxels exceeding the maximum-dose are adapted from high-dose to low-dose.

A dose-volume constraint requires a different approach. To lower a dose-volume value the voxels exceeding the critical dose are to be minimized. This can be achieved by increasing the voxel-coefficient of the voxels whose dose just exceeds the critical dose. This is depicted in the right part of figure 3.2 and visualised in figure 3.3.

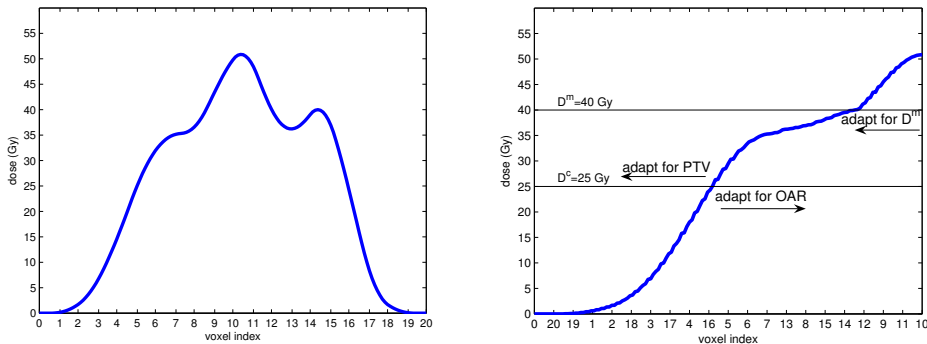


Figure 3.2: One dimensional example of the selection of voxels for adaptation of the (voxel-dependent) importance factor. The dose distribution (left) is sorted in ascending order (right). The first voxel exceeding the critical dose D^c is 16. For an OAR, the coefficient of voxels 16, 5, 6, ... are adapted. For a PTV voxels 4, 17, 3, ... If the coefficients are adapted because of a maximum-dose constraint violation, the voxels 10, 11, 9, ... are adapted.

One of the problems with this two-step approach is that the adaption of the voxels-coefficients does not have a direct relation to the criteria. It is not possible to predict the result of increasing the coefficient for a single voxel. For the maximum-dose voxel-adaption algorithm, experience learned that increasing the coefficient of the top 20% of the voxels violating the maximum-dose constraint by 0.3 proofs to be a good balance between decreasing the maximum-dose in the volume and over-emphasizing the voxels. For the dose-volume voxel-adaption algorithm, the coefficient of the first 20 voxels violating the constraint is increased by 1, unless there are less voxels violating this constraint. These settings result in a smooth convergence.

3.3 Results and discussion

The algorithm is demonstrated for a rectum cancer case. The prescribed dose is 44.65 Gy (19 fractions of 2.35 Gy) and the patient is treated with four 18 MV beams and one

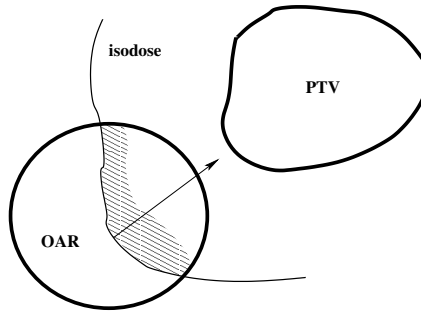


Figure 3.3: 2D example of voxel selection for voxel-coefficient adaption. The isodose line belongs to the critical dose D^c for the OAR. To reduce the amount of voxels exceeding the critical dose, the value of the voxel-coefficients of the voxels in the shaded area is increased. The result is that the isodose line moves closer to the PTV.

6 MV PA beam. 2297 beamlets of size 0.5×1.0 cm are used and 234 479 voxels of $0.4 \times 0.4 \times 0.5$ cm are considered in the patient volume. The volume-wide importance factors (see equation 3.1) for the PTV, bowel, bladder, colon and body are chosen 100, 10, 5, 5 and 1 respectively.

The constraints used are presented in table 3.1. Irradiating the tumour is the most important objective, so the constraint for the PTV is placed in the first constraint set (100% of the PTV receives a dose of 95% of the prescribed dose). The maximum PTV dose is 107% of the prescribed dose and is placed in the second constraint set, together with the maximum allowable dose in the body tissue (excluding PTV and OARs). After the constraints in the first two sets are met, the algorithm tries to meet the constraints in the third set. This set contains the high dose constraints, since high dose in a volume has a larger impact on biological damage than a lower dose. The fourth constraint set contains constraints for the lower dose range. The reason that two DVH constraints are used for the OARs is because the volumes are large. It turned out to be not efficient to only lower the high dose constraints: a lot could be gained in the low dose range as well. The last constraint on the body is to enforce more conformity and removes unnecessary dose in the unspecified tissue.

The optimization required 41 minutes for 273 iterations on a 2.4 GHz Intel Core2 processor. The results are presented in figure 3.4. The dose is highly conformal and 100% of the PTV is irradiated within the 95% – 107% dose constraint.

One of the difficulties in inverse treatment planning is the choice of the constraints and the corresponding importance factors. If possible, an algorithm will provide a solution which satisfies the constraints, but not necessarily better. A lot of human interaction would be required to find the *most optimal* constraints. This is a result of the multi-

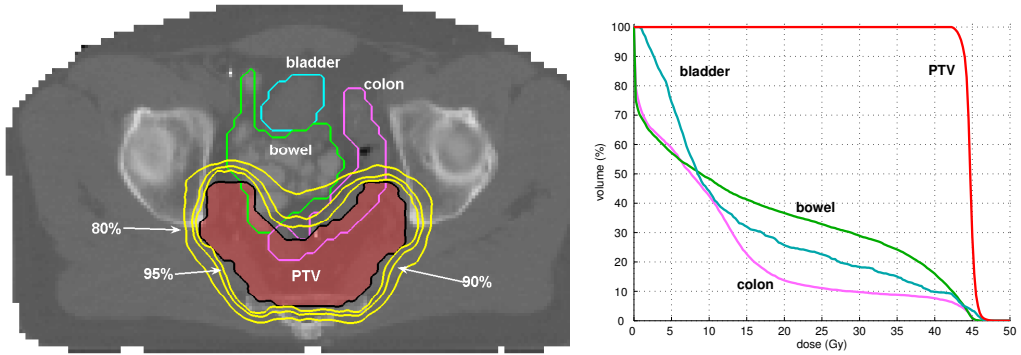


Figure 3.4: Left figure shows location of the volumes and the 80%, 90% and 95% isodose lines. The beams are placed at 85, 155, 180, 205 and 275 degrees. Right figure shows the dose-volume histogram.

criteria origin of the problem. In an upcoming paper we will present an algorithm that automatically finds the most optimal (i.e. Pareto optimal) constraints for an inverse planning process.

The time required for this optimization could be further reduced by using a parallel implementation, as mentioned in section 3.2.2.

3.4 Conclusion

In this paper we have presented an algorithm that effectively adapts voxel-dependent importance factors, used in combination with a quadratic objective function. This implemented two-step approach is capable of achieving highly conformal dose distributions.

Chapter 4

A novel approach to multi-criteria inverse planning for IMRT

Sebastiaan Breedveld¹, Pascal Storchi¹, Marleen Keijzer², Arnold Heemink²
and Ben Heijmen¹

¹ Department of Radiation Oncology, Erasmus MC Rotterdam, Groene Hilledijk 301, 3075
EA Rotterdam, The Netherlands

² Delft University of Technology, Delft Institute of Applied Mathematics, PO Box 5031,
2600 GA Delft, The Netherlands

E-mail: s.breedveld@erasmusmc.nl

Published 2 October 2007 in *Physics in Medicine and Biology*, volume **52**, pages 6339-6353

[doi:10.1088/0031-9155/52/20/016](https://doi.org/10.1088/0031-9155/52/20/016)

Abstract

Treatment plan optimization is a multi-criteria process. Optimizing solely on one objective or on a sum of *a priori* weighted objectives may result in inferior treatment plans. Manually adjusting weights or constraints in a trial and error procedure is time consuming. In this paper we introduce a novel multi-criteria optimization approach to automatically optimize treatment constraints (dose-volume and maximum-dose). The algorithm tries to meet these constraints as well as possible, but in the case of conflict it relaxes lower priority constraints so that higher priority constraints can be met. Afterwards, all constraints are tightened, starting with the highest priority constraints. Applied constraint priority lists can be used as class solutions for patients with similar tumour types. The presented algorithm does iteratively apply an underlying algorithm for beam profile optimization, based on a quadratic objective function with voxel-dependent importance factors. These voxel-dependent importance factors are automatically adjusted to reduce dose-volume and maximum-dose constraint violations.

4.1 Introduction

Traditionally, irradiating the tumour with the prescribed dose has been the primary goal in radiotherapy, as long as no critical damage is done to the OARs. Nowadays, with better planning and treatment tools available, optimal sparing of OARs has also become a major goal. One of the difficulties in plan optimization is that feasible solutions may heavily, and rather unpredictably, depend on the selected objectives and constraints, and their relative weights. In clinical practice, dosimetrists do usually optimize constraints, objectives, and/or weights in a time-consuming interactive trial-and-error process, to find some acceptable compromise. Often constraints are implemented as objectives and optimized in a weighted sum function, making it impossible to make a sharp trade-off between objectives without violating constraints. Multi-criteria optimization (or multi-objective optimization) aims at providing tools to steer this process. One approach includes generation of sets of Pareto efficient solutions (Cotrutz *et al* 2001, Craft *et al* 2005, 2006, Halabi *et al* 2006, Hoffmann *et al* 2006, Küfer *et al* 2005, Lahanas *et al* 2003).

In this paper, a novel approach to multi-criteria optimization is presented. This algorithm maximizes or minimizes objectives subjected to constraints. An objective is implemented as a *soft constraint*, a constraint which is allowed to be violated and adapted by the algorithm. (To distinguish normal constraints from soft constraints, constraints which are not allowed to be violated are called *hard constraints*.) The objectives are selected and prioritized *a priori* by the radiation oncologist and grouped together with the (hard) constraints to a *constraint priority list*. Soft constraints with a low priority may be automatically relaxed to meet higher priority or hard constraints (e.g. the volume allowed to receive more than the critical dose is increased for a dose-volume constraint). Soft constraints may also be tightened where possible. Finally, for each patient a single plan is generated with a set of constraints that just avoids constraint violations; tightening any of the final constraints will result in at least one violation for the other constraints. The final plan meets all hard constraints and the soft constraints are met as well as possible.

The proposed algorithm for multi-criteria optimization iteratively applies an in-house developed algorithm for beam profile optimization. With the latter algorithm, profiles are optimized using voxel-dependent importance factors in a quadratic dose objective function. Optimization includes automatic adjustment of these factors in order to reduce dose-volume and maximum-dose constraint violations. An algorithm for fast minimization of quadratic functions has recently been published (Breedveld *et al* 2006), and is applied here. Despite that the multi-criteria optimization algorithm is only applied to our in-house developed beam profile optimization, we believe that the algorithm can

be applied to a broader range of algorithms for constrained optimization, including, for example, aperture based optimization.

To weigh the relative importance of OARs and the tumour in inverse planning for IMRT, a volume-wide importance factor can be used for each volume (Bortfeld *et al* 1990, Brahme 1995, Spirou & Chui 1998, Wu & Mohan 2000). Because the desired dose is more easily delivered to some voxels than to others, the volume-wide importance factor can be refined to voxel-dependent importance factors. This provides more local control over the dose (Cotrutz & Xing 2002, Wu *et al* 2003). The weights of the voxels can be chosen in advance by looking at the depth and position of the organs (Shou *et al* 2005) or adapted in an iterative procedure (Cotrutz & Xing 2003, Scherrer *et al* 2005, Yang & Xing 2004).

Recently, Wilkens *et al* (2007) and Jee *et al* (2007) have also studied the use of constraint priority lists, using different optimization schemes and different underlying optimization algorithms. These papers also describe the advantage of goal programming/lexicographic ordering in treatment planning. Wilkens *et al* formulate a four-step approach which is used as a class solution for treating head-and-neck patients. The fourth step incorporates a non-clinical goal: smoothing of the fluence. In our approach, profile smoothing is an integral part of the optimization procedure, accounted for by a dedicated term in the objective function. Jee *et al* describe the application of lexicographic ordering with four levels of priority, applied to a prostate and a head-and-neck case. For the prostate case they also show the impact of changing the priorities of PTV irradiation and maximum dose to the rectum wall.

One of the main differences between the approaches of Wilkens *et al* and Jee *et al* and our approach is that their objectives are handled one by one, and in a predefined order. Our approach first tries to find a solution, fulfilling all constraints. If that is not possible, limiting (lower-priority) constraints are relaxed. However, after relaxation, the primary goal of the algorithm becomes meeting all initial constraints (as prescribed by the radiation oncologist). This process starts with the highest priority constraints that have been relaxed. If, for example, the dose in the parotid glands is within the constraints, it may be more important to first lower the dose in the oral cavity. If all the initial constraints are met (or as well as possible), an attempt is made to tighten constraints below the initially prescribed levels, again starting with the highest priority constraints.

4.2 Methods and materials

4.2.1 Global description of optimization routines

The proposed multi-criteria approach is based on algorithms for optimization of (1) beam profiles, (2) voxel weights and (3) imposed treatment constraints. To define the problem,

tumour dose prescriptions, dose-volume and maximum-dose constraints, a constraint priority list, and volume-wide importance factors have to be set. This defines the *planning protocol*. Ideally, a single protocol can be applied to patients with similar tumour types.

For the *beam profile optimization* a quadratic objective function is used to minimize the difference between the desired or prescribed doses in voxels and the attained doses. Each voxel has a *coefficient* η . The higher the coefficient, the more likely it becomes for that voxel to meet its ideal dose objective, either 0 Gy dose for organs at risk, or the prescribed dose for the tumour.

The quadratic objective function used has been discussed thoroughly in [Breedveld et al \(2006\)](#):

$$s(\mathbf{f}) = \sum_{v \in \mathcal{V}} \xi_v (\mathbf{H}\mathbf{f} - \mathbf{d}_v^p)^T \tilde{\eta}_v (\mathbf{H}\mathbf{f} - \mathbf{d}_v^p) + \kappa (\mathbf{M}\mathbf{f})^T (\mathbf{M}\mathbf{f}).$$

The first term is the quadratic dose objective, modified for use with voxel-dependent importance factors. $\mathbf{H}\mathbf{f}$ is the dose resulting from the fluence \mathbf{f} , and \mathbf{d}_v^p is the dose objective for voxels in volume v (from the set of all volumes \mathcal{V}). The volume-wide importance factors ξ_v are still used as *a priori* weighting between volumes. The vector of voxel-dependent importance factors $\boldsymbol{\eta}_v$ (which will be abbreviated as the *voxel-coefficient vector* $\boldsymbol{\eta}$ for readability) is written as a diagonal matrix $\tilde{\eta}_v$. In this approach, the dimension of the coefficient vector equals the number of patient voxels. Only the subset of the coefficients corresponding to the volume v can be unequal to zero. Because each volume has its own voxel-coefficient vector, one voxel (in the patient space) can belong to more than one volume (i.e. volumes can overlap). The second term $\kappa (\mathbf{M}\mathbf{f})^T (\mathbf{M}\mathbf{f})$ represents the squared second derivative of the fluence and ensures a smooth fluence.

Two types of constraints are used in this paper: *dose-volume* and *maximum-dose* constraints. Each constraint is put into a set C_n according to the priority for meeting the constraint level. Constraints in set C_0 are hard constraints and no relaxation is allowed. The other constraints are soft constraints. Constraints in set C_1 are the first ones considered for tightening and the last ones to be relaxed, etc. The sets C_n represent the constraint priority list. Typical examples are given in tables [4.1](#) and [4.2](#).

In the case of constraint violations, involved voxel-coefficients are adapted (sections [4.2.2.1](#) and [4.2.2.2](#)) and a new fluence is calculated by the beam profile optimization. This procedure, designated as *coefficients optimization*, is repeated until no constraint is violated, or for a maximum number of iterations (section [4.2.2](#)).

The four-stage *constraint optimization* is an iterative multi-criteria optimization mastering the coefficients optimization, based on the constraint priority list. If constraints are too tight and the coefficients optimization cannot find a feasible solution within a fixed number of iterations, constraints are first relaxed. When a feasible solution has

been found with relaxed constraints, a process is started to tighten constraints without exceeding any of the other constraints. If no constraints can be tightened anymore, the optimization is terminated (section 4.2.3).

4.2.2 Coefficients optimization

The coefficients optimization adapts the voxel-coefficient η for volumes with violated constraints by increasing the coefficient of one or more voxels. If the minimum dose constraint (mimicked by a dose-volume constraint with 100% coverage objective) for one or more PTVs is violated, only the voxel-coefficients for these constraints are adapted. Otherwise voxel-coefficients for the other violated constraints are adapted. Note that the coefficient of a voxel can be increased several times in multiple iterations (section 4.2.3, figure 4.3).

It is also possible to optimize the constraints in prioritized order in this part of the optimization, as was done in [Breedveld *et al* \(2007b\)](#). The drawback is that the constraints will not be relaxed or tightened, which may lead to a suboptimal result or even present an infeasible problem. With a multi-criteria optimization algorithm as presented in section 4.2.3, also prioritizing the constraints in this part of the optimization is superfluous.

After each adaption of voxel-coefficients, the coefficients optimization performs a beam profile optimization ([Breedveld *et al* 2006](#)) and re-evaluates the constraints. If no constraints have been violated, or after a maximum number of iterations, the coefficients optimization is terminated.

4.2.2.1 Adaptation of voxel-coefficients for dose-volume constraints.

To reduce the high dose volume in the OAR, voxels exceeding the critical dose need to have their doses reduced. Usually, voxels with a high dose are closer to the PTV. Furthermore, it is easier to decrease the dose in voxels with doses close to the critical dose than voxels with a higher dose. Therefore voxel-coefficients are increased for OAR voxels that just exceed the critical dose D^c (figure 4.1).

The selection of voxels to be adapted is illustrated in more detail in figure 4.2 for a one-dimensional example. The voxels are first sorted in ascending order by dose. For the voxels exceeding the critical dose D^c , some voxel-coefficients are increased. When applied to the PTV, the voxels are adapted from the high-dose region just below D^c to the low dose region. [Bortfeld *et al* \(1997\)](#) used the same idea applied to a penalty function. In the approach of [Cotrutz & Xing \(2002\)](#), dosimetrists have to manually select areas in the DVH that need improvement.

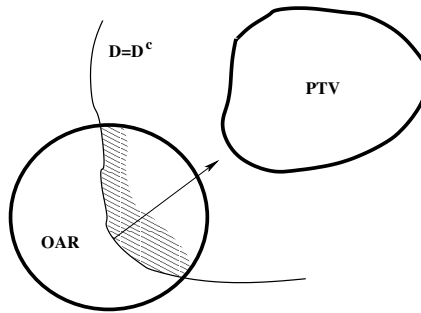


Figure 4.1: 2D example of voxel selection for iterative voxel-coefficient adaption. D^c is the critical dose for the OAR. To reduce the amount of voxels exceeding the critical dose, the value of the voxel-coefficients of the voxels in the shaded area is increased. The result is that the D^c isodose line moves closer to the PTV, because dose delivery in the shaded area is penalized.

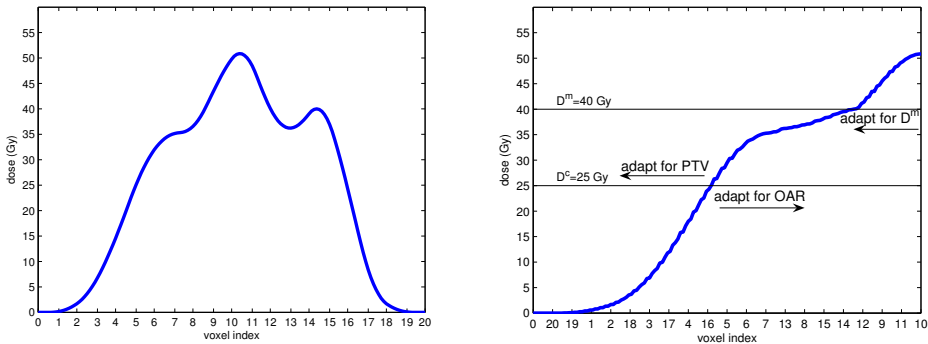


Figure 4.2: One-dimensional examples of voxel selection for voxel-coefficients adaption. The dose distribution (left) is first sorted in ascending order (right). The first voxel exceeding the critical dose D^c of the dose-volume constraint is 16. For an OAR, the coefficients of voxels 16, 5, 6, ... are then adapted. For a PTV voxels 4, 17, 3, ... In the case of a dose-maximum constraint D^m , voxels 10, 11, 9, ... are adapted.

4.2.2.2 Adaptation of voxel-coefficients for maximum-dose constraints.

A similar technique is applied to suppress high-dose regions: the coefficients for a subset of the voxels receiving a dose larger than D^m are adapted, starting with the voxels receiving the highest doses (see also figure 4.2).

4.2.3 Constraint optimization

The coefficients optimization may be used to generate a solution that meets a set of constraints, but it fails to come up with an alternative if the constraints are too tight. On the other hand, if the constraints are too loose, the solution found is sub-optimal, unless the constraints are set *just tight enough*.

In our multi-criteria approach, constraint optimization based on the initial constraints and the constraint priority list is used to generate a plan with the property that improving a single constraint is only possible if at least one other constraint is violated.

The constraint optimization is a four-stage process (figure 4.3). Each stage calls the coefficients optimization with a maximum number of iterations (N_1, \dots, N_4 for each stage). The coefficients optimization is an *evolutionary* algorithm, i.e., the voxel-coefficient vector is updated in each iteration. This property is also used in the constraint optimization because the solution of a slightly different constraint set (i.e. one constraint is more tight) lies in the proximity of the current solution. This allows a fast search through the constraint space because it is not required to start from scratch in each iteration of the constraint optimization.

4.2.3.1 Stage 1

Before the first stage starts, a single optimization is done of the quadratic objective function with voxel weights 1 for the PTV(s) and 0 for all OAR. This results in an initial dose distribution. Then the first stage is started and a maximum of N_1 iterations are done with the coefficients optimization, subjected to the initial constraints. This populates the voxel-coefficient $\boldsymbol{\eta}$ with ‘problematic’ voxels.

4.2.3.2 Stage 2

If a plan satisfying all constraints is not found in the first stage, violated soft constraints are relaxed in the second stage. The constraints in the set C_n with the lowest priority are selected for relaxation first, if there are one or more constraints violated in that set. A constraint is relaxed by setting it to the upper rounding of the current solution, so if the initial objective is 40% and the current solution is 43.21%, the new objective for the constraint is set to 44%. Then N_2 iterations with the coefficients optimization are performed to search for a solution. These iterations are also done if no constraints are suitable for relaxation (e.g. only the hard constraints are not satisfied). The second stage is repeated until a plan is found that fulfils all hard constraints and all (relaxed)

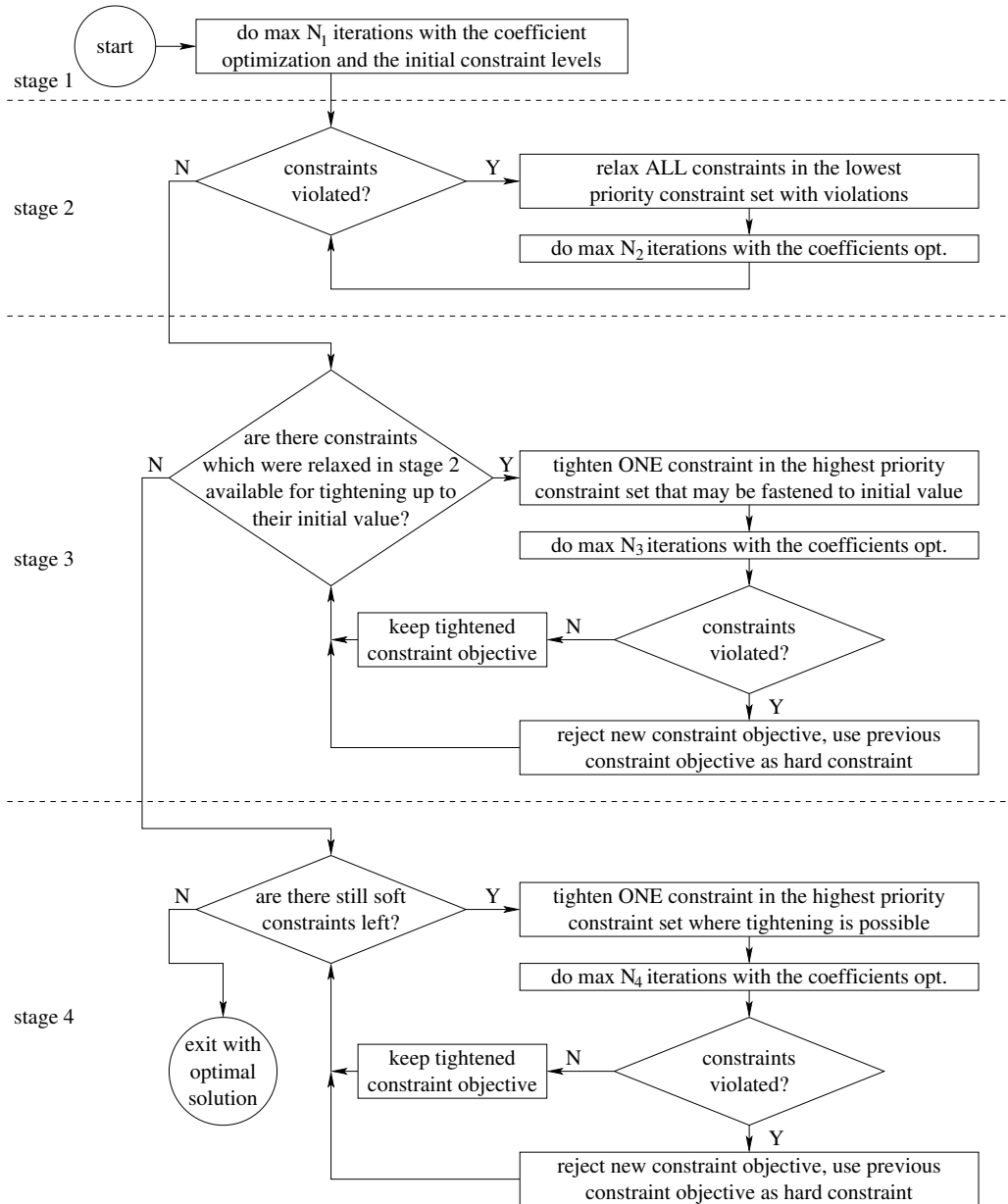


Figure 4.3: Flow diagram of the four-stage constraint optimization. The first stage populates the coefficient vector with problematic voxels. If soft constraints cannot be met, they are relaxed in the second stage. The third stage tries to undo this relaxation, by tightening relaxed constraints up to the initial constraint levels. Finally, the fourth stage tightens soft constraints until no further tightening of any of them is possible.

soft constraints. Here it is assumed that there are no conflicting hard constraints.

4.2.3.3 Stages 3 and 4

In these stages, the stage 2 plan is further optimized by tightening soft constraints one by one, so a plan is generated such that further tightening of one constraint will always lead to a violation of at least one other. In stage 3, attempts are made to tighten constraints that were relaxed in stage 2 with the ultimate goal to reach the initial values, i.e., to undo the relaxations. The first constraints to be considered are in the highest priority constraint set (C_1). If after a maximum of N_3 iterations of the coefficients optimization all constraints are met, including the tightened constraint, the tightened objective for the latter is kept. Otherwise, the constraint is reset to its previous objective, the steps of the coefficients optimization are undone, and the constraint does no longer participate in the constraint optimization, and becomes virtually a hard constraint for the rest of the constraint optimization. In this procedure, a constraint is tightened by rounding off to the lower integer, so if the current solution has a value of 43.21%, the new objective for this constraint will be 43%. For dose-volume constraints, this results in minimizing the number of voxels receiving more than the critical dose (Halabi *et al* (2006) also uses this concept in a different problem definition).

As mentioned, stage 3 aims at undoing the relaxations done in stage 2 as much as possible, with the final goal to generate a plan that fulfils to all initial constraints. Stage 4 takes this a step further. In a similar procedure as for stage 3, constraints are tightened further with an attempt to make them more strict than the initial objectives. Important to note is that in stages 3 and 4 tightening of important constraints may result in less favourable results for less important constraints. However, the tightening will never result in exceeding any of the (current) constraint levels.

4.2.4 Calculations

The algorithm used to calculate the dose deposition matrix H is from Storchi & Woudstra (1996) and uses inhomogeneity corrections for air cavities and a scatter radius of 3 cm. The Storchi and Woudstra algorithm for dose calculation is comparable to the one used in the CadPlan treatment planning system. The bixel grid size is $5 \times 10 \text{ mm}^2$ and the voxel grid size is $4 \times 4 \times 5 \text{ mm}^3$ for all patients. The numbers of iterations performed with the coefficients optimization are $(N_1, N_2, N_3, N_4) = (50, 1, 30, 20)$. Computations were performed in Matlab 7 on a 2.4 GHz Intel Core2 workstation running Gentoo Linux.

4.3 Results

The proposed method for multi-criteria inverse planning has been applied to patients suffering from rectum cancer and oropharyngeal cancer, and to a complicated head-and-neck case. For rectum and oropharyngeal cancer it has been demonstrated that the proposed

Table 4.1: Constraints and priorities for treatment of rectal cancer. Dose-volume constraints are indicated by DV.

No	Volume	Constraint type	Critical dose	Objective	Constraint set
1	PTV	DV	42.42 Gy	100%	0
2	PTV	Max		47.78 Gy	0
3	Body	Max		47.78 Gy	0
4	Bowel	DV	35 Gy	20%	1
5	Bladder	DV	40 Gy	40%	2
6	Colon	DV	40 Gy	20%	2
7	Bowel	DV	20 Gy	50%	3
8	Bladder	DV	20 Gy	75%	3
9	Colon	DV	20 Gy	30%	3
10	Body	DV	30 Gy	40%	4

approach can be used to generate class solutions for patients with the same tumour type. To find a constraint list which performs well as a class solution, different lists were tried and their results and performance were compared for four patients. The final constraint list was used on four other rectum patients to test the general performance. All generated plans are compared to the corresponding clinically applied plans made in CadPlan (referred to as *the clinical plan*). Here results are presented for the rectum cases and for the complex head-and-neck case.

4.3.1 Rectum

All patients were to be treated with a prescribed dose of 44.65 Gy (19 fractions of 2.35 Gy). The constraint list (table 4.1) has been tuned to produce desired results on four patients by defining the dose-volume points and the subdivision into constraint sets. The importance factors for the PTV, bowel, bladder, colon and body have been chosen to be 100, 10, 5, 5 and 1, respectively. To make a fair comparison, the beam directions and energies are chosen identical to the ones used in the clinical plan: five beams of 18 MV around 85, 155, 180, 205 and 275 degrees, where sometimes the beam for 180 degrees was chosen 6 MV. The performance of this protocol was verified for four other patients.

For patient 3, the resulting dose distribution is displayed in figure 4.4. It shows that the algorithm is capable of generating highly conformal dose distributions. The dose-volume histograms in figure 4.5 show that our algorithm for multi-criteria optimization does not only improve OAR dose volume histograms, but also the PTV dose homogeneity (avoidance of hot spots).

4.3.2 Complex head-and-neck case

An extensive nasopharyngeal cancer case was selected to investigate the value of the developed algorithm when a large number of structures are involved. The PTV starts

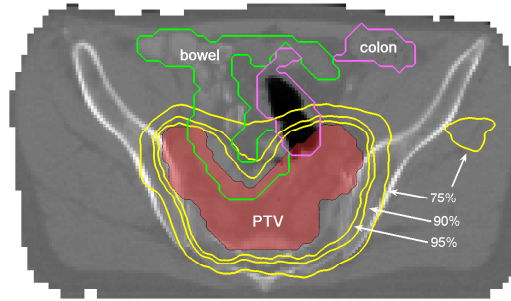


Figure 4.4: Volumes and dose distribution for the third rectum case.

halfway the eyes, branches into two neck regions (right neck is positive) and ends in front of the lung tops (level IV). The PTV length is approximately 28 *cm* and the total volume is 800 *cc*. The optical nerves and optic chiasm do partially overlap with the primary tumour/positive neck.

The constraint list used is shown in table 4.2, containing 17 constraints for the 16 volumes involved. The whole PTV should receive at least 95% of the prescribed dose of 46 *Gy* (43.7 *Gy*, hard constraint). The volume of the gross tumour (PTV70) should receive at least 66.5 *Gy*. However, because at the same time, the organs at risk have to be protected by hard (maximum-dose) constraints, the criterion to deliver 66.5 *Gy* to the PTV70 has been relaxed into a soft constraint with priority 1.

The volume-wide importance factors are 100 for the 70 *Gy* PTV, 50 for the 46 *Gy* PTV, 10 for the sella, optic chiasm, optical nerves and parotid gland, 5 for the brainstem, pons, eyes, oral cavity and pharynx/trachea and 1 for the myelum, lung tops and body. The optimized plan is compared to the clinical plan, which took experienced planners 2 weeks to achieve with 16 IMRT and wedged beams. Our setup uses nine equi-angular 6 *MV* beams.

The results are presented in table 4.2 and figure 4.6. Table 4.2 shows that using the developed multi-criteria approach all hard constraints could be met. In contrast to the clinical plan, with the multi-criteria approach the full PTV46 could be irradiated with the critical dose. Because of this improved tumour coverage, the mean dose in the parotid gland is slightly higher than in the clinical plan (27.0 *Gy* mean dose in stead of 25.6 *Gy* in the clinical plan). The dose in the oral cavity is significantly lower than in the clinical plan: the mean dose reduces from 55.5 *Gy* to 30.2 *Gy*.

Figure 4.7 shows the convergence of some dose-volume constraints. The first stage ends after 50 iterations without finding a plan meeting all hard constraints. This requires another 240 iterations (stage 2). Note the decrease in coverage of the 70 *Gy* PTV which grows to 100% in the first iterations, but decreases to 93% afterwards. The third stage,

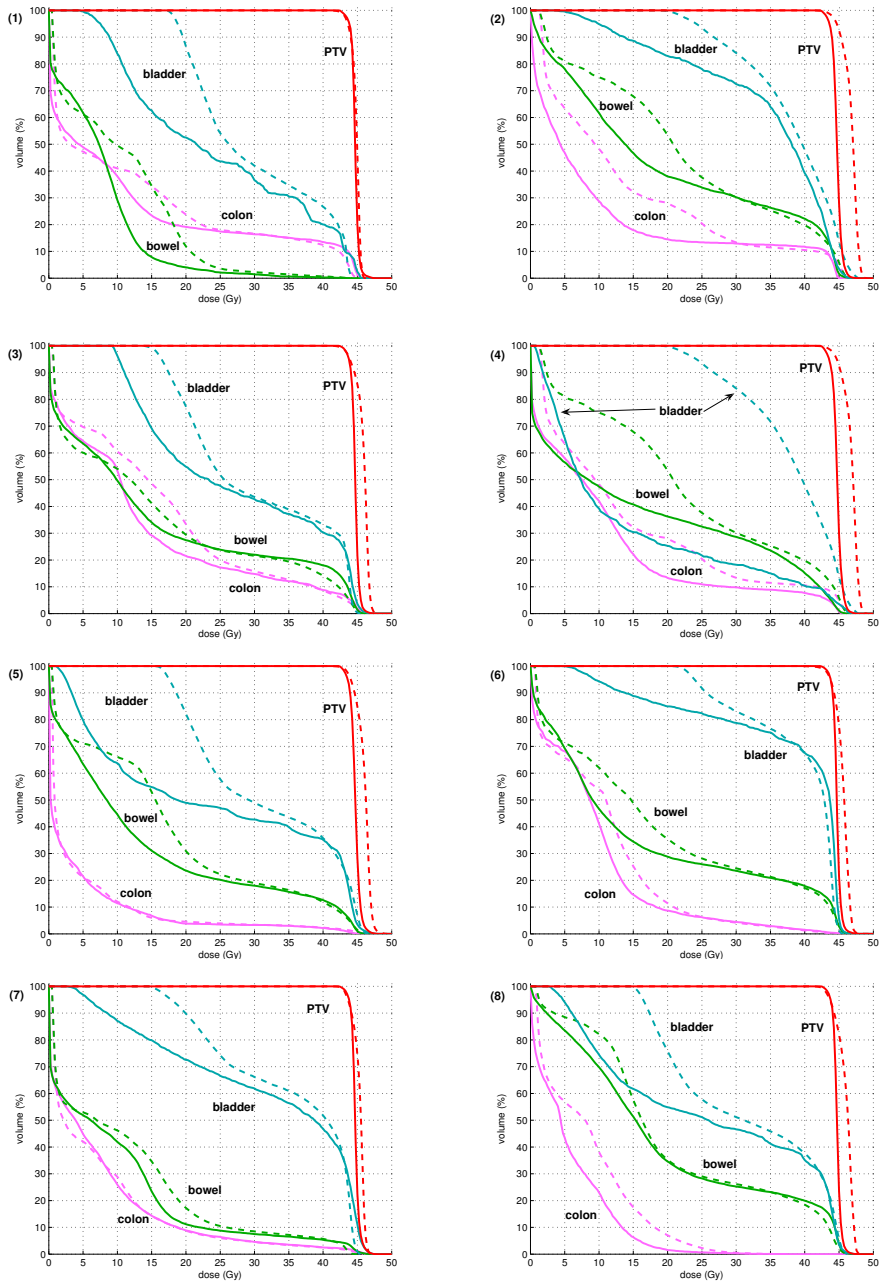


Figure 4.5: Dose-volume histograms for the eight rectum patients. Histograms are presented for the clinical IMRT plan (dashed lines) and for the plan generated with the developed method for automated multi-criteria optimization.

trying to undo the constraint relaxations of stage 2, starts after 290 iterations (indicated by (a)). Between (a) and (b), the algorithm minimizes the dose-volume constraints for the brainstem and pons (not shown in figure). After their initial objective of 0% overdose is met, the dose-volume constraint for the parotid gland is tightened (b) until its initial objective of 50% (c). The oral cavity, pharynx/trachea and lung tops are all in constraint set 4. Since the dose-volume constraint for the lung tops is not violated, only the constraints for the oral cavity and pharynx/trachea are tightened (in turn) until the initial objectives are met, (d) and (e) for the pharynx/trachea and the oral cavity, respectively. Now that all initial constraints have been met (as far as the hard constraints allow), stage 4 is initiated. Firstly, the constraint for the parotid gland is tightened which reaches its minimum value after a small reduction (f). Then the oral cavity, pharynx/trachea, and also the lung tops are considered. When no tightening is possible anymore, the algorithm tightens the constraints in the last set, containing only the body/unspecified tissue (g).

A direct comparison between the clinical plan and the automated plan is not possible for this case. This case is too extreme to be handled efficiently by CadPlan. There are 16 volumes where CadPlan can only handle 10 at a time in an optimization, so it was not possible to minimize all constraints simultaneously. Further, the 46 Gy plan and the boost plan were planned separately and combined later. The beam setup differed as well (16 IMRT and wedged beams in the clinical plan compared to 9 in our plan). CadPlan also uses a weighted sum function for optimization. A weighted sum function is inefficient in making sharp trade-offs (e.g. 100% tumour coverage and minimizing dose in a volume close to the PTV) because it mixes objectives with constraints. These reasons explain why it was possible to improve the mean dose in the oral cavity by 15 Gy.

4.3.3 Constraint list sensitivity

The final result depends on the initial objectives of the constraints and the constraint set they are assigned to. In this section we describe how the outcome of the algorithm reacts to the chosen criteria. Results are shown for the parotid gland and oral cavity of the complex head-and-neck case in figure 4.8.

When only the priorities for the parotid gland and oral cavity (3 and 4, respectively) are interchanged, the final dose-volume histograms are almost unchanged. When in the third stage of the constraint optimization the imposed objective of 50% is reached for both the parotid gland and oral cavity, the constraint on the parotid gland does not leave much space to improve the dose to the oral cavity. If the imposed objective for the parotid gland is increased (relaxed) to 70%, the oral cavity is much better spared.

When the realized objectives of the final solution were used as imposed objectives for a new optimization, the resulting dose distributions were virtually identical to the

Table 4.2: Constraints, priorities and results for the complex head-and-neck case. PTV46 is the collection of the primary tumour, positive neck and elective nodes. PTV70 is the primary tumour and the positive neck.

No	Volume	Constraint type	Critical dose	Objective	Realized objective	Mean dose	Clinical realized objective	Constraint set
1	PTV46	DV	43.7 Gy	100%	100.0%		96.5%	0
2	Sella	Max		55 Gy	55.0 Gy		52.6 Gy	0
3	Myelum	Max		45 Gy	44.8 Gy		51.6 Gy	0
4	Optic chiasm	Max		50 Gy	50.0 Gy		52.5 Gy	0
5	Optical nerve (L)	Max		55 Gy	55.0 Gy		47.3 Gy	0
6	Optical nerve (R)	Max		55 Gy	52.0 Gy		48.5 Gy	0
7	Eye (L)	Max		35 Gy	35.0 Gy		42.9 Gy	0
8	Eye (R)	Max		35 Gy	35.0 Gy		42.5 Gy	0
9	PTV70	Max		74.9 Gy	74.8 Gy		78.9 Gy	0
10	PTV70	DV	66.5 Gy	100%	93.2%		89.1%	1
11	Brainstem	DV	55 Gy	0%	0.0%		1.2%	2
12	Pons	DV	55 Gy	0%	0.0%		2.9%	2
13	Parotid (L)	DV	26 Gy	50%	46.1%	27.0 Gy	39.2%	3
14	Oral cavity	DV	26 Gy	50%	48.0%	30.2 Gy	100.0%	4
15	Pharynx/trachea	DV	40 Gy	40%	24.2%	34.5 Gy	44.3%	4
16	Lung tops	DV	18 Gy	20%	6.5%	6.5 Gy	20.0%	4
17	Body	DV	40 Gy	90%	18.9%		N/A ^a	5

^a Definition of (external) body contour differs between CadPlan and our algorithm.

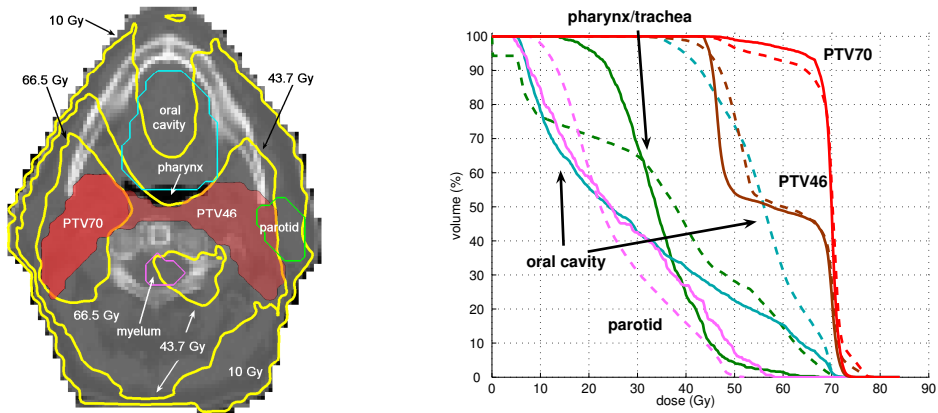


Figure 4.6: Left figure shows a CT slice with isodose lines for doses prescribed to PTV70 (66.5 Gy), PTV46 (43.7 Gy), and the 10 Gy isodose line. Right figure shows the dose-volume histograms for some interesting volumes, where the dashed lines indicate the results of the clinical plan.

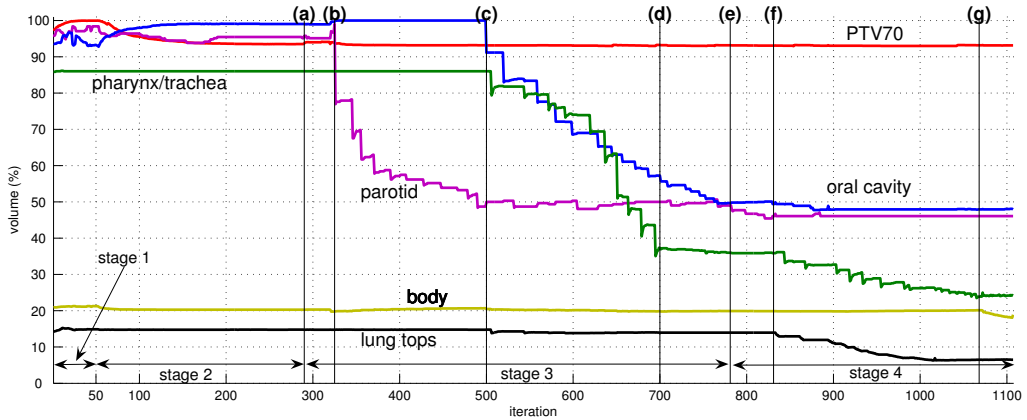


Figure 4.7: Convergence of the dose-volume constraints. The letters (a-g) are explained in the text.

previous distributions. This is an indication that the algorithm is robust, because when different starting positions (constraint lists) are used, the same result is obtained. None of the cases could be significantly improved, which demonstrates the optimality of the constraints.

But interchanging priorities or relaxing imposed objectives does not guarantee that another solution can be obtained, when the minimum-dose for the PTV is kept as a hard constraint. The physiology of the patient must also allow the desired trade-offs. For example, for the rectum patients, interchanging the priorities for the bowel and the colon, or changing the imposed objectives, does not permit much difference in the final solution: this is because the volumes are physically correlated. The placement and the number of beams used play important roles as well.

Another parameter of influence is the volume-wide importance factor for each volume. Because the voxels belonging to a certain volume are multiplied by their volume-wide importance factor, the choice of the volume-wide importance factor plays a minor role in the voxel-dependent approach, and mainly influences the number of iterations required to obtain the final solution, because it influences the impact of an adapted voxel-weight. If a volume has a large volume-wide importance factor, the effect of an adapted voxel is large as well, and the coefficients optimization needs more iterations to obtain a solution fulfilling all constraints. A rule of thumb for the volume-wide importance factors is (relative) 100 for the PTV, 50 for elective glands (PTV), 5-10 for important OARs and 1 for other OARs.

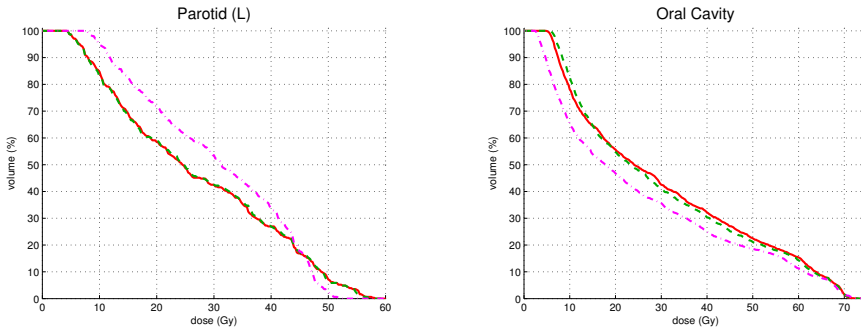


Figure 4.8: Dose-volume histograms for the parotid gland (left) and the oral cavity (right). The solid line is the original solution. The dashed line is solution when their priorities are interchanged and the dash-dotted line when the imposed objective for the parotid gland is increased to 70% as well.

4.4 Discussion and conclusions

We have developed an algorithm for multi-criteria inverse planning for IMRT. Input is a constraint priority list, to be provided by the radiation oncologist. In this list, constraints are ranked in groups, according to the priority for meeting the constraint levels. Constraints with the highest priority are considered hard constraints that necessarily have to be met, i.e., they cannot be relaxed in order to improve compliance with other constraints. In an iterative procedure, using an algorithm for optimization of voxel-dependent importance factors for the various dose-volume and maximum-dose constraints, soft constraints are optimized so that the final list of constraints has the property that if one constraint is tightened further, it would lead to a violation of at least one other constraint.

For the final constraints, this follows the definition of Pareto optimality. Our four-stage constraint optimization can be seen as an implementation of the ϵ -constraint method (Haimes *et al* 1971, Hoffmann *et al* 2006, Jee *et al* 2007). This method minimizes a set of objectives by minimizing one objective at a time, while keeping the others constrained. The minimum value for that objective is used as a constraint in the next iteration(s) where another objective is minimized.

In clinical practice, the automated approach is able to reduce the workload because it is able to come up with satisfactory plans for routine cases, where it is possible to determine the trade-offs *a priori*. Of course, there will always remain cases where an automated approach is not satisfactory. Different constraint lists have to be tried, as well as possibly different beam setups, requiring a rerun of the optimization. For these special cases, presenting the radiation oncologist with a set of (Pareto optimal) plans might be more efficient. Many authors have looked into this (e.g. Craft *et al* (2005, 2006), Halabi

Table 4.3: (Average) optimization statistics.

Case	Time	Iterations	Beamlets	Time per iteration
Rectum patients	47 (<i>m</i>)	345	2163	8.1 (<i>s</i>)
Complex head-and-neck case	38 (<i>h</i>)	1107	5293	125.2 (<i>s</i>)

et al (2006), Hoffmann *et al* (2006), Küfer *et al* (2005)). Our multi-criteria algorithm is not capable of producing multiple solutions because it was designed to provide only one solution which is within, or closest to the initial constraints, and may be even obeying tighter constraints than initially prescribed.

For rectal and oropharyngeal cancer patients, the developed multi-criteria approach was used for fully automated generation of class solutions. For the rectum patients, the class solutions were superior to the clinical plans, both regarding obtained tumour dose distributions, and with respect to OAR sparing. For the oropharyngeal cancer patients plans were similar (data not shown), but the automated procedure was faster and required less workload.

For violated constraints, voxel-weights are automatically adapted. Cotrutz & Xing (2002) use a semi-automatic approach where the dosimetrist manually has to select the part of the DVH where improvement is desired. Based on the selected areas, relevant voxel-dependent importance factors are then adjusted, followed by a new optimization. In this paper we have proposed a scheme for automatic adjustments of voxel-dependent importance factors, also based on DVH. In a later work, Yang & Xing (2004) propose a different voxel weight update scheme for automated adaption.

Some optimization statistics are given in table 4.3. The average optimization time of 47 minutes for rectal cancer is acceptable considering that the final result is a Pareto optimal solution and there is no human intervention. The optimization time is related to the number of beamlets and number of soft constraints. The complex, extended head-and-neck case with 17 constraints for 16 involved organs required almost 40 hours of calculation time. The obtained plan is superior to the corresponding clinical plan. Generation of the latter took two weeks of work of a highly experienced dosimetrist.

Acknowledgements

The authors want to thank Peter Voet for his help on defining treatment goals for the patients, and for reviewing and discussing the results. The authors would also like to thank the referees for their critical and stimulating comments.

Chapter 5

The equivalence of multi-criteria methods for radiotherapy plan optimization

Sebastiaan Breedveld, Pascal Storchi and Ben Heijmen

Department of Radiation Oncology, Erasmus MC Rotterdam, Groene Hilledijk 301, 3075
EA Rotterdam, The Netherlands

E-mail: s.breedveld@erasmusmc.nl

Published 17 November 2009 in *Physics in Medicine and Biology*, volume 54, pages 7199-
7209

[doi:10.1088/0031-9155/54/23/011](https://doi.org/10.1088/0031-9155/54/23/011)

Abstract

For multi-criteria optimization of radiation therapy treatment planning, several methods can be used. The most widely used methods are the weighted-sum method, in which the different treatment objectives are weighted, and constrained optimization methods, in which treatment goals are set and the algorithm has to find the best plan fulfilling these goals. The constrained method used in this article, the *2pec* (2-phase ϵ -constraint) method is based on the ϵ -constraint method, which generates Pareto-optimal solutions.

Both approaches are uniquely related to each other. In this article we will show that it is possible to switch from the constrained method to the weighted-sum method by using the Lagrange multipliers from the constrained optimization problem, and vice versa by setting the appropriate constraints.

In general, the theory presented in this article can be useful in cases where a new situation is slightly different from the original situation, as e.g. in online treatment planning, with deformations of the volumes of interest, or in automated treatment planning, where changes to the automated plan have to be made.

An example of the latter is given where the planner is not satisfied with the result from the constrained method and wishes to decrease the dose in a structure. By using the Lagrange multipliers, a weighted-sum optimization problem is constructed, which generates a Pareto-optimal solution in the neighbourhood of the original plan, but fulfils the new treatment objectives.

5.1 Introduction

Radiotherapy treatment plan optimization is a multi-criteria problem. To optimize for different criteria (objectives), an objective function can be used where the objectives are weighted and summed, as with e.g. quadratic objective functions (Breedveld *et al* 2006, Yang & Xing 2004) or power objective functions (Xia *et al* 2005).

However, determination of the optimal weighting factors for obtaining a good treatment plan is not trivial. Recently, with more computing power becoming available, plans for different combinations of weights are systematically computed in advance to obtain a series of plans. For these plans a Pareto front is generated and the best plan is selected through human interaction (Craft & Bortfeld 2008, Monz *et al* 2008).

Another approach in multi-criteria optimization is goal-programming, which is a form of constrained optimization. In goal-programming, objectives have prioritized goals which are to be met as well as possible (Breedveld *et al* 2007a, Jee *et al* 2007, Wilkens *et al* 2007). Our algorithm is based on the ϵ -constraint method (Haimes *et al* 1971) in which each objective is optimized separately, and then constrained while optimizing the other (lower prioritized) objectives. This algorithm is extended with goals for each priority, which we call the *2-phase ϵ -constraint* or *2pec* method. Since the solution of the *2pec* method has the same properties of the ϵ -constraint method, the term ϵ -constraint method is used when referenced to the final solution of the *2pec* method.

While the approaches are substantially different, both methods (i.e. weighted-sum and ϵ -constraint) are capable of achieving the same (Pareto-)optimal solutions. In this article we will show the relation between these methods and show how to obtain an equivalent weighted-sum problem from a solution obtained by an ϵ -constraint optimization and vice versa.

For a unique relation between the weighted-sum and ϵ -constraint method, the objectives have to be convex. Minimizing a convex function guarantees that there is only a single minimum, and therefore the solution is guaranteed to be optimal.

In the work of Chankong & Haimes (1983b), equivalence between and requirements for different multi-criteria methods are presented. For going from weighted-sum to ϵ -constraint, no convexity is required (although it is up to the optimization algorithm to find a feasible solution). However, in order to find the same solution with the weighted-sum method from an ϵ -constraint problem, the problem needs to be convex. In this article, we assume that all optimization problems are convex.

Convex objectives in radiotherapy are e.g. minimum/maximum dose, mean dose, equivalent uniform dose (EUD) and logarithmic tumour control probability (LTCP) (Alber & Reemtsen 2007). Dose-volume objectives are not convex. Romeijn *et al* (2004) and Hoffmann *et al* (2008) give an overview of transformations to convexify criteria in

radiation therapy.

A series of applications where switching between the methods is beneficial, is in automated treatment planning. The *2pec* method has proven to perform well for automated treatment planning (Breedveld *et al* 2007a). However, the planner may not be satisfied with the result from the automated plan generation (i.e. the *original* plan), and wishes to make (minor) alterations to this plan. By using the weights obtained by the *2pec* optimization, it is possible to generate plans in the Pareto-optimal neighbourhood of the original plan, fulfilling the newly requested treatment constraints. One can for example constrain an objective to a lower value, or introduce new constraints. The planner can then choose to accept or reject the new plan (see section 5.3.4). Another example is for daily treatment planning, where the anatomy of the patient differs slightly from the planning CT scan.

This article is organized as follows. First the weighted-sum, ϵ -constraint and *2pec* approaches are introduced, and the translations from weighted-sum to ϵ -constraint method and vice versa are treated in a theoretical framework. Finally, two examples are given to demonstrate application of this theory.

5.2 Methods

In this section we introduce the weighted-sum and ϵ -constraint method. The objectives are denoted by f_i , $i \in \{1, \dots, n\}$ and the constraints by g_j , $j \in \{1, \dots, m\}$. For readability, the constraints are summarized in a vector $\mathbf{g}(x)$, for which each element should be ≤ 0 .

5.2.1 Weighted-sum optimization

In the weighted-sum method, the objectives are weighted and summed together. Let the weights be denoted by $w = (w_1, \dots, w_n)$. The optimization problem to be solved becomes:

$$\begin{aligned} & \text{minimize} && w_1 f_1(x) + w_2 f_2(x) + \dots + w_n f_n(x) \\ & \text{subject to} && \mathbf{g}(x) \leq \mathbf{0} \end{aligned} \tag{5.1}$$

This optimization problem is solved for varying combinations of weights, building a database of plans (Craft & Bortfeld 2008). With appropriate tools, the user can search through this database and select the best plan (Monz *et al* 2008).

Note that the sum of the weights does not necessarily have to be normalized to 1, but this is usually done because it displays the relative weights more clearly.

5.2.2 ϵ -constraint optimization

The ϵ -constraint method (Haimes *et al* 1971) optimizes one objective at a time while keeping the others constrained. (Similar methods are goal programming and lexicographic ordering, introduced in radiotherapy treatment planning by Wilkens *et al* (2007) and Jee *et al* (2007).) This method optimizes each objective only once.

To allow for more flexibility, this method is extended to a 2-phase ϵ -constraint optimization (*2p ϵ c*), where a *goal* can be assigned to each objective. When it is possible to minimize the dose below a certain threshold (i.e. its goal) for one objective, it is often more desired to minimize the dose for other (lower priority) objectives first than to directly minimize the dose for the higher priority objectives to its fullest extent directly.

For example, if the minimum mean dose for a parotid gland drops below 26 *Gy* (e.g. 15 *Gy*) it can be considered spared. In the next step, the parotid gland is then limited to 26 *Gy* while minimizing the dose to a lower prioritized OAR (e.g. the submandibular gland). Setting the constraint for the parotid gland higher than its minimum (to 26 *Gy* instead of 15 *Gy*), increases the probability of sparing the submandibular gland as well.

This idea was introduced in Breedveld *et al* (2007a) and applied to a specific optimization method. Based on this idea we introduce the 2-phase ϵ -constraint method for general use here.

The objectives and their priorities and goals are given in a prioritized list, which we call a *wish-list*. Each priority contains an objective and a desired goal. So, for n objectives, objective $f_i(x)$ has priority i and goal b_i . Furthermore, the list contains (hard) constraints $g(x)$ which are to be met at all times. See tables 5.1 and 5.3 for practical examples.

In the first iteration of the first phase, the objective having highest priority is optimized:

$$\begin{array}{ll} \text{minimize} & f_1(x) \\ \text{subject to} & \mathbf{g}(x) \leq \mathbf{0} \end{array}$$

Depending on the result x^* , the new bound is chosen according to the following rule:

$$\epsilon_i = \begin{cases} b_i & f_i(x^*)\delta < b_i \\ f_i(x^*)\delta & f_i(x^*)\delta \geq b_i \end{cases}$$

where δ is a slight relaxation to create some space for the subsequent optimizations, usually set to 1.03 (3%). Note that in practice this relaxation is mandatory to avoid the optimization algorithm from stalling due to numerical problems. Despite that a relaxation of $\delta = 1 + \mathcal{O}(10^{-4})$ is often enough to prevent numerical problems, it is still

desirable to use $\delta = 1.03$ to prevent ending up in one of the end-points of the Pareto-curve (see section 5.3.3).

The next optimization optimizes f_2 , keeping f_1 constrained:

$$\begin{aligned} & \text{minimize} && f_2(x) \\ & \text{subject to} && \mathbf{g}(x) \leq \mathbf{0} \\ & && f_1(x) \leq \epsilon_1 \end{aligned}$$

This is repeated for all n objectives.

In the second phase of the multi-criteria optimization all objectives which met their goals are minimized to their fullest, while keeping all others constrained.

So, for each f_i which met its goal b_i solve, in order of priority:

$$\begin{aligned} & \text{minimize} && f_i(x) \\ & \text{subject to} && \mathbf{g}(x) \leq \mathbf{0} \\ & && f_k(x) \leq \epsilon_k, \quad k \in \{1, \dots, n\} \setminus i \end{aligned}$$

and then set $\epsilon_i = f_i(x^*)\delta$.

Note that this second phase resembles the original ϵ -constraint method, and therefore the solution of the *2pec* method has the same properties (i.e. Pareto-optimality) as the ϵ -constraint method.

5.3 Results

In this section, some theory is introduced for the weighted-sum and ϵ -constraint methods, and how to obtain the weights from the ϵ -constraint optimization (sections 5.3.1 and 5.3.2).

We demonstrate the relation between the *2pec* and weighted-sum methods by a simple example in section 5.3.3. In section 5.3.4 a practical situation is demonstrated for automated treatment planning where a plan for modified criteria is easily generated by using the weights from the automated plan.

The optimizations were performed using YARTOS (Yet Another Radiation Therapy Optimization Suite), an in-house developed optimization package for general non-linear optimizations and multi-criteria optimizations. It is based on interior-point optimization methods and tuned specially for radiotherapy optimization problems.

5.3.1 From weighted-sum to ϵ -constraint

The relation for going from the weighted-sum method to the ϵ -constraint method is given by the following theorem (Miettinen 1999):

Theorem 1 Let x^* be the solution of a weighted-sum optimization (5.1). Because the optimization problem is assumed to be convex, x^* is unique. Then x^* is a solution of the ϵ -constraint problem when $\epsilon_k = f_k(x^*)$ for $k \in \{1, \dots, n\} \setminus i$ and for every f_i , $i \in \{1, \dots, n\}$ as the objective function.

A proof can be found in [Miettinen \(1999\)](#).

5.3.2 From ϵ -constraint to weighted-sum

A proof that for an ϵ -constraint optimal problem there is a corresponding weighted-sum plan can be found in [Chankong & Haimes \(1983a\)](#). However the proof, which is a simple application of the generalized Gordon theorem (which is roughly speaking a nonlinear version of the Farkas lemma) ([Mangasarian 1969](#)), does not give us the weights. In their later work ([Chankong & Haimes 1983b](#)), it is mentioned that “the corresponding Kuhn-Tucker multipliers (...) furnish useful information about trade-offs”. In this section it is shown that these multipliers *are* exactly the weights. The trade-off (sensitivity) analysis is treated by [Alber et al \(2002a\)](#).

The last iteration of an ϵ -constraint problem, as described in section 5.2.2, solves the following problem (without loss of generality we can assume that the objective with priority n is the last one optimized on):

$$\begin{aligned} & \text{minimize} && f_n(x) \\ & \text{subject to} && \mathbf{g}(x) \leq \mathbf{0} \\ & && f_i(x) \leq \epsilon_i, \quad i \in \{1, \dots, n-1\} \end{aligned} \tag{5.2}$$

A way to solve a constrained problem is by rewriting the problem as an unconstrained optimization problem, which is called the *Lagrangian* ([Bertsekas 1995](#), [Wright 1997](#)). The Lagrangian for problem (5.2) is:

$$L(x, \nu, \lambda) = f_n(x) + \sum_{i=1}^{n-1} \nu_i (f_i(x) - \epsilon_i) + \sum_{j=1}^m \lambda_j g_j(x)$$

which is to be minimized with respect to x , ν and λ , where ν and λ are nonnegative vectors of *Lagrange multipliers*. A constraint is called *active* if its corresponding Lagrange multiplier is unequal to 0. As a result of the ϵ -constraint optimization all constrained objectives $f_i(x)$, $i \in \{1, \dots, n-1\}$ are active, so $\nu_i > 0$. (In this case, the Lagrange multipliers for the constrained objectives are in fact Kuhn-Tucker multipliers, to relate to the terminology used by [Chankong & Haimes \(1983b\)](#).)

For finding the optimal triplet (x^*, ν^*, λ^*) many methods are available which will not be discussed here. The method used in this article is based on *interior-point* optimization (see e.g. [Wright \(1997\)](#)).

We will now introduce and prove the following theorem:

Theorem 2 *Choosing the weights for the weighted-sum method equal to the Lagrange multipliers for the constrained objectives from the last iteration of the ϵ -constraint optimization results in an identical optimal solution.*

Proof Let $L_\epsilon(x^*, \nu^*, \lambda^*)$ be the Lagrangian for the optimal solution of the final iteration of an ϵ -constraint optimization (5.2):

$$L_\epsilon(x^*, \nu^*, \lambda^*) = f_n(x^*) + \sum_{i=1}^{n-1} \nu_i^* (f_i(x^*) - \epsilon_i) + \sum_{j=1}^m \lambda_j^* g_j(x^*)$$

Suppose we choose the weights for the weighted-sum method (5.1) equal to ν_i^* and $w_n = 1$. Then the Lagrangian for the weighed-sum problem becomes:

$$L_w(x, \lambda) = f_n(x) + \sum_{i=1}^{n-1} \nu_i^* f_i(x) + \sum_{j=1}^m \lambda_j g_j(x)$$

Adding the constant $-\sum_{i=1}^{n-1} \nu_i^* \epsilon_i$ to L_w does not change the optimal solution. Introduce:

$$\hat{L}_w(x, \lambda) = f_n(x) + \sum_{i=1}^{n-1} \nu_i^* (f_i(x) - \epsilon_i) + \sum_{j=1}^m \lambda_j g_j(x)$$

and let $\hat{L}_w(\bar{x}, \bar{\lambda})$ be the optimal solution for \hat{L}_w .

The constraints $g(x)$ can be assumed to be linear independent. In this case the set of Lagrange multipliers λ is unique (Forsgren *et al* 2002). Therefore $\bar{\lambda} \equiv \lambda^*$. Because the Lagrangian \hat{L}_w is convex in x (λ and ν are fixed), we have to conclude that $\bar{x} = x^*$. \square

5.3.3 Simple example

The relation between the weighted-sum method and the ϵ -constraint method is illustrated by a simplified head-and-neck case, where sparing of the left and right parotid glands are the only objectives, and only the PTV is subjected to minimum and maximum dose constraints (95% and 107% of the prescribed dose of 46 Gy respectively). The wish-list is given in table 5.1. The treatment setup is 5 IMRT beams.

Using the weighted-sum method (5.1), a Pareto-frontier for the parotid glands can be generated by setting $w_1 = \alpha$ and $w_2 = 1 - \alpha$ for $\alpha \in [0, 1]$ (figure 5.1). The figure shows that the extremes do not give a sane trade-off: when the dose in the left parotid gland is minimized to 29.2 Gy, the dose in the right parotid gland is to 37.1 Gy. At the cost of a slight deterioration from 29.2 to 29.4 Gy (0.7%) for the left parotid gland, the right parotid gland improves significantly from 37.1 to 23.9 Gy. This is why it is reasonable to

Table 5.1: Constraints and objectives for simplified head-and-neck case.

Constraints			
Nr	Volume	Type	Limit
1	PTV	maximum	49.22 Gy
2	PTV	minimum	43.7 Gy
Objectives			
Priority	Volume	Type	Goal
1	Parotid (R)	minimize mean	26 Gy
2	Parotid (L)	minimize mean	26 Gy

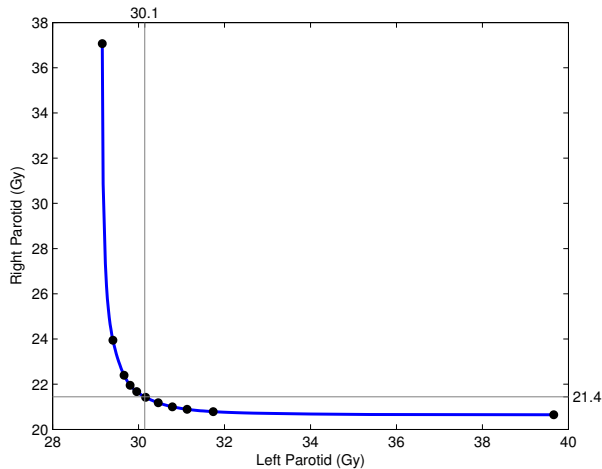


Figure 5.1: Pareto frontier. The dots are the different settings for α , starting with $\alpha = 0$ at the left side of the curve. The intersection denotes the solution of the ϵ -constraint method, coinciding with $\alpha \approx 0.5$.

allow a relaxation larger than numerically required. Experience learned that a relaxation of 3% results in a good automatic trade-off.

Using the $2pec$ method, the dose in the right parotid gland is minimized up to 26 Gy prior to minimizing the dose in the left parotid gland. Minimizing the dose in the right parotid gland again (now without a lower limit) yields the results listed in table 5.2. Comparing the result to the Pareto curve in figure 5.1, the resulted weights from the ϵ -constraint optimization coincide with the choice of $\alpha \approx 0.5$ on the Pareto curve.

5.3.4 Oropharyngeal cancer case

To reduce treatment planning time, plans can be generated automatically using a wish-list (Breedveld *et al* 2007a). However, it is possible that the planner is not satisfied with the result, and wants to reduce the dose to a structure. By using the weights from this final result, a new plan can be generated in only 1 optimization (in contrast to the $2pec$ method, which takes several optimizations), where one or more objectives have become

Table 5.2: Results for the ϵ -constraint optimization (table 5.1).

Volume	Result	Obtained weights
PTV maximum	49.22 Gy	—
PTV minimum	43.7 Gy	—
Parotid (R)	21.4 Gy	0.49
Parotid (L)	30.1 Gy	0.51

Table 5.3: Constraints and objectives for the oropharyngeal cancer case.

Constraints				
Nr	Volume	Type	Limit	
1	PTV Boost	maximum	53.5 Gy	
2	PTV	maximum	53.5 Gy	
3	Nerves†	maximum	55 Gy	
4	Unspecified Tissue	maximum	53.5 Gy	
Objectives				
Priority	Volume	Type	Goal	Parameters
1	PTV Boost	minimize LTCP	1	$\alpha = 0.75$, Sufficient = 0.5
2	PTV	minimize LTCP	1	$\alpha = 0.75$, Sufficient = 0.5
3	Eye (L)	minimize EUD	15	$a = 15$
4	Eye (R)	minimize EUD	15	$a = 15$
5	Parotid (L)	minimize mean	26	
6	Parotid (R)	minimize mean	26	

† Brainstem, Cord, Sella, Optic Chiasm, Optical Nerves

constraints.

The result from the *2pec* method is Pareto-optimal. By constraining an objective and weighting the remaining objectives, a single optimization is done with the weighted-sum method. This new solution, which is also a Pareto-optimal, lies in the neighbourhood of the first plan.

We use a oropharyngeal cancer case to demonstrate this idea. The patient is diagnosed with oropharyngeal cancer with extensions to the nasal cavity. The boost PTV has a prescribed dose of 50 Gy and the elective neck nodes 37.5 Gy. Both are implemented as LTCP objectives with cell sensitivity $\alpha = 0.75$. The other objectives are the left and right eyes (EUD with parameter $a = 15$) and the left and right parotid glands (mean dose). The wish-list is given in table 5.3. An LTCP value of 0.5 is considered sufficient for the PTVs, because low LTCP values result in overdosing the PTV. In other words: even if the LTCP value can be lower, 0.5 is set as a lower limit. The treatment setup is 8 IMRT beams.

Using the wish-list given in table 5.3, the *2pec* method requires 10 iterations (optimizations) to generate a plan (referred to as the *original* plan). A detailed list of the

Table 5.4: Step-by-step ϵ -constraint optimization for the oropharyngeal cancer patient.

Iteration	Volume	Result	New constraint
1st phase	1 PTV Boost	0.10	1.00
	2 PTV	0.01	1.00
	3 Eye (L)	20.11	20.71
	4 Eye (R)	18.12	18.66
	5 Parotid (L)	19.18	26.00
	6 Parotid (R)	19.77	26.00
2nd phase	7 PTV Boost	0.97	1.00
	8 PTV	0.01	0.50
	9 Parotid (L)	20.95	21.58
	10 Parotid (R)	24.33	24.33

Table 5.5: Numerical results for the ϵ -constraint optimization. The weights are extracted from the Lagrangian using the method presented in section 5.3.2.

Priority	Volume	ϵ -con	Weight
1	PTV Boost	1.00	0.6528
2	PTV	0.50	0.0125
3	Eye (L)	20.71	0.2734
4	Eye (R)	18.66	0.0538
5	Parotid (L)	21.58	0.0050
6	Parotid (R)	24.33	0.0026

iterations is given in table 5.4, the results are presented in table 5.5. The weights are found by applying the theorem from section 5.3.2.

Now suppose we are in the hypothetical situation where an EUD of 15 Gy to the eye would spare the eye completely. The planner is not satisfied with the result of 18.66 Gy for the right eye, since this is close enough to 15 Gy , which would spare the eye completely. By using the weights from the first (original) *2pec* optimization (table 5.5), the effect of limiting the EUD to the right eye is easily explored when solving the weighted-sum problem (5.3) (where i indexes over the priorities as given in table 5.3). The results are presented in figures 5.2 and 5.3.

$$\begin{aligned}
 & \text{minimize} && \sum_{i=\{1,2,3,5,6\}} w_i f_i(x) \\
 & \text{subject to} && f_4(x) \leq 15 \\
 & && \mathbf{g}(x) \leq \mathbf{0}
 \end{aligned} \tag{5.3}$$

Another example is to introduce a new constraint to the problem. The planner may find that the maximum-dose to the left eye is too high (27.63 Gy in the original plan) and

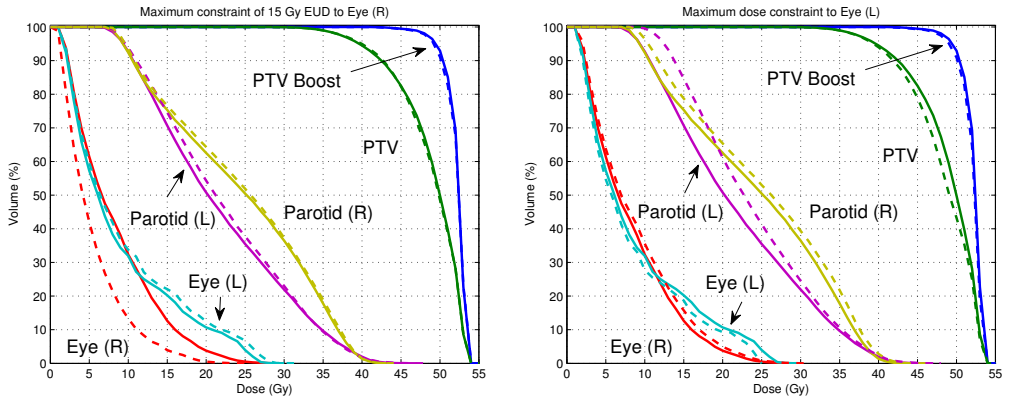


Figure 5.2: Dose-volume histograms for the case where the EUD to the right eye is limited to 15 Gy (left) and where a maximum-dose constraint of 25 Gy is introduced for the left eye (right). The solid lines represent the original $2p\epsilon c$ result and the dashed lines the modified plan.

wants to research the effect of limiting it to 25 Gy. Again, the objectives are weighted and summed, and a new constraint is added to the problem. The results are also shown in figures 5.2 and 5.3.

Both results show an improvement for the objectives that were constrained and a deterioration for the other objectives. However, the DVHs between the original and adapted plans are not structurally different, in the sense that they still lie close to each other. This suggests that the adapted plans are indeed in the neighbourhood of the original plan.

5.4 Discussion and conclusions

In this article, we established the relationship between the weighted-sum and ϵ -constraint method for multi-criteria optimization and how to switch from one to the other. This can be of practical use after an automated multi-criteria optimization where fine-tuning on some objectives is desired, or where a re-planning is required for a slightly different situation as e.g. new or revised bounds for objectives or constraints, or a re-planning on a different CT.

The 2-phase ϵ -constraint multi-criteria optimization method presented in this article can be extended in several ways. One can for example set a maximum constraint on the objectives, or remove an objective from the optimization when it cannot be minimized below a certain threshold (e.g. when a parotid or submandibular gland receives a dose > 40 Gy it is undesired to constrain this organ for subsequent optimizations, since it will only be limiting while the volume cannot be spared anyhow). Another possibility is to

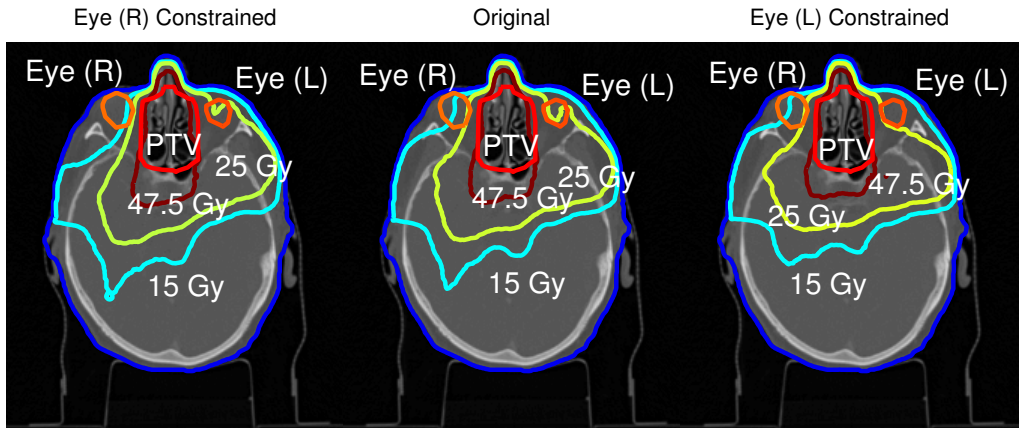


Figure 5.3: Isodose lines for the plan with the EUD to the right eye constrained is to 15 Gy (left), the original plan (middle) and the plan where the maximum-dose to the left eye is constrained to 25 Gy (right). In the left figure, the 15 Gy isodose line lies close to the PTV. The right figure shows that the 25 Gy isodose line has completely moved out of the left eye.

mix the weighted-sum and ϵ -constraint method (Chankong & Haimes 1983b, Miettinen 1999).

The theorem to extract the weights from the ϵ -constraint method applies generally to any optimization problem with constraints. Important is that the constraints of interest are *active* and the solution is Pareto optimal. The ϵ -constraint method assures both qualifications.

However, it can be questioned what influence the relaxation δ has on these qualifications (section 5.2.2): by relaxing a constraint, the Pareto optimality of the constraint-set might get lost. This is only a problem if constraints are completely independent. In radiotherapy treatment planning practice, all constraints (criteria) influence each other. When ϵ_1 is chosen and relaxed, optimizing on f_2 will make the constraint on f_1 active, if the relaxation was not too large. Despite the theoretical probability that a constraint will not be active, we have never seen this in practice.

Chapter 6

iCycle: integrated, multi-criterial beam angle and profile optimization for generation of coplanar and non-coplanar IMRT plans

Sebastiaan Breedveld, Pascal Storchi, Peter Voet and Ben Heijmen

Department of Radiation Oncology, Erasmus MC Rotterdam, Groene Hilledijk 301, 3075
EA Rotterdam, The Netherlands

E-mail: s.breedveld@erasmusmc.nl

Published 31 January 2012 in *Medical Physics*, volume **39**, pages 951-963

[doi:10.1118/1.3676689](https://doi.org/10.1118/1.3676689)

Abstract

Purpose: To introduce iCycle, a novel algorithm for integrated, multi-criterial optimization of beam angles and IMRT profiles.

Methods: A multi-criterial plan optimization with iCycle is based on a prescription called *wish-list*, containing hard constraints and objectives with ascribed priorities. Priorities are ordinal parameters used for relative importance ranking of the objectives. The higher an objective priority is, the higher the probability that the corresponding objective will be met. Beam directions are selected from an input set of candidate directions. Input sets can be restricted, e.g. to allow only generation of coplanar plans, or to avoid collisions between patient/couch and the gantry in a non-coplanar setup. Obtaining clinically feasible calculation times was an important design criterion for development of iCycle. This could be realized by sequentially adding beams to the treatment plan in an iterative procedure. Each iteration loop starts with selection of the optimal direction to be added. Then, a Pareto-optimal IMRT plan is generated for the (fixed) beam setup that includes all so far selected directions, using a previously published algorithm for multi-criterial optimization of fluence profiles for a fixed beam arrangement (Breedveld *et al* 2009a). To select the next direction, each not yet selected candidate direction is temporarily added to the plan and an optimization problem, derived from the Lagrangian obtained from the just performed optimization for establishing the Pareto-optimal plan, is solved. For each patient, a single 1-beam, 2-beam, 3-beam, etc. Pareto-optimal plan is generated until addition of beams does no longer result in significant plan quality improvement. Plan generation with iCycle is fully automated.

Results: Performance and characteristics of iCycle are demonstrated by generating plans for a maxillary sinus case, a cervical cancer patient, and a liver patient treated with SBRT. Plans generated with beam angle optimization did better meet the clinical goals than equi-angular or manually selected configurations. For the maxillary sinus and liver cases, significant improvements for non-coplanar setups were seen. The cervix case showed that also in IMRT with coplanar setups, beam angle optimization with iCycle may improve plan quality. Computation times for coplanar plans were around 1-2 hours and for non-coplanar plans 4-7 hours, depending on the number of beams and the complexity of the site.

Conclusion: Integrated beam angle and profile optimization with iCycle may result in significant improvements in treatment plan quality. Due to automation, the plan generation workload is minimal. Clinical application has started.

6.1 Introduction

In radiation therapy treatment planning, the quality of a plan depends on the choice of the beam directions, and their number. In current practice, the beam angles are either selected in a trial-and-error procedure by a dosimetrist or based on a template. The former may be time-consuming with a result dependent on the experience of the planner. Beam directions based on a template may be sub-optimal for individual patients.

Various methods for automated beam angle selection have been proposed, ranging from an aid to select suitable beams (e.g. [Das et al 2003](#), [Potrebko et al 2008](#), [Pugachev & Xing 2001](#)) to integrated beam angle optimization and beam weight/IMRT optimizations, either based on global optimization (e.g. [Aleman et al 2008, 2009](#), [Lee et al 2006](#), [Li et al 2005](#), [Rowbottom et al 1999](#), [Wang et al 2004](#)) or sequential beam selection ([Azizi Sultan & Küfer 2006](#), [Meedt et al 2003](#), [De Pooter et al 2008](#), [Woudstra & Storchi 2000](#)). An analytical approach is given by [Ehrgott et al \(2008\)](#).

In recent years, there has been a vast development in multi-criteria optimization for intensity modulated radiotherapy (IMRT). The advantage of multi-criteria optimization is that the user can select a desired solution from a database of Pareto-optimal plans in an *a posteriori* setting (e.g. [Craft & Bortfeld 2008](#), [Monz et al 2008](#)), or *a priori* define a set of criteria which may not be violated (constraints) or have to be met as well as possible, or better (objectives) ([Breedveld et al 2007a, 2009a](#), [Clark et al 2010](#), [Jee et al 2007](#)). Interactive approaches are also possible ([Azizi Sultan & Küfer 2006](#), [Ruotsalainen et al 2010](#)).

For multi-criterial beam angle optimization, an *a posteriori* method has been proposed by [Schreibmann et al \(2004\)](#) in which the algorithm generates different sets of beam angles and intensity profiles from which the user can select the plan afterward. A full multi-beam space Pareto navigation tool for *a posteriori* plan selection has been developed by [Craft & Monz \(2010\)](#). An interactive *a posteriori* method to the beam angle optimization problem is proposed by [Azizi Sultan & Küfer \(2006\)](#).

In this paper, we introduce a novel *a priori* multi-criteria approach to integrated beam angle and intensity optimization named *iCycle* (IMRT Cycle). As will be discussed in the Discussion section, we have found significant advantages of *iCycle* for generating clinical plans, and introduction in the clinic has been started. Here we report in detail on the applied algorithms and features, and for a variety of clinical cases we show the impact of beam angle optimization on plan quality.

For each patient, plan generation with *iCycle* is steered by a user-defined wish-list ([Breedveld et al 2007a, 2009a](#)), containing constraints and objectives. Objectives are optimized while taking into account ascribed priorities defined in the wish-list. Constraints have to be strictly met. For *iCycle* it is not necessary to specify the desired number of

beams in advance. Beams are sequentially added to the plan and full Pareto-optimal plans for each number of beam directions are given as output. The planner can therefore *a posteriori* make a trade-off between number of beams and plan quality.

The remainder of the paper is organized as follows: section 6.2 describes iCycle and other materials and methods used, section 6.3 demonstrates iCycle's performance using patient cases, in section 6.4 iCycle is discussed, and conclusions are presented in section 6.5.

6.2 Methods

6.2.1 Global description of iCycle

In iCycle, both selection of optimal beam orientations and beam profile optimization are based on a wish-list with prioritized objectives and constraints (section 6.2.2). Beam generation for a patient starts with an empty plan, i.e. no beams selected. Sequentially, optimal beam orientations are selected from a predefined set of candidate input directions and added to the plan. The process of adding new directions may be stopped if further improvements in the patient dose distribution are considered clinically irrelevant or if the number of beams has become impractically large. The input set can be restricted to allow only coplanar beam arrangements or extended for generation of non-coplanar plans. Directions with a risk of collisions between the patient/couch and the gantry have to be excluded from the candidate set (see also section 6.2.5).

Generation of a treatment plan is performed in an iterative procedure. Iteration i starts with selection of the i th orientation to be added to the plan. To this purpose, all not yet selected candidate beam directions (section 6.2.5) are evaluated one-by-one by solving for each of them an IMRT optimization problem for a beam arrangement consisting of the candidate plus the previously selected $i - 1$ directions (section 6.2.4). The orientation with the most favourable scores is selected as the i th orientation. The *2pec* method (section 6.2.3) is then used to generate the final Pareto optimal IMRT plan for the setup with the first i selected orientations. The output of this *2pec* optimization is then used for definition of the IMRT optimization problems to be solved for selection of orientation $i + 1$, and so on. The iterative procedure for plan generation with iCycle is schematically depicted in figure 6.1.

With iCycle, addition of a beam will always result in a higher objective value for the highest priority objective that can still be improved on. There is no need to *a priori* define the (maximum) number of orientations in a plan. If adding beams does no longer result in clinically significant plan improvements, the process of generating more plans with more orientations can be stopped. The user can then select the Pareto optimal plan with the best trade-off between number of beams used and plan quality.

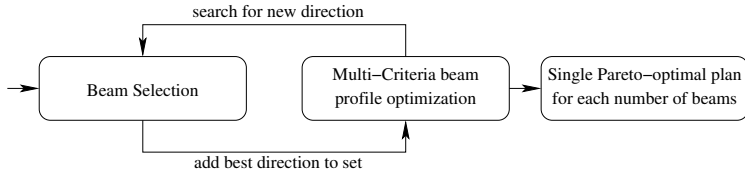


Figure 6.1: Iterative beam angle selection and profile optimization with iCycle. Each iteration (‘cycle’) starts with selection of a beam direction to be added to the plan, followed by a multi-criterial optimization of beam profiles, resulting in a Pareto-optimal plan. The output from the latter optimization is used to define the optimization problem to be solved for selection of the next beam to be added, and so on.

6.2.2 Wish-lists

Wish-lists have been introduced in [Breedveld *et al* \(2007a, 2009a\)](#). They contain user (physician) defined hard constraints and optimization objectives. Each objective has an ascribed priority. The higher the priority, the more importance is given to minimization of the objective, within imposed constraints. An example of a wish-list for a maxillary sinus case is given in table 6.1. For this patient, two PTVs were defined, to be treated with a simultaneous integrated boost (SIB) technique. The high dose PTV overlaps with the optical nerves, and the aim was to irradiate as much of the PTV as possible, without harming the optical nerves (enforced by a constraint, see below). Based on the tumour shape and its position at the patient’s left, it was upfront decided to fully focus on limiting dose delivery to right-sided organs at risk. The applied wish-list in table 6.1 contains 8 constraints and 7 objectives. All constraints are maximum-dose constraints. ‘PTV1 Shell’ and ‘PTV2 Shell’ are surfaces (ring with no width) positioned at 10 *mm* distance from PTV1 and PTV2, respectively, constructed by computerized volume expansions. The imposed maximum-dose constraints avoid high doses far from the PTVs. Objectives with priorities 1 and 2 aim at dose coverage of PTV1 and PTV2, respectively. Priorities 3-5 aim at sparing of right-sided structures.

Tables 6.3 and 6.5 show multi-level wish-lists for the studied cervix and liver cases, respectively. With a multi-level wish-list, the optimizer gradually reduces dose delivery in a group of OARs (i.e. in levels), preventing that large, initial reductions for some will prevent significant reductions for the other. In the first level, all OAR objectives have a high priority but a relatively low demand on reducing the doses (high goal values, tables 6.3 and 6.5). In lower levels, the priorities are lower but the goal values are lower as well. Defining multiple levels also allows using a wish-list as a template for a site. As the location and size of the tumour and organs-at-risk differ significantly between patients within a certain tumour site, large variations in possibilities of OAR sparing may exist.

Table 6.1: Wish-list for a maxillary sinus case.

Constraints					
	Volume	Type	Limit		
	PTV1	maximum	55 Gy	(=107% of prescribed dose PTV1)	
	PTV2	maximum	70 Gy	(=107% of prescribed dose PTV2)	
	PTV1 Shell	maximum	43 Gy	(=85% of prescribed dose PTV1)	
	PTV2 Shell	maximum	56 Gy	(=85% of prescribed dose PTV2)	
	Myelum	maximum	50 Gy		
	Nerves*	maximum	55 Gy		
	Eyes (L+R)	maximum	60 Gy		
	Unspecified Tissue	maximum	70 Gy		
Objectives					
Priority	Volume	Type	Goal	Sufficient	Parameters
1	PTV1	minimize LTCP	1	0.5	$D^p = 51 \text{ Gy}, \alpha = 0.75$
2	PTV2	minimize LTCP	1	0.5	$D^p = 65.4 \text{ Gy}, \alpha = 0.75$
3	Eye (R)	minimize gEUD	15 Gy		$a = 15$
4	Parotid (R)	minimize mean	26 Gy		
5	Submandibular Gland (R)	minimize mean	39 Gy		
6	Larynx	minimize mean	35 Gy		
7	Unspecified Tissue	minimize mean	–		

* Brainstem, Sella, Optic Chiasm, Optical Nerves

By including multiple levels, the same wish-list can be used for all patients.

In *iCycle*, target dose is generally optimized by minimizing LTCP (Logarithmic Tumour Control Probability (Alber & Reemtsen 2007)),

$$\text{LTCP} = \frac{1}{m} \sum_{j=1}^m e^{-\alpha(d_j - D^p)} \quad (6.1)$$

where m is the number of voxels in the target structure, D^p the prescribed dose, d_j the dose in voxel j and α the cell sensitivity parameter (see table 6.1). The LTCP has an exponential penalty for doses d_j lower than D^p , for doses higher than the prescribed dose the value slowly approaches 0. For a homogeneous dose equal do D^p , the LTCP equals 1.

A higher α results in less voxels with a low dose, and thus a higher percentage of the PTV receiving 95% of the prescribed dose (PTV coverage). In our practice, for clinically acceptable plans the PTV coverage is often $\geq 98.5\%$. The selected value for α is not very critical. For example, for a group of 20 head-and-neck cancer patients with a high priority for saving salivary glands, $\alpha = 0.5$ resulted in a minimum PTV coverage of 96%, while for $\alpha = 0.8$ the minimum coverage was 98.5% (Voet *et al* 2012). As visible in table 6.1, objectives may or may not have a ‘goal’, and LTCP objectives also have an ascribed ‘Sufficient’ value. Use of the ‘Goal’ and ‘Sufficient’ values for objectives in the optimization routine is explained in section 6.2.3.

6.2.3 Brief overview of the *2pec* optimization method

The *2pec* method for multi-criterial optimization of beam intensity profiles is described in detail in [Breedveld *et al* \(2009a\)](#). For a selected beam arrangement, the method generates a single Pareto optimal IMRT plan in an automated way, guided by a user-defined wish-list (section 6.2.2 and table 6.1). The generated plan strictly meets all imposed constraints defined in the list. Objectives are optimized while taking into account their ascribed priorities. The algorithm consists of two phases. In the first phase, objectives are one after the other minimized within constraints, starting with the highest prioritized objective. After each objective minimization, and based on its result, a constraint for the just minimized objective is defined, to be used as an extra constraint in the following minimizations of lower prioritized objectives. The added constraints guarantee that minimization of lower priority objectives will not jeopardize attained objective values for the higher priority objectives.

As a consequence, the lower the priority of an objective, the more constraints are used during its minimization. The result of the first phase is a plan in which each objective with a defined goal (see table 6.1 for examples) has an attained value that is equal to its goal (even if further minimization would in principle have been possible), or higher than its goal when further reduction was not allowed for by constraints.

In the second phase, objectives, that could in the first phase have been further minimized than their defined goal, are now sequentially further minimized, again starting with the highest priority objective. Apart from LTCP objectives, in the second phase all objectives are minimized to their full extent. For the LTCP objectives, minimization is stopped at the defined ‘Sufficient’ value (table 6.1), in order to leave room for minimization of lower prioritized objectives, and not to escalate the dose.

6.2.4 Selection of optimal beam direction to add to the plan; definition of IMRT optimization problems to be solved

As described in section 6.2.1 for selection of the next beam orientation i , all not yet selected candidate beam directions are evaluated one-by-one by solving for each of them an IMRT optimization problem for a beam arrangement consisting of the candidate plus the previously selected $i - 1$ directions. In this section, the IMRT optimization problems to be solved are defined.

Basis of the problem definition is the *Lagrangian* in equation (6.2), valid for the optimal solution x^* of the final iteration of the *2pec* beam fluence optimization for the first $i - 1$ beams ([Breedveld *et al* 2009a](#)):

$$L_c(x^*, \nu^*, \lambda^*) = f_n(x^*) + \sum_{k=1}^{n-1} \nu_k^* (f_k(x^*) - \epsilon_k) + \sum_{j=1}^m \lambda_j^* g_j(x^*) \quad (6.2)$$

with, f_k the objective functions and ϵ_k the constraint values for objectives k found by the *2pec* algorithm (section 6.2.3). ν_k^* are the optimal *Lagrange multipliers* belonging to objective functions f_k . The functions g_j are the (hard) constraints defined in the wish-list, with λ_j^* as their respective optimal multipliers.

In Breedveld *et al* (2009a) (Theorem 2), it is proven that a single minimization of a weighted-sum objective function with weights equal to the optimal Lagrange multipliers will generate a solution that is identical to the solution of a full *2pec* multi-criteria optimization with multiple minimizations of different objective functions, as briefly described in section 6.2.2. While the problem with one added beam is different, it is assumed here that these multipliers still give a good representation for selecting beam i .

The optimization problem to be solved for each beam direction is now defined by:

$$\begin{aligned} & \text{minimize} && \sum_{k=1}^n \nu_k^* f_k(x) \\ & \text{subject to} && \mathbf{g}(x) \leq \mathbf{0} \\ & && f_j(x) \leq \hat{\epsilon}_j \quad j \in \mathcal{J} \end{aligned} \tag{6.3}$$

where \mathcal{J} is the set of objectives $\{1, \dots, n\}$ *excluding the PTV objectives*, and their resulting constraint values $\hat{\epsilon}_j$ defined as:

$$\hat{\epsilon}_j = \begin{cases} b_j & 0.9f_j(x^*) < b_j \\ 0.9f_j(x^*) & 0.9f_j(x^*) \geq b_j \end{cases} \tag{6.4}$$

with b_j the goals as stated in the wish-list. For brevity of notation, $\nu_n^* = 1$ is defined. For selection of the first beam, where no previous *2pec* optimization has taken place, the weights ν_k^* are set equal to 1 and the bounds $\hat{\epsilon}_j$ equal the goals for the objectives as specified in the wish-list. The beam direction with the lowest value for the weighted objective functions in (6.3) is added to the set of selected orientations.

To speed up the optimization, optimization problems defined by (6.3) and (6.4) are solved with reduced beamlet resolution and/or scatter radius. If different candidate beam directions have similar objective function values, the optimization is redone with the default (high) resolution, and the best candidate beam direction is selected based on that result.

By using (6.4) to establish OAR constraints for selection of the next beam, the increased degree of freedom is used to lower OAR constraint values that exceed the pre-defined b_j . By excluding constraints resulting from previously obtained PTV objective values, it is avoided that the combination with a stricter OAR constraint would result in an infeasible problem.

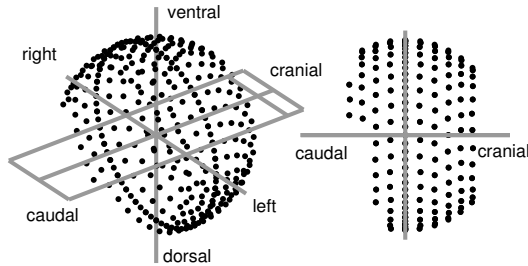


Figure 6.2: Non-coplanar candidate beam directions for the maxillary sinus case discussed in sections 6.2.2 and 6.3.1-6.3.5. The dots represent the focal spots relative to the treatment isocentre and the treatment couch. All positions can be realized without collisions, leading to irregularly distributed candidate beams caudally.

The use of a reduced beamlet resolution or scatter radius for beam angle selection (only) changes the optimization problem. Inclusion of PTV constraints as defined by (6.4) would have further increase the risk for defining an infeasible problem.

6.2.5 Candidate beam directions

In principle there are no limitations to the choice of candidate directions in the optimization problem. In practice, for the axial (coplanar) plane we allow 72 candidate beams with spacing of 5 degrees.

For non-coplanar setups, candidates are added that are homogeneously distributed across the part of a sphere for which there are no collisions between the patient/couch and the gantry. The average angular distance between two neighbouring beams is 10 degrees.

Sometimes the number of non-coplanar beams is restricted by excluding candidates that are unlikely to be selected in order to save computation time. For example, to irradiate head-and-neck patients, beams are limited to a 45 degrees cone to the cranial direction. Figure 6.2 displays the 310 non-coplanar candidate beam directions used for the maxillary sinus case discussed in sections 6.2 and 6.3, separated at an average of 10 degrees.

6.2.6 Target dose prescription for plans with small beam numbers

If in the LTCP formula (6.1) d_i is much smaller than D^p , often occurring in 1 or 2 beam plans, the value gets exponentially large, sometimes leading to numerical problems for the optimizer. Also, from trials for many cases, we learned that selection of the first few beams was often almost fully dominated by the drive to reduce the differences between d_i and D^p , largely neglecting OAR objectives. This resulted in sub-optimal selections of the first beams. To avoid this, a parameter N has been introduced, such that the

prescribed dose D_i^T for $i < N$ beams is reduced according to the following formula:

$$D_i^T = \min\left(\frac{D^p}{\arctan 3.6} \arctan \frac{3.6i}{N}, D^p\right) \quad (6.5)$$

So for $N = 4$, a PTV with 65.4 Gy prescribed dose has 36.9 Gy, 53.5 Gy and 61.2 Gy as prescribed dose in the first 3 iterations. The fourth iteration (4-beam plan) is the first which has the full 65.4 Gy prescribed to the PTV.

This formula is a result from tests with constrained (all OARs are constrained) beam angle optimization: it turned out that the maximum dose which can be delivered to the PTV behaves similar like equation (6.5). In section 6.3.4 the impact of N is illustrated with an example.

6.2.7 Optimization details

The size of the beamlets was set to $10 \times 10 \text{ mm}^2$ with 30 mm scatter radius. In the beam selection phase, only 5 mm scatter radius was used. The pencil-beam dose calculation algorithm used has equivalent path length inhomogeneity corrections (Storchi & Woudstra 1996). The CT resolution was $0.98 \times 0.98 \times 2.5 \text{ mm}^3$. For small structures (like optical nerves), all voxels took part in the optimization. For larger structures, approximately 5000 voxels were selected based on a Hammersley sequence sampling.

iCycle is part of YARTOS, our in-house developed optimization suite. YARTOS is written in Matlab, and contains functions for importing DICOM, visualize dose and dose-volume histograms, compute dose and optimize dose distributions. Our optimizer is based on primal-dual interior-point optimization and capable of solving general non-linear non-convex mathematical problems (Benson & Shanno 2007, Shanno & Vanderbei 2000). It is specially tuned for radiotherapy plan optimization and makes full use of multi-threaded computing.

6.3 Results

In this section, the performance and characteristics of iCycle are demonstrated with plans generated for a maxillary sinus case (for wish-list, see section 6.2.2 and table 6.1), a cervix case, and a liver case.

6.3.1 Maxillary sinus case - comparison of optimized coplanar and non-coplanar plans with equi-angular plans

Figure 6.3 shows dose-volume histograms for 7 and 9 equi-angular beam plans (fixed beam directions, only optimization of beam profiles with the *2pec* algorithm in iCycle, section 6.2.3), and the 7 beam coplanar and non-coplanar plans with both angles and profiles optimized with iCycle. Numerical data for parameters in the wish-list and dose distributions are presented in table 6.2 and figure 6.5, respectively. Table 6.2 shows

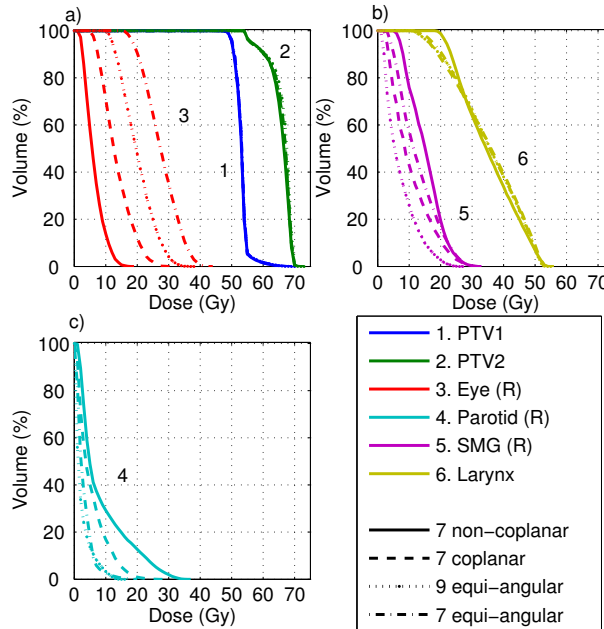


Figure 6.3: Comparison of equi-angular and optimized beam setups for the maxillary sinus case. Most notable is the reduction of dose to the right eye (a) for optimized beam angles, which was the highest priority OAR objective (table 6.1)

that all constraints in the wish-list were indeed strictly met. The coverage of the two PTVs is highly comparable for all setups (figure 6.3a, table 6.2). Full coverage of the boost PTV (PTV2) was impossible to obtain (compare tables 6.1 and 6.2), due to the overlap with the nerves, which have a maximum-dose constraint of 55 *Gy* (table 6.1). The right eye was the highest prioritized organ at risk, and the gEUD is significantly reduced when using 9 equi-angular beams instead of 7 (table 6.2). The lowest right eye gEUD was obtained with the 7 beam non-coplanar approach. Compared to the 7 beam equi-angular plan it reduced from 32.9 *Gy* to 11.8 *Gy*. With the non-coplanar 7 beam approach the right eye gEUD was almost 50% lower than with the coplanar setup with optimized angles. Doses to the right parotid and submandibular glands (SMG) are slightly enlarged for the beam angle optimized plans. However, for both OARs the attained mean dose is far lower than the goal specified in the wish-list (table 6.1). As shown in figure 6.6 (to be discussed below), selection of the 9 beam non-coplanar plan would have reduced the right eye dose somewhat further, accompanied by significantly reduced doses to the right parotid and submandibular glands. Figure 6.4 shows selected angles for optimized coplanar and non-coplanar setups.

Table 6.2: Numerical results for parameters in the wish-list (table 6.1) for the maxillary sinus case for different beam configurations. For all plans, PTV and OAR constraint values are basically equal. The 7 beam non-coplanar plan clearly has the lowest right eye gEUD, the best PTV2 LTCP, at the cost of slightly increased parotid and submandibular gland doses.

Volume	Type	7-equi	9-equi	7 coplanar	7 non-coplanar
PTV1	maximum	55 Gy	55 Gy	55 Gy	55 Gy
PTV2	maximum	70 Gy	70 Gy	70 Gy	70 Gy
PTV1 Shell	maximum	43 Gy	43 Gy	43 Gy	43 Gy
PTV2 Shell	maximum	56 Gy	56 Gy	56 Gy	56 Gy
Myelum	maximum	43.9 Gy	44.7 Gy	43.4 Gy	45.0 Gy
Nerves*	maximum	55 Gy	55 Gy	55 Gy	55 Gy
Eyes (L+R)	maximum	60 Gy	60 Gy	60 Gy	60 Gy
Unspecified Tissue	maximum	70 Gy	70 Gy	68.7 Gy	69.3 Gy
PTV1	LTCP	0.5	0.5	0.5	0.5
PTV2	LTCP	157.2	144.3	152.7	139.1
Eye (R)	gEUD	32.9 Gy	26.6 Gy	20.4 Gy	11.8 Gy
Parotid (R)	mean	2.9 Gy	2.2 Gy	5.4 Gy	8.3 Gy
Submandibular Gland (R)	mean	12.6 Gy	7.0 Gy	10.5 Gy	15.1 Gy
Larynx	mean	35.0 Gy	35.0 Gy	35.0 Gy	35.0 Gy
Unspecified Tissue	mean	5.9 Gy	5.7 Gy	5.8 Gy	5.8 Gy

* Brainstem, Sella, Optic Chiasm, Optical Nerves

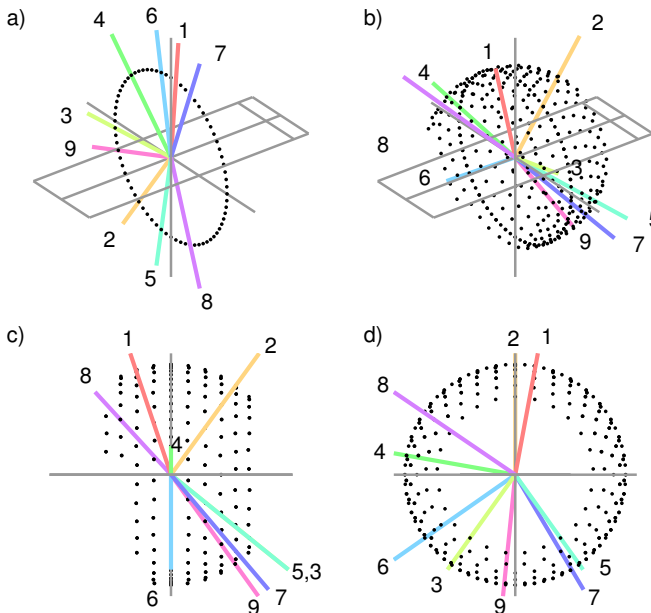


Figure 6.4: Selected beams for coplanar (a) and non-coplanar (b-d) plans of the maxillary sinus case. Numbers indicate the order in which the beams were selected. Panels (c) and (d) show left lateral and caudal views.

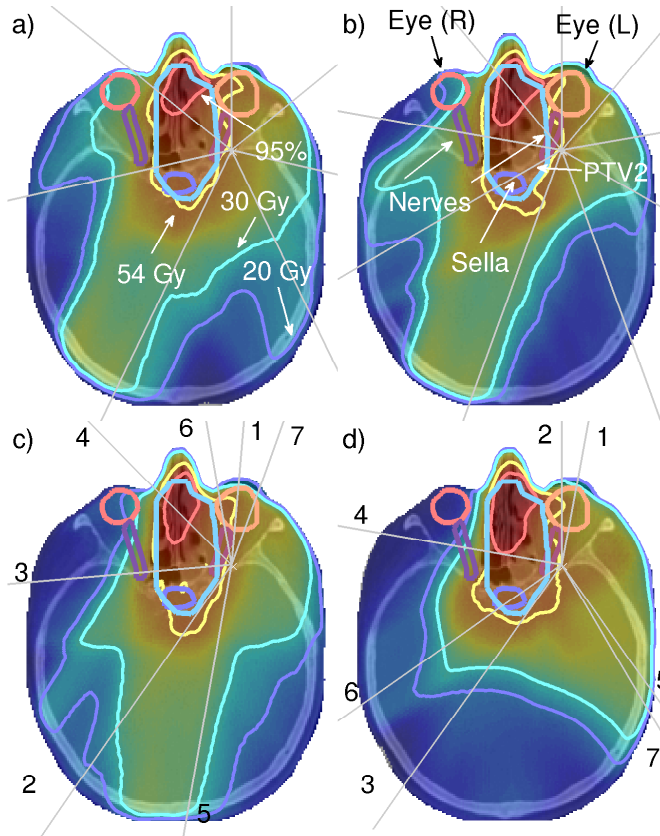


Figure 6.5: Axial CT-slice of the maxillary sinus case with dose distributions and beams for 4 different beam arrangements: 7 and 9 equi-angular (a) and (b), 7 beam coplanar with optimized beam setup (c) and 7 beams optimized non-coplanar setup (d). In (c) and (d) beam numbers are displayed in the order of selection (see figure 6.4). For the non-coplanar setup, projections of the selected beams on the axial plane are displayed.

6.3.2 Maxillary sinus case - convergence with number of beams

The lines in figure 6.6 show for coplanar and non-coplanar optimized beam setups, the obtained objective values for the objectives in the wish-list (table 6.1) as a function of the number of beams in the plan. The coverage of the boost PTV starts to level off at 4-5 beams but will probably increase also with more than the presented maximum of 12 beams. Up to 9 beams there are clear reductions in OAR doses, after that all further reductions are small. Compared to the 9 beam coplanar plan, the 9 beam non-coplanar plan has a right eye EUD that is reduced by 50%.

The diamonds in figure 6.6 allow a comparison between the 9 beam coplanar plan with optimized beam setup with the equi-angular 9 beam plan. Clearly, with beam angle

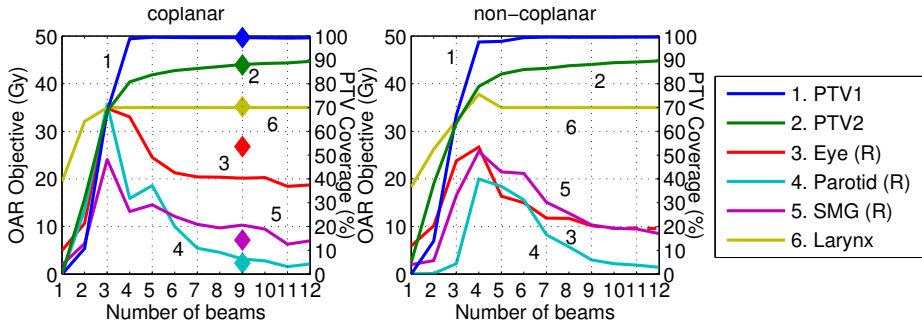


Figure 6.6: Convergence of plan objectives for the maxillary sinus case (table 6.1) for coplanar and non-coplanar setups. For the PTVs, the coverage with 95% of the prescribed dose is given (right axis) instead of the abstract LTCP value. For comparison, the diamonds in the left panel mark the values of the equi-angular 9 beam plan.

optimization the most important OAR for this patient (the right eye) could be better spared at the price of a somewhat higher dose to the submandibular gland, which had a lower priority for sparing.

6.3.3 Maxillary sinus case - alternative problem definitions for selecting the next beam

As explained in sections 6.2.1 and 6.2.4, in *iCycle*, beams are selected sequentially. In section 6.2.4 we describe the optimization problems that are solved for selecting beam orientations. Here, a comparison is made with two alternative definitions for the optimization problems to be solved. Data are provided for 7 beam coplanar plans for the maxillary sinus case, focussing on sparing of the OAR with the highest priority, i.e. the right eye (table 6.1). In the first alternative, all objectives are equally weighted in the score function (figure 6.7, ‘Simple’). The ‘Target Only’ DVH in figure 6.7 displays the result if only the target objectives participate in the objective function (Das *et al* 2003). The sparing of the right eye is superior with the *iCycle* approach (‘Lagrange’) for defining the IMRT optimization problems for selection of beam directions.

6.3.4 Maxillary sinus case - target dose prescription for plans with small beam numbers

As explained in section 6.2.6 for selection of the first N beams, the prescribed tumour dose is reduced according to equation (6.5). Figure 6.8 shows the influence of choosing different values for N for 7 beam coplanar optimized plans. When N is set to 1 there are no reductions of prescribed doses for improving the balance between PTV coverage and OAR protection in selection of the first beams (section 6.2.6). Clearly, between $N = 1, 4$ and 7, $N = 4$ results in the best OAR sparing with equal PTV coverage. For $N = 7$, it

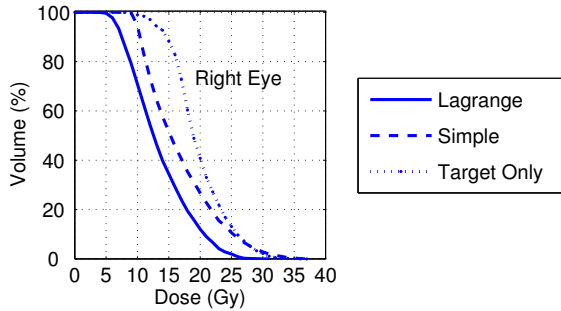


Figure 6.7: Comparing different weighted-sum objective functions for selecting beam orientations for the 7 field coplanar IMRT plan of the maxillary sinus case. DVHs for the right eye (highest OAR sparing priority, table 6.1) are shown. Lagrange: objective function as used in iCycle (section 6.2.4), Simple: equal weights, Target Only: only target objectives in objective function. The dose to the targets (not shown) is comparable.

takes too long before the final problem definition is reached, resulting in a suboptimal plan.

6.3.5 Maxillary sinus case - runtimes

Optimizations were performed on a modern 8-core computer. The runtimes are shown in figure 6.9 for the coplanar and non-coplanar optimizations. The runtime shows a polynomial behaviour with number of beams.

6.3.6 Cervical cancer case - impact of beam angle optimization for coplanar plans

Table 6.3 shows the wish-list for the cervix case, as also used in clinical practice (see section 6.4). This is an example of a *multi-level wish-list*, to gradually minimize the bowel, sigmoid, rectum and bladder mean doses. This approach is used to enforce a balanced reduction in doses to various OARs (see also table 6.5 for the wish-list of the liver case). Figure 6.10 presents DVHs for coplanar iCycle plans generated for the external beam part of the treatment of a cervical cancer patient, with a prescribed dose of 46 Gy. Numerical results and dose distributions are shown in table 6.4 and figure 6.11, respectively. The plan labelled with ‘clinical’ was generated with iCycle using the 7 predefined beam orientations as used for generation of the clinical plan in Monaco TPS (Elekta AB). All three plans have very similar PTV coverage. The plans with beam angles optimized by iCycle perform better for the OAR compared to the clinical plan, especially for the bowel and sigmoid. The 9 beam plan has best OAR sparing.

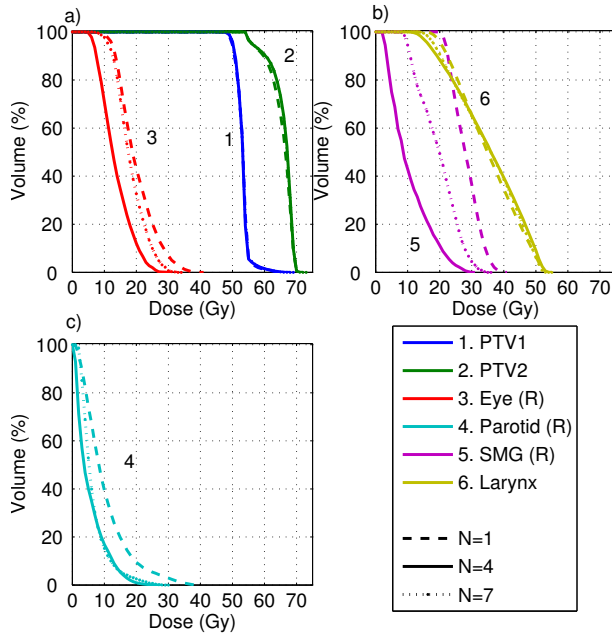


Figure 6.8: Influence of different N -values for optimization of 7 beam coplanar plans (sections 6.2.6 and 6.3.4).

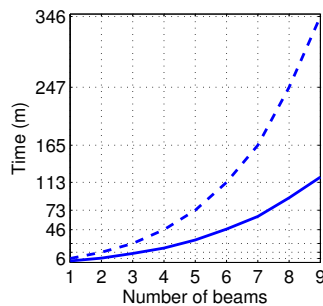


Figure 6.9: Runtimes for optimization coplanar (solid) and non-coplanar (dashed) setups for the maxillary sinus case. The ticks on the Y-axis correspond to the runtimes for the non-coplanar setup.

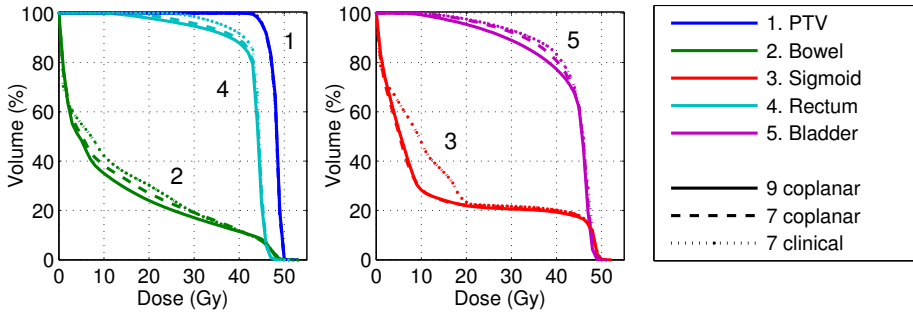


Figure 6.10: DVHs for the clinical beam setup of the cervical cancer case compared to optimized setups.

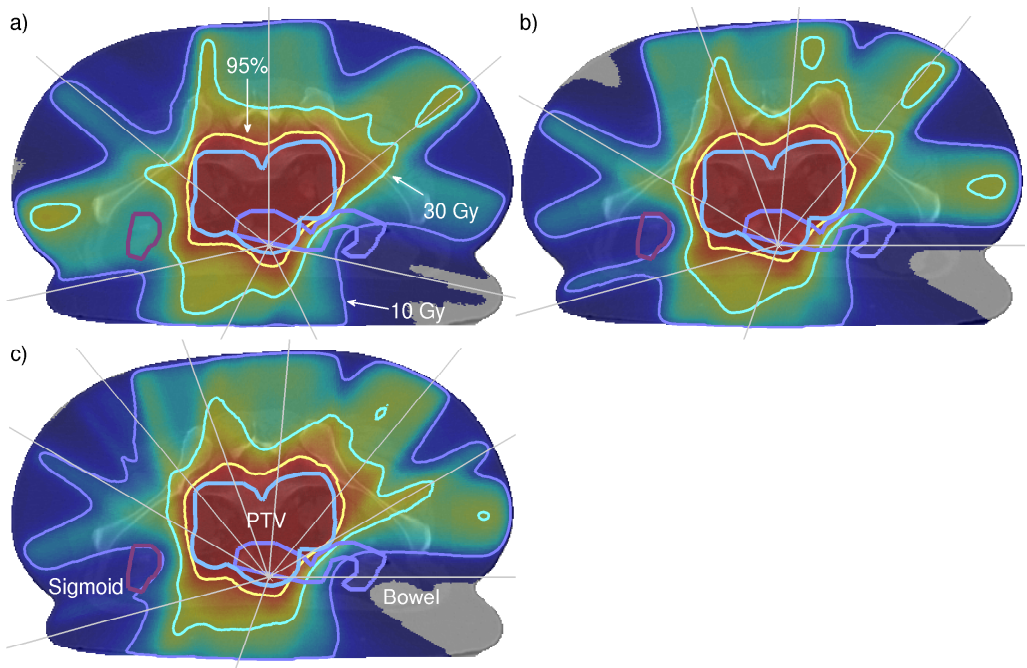


Figure 6.11: Axial CT-slice of the cervical cancer case with dose distributions and beam directions. a) 7 beam clinical beam arrangement, b) 7 beam optimized coplanar plan, c) 9 beam optimized coplanar plan.

Table 6.3: Multi-level wish-list for cervical cancer case. Mean doses to the bowel, sigmoid, rectum and bladder are gradually minimized in 3 steps, i.e. level 1, level 2 and level 3.

Constraints						
	Volume	Type	Limit			
	PTV	maximum	49.22 <i>Gy</i> (=107% of prescribed dose)			
	PTV Shell 1.5 <i>cm</i>	maximum	41.4 <i>Gy</i> (=90% of prescribed dose)			
	PTV Shell 4 <i>cm</i>	maximum	36.8 <i>Gy</i> (=80% of prescribed dose)			
	Unspecified Tissue	maximum	49.22 <i>Gy</i> (=107% of prescribed dose)			
Objectives						
Level	Priority	Volume	Type	Goal	Sufficient	Parameters
	1	PTV	minimize LTCP	1	0.5	$D^p = 46 \text{ Gy}, \alpha = 0.75$
	2	Skin Ring 3 <i>cm</i>	minimize maximum	32.2 <i>Gy</i>		(=70% of prescribed dose)
1	3	Bowel	minimize mean	40 <i>Gy</i>		
	4	Sigmoid	minimize mean	40 <i>Gy</i>		
	5	Rectum	minimize mean	40 <i>Gy</i>		
	6	Bladder	minimize mean	40 <i>Gy</i>		
2	7	Bowel	minimize mean	20 <i>Gy</i>		
	8	Sigmoid	minimize mean	20 <i>Gy</i>		
	9	Rectum	minimize mean	20 <i>Gy</i>		
	10	Bladder	minimize mean	20 <i>Gy</i>		
3	11	Bowel	minimize mean	10 <i>Gy</i>		
	12	Sigmoid	minimize mean	10 <i>Gy</i>		
	13	Rectum	minimize mean	10 <i>Gy</i>		
	14	Bladder	minimize mean	10 <i>Gy</i>		
	15	Unspecified Tissue	minimize mean	—		

Table 6.4: Numerical results for parameters in the wish-list (table 6.3) for the cervical cancer case for different beam configurations. Going from the clinical setup to 7 and 9 beam optimized coplanar setups, mean bowel, sigmoid, rectum and bladder doses gradually decrease. All other parameters values are equal for the three beam arrangements.

Volume	Type	Clinical	7 coplanar	9 coplanar
PTV	maximum	49.22 <i>Gy</i>	49.22 <i>Gy</i>	49.22 <i>Gy</i>
PTV	LTCP	0.5	0.5	0.5
PTV Shell 1.5 <i>cm</i>	maximum	41.4 <i>Gy</i>	41.4 <i>Gy</i>	41.4 <i>Gy</i>
PTV Shell 4 <i>cm</i>	maximum	36.8 <i>Gy</i>	36.8 <i>Gy</i>	36.8 <i>Gy</i>
Skin Ring 3 <i>cm</i>	maximum	32.2 <i>Gy</i>	32.2 <i>Gy</i>	32.2 <i>Gy</i>
Bowel	mean	14.1 <i>Gy</i>	13.7 <i>Gy</i>	12.9 <i>Gy</i>
Sigmoid	mean	16.6 <i>Gy</i>	14.5 <i>Gy</i>	14.3 <i>Gy</i>
Rectum	mean	43.3 <i>Gy</i>	43.0 <i>Gy</i>	42.5 <i>Gy</i>
Bladder	mean	42.9 <i>Gy</i>	42.8 <i>Gy</i>	41.9 <i>Gy</i>
Unspecified Tissue	mean	11.6 <i>Gy</i>	11.9 <i>Gy</i>	11.6 <i>Gy</i>

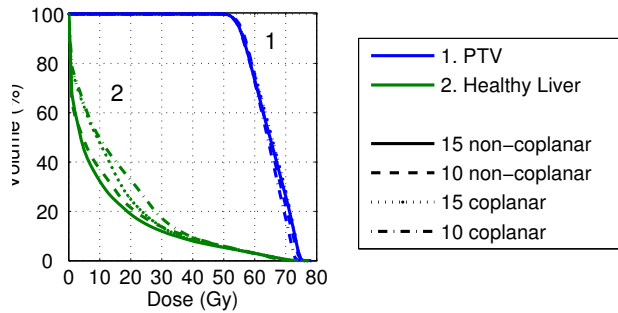


Figure 6.12: DVHs for different beam configurations for the liver case. Significant dose reduction is obtained for the healthy liver by using non-coplanar beams.

6.3.7 Liver case - impact of optimized non-coplanar beam arrangements

Table 6.5 shows the wish-list for SBRT of liver metastases. As in our clinical approach, we aimed for 3 fractions of 25 *Gy* in the isocentre and a minimum target dose of 67%. In the first iterations, the maximum PTV dose is not yet obtained. In those cases, the minimum PTV dose is 67% of the current maximum dose. Additionally, PTV subvolumes are constructed and also prescribed a relative minimum dose to enforce a dose profile in the PTV similar to previously obtained with 3DCRT (De Pooter *et al* 2007). Apart from a dose-volume constraint for the healthy liver (at least 700 *cc* has to receive a dose lower than 15 *Gy*), the highest OAR objective is minimizing the mean dose in the healthy liver tissue as far as possible. Lower priority objectives used are for the oesophagus, duodenum, stomach, heart, cord, pancreas, the kidneys, and unspecified tissues, both in maximum dose and mean dose. For all these organs there were also hard constraints. For part of the OARs, doses are reduced in a 2-level approach, see also section 6.3.6.

As can be seen in figures 6.12 and 6.13 and table 6.6, non-coplanar approaches had clear advantages regarding liver sparing, the most important OAR objectives. Obtained mean healthy liver doses were 16.4 *Gy*, 14.1 *Gy*, 12.1 *Gy* and 11.1 *Gy* for 10 coplanar, 15 coplanar, 10 non-coplanar, and 15 non-coplanar plans, respectively. The corresponding volumes of healthy liver tissue receiving less than 15 *Gy* were 884 *cc*, 963 *cc*, 1058 *cc* and 1122 *cc*. There were also striking differences between the maximum doses in the 700 *cc* healthy liver receiving the lowest doses, i.e. 8.6 *Gy*, 8.0 *Gy*, 3.7 *Gy* and 3.4 *Gy* respectively. Improved liver sparing with the optimized non-coplanar setups resulted for some other OAR in increased doses. The clinical benefit of the lower liver dose is considered more important than the observed rises in doses in the other OARs.

Table 6.5: 2-level wish-list for SBRT of liver metastases.

Constraints		Volume	Type	Limit	
		PTV	maximum	75 <i>Gy</i>	
		PTV 40% <i>vol</i>	minimum	85%	relative to current PTV maximum
		PTV 80% <i>vol</i>	minimum	75%	relative to current PTV maximum
		PTV	minimum	67%	relative to current PTV maximum
		Spinal Cord	maximum	18 <i>Gy</i>	
		Heart	maximum	30 <i>Gy</i>	
		Stomach, Oesophagus, Duodenum, Pancreas, Skin	maximum	21 <i>Gy</i>	
		Healthy Liver	dose-volume	700 <i>cc</i>	should receive < 15 <i>Gy</i>
		Kidney (L)	dose-volume	35%	should receive < 15 <i>Gy</i>
		Kidney (R)	dose-volume	35%	should receive < 15 <i>Gy</i>
Objectives					
Level	Priority	Volume	Type	Goal	
	1	PTV	maximize maximum	75	
	2	Healthy Liver	minimize mean	5 <i>Gy</i>	
1	3	Oesophagus	minimize maximum	21 <i>Gy</i>	
	4	Duodenum	minimize maximum	21 <i>Gy</i>	
	5	Stomach	minimize maximum	21 <i>Gy</i>	
	6	Pancreas	minimize maximum	19 <i>Gy</i>	
	7	Heart	minimize maximum	27 <i>Gy</i>	
	8	Spinal Cord	minimize maximum	17 <i>Gy</i>	
2	9	Oesophagus	minimize mean	5 <i>Gy</i>	
	10	Duodenum	minimize mean	5 <i>Gy</i>	
	11	Stomach	minimize mean	5 <i>Gy</i>	
	12	Pancreas	minimize mean	5 <i>Gy</i>	
	13	Heart	minimize mean	5 <i>Gy</i>	
	14	Spinal Cord	minimize mean	5 <i>Gy</i>	
	15	Kidney (L)	minimize mean	5 <i>Gy</i>	
	16	Kidney (R)	minimize mean	5 <i>Gy</i>	

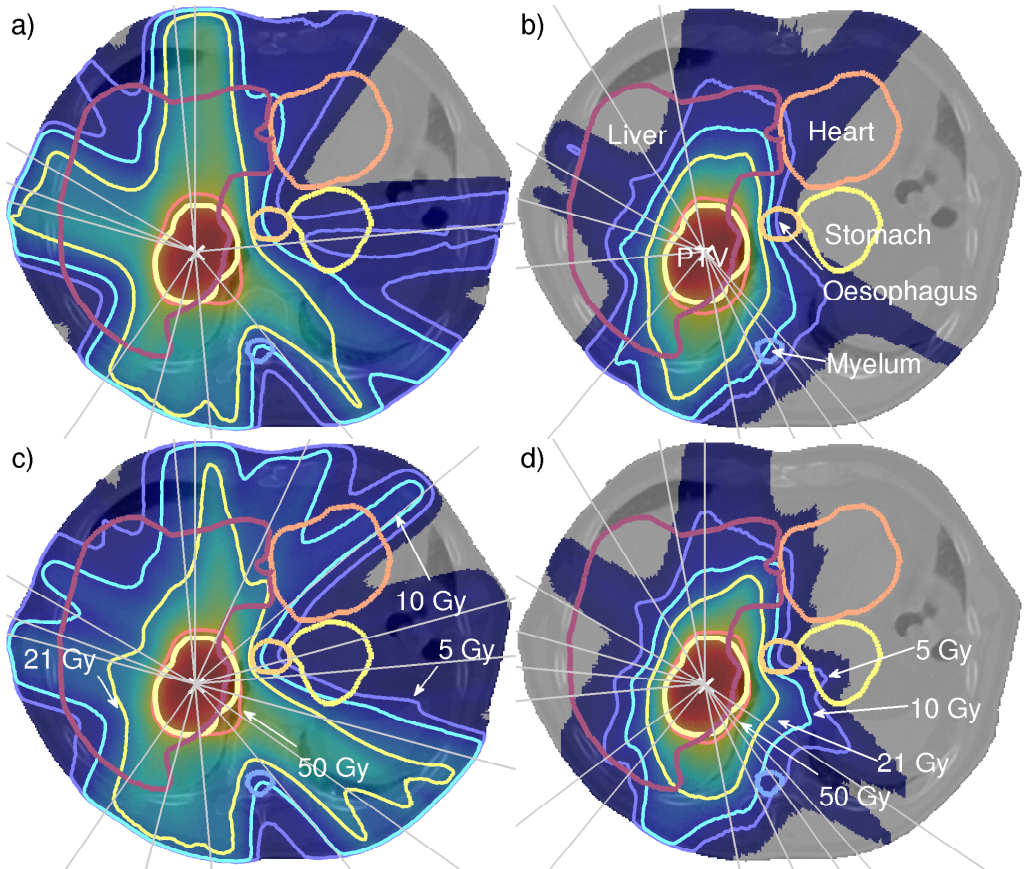


Figure 6.13: Axial CT-slice of the liver case with dose distributions and beams. a) and b): 10 beam optimized coplanar and non-coplanar plans respectively. c) and d) 15 beam optimized coplanar and non-coplanar plans respectively. For the non-coplanar setups, projections of the selected beams on the axial slice are displayed.

Table 6.6: Numerical results for different beam configurations for the liver cancer case. With practically equal PTV dose delivery, the 15 beam non-coplanar plan has the largest healthy liver volume receiving less than 15 *Gy* and the lowest mean dose delivered to healthy liver tissue. The low liver dose outweighs occasionally increased doses to other OARs.

Volume	Type	10 coplanar	15 coplanar	10 non-coplanar	15 non-coplanar
PTV	maximum	73.7 <i>Gy</i>	75.0 <i>Gy</i>	75.0 <i>Gy</i>	75.0 <i>Gy</i>
PTV 40% <i>vol</i>	minimum	62.6 <i>Gy</i>	63.8 <i>Gy</i>	63.8 <i>Gy</i>	63.8 <i>Gy</i>
PTV 80% <i>vol</i>	minimum	55.3 <i>Gy</i>	56.3 <i>Gy</i>	56.3 <i>Gy</i>	56.3 <i>Gy</i>
PTV	minimum	49.4 <i>Gy</i>	50.0 <i>Gy</i>	50.0 <i>Gy</i>	50.0 <i>Gy</i>
Healthy Liver*	dose-volume	884.0 <i>cc</i>	962.8 <i>cc</i>	1058.3 <i>cc</i>	1122.0 <i>cc</i>
Kidney (L)	dose-volume	0.0%	0.0%	0.0%	0.0%
Kidney (R)	dose-volume	4.2%	4.1%	10.0%	12.2%
Healthy Liver	mean	15.6 <i>Gy</i>	14.1 <i>Gy</i>	12.1 <i>Gy</i>	11.1 <i>Gy</i>
Oesophagus	maximum	20.2 <i>Gy</i>	19.0 <i>Gy</i>	18.6 <i>Gy</i>	19.0 <i>Gy</i>
Duodenum	maximum	3.2 <i>Gy</i>	3.1 <i>Gy</i>	14.8 <i>Gy</i>	16.4 <i>Gy</i>
Stomach	maximum	15.1 <i>Gy</i>	14.5 <i>Gy</i>	19.0 <i>Gy</i>	18.9 <i>Gy</i>
Pancreas	maximum	8.7 <i>Gy</i>	8.8 <i>Gy</i>	19.0 <i>Gy</i>	18.9 <i>Gy</i>
Heart	maximum	30.0 <i>Gy</i>	29.7 <i>Gy</i>	30.0 <i>Gy</i>	28.1 <i>Gy</i>
Spinal Cord	maximum	17.0 <i>Gy</i>	17.0 <i>Gy</i>	14.2 <i>Gy</i>	11.7 <i>Gy</i>
Oesophagus	mean	5.7 <i>Gy</i>	5.0 <i>Gy</i>	3.1 <i>Gy</i>	5.0 <i>Gy</i>
Duodenum	mean	0.2 <i>Gy</i>	0.2 <i>Gy</i>	1.7 <i>Gy</i>	1.8 <i>Gy</i>
Stomach	mean	3.1 <i>Gy</i>	3.8 <i>Gy</i>	5.0 <i>Gy</i>	5.0 <i>Gy</i>
Pancreas	mean	0.7 <i>Gy</i>	0.8 <i>Gy</i>	5.0 <i>Gy</i>	5.0 <i>Gy</i>
Heart	mean	2.6 <i>Gy</i>	3.1 <i>Gy</i>	3.3 <i>Gy</i>	5.0 <i>Gy</i>
Spinal Cord	mean	1.1 <i>Gy</i>	0.9 <i>Gy</i>	1.4 <i>Gy</i>	0.8 <i>Gy</i>
Kidney (L)	mean	0.1 <i>Gy</i>	0.1 <i>Gy</i>	3.4 <i>Gy</i>	2.2 <i>Gy</i>
Kidney (R)	mean	1.8 <i>Gy</i>	1.8 <i>Gy</i>	4.7 <i>Gy</i>	4.9 <i>Gy</i>

* part of Liver-CTV receiving less than 15 *Gy*

6.4 Discussion

To our knowledge, the presented *iCycle* application is the first published algorithm for integrated, multi-criterial optimization of beam angles and profiles, based on *a priori* defined plan criteria, allowing fully automated generation of plans. Optimization times are in the order of several hours. As discussed below, clinical validation and introduction has started. Other published algorithms for multi-criterial optimization of beam profiles and orientations are based on interactive selection of orientations ([Azizi Sultan & Küfer 2006](#)) or *a posteriori* selection of the final plan by Pareto navigation ([Craft & Monz 2010](#), [Schreibmann *et al* 2004](#)).

As a consequence of the optimization method, plans with more beams are always superior to plans with fewer beams, in the sense that at least the highest priority objective that can still be improved on, will improve. Sometimes, adding beams does only marginally improve plan quality. In the interest of minimal treatment time and/or pre-treatment dosimetrical QA, it may then be advantageous to choose a plan with a relatively small number of beams. The final choice of the number of beams has to be made by the treatment team, balancing plan quality with more practical features like

workload and treatment time. The method proposed by [Azizi Sultan & Küfer \(2006\)](#) has some similarities to our use of the Lagrangian in the beam selection phase (section 6.2.4). In their approach, a Pareto front is generated for some intermediate i beam plan. The user then interactively selects the desired plan from the front, and the corresponding weights are used to select the next beam for the $i + 1$ beam plan. Our algorithm uses the weights obtained from the $2pec$ optimization, eliminating the need for user-interaction.

As described in [Breedveld *et al* \(2009a\)](#), the $2pec$ algorithm, used by iCycle for (re-)optimizing all beam profiles each time a new orientation is added to the plan, generates Pareto-optimal plans for fixed beam setups. So for an i beam iCycle plan, a change in fluence profiles to improve on one of the objectives will always result in a less favourable output for one or more of the other objectives. It is however not possible to prove that a certain beam arrangement is Pareto-optimal in the beam space (that is, that there are no alternative beam arrangements that improve at least the highest prioritized objective). However, in the studies so far, increasing the degrees of freedom for iCycle plan generation by extension of the input set of candidate directions (e.g. allowing also non-coplanar directions), did always result in better plans for equal numbers of beams in a plan. Moreover, we have noted that it turns out to be very challenging for dosimetrists to generate plans - including selection of the number of beams and their orientations - that approach the quality of corresponding iCycle plans (below).

Plan generation with iCycle is highly intuitive. The *wish-list* is configurable using clinical criteria and priorities, and there is no need for choosing weighting factors. The only non-intuitive parameter is the target number of directions (section 6.2.6) to accommodate selection of the first few orientations in a plan. Generally 4 is a good choice. Future work is in progress to eliminate this non-intuitive parameter.

As mentioned above, with the sequential beam selection process in iCycle, there is no need to specify the number of beams in advance. This has been one of the key design features as the number of beams required for an acceptable plan varies per patient. Also, in some cases, the addition of an extra beam may result in significant additional sparing. For each beam added, the plan improves for (at least) one or more objectives, in order of priority. One can stop the beam selection process if no further improvement is seen, or add more beams if further improvement is expected. In a future version we will implement configurable convergence criteria to automatically stop the process of beam additions.

Generally, we use the LTCP as the tumour objective (formula (6.1) as it penalizes underdosage heavily (exponentially rather than polynomially like EUD), but allows still partial underdosage, in contrast to minimum-dose constraints. However, iCycle is capable of optimizing the target based on EUD or minimum-dose as well. For the OAR, preference is given to EUD, mean and maximum-dose constraints and objectives. Dose-volume

constraints may be used as well, but since they are non-convex, there is the danger of getting trapped in suboptimal plans. Often, OARs have both a hard maximum-dose constraint and an objective in the wish-list. This approach ensures that there is a guaranteed maximum, but also an active mechanism to get as low as possible (as was used for the liver case in section 6.3.7).

Since the beams are selected based on dose contribution rather than spatial preference, it is possible to mix different beam energies and/or isocentres and let the algorithm automatically select the best one. If one overlays a 6 MV beam setup and a 10 MV beam setup, there is a total of 144 candidate coplanar beams if separated at 5 degrees. An other option could be integrated photon-electron planning (Das *et al* 2004).

The Lagrange multipliers used in the objective function (section 6.2.4) fluctuate for the first few beams, but converge later on as more beams are selected. If a beam optimization is done, and the multipliers and achieved objective values of the e.g. 9-beam plan are used for all beam selections (i.e. ν_k^* and $\hat{\epsilon}_j$ in problem (6.3) are identical for all beam selections), suboptimal beam directions are selected (the final 9-beam plan is worse). Thus the final multipliers and objective values are suboptimal for the first beam selections. We also investigated how representative the multipliers and objective values obtained from the $i - 1$ plan are for selection of the i th beam. This was done by selecting beam i , compute the multipliers and objectives, remove this beam, redefine the optimization problems based on the newly obtained multipliers and objectives (section 6.2.4) and select a new one in a new iteration. This did not lead to significantly different final plans, but it doubles the total optimization time.

The purpose of this paper was to present algorithms and features of iCycle, and to show for a variety of clinical cases the impact of optimized beam angles on plan quality. In the meantime, we have also started systematic studies on the impact of plan generation with iCycle for groups of patients, i.e. head-and-neck cancer patients with sparing of salivary glands as highest priority OAR objective (Voet *et al* 2012), patients with liver metastases treated with SBRT, and cervical cancer patients. So far, all these studies point at the importance of optimized beam angles for generating the highest quality IMRT plans. Apart from the improvements in plan quality, we have also found that large reductions in planning workload may be achieved. It turned out that for each of the three mentioned patient groups, excellent plans could be generated with a single wish-list to be used for all patients in the group, without any tweaking of parameters in a trial-and-error process. In other words, iCycle could be used as a push-button system for generating highly attractive plans without any user interference. The automated push-button approach rendered plan quality independent of expertise variations among the dosimetrists working in our department. In all retrospective comparisons with clinically used plans as generated with our Monaco TPS (Elekta AB), the automatically generated

iCycle plans turned out at least equal in quality, but generally superior. iCycle was built as a research application and is not yet ready for direct use in the clinic. As a first step towards clinical benefit, we have recently introduced an indirect approach for iCycle assisted clinical plan generation with Monaco. First, a plan is generated with iCycle. Then, the beam angles found by iCycle and the achieved normal tissue dose-volume parameters are used to automatically configure Monaco for generation of the clinical plan. For cervical- and head-and-neck cancer patients, the generated Monaco plans are very similar in quality compared to the original iCycle plan that was used as input. This procedure is now in routine use for generating IMRT plans for cervical cancer patients. For head-and-neck cancer patients, we have recently started a prospective study to evaluate this procedure. For 50 randomly selected patients, two Monaco plans will be presented to the attending physician, the first generated by dosimetrists using their classical trial-and-error approach, the second generated with the automated procedure.

As shown in figure 6.9, typical runtimes with an 8 core computer for generating 9 beam plans were in the order of two hours for coplanar setups and several hours for non-coplanar plans. The process of selecting the next direction to be added to a plan can be highly parallelized. Currently, we use a 24 core high performance computer, and calculation times for non-coplanar plans have reduced by around 50%. To speed up beam direction selection, we also investigated an approach in which the dose delivered by the first $i-1$ beams was kept fixed, i.e. add new beams to an existing plan. It turned out that in the beam selection phase, the interaction between beams is already very important. Therefore, plan quality was reduced in this approach. Speeding up plan generation is a topic for continued research.

In iCycle we have chosen for an iterative sequential procedure for adding beams to a plan. This choice was made to obtain clinically acceptable calculation times and was inspired by the success of our algorithm for beam angle selection in 3DCRT, applied clinically in liver SBRT (De Pooter *et al* 2007, 2008, Woudstra & Heijmen 2003, Woudstra & Storchi 2000, Woudstra *et al* 2005, 2008). Given availability of the previously developed *2pec* method for generating Pareto optimal plans for fixed beam directions, we could have decided to base selection of the next beam on generated Pareto optimal plans, one for each candidate direction added to the already selected directions. However, with this approach we would still have ended up with unacceptable calculation times. Prior to make a definitive choice for the procedure described in section 6.2.4, many alternatives were explored. One was to enforce a minimal dose improvement in the target, comparable to section 6.2.6, but then for the full number of desired beams. In this case, the prescribed dose for the first beams is relatively low, and does not ‘push’ any constraints, leading to a poor selection of initial beams. Also important is the general shape of the target dose function (6.5): the chosen asymptotic shape works well compared to linear or parabolic

functions. On the other hand, the exact shape is of minor influence. Strategies to limit the candidate beam set based on already selected beams were also investigated. One approach is to remove candidate beams around previously selected beams, effectively locally enlarging the minimum beam separation. One other approach was to replace an old beam if the newly selected beam was within 10 degrees. Neither approach led to significantly better solutions, but the optimization times increased.

At the start of our investigations on multi-criterial beam angle and IMRT profile optimization we studied an approach that started with a plan with many directions (≈ 100), aiming at a gradual reduction of the number of beams while maintaining plan quality. We encountered two major problems: 1) Unfavourable beams were not clearly distinguishable from favourable beams, i.e. many beams have more or less an equal contribution (either measured in monitor units or mean target dose). 2) there was a drastic increase in optimization times due to the larger problem sizes, especially for non-coplanar setups.

6.5 Conclusions

We have developed a novel algorithm for integrated, multi-criterial optimization of beam angles and beam profiles, named *iCycle*. For each patient case, the output is a set of Pareto-optimal IMRT plans, i.e. one 1 beam plan, one 2 beam plan, one 3 beam plan, one 4 beam plan, etc. Plans with more beams have, by design of *iCycle*, higher quality. Plan generation is fully automated. An important design criterion was clinically feasible calculations times. In this paper, we describe the algorithms and features of *iCycle*, and its performance is illustrated with plans for some clinical cases. Based on the often observed superiority of *iCycle* plans compared to plans generated by our dosimetrists with the clinical TPS, and the reduction in workload due to the automation, introduction of *iCycle* in our clinic has started and is expanding fast.

Acknowledgements

The authors wish to thank Iskandar Bin Kassim for his continuous feed-back on *iCycle*.

Chapter 7

Integrated multi-criterial optimization of beam angles and intensity profiles for coplanar and non-coplanar head-and-neck IMRT and implications for VMAT

Peter Voet, Sebastiaan Breedveld, Maarten Dirkx, Peter Levendag and Ben Heijmen

Department of Radiation Oncology, Erasmus MC Rotterdam, Groene Hilledijk 301, 3075 EA Rotterdam, The Netherlands

E-mail: p.voet@erasmusmc.nl

Published 20 July 2012 in *Medical Physics*, volume **39**, pages 4858-4865

[doi:10.1118/1.4736803](https://doi.org/10.1118/1.4736803)

Abstract

Purpose: To quantify improved salivary gland sparing for head-and-neck cancer patients using IMRT plans based on integrated computerized optimization of beam orientations and intensity profiles. To assess if optimized nonzero couch angles also improve VMAT plans.

Methods: Our in-house developed algorithm iCycle was used for automated generation of multi-criterial optimized plans with optimized beam orientations and intensity profiles, and plans with optimized profiles for preselected beam arrangements. For 20 patients, five IMRT plans, based on one ‘wish-list’, were compared: i), ii) 7- and 9-beam equi-angular coplanar plans (iCycle_{7equi}, iCycle_{9equi}), iii), iv) 9-beam plans with optimized coplanar and non-coplanar beam orientations (iCycle_{copl}, iCycle_{noncopl}) and v) a 9-beam coplanar plan with optimized gantry angles and one optimized couch rotation (iCycle_{couch}). VMAT plans without and with this optimized couch rotation were evaluated.

Results: iCycle_{noncopl} resulted in the best salivary gland sparing, but iCycle_{couch} yielded similar results for 18 patients. For iCycle_{7equi}, submandibular gland NTCP values were on average 5% higher. iCycle_{9equi} performed better than iCycle_{7equi}. iCycle_{copl} showed further improvement. Application of the optimized couch angle from iCycle_{couch} also improved NTCP values in VMAT plans.

Conclusions: iCycle allows objective comparison of competing planning strategies. Integrated optimization of beam profiles and angles can significantly improve normal tissue sparing, yielding optimal results for iCycle_{noncopl}.

7.1 Introduction

Intensity-modulated radiotherapy (IMRT) with computer-optimized beam profiles has become standard care for curative treatments of head-and-neck cancer patients. Until now, it has been common practice that a dosimetrist selects the applied number of beams and their orientations in a trial-and-error process. This is not straightforward, especially for complex treatment sites involving many organs at risk (OARs). The quality of the final plan may thus depend on the skills and experience of the planner. Alternatively, a template solution is often used per target site to derive clinical IMRT plans.

For head-and-neck cancer patients, published data on the impact of (computer) optimized and patient-individualized beam arrangements on the quality of treatment plans are limited. In most comparative studies for head-and-neck cancer IMRT very few patients were included and equi-spaced coplanar beam arrangements were used as reference. Meedt *et al* (2003) reported on coplanar beam angle-optimization (BAO) for one laryngeal cancer patient. BAO plans with six or seven beams were compared to a manually defined 9-field plan and a plan with 15 equi-angular beams. Target coverage was improved for both BAO plans, and mean doses in OARs were reduced. Djajaputra *et al* (2003) used an extensive search from different sets of beams to derive an optimal beam angle configuration. For one head-and-neck cancer patient they showed that the use of seven or nine non-coplanar beams with optimized angles improved the plan quality over that of nine equi-angular coplanar beams. Wang *et al* (2005) investigated the effectiveness of non-coplanar BAO in ten paranasal sinus carcinoma patients. Five beams with optimized beam angles generally performed better than plans with nine equi-angular coplanar beams. Nutting *et al* (2001) determined the added value of non-coplanar BAO plans over coplanar BAO plans for 6 parotid gland carcinoma patients. Each plan consisted of 3 or 4 fields. For the non-coplanar plans, the inhomogeneity in the PTV was greater, and a higher normal brain volume received a dose of at least 54 Gy. They reported no significant advantage for non-coplanar BAO. A limitation of their study was the small number of beams used; most studies in the literature suggest that at least 7 beams are required to achieve an optimal IMRT plan.

In previous publications on BAO our group mainly investigated in-house developed algorithms for beam angle, weight and shape optimization in 3DCRT, with a special focus on liver SBRT. For IMRT, only a simple segmented approach was investigated (Woudstra & Storchi 2000), or beam angle and beam profile optimization were performed consecutively (De Pooter *et al* 2008). The latter approach started with selection of optimal beam angles for 3DCRT, using an in-house BAO algorithm. Intensity profiles for these angles were then optimized with a commercial treatment planning system (TPS). It was demonstrated that with a non-coplanar beam arrangement OARs could be better

spared than with coplanar beams only. BAO is now clinically applied for 3DCRT plan generation in liver SBRT (De Pooter *et al* 2006). Recently, we developed a multi-criterial plan optimization algorithm for integrated beam angle and beam intensity optimization, called iCycle (Breedveld *et al* 2007a, 2009a, 2012). Outputs of iCycle are Pareto-optimal IMRT plans with optimized beam setups. With Pareto-optimal we mean that none of the objectives in the applied ‘wish-list’ (see materials and methods section) can be improved any further without deteriorating one or more constraints or higher prioritized objectives. For preselected fixed beam arrangements, iCycle can also be used to optimize beam profiles only. In this study, iCycle was used to systematically compare IMRT plans for various beam angle selection strategies in 20 randomly selected head-and-neck cancer patients. Each plan aimed at maximum salivary gland sparing while obtaining the prescribed high tumour coverage. Due to the close nearness to the PTV of multiple OARS, we expected that the use of non-coplanar beam arrangements could be beneficial, like for liver SBRT patients (De Pooter *et al* 2008). Variations in the procedure for beam angle selection resulted in 7- and 9-beam equi-angular coplanar plans, coplanar plans with optimized gantry angles, fully non-coplanar plans with optimized couch and gantry angles, and coplanar plans with optimized gantry angles for various nonzero couch angles. For two patients we used a commercial TPS to compare an optimized volumetric modulated arc therapy (VMAT) plan for the regular 0° couch angle with a similar plan generated for the couch angle corresponding to the 9-beam coplanar plan generated with iCycle showing the lowest mean NTCP in the salivary glands.

7.2 Methods and materials

7.2.1 Study patients and clinical treatment plans

Twenty recently treated head-and-neck cancer patients with various tumour sites were randomly selected from our clinical database (table 7.1). For treatment, IMRT plans were made using Monaco (version 2.04, Elekta). The intention was to draw up the best clinically acceptable treatment plan for each patient on the basis of target coverage, sparing of organs at risk, and number of beams. The main focus was put on minimization of the mean dose in the salivary glands (both parotid and submandibular glands) with the intend to maintain salivary flow as much as possible (Dijkema *et al* 2010, Murdoch-Kinch *et al* 2008), while assuring that at least 98.5% of the PTV was treated with at least 95% of the prescribed dose and keeping the maximum dose in critical serial organs below a fixed threshold value. (e.g., 50 Gy for the spinal cord). In most cases this resulted in a 7-beam IMRT plan.

Table 7.1: Characteristics of patients used in this study.

Patient	Tumour type	TNM	Dose interval evaluated in this study	Followed by
1	Palatum Molle Ca.	T2N2cMO	46 Gy	CyberKnife boost
2	Tonsillar fossa Ca.	T2NOMO	46 Gy	CyberKnife boost
3	Tonsillar fossa Ca.	T3NOMO	46 Gy	CyberKnife boost
4	Tonsillar fossa Ca.	T2NOMO	46 Gy	CyberKnife boost
5	Tonsillar fossa Ca.	T2NOMO	46 Gy	CyberKnife boost
6	Tonsillar fossa Ca.	T2NOMO	46 Gy	Brachytherapy boost
7	Tonsillar fossa Ca.	T1N2aMO	46 Gy	Brachytherapy boost
8	Tonsillar fossa Ca.	TxNOMO	46 Gy	Brachytherapy boost
9	Tonsillar fossa Ca.	T2NOMO	46 Gy	Brachytherapy boost
10	Oropharynx Ca.	T3NOMO	46 Gy	CyberKnife boost
11	Oropharynx Ca.	T2NOMO	46 Gy	CyberKnife boost
12	Oropharynx Ca.	T1NOMO	46 Gy	Brachytherapy boost
13	Oropharynx Ca.	T2NOMO	46 Gy	Brachytherapy boost
14	Base of tongue Ca.	T4aN1MO	46 Gy	CyberKnife boost
15	Base of tongue Ca.	T1N1MO	46 Gy	CyberKnife boost
16	Base of tongue Ca.	cT1N2bM	46 Gy	Brachytherapy boost
17	Cheek Ca.	T4aN1MO	46 Gy	24 Gy primary tumour
18	Floor of mouth Ca.	pT4aNOMO	66 Gy post operative RT	
19	Parotid Ca.	pT2NOMO	66 Gy post operative RT	
20	Nasopharynx Ca.	T1N2MO	70 Gy	Brachytherapy boost

7.2.2 iCycle: integrated beam angle and profile optimization

iCycle is a novel in-house developed algorithm for integrated beam angle and beam profile optimization (Breedveld *et al* 2007a, 2009a, 2012). The algorithm is described in detail in (Breedveld *et al* 2012). Here we will briefly summarize the main characteristics. Core of iCycle is the 2-phase ϵ -constraint (*2pec*) algorithm for generating optimal IMRT plans for preselected (fixed) beam arrangements. This algorithm has a multi-criterial optimization approach that generates a single Pareto-optimal plan for the preselected beam angles. Basis is a user-defined ‘wish-list’ containing the clinical plan objectives that all have an ascribed priority and hard constraints to be strictly obeyed during plan generation (see table 7.2 for an example). In iCycle, beam profile optimization is integrated in an iterative procedure for selection of optimal beam directions. Starting with zero beams, new beams with optimal directions are consecutively selected from a list of candidate beams and added to the plan. For selection of a next beam orientation, first, all candidate directions not yet selected are temporarily added to the configuration established in the previous iteration, and the IMRT optimization problem is solved. In the end, the orientation with the best score is added to the beam configuration. For each orientation added this results in one new Pareto-optimal IMRT plan. Identical wish-lists can be used for groups of patients, e.g., for all head-and-neck cancer patients with the main focus on sparing of salivary glands, making plan generation fully automatic and user independent.

Table 7.2: Applied wish-list for all study patients. SMG = submandibular gland.

Constraints						
	Volume	Type	Limit			
	PTV	maximum	107% of prescribed dose			
	Spinal cord	maximum	38 Gy (48 Gy)*			
	Unspecified Tissue	maximum	107% of prescribed dose			
Objectives						
Priority	Volume	Type	Goal	Sufficient	Parameters	
1	PTV	minimize LTCP	1	0.5	$\alpha = 0.8$	
2	Parotid / SMG	minimize mean	39 Gy			
3	Parotid / SMG	minimize mean	20 Gy			
4	Parotid / SMG	minimize mean	10 Gy			
5	Parotid / SMG	minimize mean	2 Gy			
6	PTV shell 1 cm	minimize maximum	35 Gy			
7	PTV shell 2 cm	minimize maximum	30 Gy			
8	PTV shell 3 cm	minimize maximum	25 Gy			
9	PTV shell 4 cm	minimize maximum	20 Gy			
10	PTV shell 5 cm	minimize maximum	15 Gy			

* 48 Gy for patients 18-20

The *2pec* algorithm consists of two phases. First, all objectives are consecutively minimized within hard constraints, trying to reach their predefined goal values (but not below), starting with the highest prioritized objective (see table 7.2). After minimization, the objective is turned into a constraint, applying the attained value. This method ensures that in the following minimizations of lower prioritized objectives, the attained value of the just optimized objective will at least be maintained. Another advantage is that for each patient one can start with the same wish-list with demanding objectives. In the second phase, objectives that could have been reduced below their defined goal as used in the first phase are sequentially further minimized, again starting with the highest prioritized objective. Except for objectives for the target dose, in the second phase all objectives are minimized to the full extent. Minimization of the target objective is stopped at a user-defined ‘sufficient’ value, accepting small deviations from 100% coverage of the PTV with 95% of the prescribed dose to leave room for minimization of lower prioritized objectives.

Apart from the wish-list, the only input that iCycle requires to generate plans is a prescribed number of beams, and a list with candidate beam directions that may be added to the plan. This list may be restricted for generation of coplanar plans with couch angle 0° , but it may also contain a large set of orientations with various couch and gantry angles that can be delivered without crashes between the gantry and the couch or patient.

As mentioned above, in the process of generating a plan with the prescribed number of beams, Pareto-optimal plans will also be generated for smaller beam numbers. The

plan with the highest number of beams has the best plan quality regarding the highest prioritized objective that is minimized to its full extent (see above). However, differences with plans with fewer beams may be small, making a plan with fewer beams attractive because of reduced QA workload or treatment time. On the other hand, if the evaluation of plan quality as a function of beam number shows that more beams than initially prescribed would result in a better plan quality, iCycle can easily be instructed to generate more plans with higher beam numbers.

7.2.3 iCycle plan generation for the study patients

The applied wish-list is depicted in table 7.2. It contains hard constraints on the maximum allowed dose in the PTV, spinal cord and unspecified tissue. For patients 1-17, the maximum allowed dose in the spinal cord was set to 38 *Gy*, i.e., lower than our clinically used constraint, to leave sufficient room for optimizing the subsequent boost plan. The objective with priority 1 was to achieve adequate target coverage. The target dose was optimized by minimizing the Logarithmic Tumour Control Probability (LTCP) as described by Alber & Reemtsen (2007). A prescription dose and an alpha parameter, affecting the penalty given to underdosed voxels in the tumour, are inputs to derive the LTCP. On the basis of the first five study patients, alpha was set at 0.8, which ensured that at least 98.5% of the PTV volume received at least 95% of the prescribed dose for all treatment plans. Objectives 2-5 aimed at a balanced reduction of the mean dose in each of the individual salivary glands. Since the PTV objective was higher prioritized, target dose-coverage never reduced. Finally, to achieve a steep dose fall off outside the target volume, maximum dose objectives were defined for a set of shells with 0.3 *cm* thickness at 1, 2, 3, 4 and 5 *cm* of the PTV.

For coplanar BAO, beams were selected from 72 equi-angular spaced candidate beams. For non-coplanar BAO, we added non-coplanar candidate beams with a 10 degree separation, resulting in approximately 320 beams in total. The coarser separation of the non-coplanar candidate beams reduced the time required for BAO without compromising plan quality. In this study, we used a maximum non-coplanar beam angle in cranial direction of 45 degrees. Beams outside this range would never be selected due to the applied maximum dose objectives outside the PTV (objectives 6-10 in table 7.2). We also omitted candidate beams at both sides of the sphere that could result in collisions between the gantry and the patient or the treatment couch. Consequently, the list of feasible candidate beams used by iCycle for non-coplanar BAO depends on target site and treatment machine.

Using iCycle, the following plans were derived for the patients in this study:

- (i) a 7-beam coplanar equi-angular plan at couch angle 0° (iCycle_{7equi}).
- (ii) a 9-beam coplanar equi-angular plan at couch angle 0° (iCycle_{9equi}).

- (iii) a 9-beam coplanar plan with optimized gantry angles at couch angle 0° ($iCycle_{copl}$).
- (iv) a 9-beam non-coplanar plan with optimized gantry and couch angles ($iCycle_{noncopl}$).
- (v) a 9-beam coplanar plan with optimized gantry angles and an optimal couch angle ($iCycle_{couch}$). This plan was selected from 9 sequentially optimized $iCycle$ plans, generated for fixed couch angles at 340° , 345° , 350° , 355° , 5° , 10° , 15° , 20° , or 0° (i.e., $iCycle_{copl}$), based on the lowest mean NTCP for the salivary glands.

$iCycle_{couch}$ was investigated because this plan requires one single couch rotation at the start of treatment only; next, all beams can be delivered without the technicians having to enter the treatment room in between. In contrast, treatment of fully non-coplanar plans is more labour-intensive and time-consuming, as technicians have to enter the treatment room to manually execute prescribed couch rotations.

7.2.4 Impact of couch angle on VMAT plans

For the two study patients who benefited most from using an optimized couch angle for the coplanar plan (i.e., showing the largest difference in mean salivary gland NTCP when comparing $iCycle_{copl}$ and $iCycle_{couch}$), we investigated whether VMAT plans could be improved by using this optimized couch angle, instead of the commonly used zero couch angle. Single, full-arc VMAT-plans were generated with Monaco for both situations. Differences in salivary gland sparing were quantified.

7.2.5 Comparison of treatment plans

Like in our clinically used plans, plan evaluation was mainly focused on the achieved salivary gland sparing. We compared mean doses in each of the glands. Moreover, these mean doses were converted into NTCP values, using published dose-response models for parotid (Dijkema *et al* 2010) and submandibular glands (Murdoch-Kinch *et al* 2008). Both NTCP models are based on the probability of Grade 4 toxicity (i.e., salivary flow rate $< 25\%$ of baseline pre-radiotherapy). A two-sided Wilcoxon matched-pair signed-rank test (McDonald 2009) was used to compare the different $iCycle$ plans for the patient group.

7.3 Results

7.3.1 Comparison of $iCycle$ plans

With the applied wish-list, at least 98.5% of the PTV received 95% of the prescribed dose for all plans. For most plans this applied for even more than 99% of the PTV. Due to applied hard constraint in the wish-list, observed maximum doses in the spinal cord remained below 38 Gy for patients 1-16, and below 48 Gy for patients 17-20. For patient 20, the observed maximum dose for brainstem was 48 Gy, while the maximum doses in

the optical chiasm, optical nerves and eyes were less than 40 *Gy*. In all other patients the maximum doses in the brainstem were below 38 *Gy*.

Figure 7.1 compares mean salivary gland doses for $iCycle_{noncopl}$ with the corresponding doses in the other $iCycle$ plans. Figure 7.2 shows the NTCP differences between $iCycle_{noncopl}$ and the other plans. In table 7.3, these differences are summarized. The lowest mean salivary gland doses were observed for $iCycle_{noncopl}$. Differences with $iCycle_{7equi}$, $iCycle_{9equi}$, and $iCycle_{copl}$ were statistically significant ($p < 0.001$, table 7.3). Compared to $iCycle_{couch}$, only the differences in mean submandibular gland dose were statistically significant ($p = 0.05$). For $iCycle_{7equi}$, $iCycle_{9equi}$ and $iCycle_{copl}$, the observed increases in mean salivary gland doses compared to $iCycle_{noncopl}$ also translated in statistically significant increased NTCPs (table 7.3). $iCycle_{7equi}$ yielded higher mean salivary gland doses and NTCPs than each of the 9-beam techniques. BAO for $iCycle_{copl}$ resulted in better salivary gland sparing than achieved with $iCycle_{9equi}$.

The observed mean NTCP differences between different planning techniques are small. However, one should keep in mind that the mean NTCP values for $iCycle_{noncopl}$ were 7% for the parotid glands and 30% for the submandibular glands. Therefore, in a relative sense, $iCycle_{noncopl}$ had a far lower risk for damaging parotid glands than e.g., $iCycle_{7equi}$. Moreover, the gain of applying a more advanced planning technique was patient dependent (see table 7.3). For example, the mean difference in NTCP for the submandibular glands between $iCycle_{7equi}$ and $iCycle_{9equi}$ was 2.2%; whereas, in patient 5 the use of 9-beams reduced the NTCP for the right submandibular gland from 40% to 29%. For the parotid glands, the mean NTCP difference between $iCycle_{9equi}$ and $iCycle_{copl}$ was 0.9%, but in patient 20 the NTCPs reduced from 53% to 47% and 44%, respectively.

Compared to $iCycle_{copl}$, use of the optimal couch angle ($iCycle_{couch}$) improved the NTCP for parotid glands by up to 4% and for submandibular glands by up to 3%. For 18 of the 20 patients, NTCPs for $iCycle_{couch}$ were similar to the values for $iCycle_{noncopl}$.

7.3.2 Calculation times for generating $iCycle$ plans

The calculation time for the beam angle optimization phase in $iCycle$ scales linearly with the number of candidate beams. For the multi-criterial optimization, the required time grows to the power of three with the number of beams. Moreover, it depends on the number of constraints and objectives in the wish-list. For this part, calculation times are similar for coplanar and non-coplanar $iCycle$ plans.

Using a modern 8-core server, calculation times were typically 3 hours for the 9-beam coplanar BAO plans and 12 hours for the non-coplanar plans.

7.3.3 Impact of couch optimization on VMAT plans

Patients 4 and 18 had the largest reduction in mean salivary gland NTCP when changing from $iCycle_{copl}$ to $iCycle_{couch}$. For these patients, the optimal couch angle was 340° and

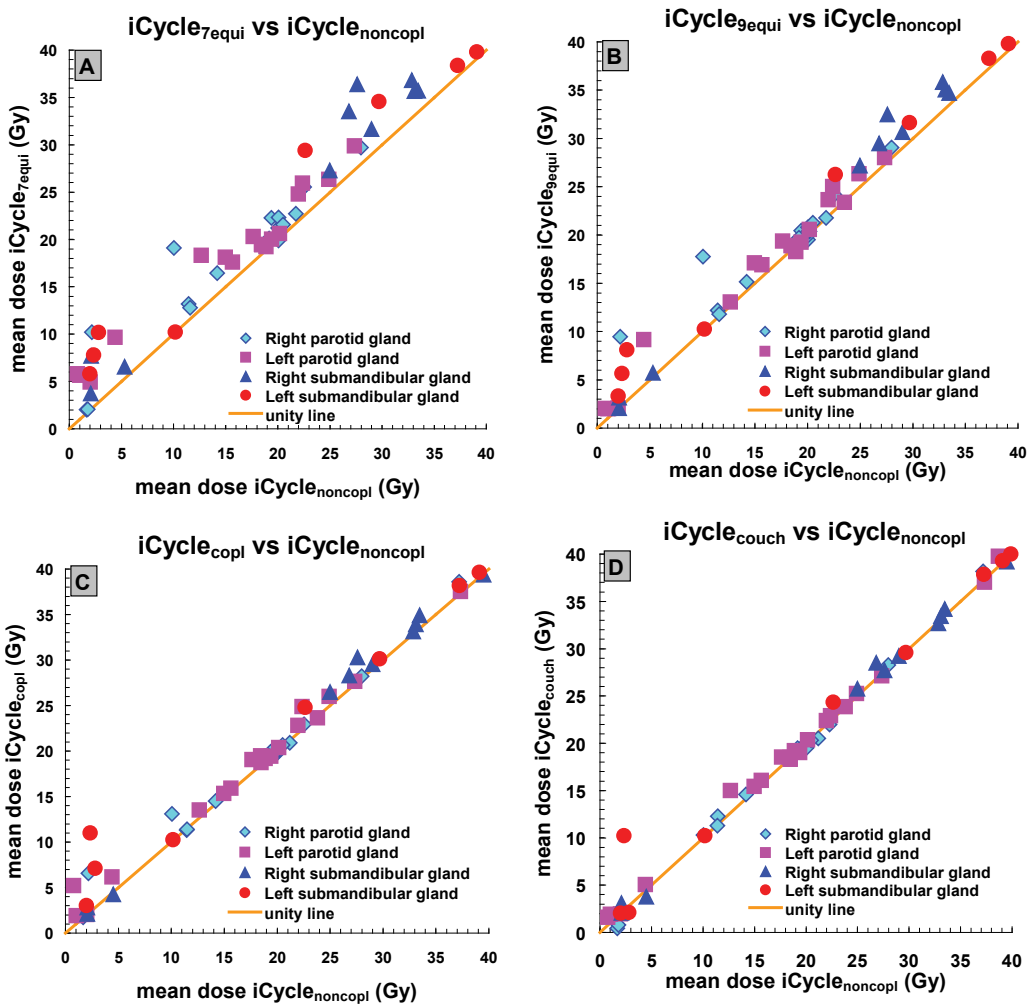


Figure 7.1: Mean salivary gland doses for all coplanar techniques compared to $iCycle_{noncopl}$.

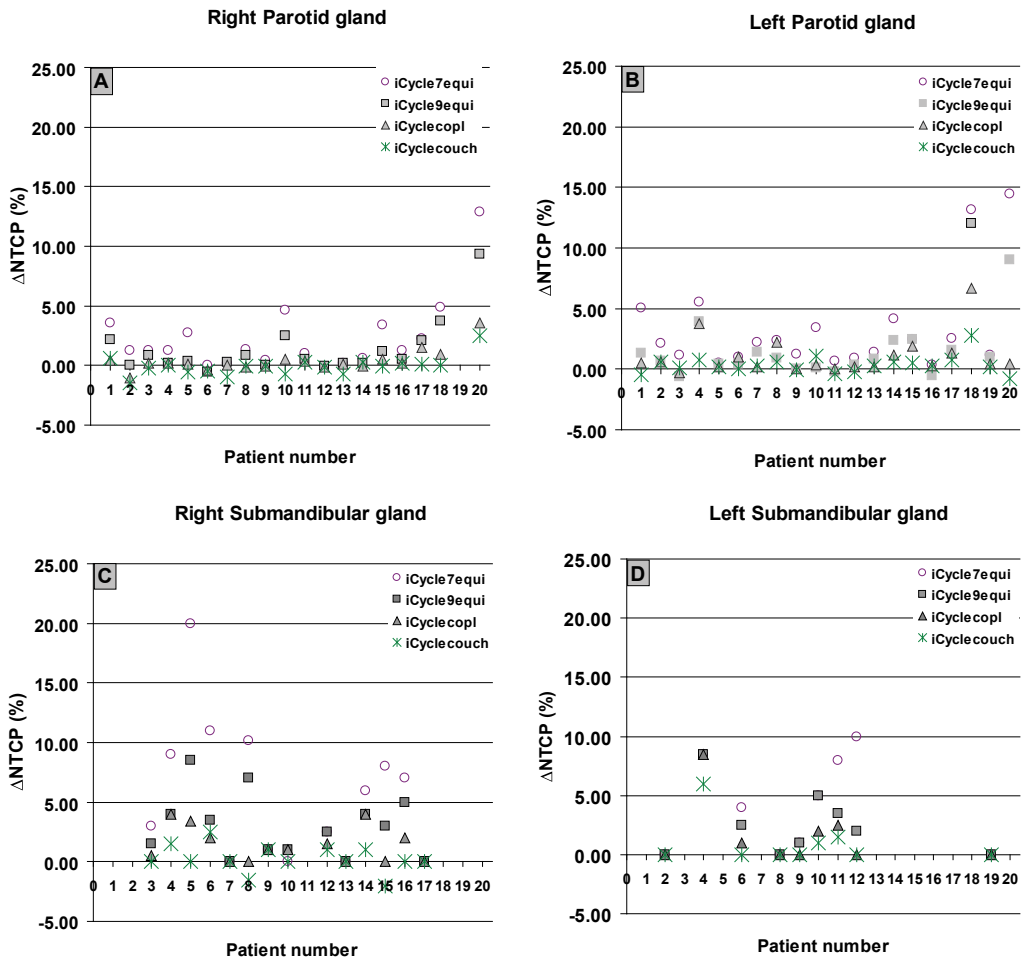


Figure 7.2: Differences in NTCP values for all plans relative to $iCycle_{noncopl}$, visualized per salivary gland. NTCP values of glands that could not be spared, because they were entirely enclosed in the PTV, were omitted.

Table 7.3: Differences between $iCycle_{noncopl}$ and all other plans in mean salivary gland dose and NTCP, averaged over the 20 study patients, for both parotid and submandibular glands. For $iCycle_{noncopl}$, the mean parotid and submandibular gland doses were 17.5 Gy (range: 0.8 – 38.7 Gy) and 24.5 Gy (range: 2.0 – 41.0 Gy), respectively. Mean NTCPs were 7% (range: 1 – 47%) and 30% (range: 10 – 65%).

Parotid glands	$iCycle_{7equi}$	$iCycle_{9equi}$	$iCycle_{copl}$	$iCycle_{couch}$
mean dose* (Gy)	2.5	1.4	0.7	0.1
SD (Gy)	2.2	1.9	1.2	0.7
Range (Gy)	-0.2 to 9.1	-0.6 to 7.7	-0.8 to 4.4	-1.2 to 2.3
p-value*	<0.001	<0.001	<0.001	0.203
NTCP* (%)	2.8	1.6	0.7	0.1
SD (%)	3.5	2.7	1.4	0.8
Range (%)	-0.2 to 14.4	-0.7 to 12.0	-1.1 to 6.7	-1.5 to 2.8
p-value*	<0.001	<0.001	0.005	0.629
Submandibular glands	$iCycle_{7equi}$	$iCycle_{9equi}$	$iCycle_{copl}$	$iCycle_{couch}$
mean dose* (Gy)	3.1	1.7	1.2	0.6
SD (Gy)	2.6	1.5	2	1.7
Range (Gy)	-0.5 to 8.8	-0.0 to 5.3	-1.1 to 8.6	-1.5 to 7.9
p-value*	<0.001	<0.001	<0.001	0.05
NTCP* (%)	5	2.8	1.5	0.5
SD (%)	5.1	2.7	2	1.5
Range (%)	0 to 20.0	0 to 8.5	0 to 8.5	-2.0 to 6.0
p-value*	<0.001	<0.001	<0.001	0.085

* Compared to $iCycle_{noncopl}$

350° respectively. Table 7.4 shows salivary gland doses for VMAT plans with couch angles 0° and 340°/350°. Like observed for $iCycle_{couch}$, use of the optimal couch angle improved the salivary gland sparing for VMAT plans as well.

7.4 Discussion

To our knowledge, this is the first systematic study on the impact of beam angles on salivary gland sparing in head-and-neck cancer patients, based on integrated computerized optimization of beam angles and intensity profiles. By using a single wish-list with plan objectives and constraints for all patients and techniques, plan generation became fully

Table 7.4: Mean doses in salivary glands (Gy) for VMAT plans with a couch angle of 0° and with the optimized couch angle from $iCycle_{couch}$. Submandibular glands for patient 18 were omitted in the table since they were fully included in the PTV.

	Patient 4		Patient 18	
	VMAT 0°	VMAT 350°	VMAT 0°	VMAT 340°
Right parotid	22.7	20.6	13.9	9.2
Left parotid	26.6	24.8	42.5	39.1
Right submandibular gland	44.3	42.7	-	-
Left submandibular gland	35.6	35.2	-	-

user independent, ensuring objective plan comparisons. Plans with 9 beams performed better than plans with 7 beams, and coplanar plans with optimized gantry angles had better gland sparing than equi-angular plans. Non-coplanar plans with optimized gantry and couch angles had the lowest gland NTCPs, although differences with coplanar plans with an optimized couch angle were negligible for most patients.

iCycle generates multi-criterial optimized treatment plans. Other algorithms for multi-criterial plan optimization have been evaluated clinically, showing a benefit for plan quality and plan efficiency (Craft *et al* 2012, Thieke *et al* 2007). But in these studies the number of treatment beams and their orientations were still manually selected. The regular labour-intensive trial-and-error process for selecting beam orientations and number of beams in IMRT treatment planning may result in variations in plan quality, depending on the skills and experience of the dosimetrist. Class solutions for beam arrangements may be suboptimal for individual patients. iCycle is an algorithm for fully automated generation of plans with optimized beam angles and intensity profiles. Therefore, the workload for generating plans is almost negligible. Prior to the start of the investigations described in this paper, for 10 of the 20 selected patients we compared the clinical plan as generated with the Monaco TPS with the coplanar iCycle plan with optimized gantry angles (iCycle_{copl}). For each of these patients, salivary gland sparing in the iCycle plan was superior. On average, the mean gland NTCP reduced from 29.2% to 19.4%.

iCycle has been developed in a research setting and not for clinical use; a segmentation algorithm is currently lacking. However, it turned out that using the optimal beam angles and mean gland doses as established with iCycle as input, Monaco could be steered to generate a clinically acceptable plan that was almost identical to the iCycle plan with respect to the obtained gland NTCPs. The procedure for converting an iCycle plan into a Monaco plan has recently been automated. As a result, high quality IMRT plans for head-and-neck cancer patients can now be generated in two automated steps. The first step is generation of a plan in iCycle; the second is the conversion into a clinically deliverable Monaco plan. We recently performed a prospective study for head-and-neck patients, showing a clear benefit for this automated plan generation approach (Voet *et al* 2013). In that study, we took into account more relevant critical structures, like oral cavity, larynx and swallowing muscles, during plan optimization.

We demonstrated that iCycle_{couch} plans were sometimes superior to the corresponding plans for couch angle 0°. This was especially true in unilateral neck treatments, in which rotation of the couch often resulted in a free projection of the contra-lateral salivary glands, yielding reductions in delivered gland doses. As demonstrated for two patients, also with VMAT the optimal nonzero couch angles resulted in lower salivary gland doses than plans for couch angle 0°.

All iCycle plans in this study were automatically generated based on one identical wish-list. This allows for an objective comparison of competing treatment strategies for individual patients. For none of them, clinically relevant plan improvements were observed when using more than 9 beams. Patients with unilateral targets showed very little improvement in plan quality after adding beams eight or nine. However, adding extra beams never deteriorated plan results. The investigations revealed that the gain of more complex or time-consuming treatment techniques was patient dependent. As planning with iCycle is fully automated, a possible future clinical application is to generate for each patient 9-beam coplanar plans for couch angle 0° and several nonzero angles, and a 9-beam non-coplanar plan. Based on the differences in NTCP and involved treatment time, one could then choose for each individual patient the most appropriate treatment technique.

7.5 Conclusions

iCycle is a novel plan optimization algorithm for user-independent generation of treatment plans with optimized beam angles and intensity profiles, allowing objective comparison of competing planning strategies. For head-and-neck cancer patients, plan generation with iCycle can result in improved salivary gland sparing with a largely reduced planning workload. Observed sparing was best for fully non-coplanar plans. VMAT with an optimized couch angle can improve salivary gland sparing compared to the commonly applied zero couch angle.

Chapter 8

Toward fully automated multi-criterial plan generation: a prospective clinical study

Peter Voet, Maarten Dirkx, Sebastiaan Breedveld, Dennie Fransen, Peter Levendag and Ben Heijmen

Department of Radiation Oncology, Erasmus MC Rotterdam, Groene Hilledijk 301, 3075 EA Rotterdam, The Netherlands

E-mail: p.voet@erasmusmc.nl

Published 31 March 2013 in *International Journal of Radiation Oncology*Biography*Physics*, volume **85**, pages 866-872

[doi:10.1016/j.ijrobp.2012.04.015](https://doi.org/10.1016/j.ijrobp.2012.04.015)

Abstract

Purpose: To prospectively compare plans generated with iCycle, an in-house developed algorithm for fully automated multi-criterial IMRT beam profile and beam orientation optimization, with plans manually generated by dosimetrists with the clinical treatment planning system.

Methods and Materials: For 20 randomly selected head-and-neck cancer patients with various tumour locations (of whom 13 received sequential boost treatments) we offered the treating physician the choice between an automatically generated iCycle plan and a manually optimized plan following standard clinical procedures. While iCycle used a fixed ‘wish-list’ with hard constraints and prioritized objectives, the dosimetrists manually selected the beam configuration and fine-tuned the constraints and objectives for each IMRT plan. Dosimetrists were not informed in advance whether or not a competing iCycle plan was made. The two plans were simultaneously presented to the physician, who then selected the plan to be used for treatment. For the patient group, differences in PTV coverage and sparing of critical tissues were quantified.

Results: In 32/33 plan comparisons the physician selected the iCycle plan for treatment. This highly consistent preference for automatically generated plans was mainly caused by improved sparing for the large majority of critical structures. With iCycle, the NTCPs for parotid and submandibular glands were reduced by $2.4\% \pm 4.9\%$ (maximum: 18.5%, $p = 0.001$) and $6.5\% \pm 8.3\%$ (maximum: 27%, $p = 0.005$), respectively. The reduction in mean oral cavity dose was $2.8 Gy \pm 2.8 Gy$ (maximum: 8.1 Gy, $p = 0.005$). For swallowing muscles, oesophagus and larynx, the mean dose reduction was $3.3 Gy \pm 1.1 Gy$ (maximum: 9.2 Gy, $p < 0.001$). In addition, for 15 of the 20 patients, target coverage was improved as well.

Conclusions: In 97% of cases, automatically generated plans were selected for treatment because of superior quality. Apart from improved plan quality, automatic plan generation is economically attractive because of reduced workload.

8.1 Introduction

Intensity modulated radiotherapy (IMRT) is commonly applied as curative radiotherapy treatment for head-and-neck cancer patients. As input for computerized optimization of the beam profiles, the number of beams, their configuration, the constraints and the objectives need to be defined by the dosimetrist. It is often difficult for dosimetrists to select these input parameters and to assess whether and how a plan can be further optimized by modifying them for a second optimization attempt. This may result in a time-consuming trial and error process. Moreover, the realized plan quality may highly depend on the complexity of the case, the time available for plan generation, and the skills and ambition of the dosimetrist.

In a previous study on head-and-neck cancer patients we compared IMRT plans with computer-optimized beam arrangements with plans based on equi-angular set-ups (Voet *et al* 2012). All plans were automatically generated with iCycle (Breedveld *et al* 2007a, 2009a, 2012), an in-house developed algorithm for multi-criterial optimization of beam profiles and gantry angles. Compared to equi-angular arrangements, we demonstrated improved salivary gland sparing for optimized beam set-ups. Nine beam plans were often superior to seven field plans.

In this study we prospectively compared for a group of randomly selected head-and-neck patients two plans: one generated by dosimetrists using our clinical treatment planning system Monaco (Elekta AB, Sweden), the other based on automatic plan generation by iCycle. iCycle optimized both beam profiles and coplanar beam arrangements. Patients were treated according to the best plan, as selected by the treating physician. Plans were compared based on physicians' preferences and quantitative assessments.

8.2 Methods and materials

8.2.1 Patients

Table 8.1 gives an overview of the 20 patients included in our study. Treatments for the indicated dose intervals were delivered at an Elekta Synergy linear accelerator using 6 MV photon beams. For 17 of the 20 patients, a sequential boost followed the initial treatment up to 45 or 46 Gy. Since boosts delivered with brachytherapy or CyberKnife were excluded in our analyses, the treating physicians made in total 33 plan comparisons and selections.

Prior to plan generation, the treating physician contoured the CT-scan of the patient, largely assisted by the auto-contouring program ABAS (Teguh *et al* 2011). Apart from the clinical target volumes (CTV), the parotid and submandibular glands, oral cavity, swallowing muscles, first centimetre of the oesophagus (Levendag *et al* 2007), larynx, spinal cord, and brain stem were delineated. For planning, CTVs were extended with a

Table 8.1: Characteristics of patients included in this study.

Patient	Tumour type	TNM	Dose intervals evaluated (Gy)	Followed by
1	Hypopharynx cancer	T4aN2bM0	0-66	
2	Oral cavity cancer	T4aN0M0	0-46 + 46-66	
3	Tonsil cancer	T2N0M0	0-46	Brachytherapy
4	Larynx cancer	T4N2bMx	0-46 + 46-70	
5	Larynx cancer	T4aN1M0	0-46 + 46-70	
6	Nasopharynx cancer	T1N1Mx	0-46 + 46-70	
7	Oral cavity cancer	T2N0M0	0-46	CyberKnife boost
8	Base of tongue cancer	T2N2bM0	0-46	CyberKnife boost
9	Hypopharynx cancer	T2N2bM0	0-46 + 46-70	
10	Sinus piriformis cancer	TxN2bMx	0-46 + 46-66	
11	Tonsil cancer	T3N2bMx	0-46	CyberKnife boost
12	Hypopharynx cancer	T4aN0M0	0-46 + 46-70	
13	Hypopharynx cancer	T2N0M0	0-46 + 46-70	
14	Tongue cancer	T4N2cM0	0-46 + 46-66	
15	Larynx cancer	T3N0M0	0-46 + 46-70	
16	Base of tongue cancer	T2N0M0	0-46 + 46-70	
17	Lip cancer	TxN0M0	0-45 + 45-62.5	
18	Left neck (mesothelioma)		0-44	
19	Oral cavity cancer	T2N0M0	0-66	
20	Larynx cancer	T3N0M0	0-46 + 46-70	

5 mm margin to generate planning target volumes (PTV).

8.2.2 Study design

The design of our study is schematically presented in figure 8.1. During the study period, the standard protocol for IMRT included “manual” generation of treatment plans ($IMRT_{dos}$) by dosimetrists using Monaco version 2.04. For each IMRT plan the beam configuration was manually selected and the constraints and objectives were fine-tuned. For the study patients, a second plan ($IMRT_{iCycle}$) was generated, based on an automated plan generation with iCycle (Breedveld *et al* 2012, and next section). Neither the involved dosimetrist, nor the treating physician knew in advance whether a competing iCycle plan would be developed.

iCycle is not commissioned for clinical use. Therefore, one of the investigators (PV) used Monaco for conversion of iCycle plans into highly similar, clinically deliverable plans ($IMRT_{iCycle}$). First, a Monaco plan-template was automatically generated including the optimized beam angles and achieved plan-parameters for organs at risk (OAR) in iCycle. With minimal user interference, these values could then be reproduced in Monaco within 1 Gy difference for all OARs. To prevent any bias, PV did not have access to the $IMRT_{dos}$ plan while generating $IMRT_{iCycle}$.

$IMRT_{dos}$ and $IMRT_{iCycle}$ were together presented to the treating physician for plan selection, using identical lay-outs of plotted dose distributions and dose-volume histograms. Seven experienced dosimetrists, experienced in IMRT planning, generated the standard

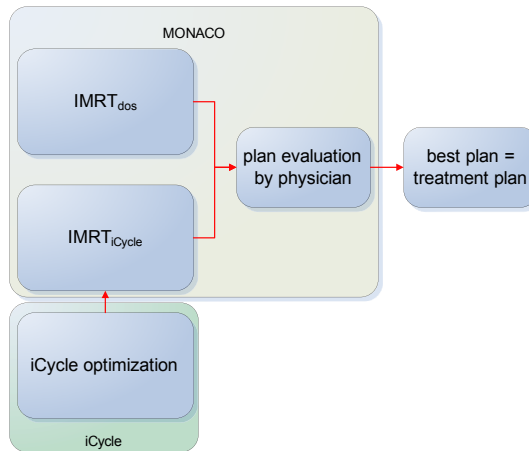


Figure 8.1: Workflow of study. Note that the intensity modulated radiation therapy plans generated manually (IMRT_{dos}) and those generated with iCycle, an in-house-developed algorithm ($\text{IMRT}_{\text{iCycle}}$) were presented to the treating physician in the same program (Monaco).

plans with Monaco. Seven head-and-neck radiation oncologists entered patients and evaluated competing $\text{IMRT}_{\text{iCycle}}$ and IMRT_{dos} plans to select the best plan for treatment.

In addition to physicians' preferences, we compared plans based on quantitative analyses of achieved PTV coverage and OAR sparing. For patients with a sequential boost, not delivered with brachytherapy or CyberKnife, summed dose distributions were evaluated. Target coverage was quantified by the dose delivered to 99% of the PTV ($D_{99\%}$). For the spinal cord and brainstem, maximum doses were compared. Mean doses were evaluated for the other OARs. For salivary glands, mean doses were converted into NTCP values, using published dose-response models for parotid (Dijkema *et al* 2010) and submandibular glands (Murdoch-Kinch *et al* 2008). Both models are based on the probability of Grade 4 toxicity (i.e., salivary flow rate < 25% of baseline pre-radiotherapy). For the group of patients, two-sided Wilcoxon matched-pair signed-rank tests were used to derive the statistical significance of observed differences in plan parameters.

For both IMRT_{dos} and $\text{IMRT}_{\text{iCycle}}$, the required hands-on planning time was logged. Time for optimization, segmentation and dose calculation, which did not require any manual interference, was excluded.

8.2.3 iCycle plan generation

iCycle is an algorithm for multi-criterial optimization of both beam orientations and IMRT fluence profiles. Its features have been described in detail in (Breedveld *et al* 2012). Here a brief summary is provided. Basis for a plan optimization is an a priori

defined ‘wish-list’ containing hard constraints to be strictly obeyed and prioritized objectives. Per patient category, a fixed wish-list is used. Treatment plan generation is fully automated, i.e. without any user interaction such as tweaking of objective weights. Core of iCycle is the 2-phase ϵ -constraint ($2p\epsilon$) algorithm for generating Pareto-optimal plans for preselected (fixed) beam arrangements (Breedveld *et al* 2007a, 2009a). In the generated Pareto-optimal plans none of the objectives can be improved any further without deteriorating one or more constraints or higher prioritized objectives.

In iCycle, beam profile optimization is integrated in an iterative procedure for selection of optimal beam directions. Starting with zero beams, new beams with optimal directions are consecutively selected from a list of candidate beams and added to the plan. For selection of a next beam orientation, all candidate directions not yet selected are temporarily added to the configuration established in the previous iteration, and the IMRT optimization problem is solved. In the end, the orientation with the best score is added to the beam configuration. For each orientation added this results in one new Pareto-optimal IMRT plan. Addition of a new beam improves plan quality regarding the highest prioritized objective that can still be improved on. In this study, in total 9 directions were used for plan generation for each of the patients, resulting in Pareto optimal plans with 9, 8, 7, ... beams. With more than 9 beams, clinically relevant plan improvements were not observed (Voet *et al* 2012). Based on a minimum gain of 0.5 Gy per added beam in at least one of the objectives, we decided on the number of beams for generating IMRT_{iCycle} plans.

In this study iCycle was used for generating Pareto-optimal coplanar plans at couch angle 0°. Beam directions were automatically selected from 72 equi-spaced candidate directions (5° separation), including 0°.

Table 8.2 shows the applied wish-list for the first dose interval of each patient. It was established using the clinical protocol, previous experiences (Voet *et al* 2012), trial runs of iCycle for a small group of patients, and discussions with two of the seven involved clinicians. iCycle has a mechanism to reduce, if possible, the objective functions in the wish-list to values lower than the indicated goal values, with an accent on the objectives with the highest priorities. PTV coverage had the highest priority. To enforce that the PTV $D_{99\%}$ was at least 95% of the prescribed dose, the Logarithmic Tumour Control Probability (LTCP) was used (Alber & Reemtsen 2007, Breedveld *et al* 2012). For a homogeneous target dose, equal to the prescribed dose, $LTCP = 1$. A lower target dose results in a strongly enhanced LTCP, while higher target doses decrease the LTCP to a minimum value of 0 for a clinically infeasible, infinite dose. To guarantee good target coverage, an alpha value of 0.8 was used. A higher alpha puts a higher penalty on cold spots in the PTV. Reduction of the mean salivary gland doses was performed using a multi-level approach (Breedveld *et al* 2009a), i.e., by repeated use of the objective func-

Table 8.2: Applied wish-list for first dose interval of each patient, containing hard constraints and prioritized objectives.

Constraints			
	Volume	Type	Limit
	PTV	maximum	107% of prescribed dose
	Spinal cord	maximum	48 Gy*
	Unspecified Tissue	maximum	107% of prescribed dose
Objectives			
Priority	Volume	Type	Goal
1	PTV	minimize LTCP	1
2	Parotid / SMG	minimize mean	39 Gy
3	Parotid / SMG	minimize mean	20 Gy
4	Oral cavity	minimize mean	39 Gy
5	Spinal cord / brain stem	minimize maximum	30 Gy
6	External ring †	minimize maximum	90% of prescribed dose
7	Larynx + swallowing muscles	minimize mean	75% of prescribed dose
8	PTV shell 1 cm ‡	minimize maximum	75% of prescribed dose
9	Parotid / SMG	minimize mean	10 Gy
10	PTV shell 4 cm ‡	minimize maximum	40% of prescribed dose
11	Parotid / SMG	minimize mean	2 Gy

* For patients treated with a sequential boost technique, a spinal cord constraint of 38 Gy was applied to leave room for optimizing the boost plan.

† Structure 2 cm distance interior from patient surface, preventing high superficial doses in incident beams.

‡ PTV shells 1 cm and 4 cm from PTV to control dose gradient outside PTV.

tion with decreasing priorities and goal values (table 8.2). iCycle first tried to minimize the mean dose in each of the salivary glands to 39 Gy (corresponding to an NTCP of about 50%, objective 2), and then to 20 Gy (NTCP of about 10%, objective 3). Before minimizing the dose in the salivary glands even further (priorities 9 and 11), the mean oral cavity dose (priority 4), the maximum dose in spinal cord and brainstem (priority 5) and the mean dose in the larynx and swallowing muscles (priority 7) were optimized. When for instance the dose in the oral cavity would not be considered first, the salivary glands might be spared at the cost of an unacceptable high dose in the oral cavity. The volumes External ring, PTV shell 1 cm and PTV shell 4 cm aimed at reducing the entrance dose, and steering the dose gradient outside the PTV, respectively.

For patients with a sequential boost (see table 8.1) we used the same wish-list for the boost phase. Only the constraints for the spinal cord and brain stem were adjusted according to the dose interval.

8.3 Results

IMRT_{iCycle} and IMRT_{dos} plans consisted of 6-9 beams (average 8.6), and 5-9 beams (average 7.3), respectively. In 32/33 plan comparisons, the physician selected IMRT_{iCycle} for treatment, in the vast majority of cases due to reduced dose delivery to OARs with neg-

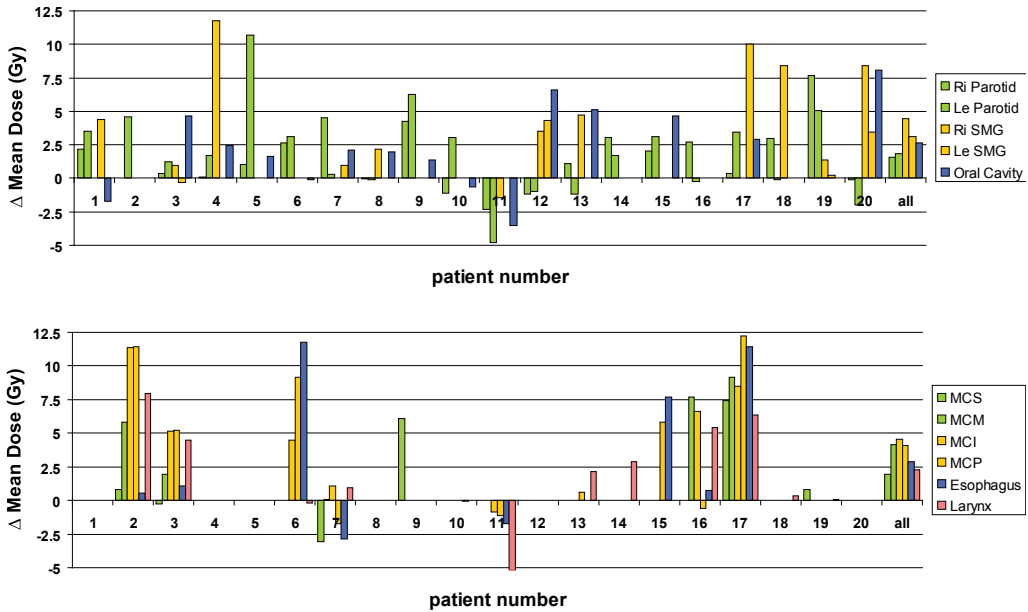


Figure 8.2: Differences in OAR mean doses between $IMRT_{dos}$ and $IMRT_{iCycle}$ for the 20 study patients with at the right end ('all') the patient group averages. Positive values indicate lower OAR doses for $IMRT_{iCycle}$. Results for OARs that could not be spared, because they are completely embedded in the PTV, were omitted. MCS = musculus constrictor superior; MCM = musculus constrictor medius; MCI = musculus constrictor inferior; MCP = musculus constrictor cricopharyngeus. SMG = submandibular gland.

ligible loss in PTV coverage, equal coverage, or even improved coverage. For patient 11, $IMRT_{iCycle}$ was selected notwithstanding the higher OAR doses. In this case, $IMRT_{dos}$ had a too low PTV coverage, which was avoided in $IMRT_{iCycle}$.

Figure 8.2 compares obtained OAR doses. In case a patient had plans for two dose intervals (see table 8.1), data for the summed plan are provided. For the $iCycle$ plans the mean NTCP was reduced by 2.4% (maximum: 18.5%, $p = 0.001$) for the parotid glands and by 6.5% (maximum: 27%, $p = 0.005$) for submandibular glands. The mean dose in the oral cavity reduced by on average 2.8 Gy (maximum: 8.1 Gy, $p = 0.005$). The mean dose reduction in the swallowing muscles, oesophagus and larynx was $3.3 Gy \pm 1.1 Gy$ (maximum 9.2 Gy, $p < 0.001$). For $IMRT_{iCycle}$ the maximum doses in the spinal cord and in the brain stem were well below tolerance with average values of 34.8 Gy and 21.8 Gy, respectively. Relative to $IMRT_{dos}$ the maximum doses in the spinal cord and the brain stem were reduced by $3.3 Gy \pm 4.0 Gy$ ($p = 0.04$) and $1.1 Gy \pm 6.4 Gy$ ($p = 0.531$), respectively.

Figure 8.3 illustrates the balance between target coverage and NTCP for the salivary

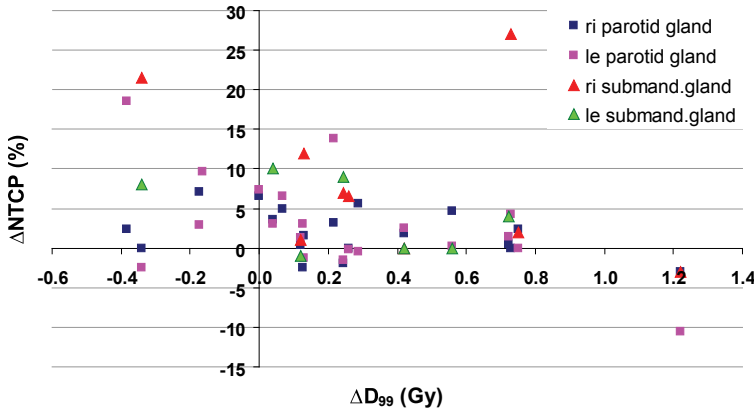


Figure 8.3: Differences between IMRT_{dos} and $\text{IMRT}_{\text{iCycle}}$ in $D_{99\%}$ and NTCP values for the individual salivary glands, for the 20 study patients. Results for salivary glands that could not be spared, because they were completely embedded in the PTV, were omitted. For points in the upper right quadrant, $\text{IMRT}_{\text{iCycle}}$ showed both a better target coverage and improved OAR sparing.

glands. Overall, the target coverage was slightly better for the $\text{IMRT}_{\text{iCycle}}$ plans. The mean improvement in $D_{99\%}$ was $0.24 \text{ Gy} \pm 0.4 \text{ Gy}$ ($p = 0.07$). 75% of salivary glands had lower NTCPs in the $\text{IMRT}_{\text{iCycle}}$ plan (upper left and right quadrants in figure 8.3). 59% of the glands are in the upper right quadrant, indicating that $\text{IMRT}_{\text{iCycle}}$ had both the lowest mean gland dose and improved target coverage.

For each patient, we estimated both for IMRT_{dos} and $\text{IMRT}_{\text{iCycle}}$ the probability that the function of at least one parotid gland could be preserved, and the probability that at least one submandibular gland could be spared. These probabilities, P , were calculated according to $P = (1 - \text{NTCP}_{\text{left}} \cdot \text{NTCP}_{\text{right}})$. Figure 8.4 clearly shows that this probability is higher for the $\text{IMRT}_{\text{iCycle}}$ plans, except for patient 11 (see also above). In case IMRT_{dos} has already a high sparing probability (i.e., close to 100%), there is naturally limited room for improvement with $\text{IMRT}_{\text{iCycle}}$. But for patients with a lower probability of sparing at least one of the glands, sparing could be substantially enhanced by $\text{IMRT}_{\text{iCycle}}$.

The average hands-on time spent by dosimetrists on generating IMRT_{dos} plans was 3.3 hours (range 1 – 6.5 hours). As described in the Methods and Materials section (8.2), generating an iCycle plan is fully automated. Conversion into a Monaco plan to arrive at the clinically applicable $\text{IMRT}_{\text{iCycle}}$ plan, as performed in this study, took on average 1.5 hours (range 1 – 2.5 hours).

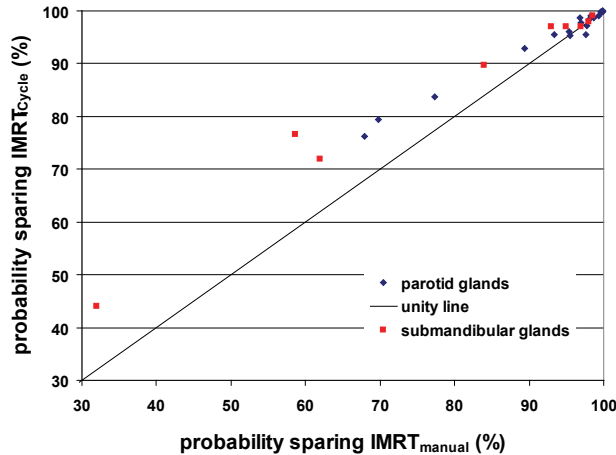


Figure 8.4: Probability of sparing at least one of the salivary glands when using either $\text{IMRT}_{i\text{Cycle}}$ or IMRT_{dos} .

8.4 Discussion

To our knowledge, this is the first prospective clinical study, evaluating possibilities for automated treatment plan generation. We included patients with a broad range of head-and-neck tumour sites in this study. For each study patient/dose interval, a plan generated with iCycle, our in-house algorithm for automated, multi-criterial optimization of beam angles and profiles, was compared with a plan manually generated by the dosimetrists, following the routine clinical protocol. In 32 out of 33 cases, physicians selected the automatically generated plan for treatment. Generally, $\text{IMRT}_{i\text{Cycle}}$ plans showed higher quality for a very broad range of plan parameters (see figure 8.2). This could explain the high consistency in the physicians' preferences for the automatically generated plans. Only once, a physician selected the IMRT_{dos} plan for treatment (patient 9; 0 – 46 Gy). In this case, $\text{IMRT}_{i\text{Cycle}}$ showed larger hotspots (107% of the prescribed dose) in parts of the PTV adjacent to the parotid glands. The fact that these hotspots resulted in reduced parotid gland mean doses was considered less important. With some minor adjustments in the standard wish-list used by iCycle, these hotspots could have been avoided (Breedveld *et al* 2007a). For the sequential boost of this patient, the physician preferred the $\text{IMRT}_{i\text{Cycle}}$ plan for treatment.

As demonstrated in previous studies, iCycle can also be used for optimizing fully non-coplanar IMRT plans (Breedveld *et al* 2012, Voet *et al* 2012). Compared to coplanar beam arrangements, minor improvements in OAR sparing were observed for the majority of head-and-neck cancer patients. Because delivery of non-coplanar plans would be more labour-intensive and time-consuming, as technicians have to enter the room to manually execute prescribed couch rotations, coplanar beam arrangements were used in this study.

Due to the applied wish-list, with multi-level objectives for the salivary glands, the sparing of different OARs was better balanced with IMRT_{iCycle}. For some patients, this resulted in less sparing for a lower-prioritized OAR, in benefit of higher prioritized ones. As an example, in patient 1, the mean dose in the oral cavity was 1.7 Gy higher for IMRT_{iCycle}, but the sparing of both the parotid glands and left submandibular gland was improved (mean dose reductions of 2.2 Gy, 3.5 Gy and 4.4 Gy, respectively).

For the patient group, differences between IMRT_{dos} and IMRT_{iCycle}, appear to be small. Nevertheless, individual patients may highly benefit from automated plan generation with iCycle, as shown by differences in NTCP values up to 18.5% for parotid glands and up to 27% for submandibular glands (see figure 8.3).

The basis of automated plan generation with iCycle is the automated steering of plan optimizations, using a wish-list with plan criteria that is identical for all patients. The observed high clinicians' preference and the favourable plan parameters for the IMRT_{iCycle} plans demonstrate that automated plan generation can indeed be successfully performed. As mentioned also in the Methods and Materials section (8.2), the wish-list used in this study was compiled based on discussions with two of the seven clinicians participating in the study. Obviously, with the input of only two of the clinicians, it was possible to generate a wish-list that served the needs of the others as well.

Other recent papers also addressed the possibility of (semi-)automatic treatment planning. Thieke *et al* (2007) described a multi-criterial optimization technique with an interactive plan navigation tool. They automatically generated a database with Pareto optimal IMRT plans. By interactively exploring this database the optimal treatment plan was identified. Teichert *et al* (2011) enhanced this algorithm such that the user could also navigate between plans with different beam configurations. In contrast to iCycle, the number of treatment beams and the beam configurations were manually predefined. Craft *et al* (2012) reported on multi-criterial plan generation for glioblastoma and pancreatic cancer patients, showing clear benefits in treatment planning efficiency and plan quality compared to manually generated treatment plans. Also in this work the beam arrangement was predefined. Another limitation of both multi-criterial optimization approaches is that manually selecting an optimal plan from the Pareto front might be very difficult and subjective, especially when many OARs are involved.

Zhang *et al* (2011) described an algorithm for automatic intensity-modulated radiation treatment planning for lung cancer. In their work the beam angle configuration was selected from an expert database, depending on tumour size and position. A drawback of this approach is that it remains unclear whether this configuration is optimal for a next patient.

As mentioned in the Methods and Materials section (8.2), iCycle can currently not be used in a direct way for generating clinical plans. Therefore, in this study, fully auto-

matically generated iCycle plans were “manually” converted into corresponding Monaco plans ($\text{IMRT}_{\text{iCycle}}$) of highly similar quality. Based on the superiority of $\text{IMRT}_{\text{iCycle}}$ plans compared to manually generated plans (IMRT_{dos}), we conclude that fully automated planning with iCycle becomes feasible, once the system has been prepared for direct clinical use. For the current study, there was however also an advantage of the conversion of iCycle plans. As both plans were in the end available in Monaco, the layout of presented dose distributions and dose-volume histograms was equal for $\text{IMRT}_{\text{iCycle}}$ and IMRT_{dos} , avoiding plan selection bias.

In an on-going project we aim at direct use of iCycle plans in the clinic, avoiding conversion into Monaco plans. In the meantime we have started to routinely apply iCycle for treatment of head-and-neck cancer patients as described in this paper, i.e. use of iCycle for generation of an IMRT plan, followed by conversion into a deliverable plan with highly similar quality in Monaco. More comparative studies are needed to investigate the importance of automated treatment planning for other tumour sites.

8.5 Conclusions

Compared to plans generated by dosimetrists with Monaco, plans automatically generated with iCycle were highly preferred by treating physicians. Quantitative plan analyses were in line with this preference. By routinely applying iCycle, optimized, patient specific treatment plans can be generated for large groups of patients with minimal user interaction.

Acknowledgements

The authors would like to thank the dosimetrists who generated the IMRT_{dos} plans and the physicians for entering patients in the study and evaluating the treatment plans.

Chapter 9

On the beam direction search space in computerized non-coplanar beam angle optimization for IMRT – prostate SBRT

Linda Rossi^{1,2}, Sebastiaan Breedveld¹, Ben Heijmen¹, Peter Voet¹, Nico Lanconelli²
and Shafak Aluwini¹

¹Department of Radiation Oncology, Erasmus MC Rotterdam, Groene Hilledijk 301, 3075
EA Rotterdam, The Netherlands

²Alma Mater Studiorum, Department of Physics, Bologna University, Italy

E-mail: s.breedveld@erasmusmc.nl

Published 3 August 2012 in *Physics in Medicine and Biology*, volume 57, pages 5441-5458

[doi:10.1088/0031-9155/57/17/5441](https://doi.org/10.1088/0031-9155/57/17/5441)

Abstract

In a recent paper we have published a new algorithm, designated ‘iCycle’, for fully-automated multi-criteria optimization of beam angles and intensity profiles. In this study, we have used this algorithm to investigate the relationship between plan quality and the extent of the beam direction search space, i.e. the set of candidate beam directions that may be selected for generating an optimal plan. For a group of 10 prostate cancer patients, optimal IMRT plans were made for Stereotactic Body Radiation Therapy (SBRT), mimicking High Dose Rate (HDR) brachytherapy dosimetry. Plans were generated for 5 different beam direction input sets, a coplanar set and four non-coplanar sets. For coplanar (CP) treatments, the search space consisted of 72 orientations (5° separations). The non-coplanar CK-space contained all directions available in the robotic CyberKnife treatment unit. The fully non-coplanar (F-NCP) set facilitated the highest possible degree of freedom in selecting optimal directions. CK⁺ and CK⁺⁺ were subsets of F-NCP to investigate some aspects of the CK-space. For each input set, plans were generated with up to 30 selected beam directions. Generated plans were clinically acceptable, according to an assessment of our clinicians. Convergence in plan quality occurred only after around 20 included beams. For individual patients, variations in PTV dose delivery between the 5 generated plans were minimal, as aimed for (average spread in $V_{95\%}$: 0.4%). This allowed plan comparisons based on organ at risk (OAR) doses, with the rectum considered most important. Plans generated with the non-coplanar search spaces had improved OAR sparing compared to the CP search space, especially for the rectum. OAR sparing was best with the F-NCP, with reductions in rectum D_{Mean} , $V_{40\text{Gy}}$, $V_{60\text{Gy}}$ and $D_{2\%}$ compared to CP of 25%, 35%, 37%, and 8%, respectively. Reduced rectum sparing with the CK search space compared to F-NCP could be largely compensated by expanding CK with beams with relatively large direction components along the superior-inferior axis (CK⁺⁺). Addition of posterior beams (CK⁺⁺ \rightarrow F-NCP) did not lead to further improvements in OAR sparing. Plans with 25 beams performed clearly better than 11-beam plans. For coplanar plans, an increase from 11 to 25 involved beams resulted in reductions in rectum D_{Mean} , $V_{40\text{Gy}}$, $V_{60\text{Gy}}$ and $D_{2\%}$ of 39%, 57%, 64%, and 13%, respectively.

9.1 Introduction

SBRT involves hypofractionated delivery of high radiation doses and requires highly conformal treatment plans and optimal geometrical precision in daily dose delivery (Blomgren *et al* 1995). Hypofractionation may result in a treatment benefit for prostate cancer, as the α/β ratio could be as low as 1.5 (Brenner & Hall 1999, Fowler *et al* 2001, King & Fowler 2001, Miralbell *et al* 2012). Several randomized studies have demonstrated advantages of moderate hypofractionation in prostate cancer (Arcangeli *et al* 2011, Norkus *et al* 2009, Pollack *et al* 2006, Yeoh *et al* 2011).

Based on promising results with the strongly hypofractionated prostate HDR brachytherapy (Demanes *et al* 2005, Grills *et al* 2004), interest has grown in developing non-invasive external beam radiotherapy (EBRT) techniques with as little as four fractions. Several of these studies were based on the robotic CyberKnife treatment unit (Accuray, Inc) with its image-guided tumour tracking technology and easy use of non-coplanar beams (Aluwini *et al* 2010, Freeman & King 2011, Freeman *et al* 2010, Fuller *et al* 2011, 2008, Jabbari *et al* 2012, Katz & Santoro 2009, Kilby *et al* 2010, King *et al* 2003, 2011, Townsend *et al* 2010).

The impact of beam angle optimization on the quality of treatment plans has been investigated in many studies (Aleman *et al* 2009, De Pooter *et al* 2008, Pugachev & Xing 2001, Voet *et al* 2012, Van de Water *et al* 2011a, Woudstra & Storchi 2000). To our knowledge, very little is known on the importance of the extent of the beam angle search space in computer optimization of beam orientations, especially for non-coplanar techniques.

Computer optimization of beam angles has been investigated for many years in our institution (De Pooter *et al* 2008, Voet *et al* 2012, Van de Water *et al* 2011a, Woudstra & Storchi 2000). Most papers relate to 3D conformal techniques (De Pooter *et al* 2008, Voet *et al* 2012, Woudstra & Storchi 2000), or to CyberKnife treatments with circular cones, (Van de Water *et al* 2011a). Recently, we developed a new algorithm, designated ‘iCycle’, (Breedveld *et al* 2012), for multi-criterial optimization of beam angles and IMRT fluence profiles. In this study we have used iCycle to investigate the importance of the beam angle search space in computer optimization of prostate SBRT plans that mimic HDR brachytherapy dose distributions. Plan comparisons were made for 5 different search spaces, including one with only coplanar directions, and one with the orientations available at the CyberKnife.

9.2 Methods and materials

9.2.1 Patients

Planning CT-scans of ten prostate cancer patients, previously treated in our institution with the CyberKnife, were included in this study. Patients were treated with a dose of 38 Gy, delivered in 4 fractions with a dose distribution that resembled prostate HDR brachytherapy. The CT-scan slice distances were 1.5 mm, the average scan length was 47.4 ± 6.7 cm (range: 35.7-55.7 cm). PTVs included the entire delineated GTV plus a 3 mm margin. The average volume was 90.8 ± 23.1 cc (range: 69.5-145.4 cc). Within the GTV, the peripheral zone (PZ) was defined with the help of MR-images. Patients had 4 implanted markers for image guidance and were treated supine with their feet towards the robotic manipulator.

9.2.2 iCycle

All treatment plans were generated with iCycle, our novel in-house developed algorithm for automated, multi-criterial optimization of beam angles and IMRT fluence profiles. The algorithm is described in detail in [Breedveld *et al* \(2012\)](#). Here a brief summary of its features is provided.

Fully-automated plan generation with iCycle is based on a ‘wish-list’, defining hard constraints that are strictly met and prioritised objectives ([Breedveld *et al* 2007a](#)). The higher the priority of an objective, the higher the chance that the goal will be approached closely, reached or even exceeded. Furthermore, a list of candidate beam orientations for inclusion in the plan is needed. The beam direction search spaces and wish-list used in this study are described in detail below in the sections [9.2.3](#) and [9.2.4](#), respectively. A plan generation starts with zero beams. Optimal directions are sequentially added to the plan in an iterative procedure, up to a user-defined maximum number of beams. After each beam addition, iCycle generates a Pareto optimal IMRT plan including the beam directions selected so far. Consequently, plan generation for a patient always results in a series of Pareto optimal plans with increasing numbers of beams. For example, in this study the selected maximum number of beams is 30, resulting for each case in Pareto optimal IMRT plans with 30, 29, 28, 27, ... beams. By design, addition of a beam improves plan quality regarding the highest prioritized objective that can still be improved on ([Breedveld *et al* 2012](#)).

9.2.3 Investigated beam direction input sets (search spaces)

In this study, the isocentre was placed in the centre of the tumour. Beam directions were defined by straight lines (beam axes) connecting the isocentre with focal spot positions situated on a sphere centred around the isocentre. The five investigated beam direction search spaces were defined as follows:

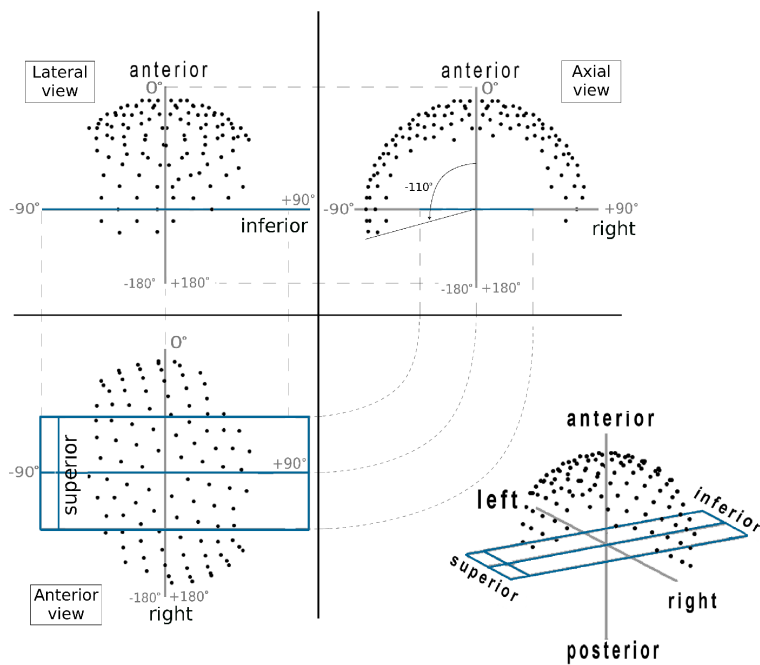


Figure 9.1: CyberKnife (CK) search space. Dots represent focal spot positions.

1. **CP** (coplanar): 72 equi-angular orientations in the axial plane through the isocentre, covering 360° around the patients (angular separation 5°).
2. **CK** (used by the CyberKnife robotic treatment unit): graphical presentation shown in figure 9.1. The set consists of 117 directions. Interesting features are the absence of beams with a large posterior component (right upper panel in figure 9.1: available directions in the axial plane are limited to $[-110^\circ, 110^\circ]$), and the asymmetry in the beam direction set (left lower panel in figure 9.1) related to the asymmetric position of the robotic manipulator relative to the treatment couch.
3. **F-NCP** (fully non-coplanar): largest set of all 5, theoretical, i.e. not related to a particular treatment device. Ideally, it should represent the search space as defined by all focal spots on a complete sphere around the isocentre. In the axial plane, through the isocentre, the angular distance between directions is 5° (F-NCP includes CP). Non-coplanar directions are separated by 10° . However, iCycle removes the non-coplanar treatment beams that enter (partially) through the end of the CT dataset, which limits the available number of beam directions due to the finite lengths of the CT data sets (section 9.2.1). Because of this limitation, the maximum deviation from the AP-axis in the sagittal plane is around 55° . F-NCP includes around 500 beam orientations, depending on the patient.
4. **CK⁺⁺**: as F-NCP, however excluding (*only*) directions with a posterior component outside the borders of the CK search space. In the axial plane this results in exclusion of beams outside the $[-110^\circ, 110^\circ]$ range (figure 9.1, upper right panel). Depending on the patient, CK⁺⁺ has around 300 beam directions.
5. **CK⁺**: as F-NCP, however excluding *all* directions outside the borders of the CK search space (figure 9.1). Because of the higher focal spot density, the number of available directions in CK⁺ is higher than for CK, i.e. 186 vs. 117.

9.2.4 iCycle generation of prostate SBRT plans

iCycle was used to optimize beam angles and intensity profiles for high quality SBRT plans, mimicking HDR brachytherapy dose distributions. Table 9.1 shows the applied wish-list with planning constraints and objectives in the upper and lower parts, respectively. The wish-list was established in a trial-and-error procedure to ensure for this patient population, generation of high quality plans with the desired balance between the clinical objectives (see also Breedveld *et al* (2012), Voet *et al* (2012)). Most important clinical goals were adequate PTV coverage and a maximally reduced rectum dose.

The two highest priority objectives, defined with Logarithmic Tumour Control Probability (LTCP) functions (Alber & Reemtsen 2007) aimed at adequate PTV dose delivery.

Table 9.1: Applied wish-list for all study patients. For definition of Ring 1, 2 and 3 see section 9.2.4.

Constraints				
	Structure	Type	Limit	
	PTV	maximum	59-69 Gy	
	Rectum	maximum	38 Gy	
	Urethra	maximum	40 Gy	
	Bladder	maximum	41.8 Gy	
	Penis Scrotum	maximum	4 Gy	
	Penis Scrotum	mean	2 Gy	
	Ring 2	maximum	15 Gy	
	Ring 1	maximum	20 Gy	
Objectives				
Priority	Structure	Type	Goal	Parameters
1	PTV	LTCP	1	$D_p = 34-38 Gy, \alpha = 0.7,$ Sufficient = 0.003-0.20
2	PTV	LTCP	4	$D_p = 55-60.8 Gy, \alpha = 0.1-0.2,$ Sufficient = 4-26
3	Rectum	mean	0 Gy	
4	PZ	LTCP	1	$D_p = 45 Gy, \alpha = 0.9$
5	Urethra	mean	0 Gy	
6	Bladder	mean	0 Gy	
7	Ring 3	maximum	15 Gy	
8	Rectum	maximum	30 Gy	
9	Bladder	maximum	35 Gy	
10	Penis Scrotum	maximum	0 Gy	
11	Left and right Femur head	maximum	24 Gy	

The first focused on control of PTV doses around 34-38 Gy , while the second mainly steered PTV doses around 55-60.8 Gy . For each patient, the goal was to generate, for all 5 beam angle search spaces (section 9.2.3), plans with highly similar PTV dose delivery, all close to the dose delivered in the clinical plan, allowing comparison of search spaces based on OAR plan parameters. To this purpose, prior to the final plan generations for a patient, trial plans were generated to fine-tune the LTCP sufficient and α parameters (Breedveld *et al* 2009a) for a PTV maximum dose constraint (table 9.1) equal to the maximum dose in the clinical plan. For each patient, a fixed set of sufficient, α , and PTV maximum dose values was used for the final plan generation for all five search spaces.

As in clinical practice, reduction of rectum dose delivery was the most important OAR objective (priority 3 in table 9.1), aiming at a mean dose of 0 Gy . With this choice, the optimizer would only reduce doses to other OARs to the extent that this would not compromise reaching the lowest possible mean rectum dose. Other OAR considered with lower priorities were urethra, bladder, penis, scrotum and femoral heads. Other structures, *Rings*, were defined to control and reduce the dose to healthy tissues: ‘Ring 1’ includes all tissue between 2 and 3 cm from the PTV, ‘Ring 2’ was all tissue between

the body contour and the body contour-2cm and ‘Ring 3’ referred to all tissue in between Ring 1 and Ring 2. Hard constraints on Ring 1 and Ring 2 had to enforce a steep dose fall-off outside the target and to limit the entrance dose, respectively. The priority 7 objective on Ring 3 aimed at dose reduction to healthy tissues, also if not part of an OAR.

For all beam direction search spaces considered in this study, the simulations assumed that beam collimation was performed with a dynamic multi-leaf collimator (MLC) with a 5 mm leaf width. Maximum field size was $10 \times 12 \text{ cm}^2$ and leaves had full interdigitation and overtravel. For dose calculations, percentual depth dose curves and profiles of an Elekta Synergy 6 MV beam, collimated with an MLCi2, were used. Pencil beam kernels for optimization were derived as described in [Storchi & Woudstra \(1996\)](#). Equivalent path length correction was used for inhomogeneity correction.

9.2.5 Details on plan evaluation and comparison

The plans in this study were evaluated by a clinician (SA) to check clinical acceptability. In accordance with the ICRU-83 report ([ICRU Report 83 2010](#)), $D_{2\%}$ and $D_{98\%}$ were reported instead of maximum and minimum doses, respectively. In line with QUANTEC findings ([Michalski et al 2010](#)), rectum dose delivery reporting included $V_{40\text{Gy}}$ and $V_{60\text{Gy}}$, calculated by first converting delivered doses to a 2 Gy/fraction regime using an alpha/beta parameter of 3 Gy. Apart from doses delivered to the PTV, PZ and OARs, we also analyzed $V_{10\text{Gy}}$, $V_{20\text{Gy}}$, and $V_{30\text{Gy}}$, the patient volumes receiving more than 10, 20, and 30 Gy, respectively. Evaluations also included the conformity index (CI) calculated as the ratio of the total tissue volume receiving 38 Gy or more and the PTV (almost 100% of the PTV received 38 Gy, see Results section). Hard constraints on dose delivery to the penis and the scrotum guaranteed negligible doses to these structures in all plans (table 9.1), which are not reported in the Results section.

As described in section 9.2.4, for each patient we aimed at highly similar PTV doses for all five search spaces. In the Results section it is demonstrated that differences were indeed very small. For this reason comparison of plans and search spaces could be based on doses delivered to healthy tissues with the rectum being the most important one. The two-sided Wilcoxon signed-rank test was used to compare plan parameters in the various search spaces. A p -value of <0.05 was defined as statistically significant.

9.2.6 Treatment time calculation for the CK search space

We calculated treatment times for the hypothetical situation that the CyberKnife would be equipped with an MLC. Treatment times consist of beam-on time, linac travel time, and imaging time. For calculation of beam-on times, we used a leaf sequencing algorithm described in [van Santvoort & Heijmen \(1996\)](#), assuming a linac output of 1000 MU/min (as available for the current CyberKnife), a maximum leaf speed of 2.5 cm/s and full

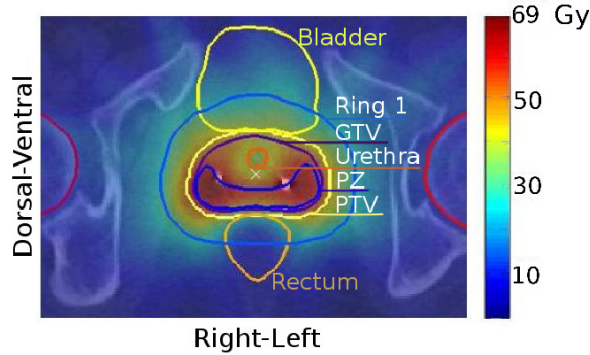


Figure 9.2: Axial dose distribution for the 25-beam plan generated with the CK search space for the first study patient. For definition of Ring 1 see section 9.2.4.

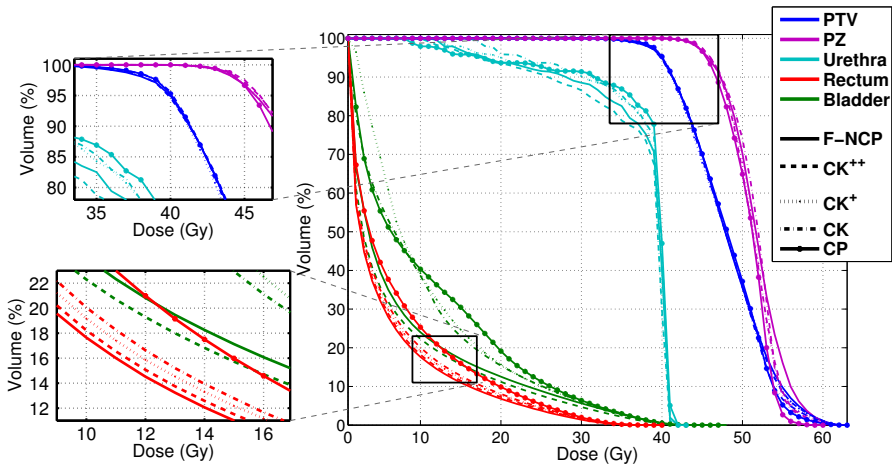


Figure 9.3: DVH comparison for patient 1 for five 25-beam plans, each generated for one of the five studied search spaces.

leaf interdigitation and overtravel (see also section 9.2.4). Leaf synchronization was not applied. The linac travel time is the time to travel through all selected focal spot positions. However, CyberKnife movements are not totally free, i.e. it cannot freely travel from each spot position to any other, but it sometimes has to pass unselected (but allowed, figure 9.1) positions to reach a next selected position. The applied travel time calculation algorithm selects the shortest path, considering all possible movements between spot positions (Van de Water *et al* 2011a). For the treatment time calculations, we assumed that prior to dose delivery from a focal spot position, images were acquired to verify, and if needed, correct alignment of the beam to be delivered with the current

tumour position. Imaging time takes only 2 seconds. However, CK has some node positions from which it is not possible to take an image. To handle this, the machine has to travel to the nearest node position from which imaging is allowed and come back to the delivery position. This aspect was also considered in the calculation of the treatment times.

9.3 Results

9.3.1 Generated plans

In this section, plans and analyses performed for the first study patient are described in some detail to provide examples of the investigations performed for all 10 patients.

Figure 9.2 shows an axial dose distribution for the 25-beam plan generated with the CK search space. Clearly visible are the high degree of rectum sparing, the reduced dose in the urethra, and the increased dose in the peripheral zone (PZ), as enforced by the applied wish-list (table 9.1).

Figure 9.3 shows DVHs for the 25-beam plans generated with each of the 5 search spaces in this study. As aimed for (section 9.2.4), PTV coverages for the 5 plans were highly similar (upper left zoom). Rectum sparing was best for F-NCP and CK⁺⁺, while for the coplanar (CP) plan, rectum dose was clearly highest (lower left zoom). F-NCP was best for bladder and CK⁺⁺ for urethra, with F-NCP second. Obviously, plans for the non-coplanar search spaces with the largest extents (F-NCP and CK⁺⁺) were most favourable for this patient.

Figure 9.4 shows plan parameters as a function of the number of beams in the plan. For all beam numbers, PTV coverage was very similar for the 5 search spaces. The second row shows that for all search spaces, rectum dose parameters improved with increasing numbers of beams, with some levelling off between 15-20 beams. Also bladder D_{Mean} , urethra D_{Mean} , $V_{10\text{Gy}}$, $V_{20\text{Gy}}$, and $V_{30\text{Gy}}$ improved with increasing numbers of beams. A very similar behaviour of plan quality on numbers of involved beams was seen for all 10 patients in this study. In the next section, population data will be provided for PTV and rectum.

9.3.2 Plan quality vs number of beams in plans, PTV and rectum

The left panel in figure 9.5 shows the average PTV $V_{95\%}$ and PTV $D_{98\%}$ for the 10 study patients, as a function of the number of beams in the plans, normalized to the CP 10-beam plan. For each search space, these quantities are largely independent of the number of beams (normalized values differ up to 0.8% and 2% for average PTV $V_{95\%}$ and $D_{98\%}$, respectively). The trend to slightly reduced PTV dose delivery with increasing number of beams is (partly) related to enhanced urethra sparing with more beams (no data presented). For all beam numbers, these PTV dose parameters are also highly

similar for the 5 search spaces with variations up to less than 0.5%. The right panel demonstrates substantial differences between the search spaces in population averaged rectum D_{Mean} and rectum $V_{60\text{Gy}}$, with lowest values for F-NCP and least favourable values for CP. For 20 beams, F-NCP averaged rectum D_{Mean} and $V_{60\text{Gy}}$ were 29% and 45% lower compared to CP. For all 5 search spaces, rectum dose improved with increasing number of beams. None of the curves in the right panel fully levels off, but reductions with beam number are clearly most prominent up to around 20 beams. In the remainder of this paper, data for 25-beam plans will be reported, unless stated otherwise.

9.3.3 25-beam plans - Coplanar (CP) vs non-coplanar beam direction search spaces

Table 9.2 provides a comparison of the CP search space with the four non-coplanar spaces regarding plan parameters of the generated 25-beam plans.

As aimed for (section 9.2.4), differences in PTV D_{Mean} , PTV $V_{95\%}$ and PTV $D_{98\%}$ between the 5 search spaces were clinically and/or statistically insignificant. Compared to CP, only PTV $D_{2\%}$ was around 3% higher for non-coplanar set-ups ($p < 0.05$), but clinically these increases were considered unimportant. No relevant differences were observed in the PZ parameters. Because of this high similarity in target dose for the 5 search spaces, in the remainder of this paper, plan comparisons are focused on organs at risk and especially on the rectum.

The rectum population mean plan parameters were clearly lowest for the 4 non-coplanar search spaces (table 9.2). For the largest search space, F-NCP, population mean reductions relative to CP in rectum D_{Mean} , $V_{40\text{Gy}}$, $V_{60\text{Gy}}$, and $D_{2\%}$ were as large as 25.0%, 34.9%, 36.5%, and 7.5%, respectively. For CK, these reductions were smallest but still highly relevant (18.5%, 23.2%, 21.4% and 3.9%, respectively). Figure 9.6 demonstrates that the superiority of the non-coplanar search spaces holds for all individual patients. Patient 7 had the highest CP rectum dose parameters, while percentual reductions with the non-coplanar set-ups were also highest (figure 9.6). Regression analyses showed, for all 4 non-coplanar search spaces, increasing percentual reductions in rectum dose parameters for increasing CP parameters ($p=0.001-0.03$), i.e. patients with less favourable CP rectum parameters had largest reductions when switching to a non-coplanar plan.

Population mean urethra doses were equal for all 5 search spaces (table 9.2). Differences between non-coplanar spaces and CP in mean bladder dose were highly patient specific. F-NCP and CK⁺⁺ had on average $\approx 9\%$ lower mean bladder doses, while for CK⁺ and CK, mean bladder doses were around $\approx 11\%$ higher compared to CP. None of these differences were statistically significant. With CP, doses in the femoral heads were already low, but substantial percentual reductions were seen for the non-coplanar beam sets. Also $V_{10\text{Gy}}$ and $V_{20\text{Gy}}$ were lowest for the non-coplanar sets.

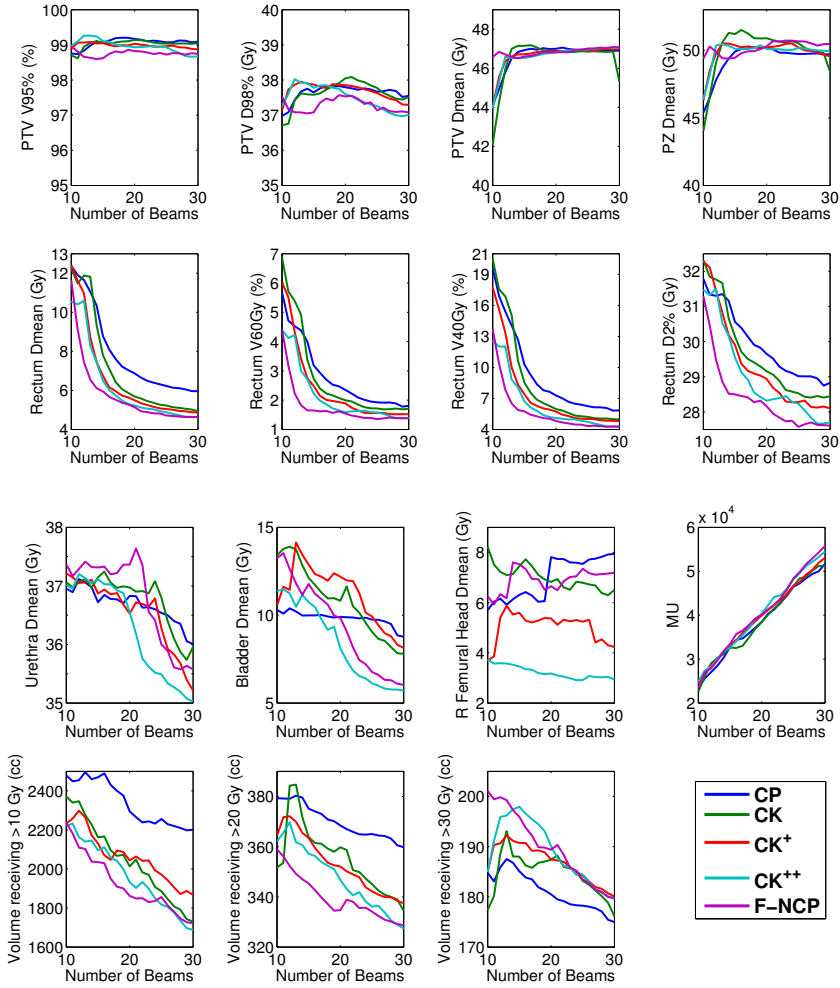


Figure 9.4: Dosimetrical results for patient 1 for plans with 10 up to 30 beams for the 5 studied input beam sets.

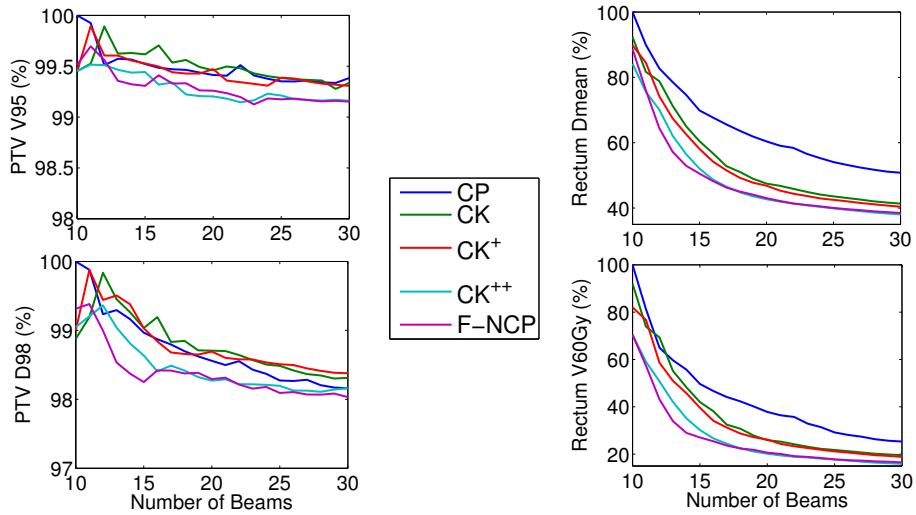


Figure 9.5: Population averaged PTV (left) and rectum (right) plan parameters as function of beam number, for 10-30 beam plans. All percentages are relative to absolute population mean values of the CP 10-beam plan, i.e. PTV $V_{95\%}=99.5\%$, PTV $D_{98\%}=37.8 Gy$, Rectum $D_{Mean}=11.3 Gy$ and Rectum $V_{60Gy}=8\%$.

V_{30Gy} , the total delivered number of MU and the conformity index (CI) were the only parameters for which CP plans did on average (slightly) better than non-coplanar set-ups. V_{30Gy} and MU were 3-5% and 8% lower in the CP plans. The mean CI in the CP plans for the 10 study patients was 1.2, which increased to 1.27-1.31 for the non-coplanar sets.

Table 9.2: Comparison of dosimetric plan parameters of the generated 25-beam plans, for the five investigated beam angle search spaces. Mean values, standard deviations (SD) and ranges refer to the 10 patients in the study. The first data column reports the results obtained with the coplanar (CP) search space. In the next columns, percentage differences of the other spaces with CP are shown, i.e. $100 \times (\text{other_search_space} - \text{CP}) / \text{CP}$. (*) refers to all tissues receiving >10 , >20 or >30 Gy. Statistically non-significant (NS) for $p > 0.05$.

Target	CP	F-NCP - CP (%)	CK ⁺⁺ - CP (%)	CK ⁺ - CP (%)	CK - CP (%)
	Mean \pm 1SD [Range]	Δ Mean \pm 1SD [Range]	p	Δ Mean \pm 1SD [Range]	p
Rectum					
D_{Mean}	46.7 \pm 2.2 (Gy)	0.4 \pm 1.2	NS	0.3 \pm 1.0	NS
$V_{100\%}$	99.0 \pm 0.6 (%)	-0.3 \pm 0.5	NS	-0.1 \pm 0.3	NS
$D_{95\%}$	37.2 \pm 0.7 (Gy)	-0.3 \pm 1.2	NS	0.1 \pm 1.1	NS
$D_{98\%}$	56.5 \pm 3.8 (Gy)	2.7 \pm 4.0	NS	3.1 \pm 4.1	NS
$D_{2\%}$	50.4 \pm 2.3 (Gy)	0.9 \pm 2.0	NS	0.5 \pm 1.9	NS
Urethra					
D_{Mean}	6.2 \pm 2.1 (Gy)	-25.0 \pm 9.0	.002	-20.2 \pm 8.1	.002
$V_{100\%}$	6.6 \pm 2.7 (%)	-34.9 \pm 14.2	.002	-25.8 \pm 13.3	.002
$D_{95\%}$	2.4 \pm 1.1 (%)	-36.5 \pm 19.3	.002	-22.6 \pm 21.8	.004
$D_{2\%}$	29.5 \pm 2.2 (Gy)	-7.5 \pm 4.3	.002	-4.4 \pm 3.3	.002
Bladder					
D_{Mean}	32.2 \pm 3.5 (Gy)	-0.4 \pm 1.3	NS	-0.3 \pm 1.6	NS
$D_{2\%}$	40.0 \pm 0.2 (Gy)	-0.4 \pm 0.6	NS	-0.4 \pm 0.6	NS
Femoral Heads					
D_{Mean}	8.8 \pm 2.4 (Gy)	-9.0 \pm 18.4	NS	11.2 \pm 17.3	NS
$D_{2\%}$	34.4 \pm 3.4 (Gy)	0.9 \pm 1.6	NS	2.4 \pm 2.1	.01
Other					
R D_{Mean}	9.1 \pm 2.7 (Gy)	-35.1 \pm 21.5	.002	-34.3 \pm 15.5	.002
R $D_{2\%}$	15.6 \pm 0.7 (Gy)	-24.2 \pm 13.9	.002	-18.7 \pm 4.5	.002
L D_{Mean}	9.0 \pm 2.5 (Gy)	-32.6 \pm 26.9	.004	-31.3 \pm 19.6	.004
L $D_{2\%}$	15.4 \pm 0.8 (Gy)	-19.9 \pm 15.0	.002	-18.9 \pm 13.8	.004
V _{100%} *	2020 \pm 331 (cc)	-17.0 \pm 5.8	.002	-13.4 \pm 4.7	.002
V _{200%} *	352 \pm 63 (cc)	-8.3 \pm 2.2	.002	-5.3 \pm 1.8	.002
V _{300%} *	169 \pm 31 (cc)	3.4 \pm 2.5	.006	4.5 \pm 2.3	.004
CI	1.2 \pm 0.1	7.0 \pm 2.9	.002	7.1 \pm 2.2	.002
MU	43533 \pm 2694	8.4 \pm 4.8	.002	7.4 \pm 6.0	.002

9.3.4 25-beam plans - Comparison of non-coplanar search spaces

As described in detail in section 9.2.3, non-coplanar search spaces increased in extent when going from CK to CK⁺ to CK⁺⁺ and finally to F-NCP. Briefly, CK⁺ had the same boundaries as CK but a higher spot density, CK⁺⁺ was an expansion of CK⁺ with beams with relatively large direction components along the superior-inferior axis and F-NCP was an extension of CK⁺⁺, making it the only non-coplanar search space with posterior beams. In this section, changes in plan parameters related to these increases in degree of freedom for selecting optimal non-coplanar beam angles are discussed.

CK → CK⁺ As also visible in table 9.2, CK has the highest mean rectum dose parameters of the 4 non-coplanar beam direction search spaces. Increasing the focal spot density did only marginally improve rectum dose delivery, although reductions in D_{Mean} of 2.2% and in $V_{40\text{Gy}}$ of 3.2% were statistically significant. For urethra and bladder, differences in delivered dose were negligible (table 9.2). Significant differences were found for femoral head doses. With CK⁺, D_{Mean} and $D_{2\%}$ for right and left head decreased by 15%, 9%, 11% and 10%, respectively (p -values: 0.02, 0.04, 0.04, 0.03). Small, but statistically significant, differences were found for $V_{20\text{Gy}}$ (CK⁺ 1% lower, $p=0.01$), $V_{30\text{Gy}}$ (CK⁺ 1.1% higher, $p=0.02$), and for CI (CK⁺ 1.5% higher, $p=0.01$).

CK⁺ → CK⁺⁺ With this increase in search space, population mean rectum D_{Mean} , $V_{40\text{Gy}}$, $V_{60\text{Gy}}$ and $D_{2\%}$ were reduced by as much as 6.8%, 12.0%, 16.9%, and 3.5%, respectively ($p=0.002$). Large improvement was also found for the bladder with a reduction in D_{Mean} of 26.9% ($p=0.01$). $V_{20\text{Gy}}$ was also improved with CK⁺⁺ (1.7%, $p=0.002$). CI was slightly better for CK⁺ (2.3%, $p=0.001$).

CK⁺⁺ → F-NCP Adding posterior beams by going from CK⁺⁺ to F-NCP did not result in relevant further reductions in rectum dose (table 9.2). Very small improvements were seen for $V_{20\text{Gy}}$ (1.5%, $p=0.006$), $V_{30\text{Gy}}$ (1.6%, $p=0.001$), and CI (2.0%, $p=0.004$).

9.3.5 25-beam plans - Distribution of selected beam orientations

Figure 9.7 shows selected beam directions for the 25-beam F-NCP plan of each individual study patient. Clearly, there is a preference for beams with a large lateral component. Comparison of the right panels of figures 9.7 and 9.8 shows that most high-weight beams in the F-NCP plans are within the CK⁺⁺ search space. Apparently, beams with a large posterior component are not frequently selected or have low weights.

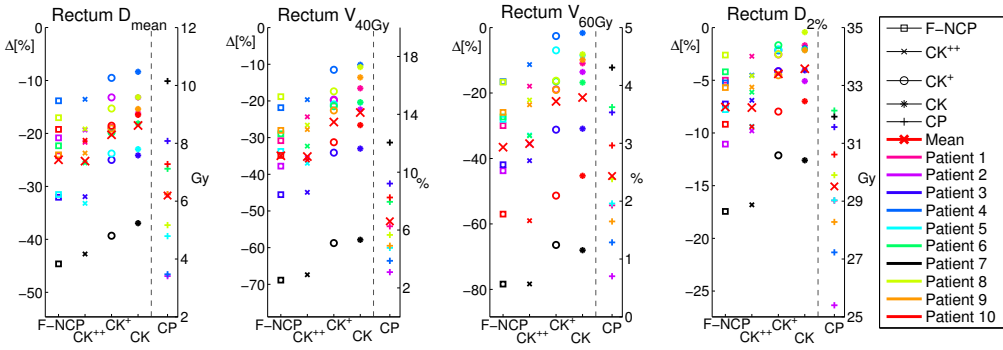


Figure 9.6: Comparison of the CP search space with the four non-coplanar spaces for four rectum plan parameters. On the right of each panel, the CP absolute values for each patient are reported. The four columns on the left report the percentage differences for non-coplanar search spaces with the CP plan. For all patients and all parameters, differences $\Delta[\%]$ are below zero, showing the improved rectum sparing with non-coplanar beam search spaces. All plans are with 25 beams.

9.3.6 25-beam plans - Treatment times for the CK search space

Treatment times for the 25-beam CK plans were on average 18.1 ± 0.5 minutes, including dose delivery, robot motion and imaging and set-up correction prior to delivery of each beam (section 9.2.6).

9.3.7 11 vs 25-beam coplanar plans

As visible in figure 9.4 for patient 1 and in the right panel of figure 9.5 for the patient population, OAR plan parameters may substantially improve with increasing numbers of beams in the plans. On regular treatment units, IMRT plans are generally delivered with coplanar beam set-ups with ≤ 11 beams. Table 9.3 compares coplanar plans with 11 and 25 beams. Although differences in PTV parameters are statistically significant, they are small, and clinically the obtained PTV doses are considered highly comparable. An important consideration here is that the difference in PTV $V_{95\%}$, our most important parameter for PTV dose evaluation, is very small. The most striking differences were found for the rectum with improvements in D_{Mean} , $V_{40\text{Gy}}$, $V_{60\text{Gy}}$ and $D_{2\%}$ of 39.2%, 57%, 63.7%, and 12.6% ($p=0.002$), when increasing the number of beams from 11 to 25. Bladder D_{Mean} and $D_{2\%}$ reduced by 14.4% ($p=0.002$) and 5.3% ($p=0.004$), respectively, and $V_{10\text{Gy}}$ improved by 11.1% ($p=0.002$). When switching to 25-beam plans, the MU increased on average by 75.7% ($p=0.002$).

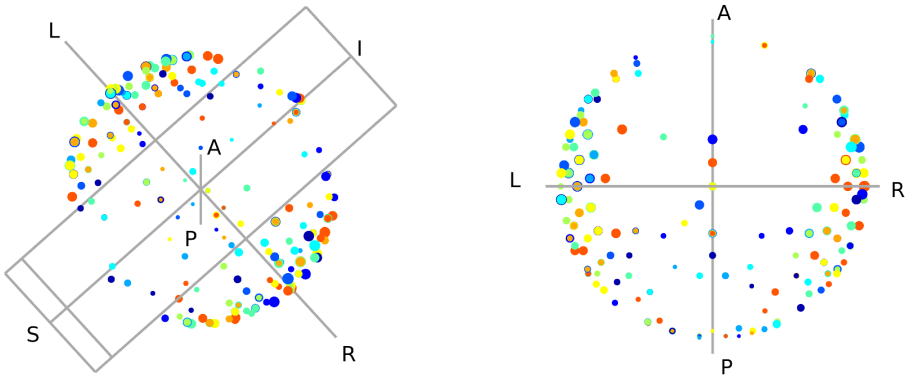


Figure 9.7: Selected focal spots/beams by iCycle for 25-beam F-NCP plans for all 10 patients in a 3D (left) and an axial view (right). Colours refer to different patients, beam weights are proportional to the dot diameters.

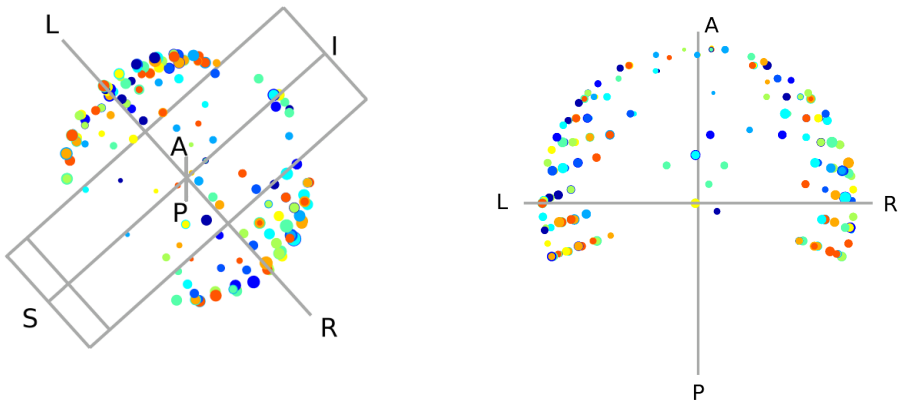


Figure 9.8: Selected focal spots/beams by iCycle for 25-beam CK⁺⁺ plans for all 10 patients in a 3D (left) and an axial view (right). Colours refer to different patients, beam weights are proportional to the dot diameters.

Table 9.3: Results for 10 patients for 11 and 25 coplanar beam plans. The first column reports the results obtained with the 11 beam coplanar configuration. In the next columns, the percentage decrease from the 11 beams CP results are shown. (*) refers to all tissues receiving >10, >20 or >30 Gy.

	11 beams, CP		25 vs 11 beams, CP (%)		
	Mean \pm 1SD	[Range]	Δ Mean \pm 1SD	[Range]	p-value
Target					
PTV D_{Mean}	45.1 \pm 1.0 (Gy)	[43.4,46.7]	3.4 \pm 3.1	[0.2,9.1]	.002
PTV $V_{95\%}$	99.4 \pm 0.4 (%)	[98.7,99.9]	-0.5 \pm 0.5	[-1.8,0.3]	.01
PTV $D_{98\%}$	37.8 \pm 0.5 (Gy)	[37.1,38.6]	-1.5 \pm 1.4	[-3.9,1.6]	.02
PTV $D_{2\%}$	52.8 \pm 1.8 (Gy)	[49.5,56.1]	7.0 \pm 4.2	[1.6,13.2]	.002
PZ D_{Mean}	48.1 \pm 0.9 (Gy)	[46.5,48.9]	4.6 \pm 4.5	[-0.8,11.5]	.006
PZ $D_{98\%}$	42.5 \pm 1.0 (Gy)	[39.8,43.3]	-12.4 \pm 2.8	[-16.4,-5.4]	.002
Rectum					
D_{Mean}	10.2 \pm 2.9 (Gy)	[5.5,13.7]	-39.2 \pm 9.0	[-48.0,-18.6]	.002
$V_{40\text{Gy}}$	15.2 \pm 4.9 (%)	[7.8,22.2]	-57.0 \pm 9.2	[-63.3,-34.3]	.002
$V_{60\text{Gy}}$	6.5 \pm 2.4 (%)	[3.2,10.9]	-63.7 \pm 9.3	[-78.1,-46.9]	.002
$D_{2\%}$	33.7 \pm 1.5 (Gy)	[31.3,35.4]	-12.6 \pm 4.2	[-19.0,-7.4]	.002
Urethra					
D_{Mean}	33.1 \pm 3.3 (Gy)	[27.5,36.9]	-2.6 \pm 1.2	[-4.7,-0.9]	.002
$D_{2\%}$	40.0 \pm 0.2 (Gy)	[39.7,40.5]	-0.2 \pm 0.5	[-1.2,0.7]	NS
Bladder					
D_{Mean}	10.2 \pm 2.3 (Gy)	[5.1,13.7]	-14.4 \pm 9.1	[-28.1,-2.5]	.002
$D_{2\%}$	36.3 \pm 3.0 (Gy)	[27.9,37.9]	-5.3 \pm 3.7	[-9.8,0.6]	.004
Femoral Heads					
R D_{Mean}	7.8 \pm 2.5 (Gy)	[4.7,12.3]	19.9 \pm 30.1	[-14.0,92.1]	NS
R $D_{2\%}$	15.3 \pm 2.0 (Gy)	[12.9,18.4]	3.5 \pm 13.0	[-11.0,27.4]	NS
L D_{Mean}	8.0 \pm 1.7 (Gy)	[6.0,10.8]	12.7 \pm 17.3	[-19.5,44.5]	.03
L $D_{2\%}$	15.2 \pm 1.3 (Gy)	[13.8,17.3]	2.0 \pm 8.7	[-12.2,12.5]	NS
Other					
$V_{10\text{Gy}}^*$	2274 \pm 382 (cc)	[1824,3163]	-11.1 \pm 2.6	[-15.2,-6.9]	.002
$V_{20\text{Gy}}^*$	365 \pm 67 (cc)	[295,520]	-3.4 \pm 2.7	[-7.4,2.2]	.006
$V_{30\text{Gy}}^*$	178 \pm 33 (cc)	[143,257]	-4.8 \pm 3.0	[-9.4,0.2]	.004
CI	1.2 \pm 0.1	[1.1,1.3]	-2.5 \pm 4.5	[-10.0,3.1]	NS
MU	24791 \pm 1302	[22624,26844]	75.7 \pm 9.2	[56.8,91.7]	.002

9.3.8 Calculation times

iCycle simulations were done in Matlab 7.12, R2011a, The Mathworks Inc., on a 4 socket 10-core Intel Xeon E7. Plan optimization required ≈ 35 hours to generate for one patient F-NCP plans with up to 25 beams, i.e. 25 complete plans have been generated and all data are individually available, and around ≈ 45 hours for up to 30 beams. These times reduced to ≈ 15 and ≈ 25 hours to generate coplanar treatment plans.

9.4 Discussion

Recently, we have presented iCycle, our in-house developed algorithm for integrated, multi-criterial optimization of beam angles and profiles (Breedveld *et al* 2012). For plan generation, iCycle uses a *priori* defined plan criteria (wish-list, section 9.2.4 and table 9.1) and a beam direction search space. The wish-list is used to fully automatically generate high quality plans without interactive tweaking of parameters such as weighting factors in the cost function. For a plan with N selected orientations, the solution is Pareto optimal regarding the generated beam profiles (Breedveld *et al* 2009a, 2012). To ensure generation of clinically acceptable plans with favourable balances in the outcomes for the various plan objectives, wish-lists are developed in close collaboration with treating clinicians. This study is based on 1500 treatment plans generated with iCycle (10 patients, 5 beam sets, 30 beams). Due to the automation, the plan generation workload was minimal and plan quality was independent of the experience and skills of human planners. To our knowledge, this is the first paper investigating in details the impact of the extent of the beam angle search space in computer optimization of IMRT dose distributions.

For each individual patient, PTV doses in the iCycle generated plans for the five investigated search spaces were highly similar (figures 9.3, 9.4, 9.5 and table 9.2), and tuned to be in close agreement with the clinically delivered dose. This allowed focusing plan comparisons on OARs, and specifically on the highest priority OAR, the rectum. Rectum doses for all four non-coplanar beam direction search spaces were clearly superior when compared to doses obtained with the coplanar search space (figures 9.3, 9.4, 9.5, 9.6 and table 9.2). Also for the femoral heads, $V_{10\text{Gy}}$ and $V_{30\text{Gy}}$, non-coplanar plans performed better (table 9.2). Coplanar plans had (slightly) improved $V_{30\text{Gy}}$, CI and MU .

The CK^+ and CK^{++} search spaces were used to study dosimetrical consequences of limitations in the extent of the CK space (figure 9.1, sections 9.2.3, 9.3.4 and 9.3.5). The data presented in section 9.3.4 do clearly demonstrate that extension of the CK space to include beams with larger direction components along the superior-inferior axis could substantially enhance plan quality ($CK^+ \rightarrow CK^{++}$). On the other hand, further addition of beams with larger posterior components did not improve plans ($CK^{++} \rightarrow \text{F-NCP}$). Comparison of the right panels in figures 9.7 and 9.8 shows that also in case of

availability of the posterior beams (F-NCP), most selected high-weight beams are within the borders of the CK⁺⁺ space that lacks posterior beams. As plan quality for F-NCP and CK⁺⁺ is highly similar, it may be concluded that omission of posterior beams does not limit the quality of generated plans.

As demonstrated in figures 9.4 and 9.5, for all search spaces, plan quality continued to improve with increasing numbers of involved beams, with some levelling off for >20 beams. Table 9.3 details the very significant improvements that can be obtained with 25 coplanar beam configurations compared to 11 coplanar beams. This observation might seem in striking contrast with the broadly applied ≤ 9 beams for prostate in clinical practices. However, it has to be considered here that HDR like dose distributions were investigated in this paper, aiming at highly inhomogeneous PTV doses with some sparing of the urethra and enhanced dose delivery in the peripheral zone. In an on-going study we are investigating the use of large numbers of beams for more regular prostate IMRT dose distributions.

Also for very large beam numbers, non-coplanar configurations performed clearly better than coplanar set-ups (figures 9.5, 9.6, table 9.2). On conventional treatment units with L-shaped gantries, delivery of non-coplanar plans with many beams would result in impractically long treatment times and a high workload because of the involved couch rotations. The latter would also limit treatment accuracy. The performed treatment time calculations for a robotic CyberKnife equipped with an MLC (sections 9.2.6 and 9.3.6) demonstrated that treatment times of around 18 minutes could be obtained with such a system, including intra-fraction imaging and position correction prior to delivery of each of the 25 beams.

As mentioned in section 9.2.4, for each patient, PTV doses in iCycle plans were highly similar to the dose in the plan generated with the clinical treatment planning system for actual treatment with the CyberKnife. On the other hand, it was observed that rectum doses in iCycle plans were highly superior to corresponding doses in the clinical plans (not described in detail in this paper). This may seem unexpected for the CK search space that contains the feasible beam directions of the CyberKnife treatment unit. A possible explanation may be that clinical plans were generated with 3 circular cones per patient, while for the iCycle simulations it was assumed that beam collimation was performed with an MLC. These observations are now being investigated in great detail, to be reported in a separate paper.

In this study, minimization of the mean rectum dose was used as the highest priority objective, aiming at rectum sparing (table 9.1). Many studies have been performed to establish plan parameters that correlate most with rectum toxicity, see Michalski *et al* (2010) for an overview. The QUANTEC group suggests V_{60} , but using this objective directly in the optimization leads to less desirable results because of the focus on a single

dose-point. Instead we used rectum D_{Mean} as an objective in the optimizations, while V_{60} was included in plan evaluations.

In iCycle, the wish-list is used to generate plans with favourable balances between the various treatment goals. In our investigations we imposed a very strong drive for minimization of the mean rectum dose (table 9.1: priority 3, Goal: 0 Gy). Such a focus on rectum dose minimization has a danger that slightly higher rectum doses could potentially result in (unobserved) much improved doses to other OAR. In the trial plan generations for creating the applied wish-list (section 9.2.4), no evidence was found that this would actually occur. In the near future, we will however study the value of navigation tools (Craft & Bortfeld 2008, Monz *et al* 2008, Thieke *et al* 2007) for exploring the solution space around iCycle generated plans. Anyway, as in this study the same wish-list was used for all search spaces, numbers of involved beams and patients, it is believed that the impact of not performing navigation on main conclusions of the work will be minimal.

In this paper we compared plan quality of treatments with up to 30 optimized coplanar beam directions with optimized non-coplanar techniques. There is no existing machine that can deliver treatments for all investigated beam search spaces. The CyberKnife search space does not include 72 equi-angular coplanar beams, neither does it contain all directions defined for CK⁺ and CK⁺⁺. The fully non-coplanar (F-NCP) space cannot be realized with any of the commercially available systems, e.g. because of linac-bunker floor collisions, gantry-couch collisions, or beams going through heavy couch elements. However, the F-NCP dose distributions give an upper limit of what could theoretically be obtained with optimized non-coplanar set-ups. To make conclusions on the impact of the beam search space on plan quality independent of the applied optimizer, the type of beam shaping, and the beam characteristics, all optimizations were performed with the iCycle optimizer, using the same dose calculation engine for the same MLC (section 9.2.4).

Optimization results may depend on dose calculation accuracy (Jeraj *et al* 2002). It is well known that dose calculations using pencil beams and equivalent path length correction have limited accuracy, especially in low density tissues. In this study on prostate cancer, these tissues were largely absent in the treatment fields. Moreover, the same dose calculation algorithm was used for all beam direction search spaces. Therefore, we believe that limitations in the applied dose calculation engine do not jeopardize our main conclusions on ranking of the beam search spaces.

As described in section 9.3.8, optimization times were long, especially for the largest non-coplanar search spaces. There are many possibilities for substantial reductions and this is an area of active research in our group. On the other hand, based on an *a priori* defined, fixed wish-list per patient group, iCycle optimized plans are generally of very high quality, and do not require further iterations with new iCycle runs (Breedveld

et al 2012) (as explained in section 9.2.4, in this study, PTV constraints and objectives were tuned per patient to reproduce different clinical PTV dose distributions). In a recent prospective clinical study for evaluation of iCycle in head-and-neck IMRT, for each patient the treating physician was presented a plan based on iCycle and a plan made by dosimetrists with the clinical treatment planning system. In 32 out of 33 plan selections, the treating physician selected the iCycle based plan. Also objectively, the latter plans were clearly of higher quality (*Voet et al 2013*).

This study focused on generation of prostate SBRT plans that mimicked HDR brachytherapy dose distributions. Conclusions on the importance of non-coplanar beams, on the favourable use of large numbers of beams (>20), and on the limited importance of posterior beams may not be valid in other circumstances. Recently, we demonstrated for a group of head-and-neck cancer patients that inclusion of non-coplanar beams in the search space did only marginally improve IMRT plans (*Voet et al 2012*). Studies for other treatment sites are on-going.

9.5 Conclusion

For prostate SBRT, IMRT plans generated with all four investigated non-coplanar search spaces had clearly improved organ at risk (OAR) sparing compared to the coplanar (CP) search space, especially for the rectum which was the most important OAR in this study. OAR sparing was best with the fully non-coplanar search space (F-NCP), with improvements in rectum D_{Mean} , $V_{40\text{Gy}}$, $V_{60\text{Gy}}$ and $D_{2\%}$ compared to CP of 25%, 35%, 37%, and 8%, respectively. Reduced rectum sparing with the CyberKnife (CK) search space compared to F-NCP could be largely compensated by extending the CK space with beams with relatively large direction components along the superior-inferior axis (CK⁺⁺). Further addition of posterior beams to define the F-NCP search space, did not result in plans with clinically relevant further reductions in OAR sparing. Plans with 25 beams performed clearly better than plans with only 11 beams. For coplanar set-ups, an increase in involved number of beams from 11 to 25 resulted in reductions in rectum D_{Mean} , $V_{40\text{Gy}}$, $V_{60\text{Gy}}$ and $D_{2\%}$ of 39%, 57%, 64%, and 13%, respectively.

Chapter 10

Adaptive liver stereotactic body radiotherapy: can automated daily plan re-optimization prevent dose delivery degradation caused by anatomy deformation?

Suzanne Leinders^{1,2}, Sebastiaan Breedveld¹, Alejandra Méndez Romero¹,
Dennis Schaart², Yvette Seppenwoolde¹ and Ben Heijmen¹

¹Department of Radiation Oncology, Erasmus MC Rotterdam, Groene Hilledijk 301, 3075
EA Rotterdam, The Netherlands

²Delft University of Technology, Delft Institute of Applied Sciences, PO Box 5, 2600 AA
Delft, The Netherlands

E-mail: y.seppenwoolde@erasmusmc.nl

Published 1 December 2013 in *International Journal of Radiation Oncology*Biography*Physics*,
volume **87**, pages 1016-1021

[doi:10.1016/j.ijrobp.2013.08.009](https://doi.org/10.1016/j.ijrobp.2013.08.009)

Abstract

The purpose of this study was to investigate how dose distributions for liver Stereotactic Body Radiation Therapy (SBRT) can improve by automated, daily plan re-optimization to account for anatomy deformations, compared to set-up corrections only. For 12 tumours, three different strategies for dose delivery were simulated. In the first strategy, CT-scans made before each treatment fraction were used only for patient re-positioning prior to dose delivery for correction of detected tumour set-up errors. In the adaptive second and third strategies, in addition to the isocentre shift, IMRT beam profiles were re-optimized, or both intensity profiles and beam orientations were re-optimized, respectively. All optimizations were performed with a recently published algorithm for automated, multi-criteria optimization of both beam profiles and beam angles. In six of 12 cases, violations of organs at risk (OAR; heart, stomach, kidney) constraints of 1 – 6 Gy in single fractions occurred in case of tumour re-positioning only. With the adaptive strategies these could be avoided (< 1 Gy). For one case, this needed adaptation by slightly underdosing the PTV. For two cases with restricted tumour dose in the planning phase to avoid OAR constraint violations, fraction doses could be increased by 1 and 2 Gy due to more favourable anatomy. Daily re-optimization of both beam profiles and beam angles (third strategy) performed slightly better than re-optimization of profiles only, but the latter required only some minutes computation time while full re-optimization took a few hours. This simulation study demonstrated that re-planning based on daily acquired CT-scans can improve liver SBRT dose delivery.

10.1 Introduction

SBRT for liver metastases has a high local control rate with acceptable toxicity (Dawson *et al* 2006, Kavanagh *et al* 2006, Méndez Romero *et al* 2006, Van der Pool *et al* 2009, Rule *et al* 2011, Wulf *et al* 2006). To allow large radiation doses in only a few fractions, PTV margins have to be small, requiring high accuracy in daily tumour set-up. The patients in this study were treated in a stereotactic body frame with abdominal compression. Before each treatment fraction, a contrast enhanced CT-scan was acquired to verify and correct tumour set-up, resulting in a good treatment accuracy with individualized margins (Wunderink *et al* 2004, 2006, 2007). In a recent dosimetrical study (Méndez Romero *et al* 2009), adequate PTV coverage for this procedure was confirmed, but it was also demonstrated that daily tumour re-positioning could sometimes not avoid large deviations in OAR doses, caused by anatomical deformations, an observation that is comparable to that of Velec *et al* (2012) who observed that the majority of patients had accumulated dose deviations $> 5\%$ relative to the static plan. Li *et al* (2011) and Liu *et al* (2012) observed that for pancreatic cancer the internal organ configuration in the abdomen varied over time and that an online adaptive re-planning technique based on a daily respiration-gated diagnostic-quality CT could effectively correct for those inter-fraction variations.

In the current study we investigate to what extent automated, daily re-optimization of IMRT profiles and beam angles, based on a daily CT-scan, can improve SBRT dose delivery for liver metastases.

10.2 Methods and materials

10.2.1 Patients

For this study we retrospectively used contrast-enhanced helical CT-scans of 8 liver metastasis patients with in total 12 targets, previously treated in our institution with liver SBRT (table 10.1). In case more than one target was present in a patient, the simulations in this study were performed independently for each of the targets.

Table 10.1: Patient characteristics and results of re-planning strategies. Targets 9-10 and 11-12 are multiple tumours of patients 1 and 7, respectively. For each patient is indicated which OAR constraints were violated, the fraction and the amount of overdose per re-planning strategy per fraction. For the PTV the amount of underdose (D_{95}) is indicated.

Patient characteristics			Re-planning strategy, constraint violations				Re-planning strategy, PTV- D_{95}				
Target	Gender	Tumour size (cm)	Tumour volume (cm ³)	Liver segment	OAR	TSO	Adapt-I	Adapt-IA	TSO	Adapt-I	Adapt-IA
1	Male	6	64	2	Heart	3	3 Gy		3	< -1 Gy	3
2	Male	2.5	26	1	Heart	1	1 Gy		All	-4 Gy	All
3	Male	2.5	14	1	Stomach	1	1 Gy		All	-7 Gy	All
4	Male	4, 1	41*	7, 7	Kidney	3	< 1 Gy		All	< -1 Gy	All
5	Female	4, 1.5	61*	4, 4	Stomach	1	< 1 Gy		All	-10 Gy	All
6	Male	5	184	4	Kidney	1	6 Gy		All	-9 Gy	All
7	Male	5	85	8		2	< 1 Gy		All	-7 Gy	All
8	Male	3	76	8		3	< 1 Gy	1 Gy	All	-7 Gy	All
9 (1)	Male	4	17	4		1	< 1 Gy		All	< -1 Gy	All
10 (1)	Male	3	10	4		2	< 1 Gy		All	-10 Gy	All
11 (7)	Male	3.5	58	6	Kidney	1	< 1 Gy	1	All	-9 Gy	All
12 (7)	Male	1	2	6		3	3 Gy		All	-9 Gy	All
12 (7)	Male										

* Because of close proximity of the tumours, they were treated as one volume.

Apart from the planning CT-scan, 3 repeat contrast-enhanced helical CT scans were available for each patient, each acquired prior to dose delivery of one of the 3 treatment fractions. For all scans, patients were positioned in a Stereotactic Body Frame (Elekta Instrument, Stockholm, Sweden) with abdominal compression, as during treatments. Details of this technique can be found in the study of Méndez Romero *et al* (2009). OAR in repeat scans were delineated retrospectively by a single radiation oncologist (AMR). The PTV in the planning CT was copied into each repeat scan and repositioned to the correct tumour position, taking into account the clinically established (grey value 3D matching) tumour shift in the repeat scan (Méndez Romero *et al* 2009), hereby avoiding effects of intra-observer variance in tumour delineation, while presuming that tumour shrinkage or deformation was absent during the short overall treatment time.

10.2.2 Study design

Computer simulations were performed retrospectively for three planning strategies. The first was the current clinical approach using daily Tumour Set-up corrections Only (TSO). In this strategy, for each repeat scan the dose optimized on the corresponding planning CT-scan (see next paragraph) was shifted to the tumour position in that fraction. For the second and third adaptive strategies, additional to tumour repositioning, beam intensity profiles were re-optimized based on the fraction CT-scan (Adapt-I), or both intensities and beam angles were re-optimized (third strategy, designated Adapt-IA). Strategies were compared regarding single fraction dose distributions.

10.2.3 Optimization of dose distributions

All treatment plan optimizations, including the planning phase, were performed with an in-house developed algorithm for automated multi-criterial optimization of beam intensities and beam directions that is based on a prescription called wish-list, containing hard constraints and objectives (iCycle; Breedveld *et al* (2012)). Optimal beam directions are selected from an input set of candidate directions, that can be restricted e.g. to avoid collisions between patient/couch and the gantry in a non-coplanar setup. Generated plans are Pareto-optimal for optimized profiles. In this study, optimized plans consisted of around 10 IMRT beams in a non-coplanar configuration.

In planning and re-optimization, the goal for each of the 3 fractions was that at least 95% of the PTV would receive a dose of 67% of the prescribed 25 Gy isocentre dose. The OAR constraints and treatment objectives as used by iCycle for plan optimization (Breedveld *et al* 2009a, Méndez Romero *et al* 2009) are summarized in table 10.2. When 25 Gy could not be delivered without constraint violations (deviation > 1 Gy), the prescribed dose was reduced such that violations could just be avoided.

Table 10.2: Constraints and objectives for automated generation of plans for the complete treatment (3 fractions).

Constraints			
	Volume	Type	Limit
	PTV	minimum	$0.67 \cdot 75 \text{ Gy}$
	Liver-CTV	maximum $D_{33\%}$	21 Gy
	Liver-CTV	maximum $D_{50\%}$ or D_{700cc}	15 Gy
	Heart	maximum D_{1cc}	30 Gy
	Spinal Cord	maximum $D_{99\%}$	18 Gy
	Duodenum	maximum D_{1cc}	21 Gy
	Oesophagus	maximum D_{1cc}	21 Gy
	Stomach	maximum D_{1cc}	21 Gy
	Kidneys	maximum $D_{35\%}$	15 Gy
	Unspecified Tissue	maximum D_{1cc}	21 Gy

Objectives			
Priority	Volume	Type	Goal
1	Liver	minimize mean	0 Gy
2	Heart	minimize maximum	5 Gy
3	Stomach	minimize maximum	5 Gy
4	Duodenum	minimize maximum	5 Gy
5	Oesophagus	minimize maximum	5 Gy
6	Heart	minimize mean	0 Gy
7	Stomach	minimize mean	0 Gy
8	Duodenum	minimize mean	0 Gy
9	Oesophagus	minimize mean	0 Gy

10.3 Results

For TSO, 5 of the 36 fraction dose distributions showed OAR constraint violations $\geq 1 \text{ Gy}$, table 10.1. Such violations did not occur in Adapt-I and Adapt-IA. The $\geq 3 \text{ Gy}$ OAR constraint violations of the heart (target 1) and the kidney (targets 6 and 11) for TSO (table 10.1, figure 10.1) were all related to anatomy deformations, moving the OAR in the high dose area. With the 6 Gy kidney constraint violation for target 6 in the first fraction, TSO would have resulted in a dose more than double the constraint dose of 5 Gy (table 10.2). For patient 1, avoidance of heart constraint violation with the adaptive approaches was obtained by slightly underdosing the PTV.

In the planning phase, the prescribed PTV dose could not be attained for 3 out of 12 targets due to an unfavourable position of the surrounding OARs, resulting in a lower prescribed dose, that stayed at the same low level for the TSO strategy. For target 2, in each of the fractions the patient anatomy had changed in a way that provided more room to deliver the required tumour dose; re-planning with Adapt-I and Adapt-IA improved the PTV D_{95} by 15% and 18% respectively compared to the TSO PTV D_{95} , without compromising the OARs. For target 5 the target dose could be up scaled by 1 Gy in all fractions, while the adaptive strategies could not reduce target underdose in target 3.

To get an overall quantitative impression of the impact of the adaptive strategies,

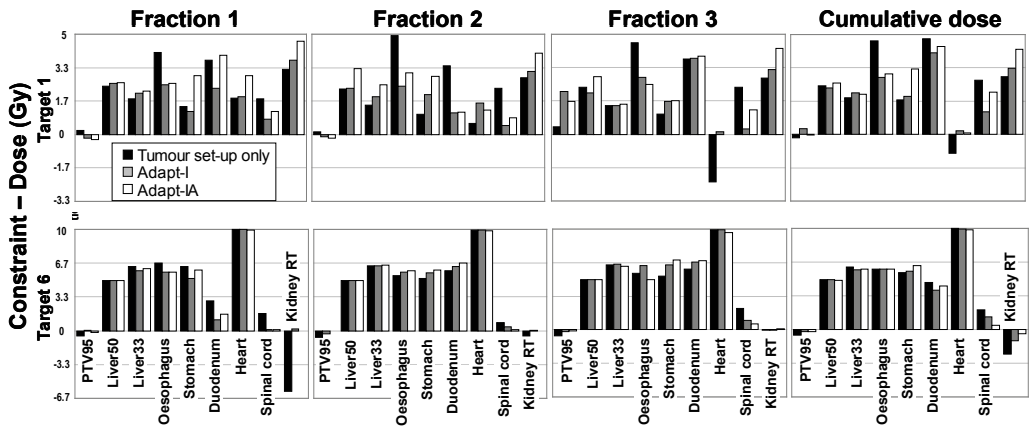


Figure 10.1: Plan comparisons for the three studied treatment strategies for two targets per fraction. Dosimetric parameters correspond to the constraints, except for the PTV where the D_{95} is evaluated. For the OAR, the bars show how much delivered doses were below the imposed constraint values. A negative value for an OAR indicates constraint violation, while a negative bar for the PTV means that PTV dose delivery was better than prescribed. PTV95 means PTV D_{95} and Liver₅₀ and Liver₃₃ refers to the 50% dose and 33% dose of the Liver respectively.

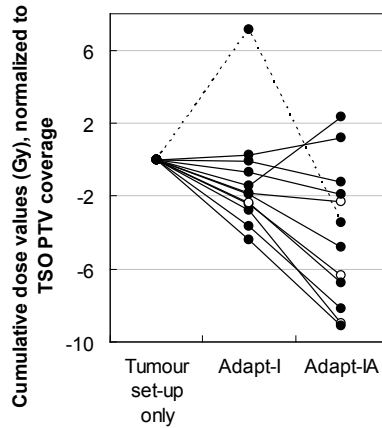


Figure 10.2: For the 12 targets, differences between the sum of all OAR dose parameters for the clinical strategy and the sum for Adapt-I and Adapt-IA respectively. Dose distributions for Adapt-I and Adapt-IA were normalized for equal PTV coverage in the clinical strategy. The lower the value, the less total dose organs received. Open circles represent the patients with remaining constraint violations (all $\approx 1 \text{ Gy}$) in the adaptive plans; dose to all the organs of the plans with a higher total dose parameter value than the TSO plan stayed below the constraint value.

we added for each strategy all dose values of all OARS after the PTV coverage of the Adapt-I and Adapt-IA plans were normalized to the PTV D_{95} of the TSO plan. In this way the influence of dissimilar tumour doses was eliminated and the cumulative effect on the OARS could be compared between the strategies; the smaller the value, the less dose the OARs received. The results as presented in figure 10.2 assume that all organs are of equal importance. Clearly, the adaptive strategies resulted in a significantly lower total dose to the OARs ($p = 0.001$ and $p = 0.006$ without the outlier and $p = 0.190$ and $p = 0.003$ with the outlier for Adapt-I and Adapt-IA, respectively, in a two-tailed paired t-test). The outlier in figure 10.2 was caused by a beam that was directed through the spinal cord that initially had a low weight, gained a relatively high weight (but not reaching the spinal cord constraint) in the Adapt-I plan due to constraints to the other OARs. In the Adapt-IA plan, the beam directions were changed and thus not directed through the spinal cord anymore.

10.4 Discussion

To our knowledge this is the first paper systematically investigating potential advantages of fully automated daily re-planning in liver SBRT compared to tumour set-up correction only. In five of the studied 12 targets, OAR constraint violations $\approx 1 \text{ Gy}$ occurred in one of the fractions when tumour set-up only (TSO) was used. By using adaptive RT

with re-optimization of the IMRT fluence patterns and/or beam directions, this could be avoided. In two cases, when the prescribed dose to the PTV could not be reached in the planning to avoid OAR constraint violation, daily re-optimization resulted in a higher dose in the PTV.

Plan (re-)optimization in iCycle is fully automated, based on the prescription wish-list (above). The calculation time for re-optimization of beam profiles only (Adapt-I) was 6-15 minutes, while the time needed for re-optimization of both beam profiles and beam orientations (Adapt-IA) was quite long (up to till 5 hours). Dose distributions were only slightly better for Adapt-IA. Certainly for Adapt-IA, current calculation times are prohibitively long for on-line clinical use. Both for Adapt-I and Adapt-IA, investigations on reductions of computation times are on-going. It is expected that for Adapt I this will soon result in 1-2 minutes calculation time.

In this retrospective study, iCycle was used to automatically generate IMRT plans for all planning CT- and repeat scans. The quality of obtained dose distributions for the planning CT-scans was clearly enhanced compared to the clinically applied 3D conformal plans, especially regarding conformality. This might explain the sometimes modest improvements of the adaptive strategies relative to TSO. Due to the high conformality, there is some space for repositioning of OARs without exceeding tolerance doses. The high quality of iCycle dose distributions has been demonstrated in several studies ([Breedveld *et al* 2012](#), [Rossi *et al* 2012](#), [Voet *et al* 2013](#)). Currently, iCycle is clinically used for all liver SBRT patients.

Although the results above are promising, this study has a few limitations. Dose variations caused by respiratory motion in the SBF were not explicitly taken into account. However, the expected impact of respiratory effects is very limited ([Eccles *et al* 2011](#), [Wu *et al* 2008](#)), because with abdominal compression the breathing motion generally reduces to < 5 mm ([Wunderink *et al* 2008](#)). The study of [Velec *et al* \(2012\)](#) showed that organ deformation can cause changes in the intended dose distribution, even if the planning corrected for breathing motion.

The re-optimizations in this study were performed without taking into account doses delivered in previous treatment fractions (dose accumulation), as this is not yet featured in iCycle. With such a procedure, the impact of daily re-planning could be further enhanced for example by boosting underdosed areas in the last fraction, requiring on-line non-rigid registration of CT datasets. The algorithm we have available for non-rigid registration ([Bondar *et al* 2010](#), [Vásquez Osorio *et al* 2009](#)) looks promising and validation of non-rigid dose addition is under current investigation ([Vásquez Osorio *et al* 2011](#)).

Daily re-planning requires fast and accurate segmentation of the tumour and OARs. As manual delineation would be too time consuming, auto-segmentation is essential.

There are a few auto-segmentation algorithms available used for head-and-neck cases (Sims *et al* 2009, Teguh *et al* 2011, Wang *et al* 2008, Zhang *et al* 2007). There are also some algorithms available for liver cases (Campadelli *et al* 2010, Freiman *et al* 2011), but there is no auto-segmentation algorithm available yet that is accurate and fast enough to use it for online adaptive planning in daily clinical practice.

10.5 Conclusion

Daily automated re-optimization of dose distributions, additional to tumour set-up corrections, can improve liver SBRT dose delivery by accounting for inter-fraction anatomy variations. Clinical implementation requires availability of a fast and accurate auto-segmentation routine and (preferably) a fast and reliable non-rigid registration algorithm. Further research is needed, including assessment of clinical relevance.

Acknowledgements

The authors want to thank Eliana Vásquez Osorio, Luiza Bondar and Mischa Hoogeman for useful discussions.

Chapter 11

Discussion

11.1 Introduction

During this work, basically two multi-criterial algorithms have been developed for automated plan generation, the first described in chapters 2-4, the second, called iCycle, described in chapters 5 and 6 and investigated for clinical treatment planning in chapters 7-10. iCycle is clearly the more general and powerful one, suited for multi-criterial optimization of not only IMRT profiles but also beam angles. In a multi-criterial problem there is no single optimal solution, but a front is constructed out of so-called Pareto optimal plans (Miettinen 1999). A key feature of iCycle is that for each patient plan with n optimized angles, it will pick a single Pareto optimal IMRT plan, based on a wish-list with clinical hard constraints and prioritized treatment objectives. In this Discussion section we will focus on iCycle.

11.2 iCycle automated plan generation and plan quality

As described in chapters 5-10, a single wish-list is used for automated generation of plans for all patients in a group, e.g. all head-and-neck cancer patients with a main focus on sparing of salivary glands, while obtaining a high tumour coverage (chapter 8). So there is no need for manual fine-tuning for individual patients to obtain high quality plans; the full process is automatic. A very powerful proof for this statement is delivered in chapter 8, describing a prospective clinical study comparing plans generated in the traditional way by dosimetrists with automatically generated iCycle plans. In 32 of 33 cases, the treating physician selected the iCycle plan. Also in chapter 9 we noted that our clinical plans were of much lower quality than the plans generated by iCycle. More examples are give in section 11.3 below. To achieve this, fine-tuning of the wish-list is of utmost importance. This is done in close collaboration between dosimetrists and physicians in an iterative trial-and-error process generating plans for a small group of patients for an

evolving wish-list. An advantage of automated planning based on a wish-list is also that the number of objectives and constraints may easily be chosen larger than used in clinical treatment planning. In the latter, an overload of criteria will confuse the planner. In recent years we have gained confidence that the quality of iCycle plans is indeed very high. On the other hand, tools for easily checking this on a per patient basis are currently lacking. In a future work, we will add Pareto navigation tools ([Craft & Bortfeld 2008](#), [Monz et al 2008](#), [Teichert et al 2011](#), [Thieke et al 2007](#)) to iCycle to investigate the space around the proposed Pareto optimal plan. These tools may also aid in the construction of a general wish-list, but also other aspects may be helpful, like quantifying the most effective decision criteria ([Holdsworth et al 2011](#), [Moore et al 2012](#)).

11.3 iCycle for optimizing beam angles and generation of non-coplanar plans

Planning systems for integrated, multi-criterial beam profile and angle optimization are hardly available. As a consequence, the value of beam angle optimization in IMRT and the value of optimized non-coplanar beam arrangements have hardly been investigated. In this thesis we have demonstrated that beam angle optimization may result in highly improved plans, compared to beam angles selected clinically or equi-angular set-ups. The added value of non-coplanar set-ups became especially clear for prostate cancer patients (chapter 9) and for some head-and-neck cancer patients (chapter 7). In a recent study on liver SBRT, we also saw large plan improvements for optimized non-coplanar set-ups (one example in section 6.3.7 in chapter 6, article in preparation). It is well known that delivery of non-coplanar treatments on regular L-shaped linacs may result in seriously prolonged treatment times. This is especially problematic if many fields (> 20) are clearly more favourable than e.g. 10 fields, as observed for the prostate cancer patients studied in chapter 9. For these non-coplanar treatments, a robotic treatment unit such as the CyberKnife (but preferentially equipped with an MLC) might be a better option. A point of caution with introduction of non-coplanar treatments is the need of delineating and constraining more structures. Without this, high dose might unexpectedly appear in places that were previously not at risk. The extra contouring will currently result in some increase in workload. Fortunately, a lot of development is going on in the field of auto-segmentation of images ([Anders et al 2012](#), [Bondar et al 2012](#), [Gu et al 2010](#)).

11.4 iCycle automated plan generation to reduce workload and enhance treatment efficiency

Apart from enhanced and consistent plan quality (above), automated plan generation also reduces workload, making it an economically attractive feature. As described in chapter 8, iCycle plans cannot yet be used directly in the clinic because of technical and

QA issues. Currently, generated iCycle plans are used to generate a template for plan generation with our commercial TPS. The template is used for reverse engineering of the high quality iCycle plan. Due to this procedure, workload reduction is compromised but still considerable. In an on-going project, we are preparing iCycle for direct generation of clinical plans.

In the coming decennia the number of patients that will be treated with radiation therapy will grow world-wide. This is a result of aging of the population, or growth in prosperity, or both. For The Netherlands, the number of patients newly diagnosed with cancer is expected to increase by 40% from 87.000 in 2007 to 123.000 in 2020. For patients who have been diagnosed with cancer, these numbers are 420.000 and 660.000 respectively ([Dutch Cancer Society 2011](#)). Incidences of other diseases are expected to grow as well. There is a general concern that it may become difficult to get enough (young) and well-trained people employed in health care. Workload reduction by automated plan generation might be a way to circumvent this problem in radiotherapy and maintain a high quality of treatment plans.

An interesting question is whether a *Nash-equilibrium* ([Osborne 2003](#)) exists for radiotherapy. Suppose the whole trajectory of contouring, planning and verification is automated and does not have a limit on quantity. In that case, only the treatment device capacity is the limiting factor. Can we then improve individual treatments (in the sense of *quality-of-life*) by *not* delivering the ultimate best plan for that individual patient, but avoiding a waiting list?

The rationale here is that if a patient is treated directly after diagnosis, the tumour is smaller and easier to irradiate than when a patient has to wait several weeks before starting with the treatment. [Murai et al \(2012\)](#) showed for non-small-cell lung cancer that for 21% of the patients waiting for more than 4 weeks, the stage progressed from T1 to T2. If the treatment is easier to deliver, it will take less time, and therefore more patients can be treated with the same treatment device capacity. An important condition is that adding complexity to the treatment plan (and thereby adding treatment time) is indeed stopped if only minor improvements would result. For example, a dose reduction from 15 Gy to 5 Gy in a parotid gland only results in an NTCP reduction of 5.5% to 3% ([Houweling et al 2010](#)), while the treatment time may be increased by as much as 10% to obtain the 1.5% gain. In the end, 10 of such patients a day creates time for treatment of another patient. To study this, plan quality in relation to treatment time and tumour growth due to waiting time should first be quantified, and later be considered in treatment planning.

Despite the seemingly contradictory origin of this hypothesis – not delivering the best treatment plan while the patient is treated better –, more patients can be treated while the probability of complications should reduce. Striking observations are in the field

of transportation planning. Examples include that closing 42nd street in New York for maintenance resulted in a higher throughput (Kolata 1990); South Korea even invested \$380 million to tear down one of the three main bridges to Seoul (Easley & Kleinberg 2008).

11.5 iCycle in treatment planning studies

A severe caveat in many treatment planning studies is that the quality of generated plans may be dependent on the skills and ambitions of the planner(s), and the allotted time for generating plans may be limited and variable. With iCycle automated plan generation, all these issues can be avoided. The investigations in chapter 9 are based on a total of 1500 automatically generated plans with beam angle and profile optimization. For a human planner, generating this amount of plans would be infeasible.

11.6 iCycle in clinical practice

As described in section 11.4, iCycle automated plan optimization is nowadays used in an indirect way to generate for each patient a template for design of a plan of equal high quality with the clinical TPS. This results in higher quality plans and reduced planning workload. Currently, this procedure is performed for the major part of head-and-neck cancer patients, and the percentage is still increasing. Also all liver SBRT patients are planned using iCycle and iCycle is also used to automatically generate treatment plans for cervix cancer patients treated with an adaptive protocol (Ahmad *et al* 2011, Bondar *et al* 2011, Vázquez Osorio *et al* 2009). For these patients, treatment is based on a library of plans. Based on a daily cone beam CT scan, the plan best fitting the anatomy of the day is selected for treatment. Studies on the clinical implementation for other major tumour sites are in progress. With this approach, the department is aiming for more consistent high plan quality and a reduction in planning workload. It is believed that the majority of patients will in the end be treated with an automatically generated plan. Due to the reduced planning efforts for these patients, more time will become available for difficult, rare cases, for whom a tuned wish-list is not available. Moreover, advanced adaptive treatment might in the future require more highly skilled manpower at the treatment units.

11.7 Plan quality control

When plans are automatically generated, the planner has less affinity with the patient's anatomy and resulting plan. It can be helpful to have a tool which looks more global to the treatment plan, and gives the planner a list of "questionable" items which eases plan verification (Buettner *et al* 2010, Yang & Moore 2012, Zhao *et al* 2010). This is essential for online treatment planning, where the time to verify a plan is very limited.

Even if all plans generated fulfil the clinical constraints, it may still occur that a

plan is significantly worse than it could be, due to bugs or flaws in the software. If the majority of the plans are generated automatically, and are of high-quality, the planner may lose insight in what is achievable for an individual patient, and may therefore not detect the lower quality. One other danger is that people may become trustworthy to the generated plans, and therefore less critical.

To counterfeit this, all plans should ideally be re-planned using a completely different and independent approach. This goes much further than recomputing only the dose with an independent dose-engine. These “shadow” plans could be simplified versions of the actual planning, e.g. without beam angle optimization and with coarse beamlet and dose resolution, but should still result in an acceptable plan.

A more lightweight approach is given by [Petit *et al* \(2012\)](#), where a database of plans of previously treated patients is used to predict achievable doses in organs at risk for a new patient, based on distances of the organ to the target. If the achieved dose of the generated plan lies outside the confidence interval computed by the model, the plan is likely non-optimal.

11.8 The optimizers

In the first part of this work (chapters 2-4), an optimizer was used that uses voxel-dependent importance factors to optimize a plan. In our later work (chapters 5-10) the switch was made to a more general optimizer. In this section we will discuss some aspects of the different optimizers.

11.8.1 Iterative constrained optimizer

The first optimizer is a very good method if one can pinpoint the voxels where the dose should be changed for the highest yield. If one wants to reduce the maximum dose, reduce the dose in the voxels receiving the highest amount of dose. Also for dose-volume constraints the approach is very intuitive (see figure 4.1). As a result, this method is very effective in optimizing on traditional dose-volume criteria, but is not capable of optimizing on more global criteria, like mean dose or EUD.

This optimizer only works for *constrained optimization*, but lacks a check for optimality conditions. The *feasibility checking* is iteratively performed by increasing weights to individual voxels, and solve a quadratic subproblem. This is the *inner-loop*, and due to the iterative nature there is no hard guarantee whether a problem is feasible or not. For the multi-criteria optimization, the problem is even worse: as there is no “objective”, the multi-criteria optimization is done by iteratively reducing the constraints step-by-step (e.g. 1 Gy or 1%) in an *outer-loop*.

11.8.2 Interior-point optimizer

For the development of iCycle it was necessary to use a more transparent and flexible optimizer. iCycle now uses an *interior-point* based optimizer (Nocedal & Wright 2000, Wright 1997). This optimization method is considered to be one of the top-performing optimizers for medium-scale problems, and is very flexible in the criteria which can be optimized on. All smooth and convex criteria should work flawlessly, and also non-convex problems are usually solved well. As often applied dose-volume objectives are non-convex, this is an important aspect.

As the optimizer will only be used for the field of radiotherapy, it was decided to implement this ourselves, in order to exploit the field-specific elements to its maximum, and tune all parameters. We have mainly followed the work of LOQO by (Benson & Shanno 2007, Shanno & Vanderbei 2000, Vanderbei 1999, Vanderbei & Shanno 1999), improved with predictor-corrector techniques (Gondzio 1996, Mehrotra 1992).

The field-specific implementation includes:

- preprocessing: this is done on a much higher level than in general purpose optimizers, namely on the wish-list level. For example, redundant constraints will never occur (unless the wish-list is purposely misleading or ill-constructed). Not preprocessing at all saves time for every optimization.
- warmstarting: helps to reduce the number of iterations. Warmstarting is more problematic in interior-point methods than for simplex-based methods, but there is still active research ongoing (Gondzio & Grothey 2008, Pagès *et al* 2009, Yildirim & Wright 2002). We are able to effectively warmstart by solving a least-squares problem that only irradiates the tumour with the prescribed dose balanced with smoothing. Warmstarting in a multi-criteria phase is still not as efficient as with simplex methods, but decreasing/increasing the dose by a few percent already takes off a few iterations, keeps the problem stable (when non-convex dose-volume criteria are part of the problem) and is much cheaper than solving a least-squares problem.
- derivatives: as only a limited set of criteria is used (mean, minimum, maximum, EUD, LTCP, etc.) all criteria have hard-coded first- and second derivatives. As a by-effect, the expensive matrix-matrix multiplication for construction of the dual-norm matrix requires only 1 multiplication per structure, even if that structure has more than 1 constraint or objective.
- efficient memory management and computation: the dose matrices may be sparse or dense, depending on the structure it represents. Storing all matrices together (e.g. for the linear constraints) in a single storage scheme, results in a highly inefficient storing and computation. Instead, the matrices are stored individually,

and are reordered and pre-tiled. A matrix-vector product is computed *matrix-free* on demand. Our own matrix-matrix multiplication has become highly efficient: it is twice as fast on average (but with extremes over 10 times faster) compared to naive methods (which either uses dgemm (Anderson *et al* 1999) for dense matrices or our own (OpenMP) implementation (Gustavson 1978, section 2.B in this thesis)), which already takes into account that the resulting matrix is a dense matrix. It also improves scaling when using more threads.

- Newton-system: the mixed-density of the matrices prevents construction of the a reduced Karush-Kuhn-Tucker system (as most optimizers do). The further reduced dual-norm matrix is a dense matrix. Our sparse algorithms can therefore skip the symbolic multiplication.
- feasibility checks: when the optimizer is run in the 1st phase of the 2-phase ϵ -constraint optimization, the optimizer terminates as soon as the goal is found feasible, but continues to optimize to optimality otherwise. This early termination saves a lot of iterations.
- dose-volume objectives: these are non-smooth non-convex, but can be used under certain conditions and some safeguards (see section 11.9).

Aleman *et al* (2010) also researched optimal settings for an interior-point optimizer in the field of radiation therapy.

Another nice property of interior-point optimizers is that optimality conditions can be measured: it is known whether or not a problem is feasible, and how far the solution is from optimality. This is interesting for the 2-phase ϵ -constraint multi-criteria optimization, where the optimizer can terminate as soon as a problem is feasible. In the rare case that a problem cannot be solved to optimality (this can happen in difficult problems), one can still accept the (intermediate) non-optimal solution if it is rendered feasible. Lagrange multipliers are used internally in the optimizer to find a solution, but also furnish information about relative sensitivity between objectives (Alber *et al* 2002a), making it possible to rewrite an ϵ -constraint formulation to a weighted-sum problem (Breedveld *et al* 2009a, chapter 5 in this thesis). This feature was used to improve beam selection in iCycle (figure 6.7 on page 73).

11.9 The dose-volume problem

Computer optimization using dose-volume criteria is (still) used a lot in modern treatment planning. The main problem from a mathematical point of view is that dose-volume criteria are not convex and not smooth. The non-convexity was analysed by Deasy (1997), Wu *et al* (2003) for 3D conformal radiotherapy, but later research for IMRT showed that

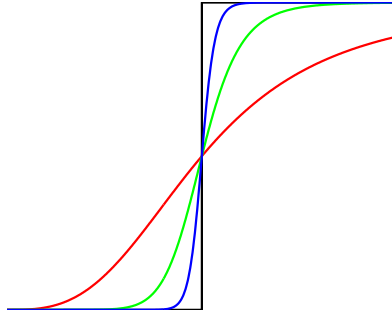


Figure 11.1: Sigmoid approximations for the Heaviside step function. The turn-point is at the critical dose level. Steeper sigmoid functions result in a better approximation.

local minima are hardly significantly different from the global minimum (Llacer *et al* 2003). This is a result of the degeneracy of the IMRT problem (Alber *et al* 2002b) and the fact that (physical) dose is continuous and differentiable.

There has been active research in incorporating dose-volume objectives in modern optimizers, including mixed-integer programming (Halabi *et al* 2006), conditional variables at risk (CVaR) (Romeijn *et al* 2003) or using a series of gEUD constraints (Zinchenko *et al* 2008). We have adopted the more direct approach by Alber & Reemtsen (2007) in which the dose-volume objective is represented at first as a summation of Heaviside step functions, and then smoothed into a sigmoid function, making the function differentiable.

Figure 11.1 shows the Heaviside function and approximations with different steepnesses. A steep sigmoid function provides the best approximation, but is also hard to optimize on as the gradient becomes too large. A shallow sigmoid works fine, but is a bad approximation to the Heaviside function. In our approach, we adapt the steepness of the approximation *during the interior-point iterations*. In the beginning, the steepness is gradually increased, until a certain accuracy is reached, currently set to be within 1 percent-point of the real dose-volume value. Later on the steepness is decreased again as a steep gradient may become problematic later on during convergence. This “folding” of the solution search-space during the optimization disturbs the behaviour of the default path-following-based algorithm. However, by using some safeguards for a more robust optimization over speed, carefully increasing/decreasing the steepness of the approximation and proper warmstarting strategies in a multi-criteria optimization makes this approach a very well working one.

A drawback of the sigmoid approximation to the Heaviside step function is that it can only be used for protection of organs at risk, but not for target coverage. The reason

is that around the critical dose point, there is a large error (area between sigmoid and step function, figure 11.1). If voxels are far away from this point, the error is negligible. Normally, for an organ at risk, the dose in the voxels range between 0 Gy and the prescribed dose. However, for a target, most voxels have a dose very close to the critical dose point, and thus results in a high accumulated error between the approximation and the real function. Another implication of the sigmoid approximation is that 100% coverage is never possible. This impossibility leads to an ill-conditioned and ill-posed problem definition. Thus, for partial target coverage, a different method should be applied.

11.10 Calculation times and online re-planning

Current calculation times range between 5 minutes for a 9-beam plan with fixed gantry angles to 15 hours for a 30-beam plan with optimized directions. The main factor that determines the optimization time is the number of beamlets participating in an optimization, which has a *quadratic* relation to the optimization time. The number of beamlets is influenced by the number of beams, size of the PTV and the resolution of the beamlet grid. The number of participating volumes of interest and resolution (or generally: voxels), the number of prioritized objectives in the wish-list, and the number of candidate beam directions have a *linear* relation to the optimization time. The linear-quadratic relation is a result of the design of the interior-point optimizer. Reducing the Newton system to the dual-norm equations results in a series of matrix-matrix computations (see section 11.8.2), where the inner dimensions are equal to the number of voxels and the outer dimension to the number of beamlets. As roughly 80% – 90% of the runtime is consumed by this operation, the scalability of the algorithm is largely determined by the number of beams. It also explains why adding a single beam to a 10 beam plan is much faster than adding one beam to a 30 beam plan. Figure 11.2 shows runtimes for a prostate cancer patient treated with up to 30 beams.

The algorithm for generation of Pareto-optimal plans is multi-threaded, and scales well up to 20 threads. The beam selection phase is distributed into single-threaded jobs, each of them evaluating a single beam direction. On a modern server with 40 CPU cores, a full iCycle optimization for 9 coplanar beams takes between 1 and 3 hours for clinical head-and-neck patients, and 15 hours for a 30-beam (non-coplanar) plan. Our cluster currently consists of 3 machines with 130 CPU cores in total, including scheduling software that optimally distributes the computations over the cluster.

Currently, these calculation times are acceptable as plans can be generated automatically during the night. Certainly for online re-planning, a speed increase is required. There are 3 levels where things can be improved: the beam angle optimization, the *2pec* multi-criteria plan optimization and the interior-point optimizer.

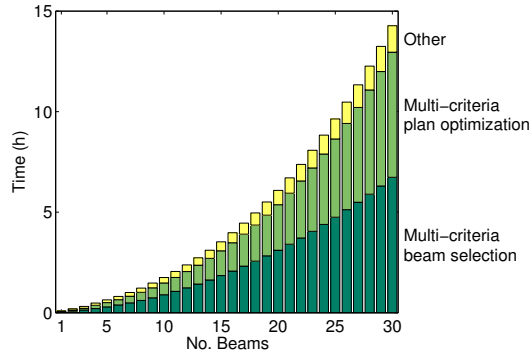


Figure 11.2: Runtimes for a prostate cancer patient treated with up to 30 IMRT beams. “Other” accounts for dose computation, segmentation, patient import, and all other overhead.

Improvement on the highest level, the beam angle optimization, is the most difficult, but possibly not very relevant for online treatment planning. In the study described in chapter 10 (Leinders *et al* 2013), re-optimization of the beam angles for each fraction resulted in only slightly better doses.

Reducing the number of optimizations in the 2-phase ϵ -constrained multi-criteria optimization directly results in a significant speed-up: rather than optimizing each objective individually, the idea is to perform a single optimization to optimize all criteria at once. In Breedveld *et al* (2009b) this was attempted by optimizing the Lagrangian, obtained from the reference plan, for each fraction. This worked for simple sites with few objectives, but behaved unpredictably on more complex cases. Our future research on this includes *aspiration-based* methods (Granat & Makowski 2000, Ogryczak & Kozłowski 2011).

More fundamental is improvement of the interior-point optimizer itself, as all other functions utilize it (multi-criterial beam selection and/or plan optimization) directly benefit. As described above, the main difficulty is construction of the dual-norm matrix. In order to speed-up the required matrix-matrix multiplication, the numerical subroutines should be revised. There are many different approaches possible: more efficient machine implementation (e.g. (manually) utilizing vector registers like VMX), a mixed precision arithmetic (MPA) or utilizing Strassen’s matrix multiplication algorithm (Strassen 1969). Within the bounds of the current interior-point algorithm, a GPU can be useful to offload the (default) matrix-matrix multiplications with the GPU BLAS (Basic Linear Algebra Subsystem), or use an advanced library like MAGMA (2011), which has a highly efficient scheduling algorithm included in the BLAS operations. On the other hand, there is a

possibility to eliminate the matrix-matrix multiplication altogether by using a matrix-free implementation, such as quasi-Newton methods like L-BFGS-B (limited memory Broyden-Fletcher-Goldfarb-Shanno for bounded problems) (Byrd *et al* 1995), or solve the reduced Karush-Kuhn-Tucker system (so not building the dual-norm matrix) by an iterative direct solver (Gondzio 2012, Sonneveld & van Gijzen 2008), utilizing only matrix-vector operations. Both approaches risk an increase in the number of interior-point iterations, but the computational cost per iteration should be significantly lower, and the scalability of the algorithm becomes linear rather than quadratic with the number of beamlets.

11.11 Direct aperture optimization

The current implementation of iCycle is based on fluence map optimization, followed by a segmentation for delivery with dynamic multileaf collimation (Rossi 2012, van Santvoort & Heijmen 1996). Direct Aperture Optimization (DAO) may hold several advantages such as faster delivery and higher plan quality, as the optimized dose corresponds to deliverable fluence. Profile smoothing during fluence optimization (Alber & Nüsslin 2001, Breedveld *et al* 2006, Zhu *et al* 2008) may also keep delivery times low and largely prevent loss in plan quality due to differences between optimized profiles and profiles after sequencing. Unfortunately, such smoothing can only be applied globally, while better treatment times can be obtained when smoothing is done locally (Matuszak *et al* 2008). As a consequence, optimizing a treatment plan with smoothing can never use all degrees of freedom in dose or delivery time, and thus may produce suboptimal treatment plans.

As DAO is a non-convex and NP-hard optimization problem (Baatar *et al* 2005), different heuristics have been developed (Bedford & Webb 2006, Gunawardena *et al* 2006, Men *et al* 2007, Shepard *et al* 2002, Süß *et al* 2007). Jin *et al* (2010) were the first to model dynamic leaf sequencing into a convex optimization problem.

The work of Men *et al* (2007) makes it possible to perform a full *what you see is what you get* optimization. The problem is separated in a pricing and a master problem, which are called sequentially in an iterative loop. The pricing problem determines the optimal apertures to be added to the problem and, if the machine and collimator are fully modelled, the chosen apertures reflect the physical capabilities of the treatment device including tongue-and-groove design of the collimator (Salari *et al* 2011), account for leaf and interleaf leakage, and can also model the treatment head. Dose computation can be done using the actual equivalent field-size, or use more sophisticated methods like Monte-Carlo. With the generated apertures, the master problem performs a normal optimization, based on treatment goals. A single pricing problem can be solved within a second using a GPU (Men *et al* 2010), and grows linear in the number of beamlets

(Romeijn *et al* 2005). The master problem only optimizes apertures, which is a relatively small amount (20-200) compared to beamlet based optimizations (300-5000). As this DAO is exact, has low computation times and is accurate, this approach will be implemented in iCycle in the future.

A powerful extension of direct aperture optimization is that the delivery time may also be actively optimized on (Craft *et al* 2007). If the treatment time can be accurately incorporated in the optimization (as an objective), one can look for an optimal treatment that is deliverable using the full time available in a time-slot.

11.12 iCycle for other treatment modalities

As the optimizer is a general purpose optimizer, it is straightforward to use for other treatment modalities, such as circular cone based CyberKnife treatments or intensity modulated proton therapy (IMPT). The degrees of freedom are much larger for these treatment modalities, so the iCycle optimizer cannot be efficiently used directly. Van de Water *et al* (2011a) introduced a method for dimensionality reduction for CyberKnife treatments and IMPT.

For circular cone based treatments with the CyberKnife, there are 117 fixed node positions, and 12 fixed cone sizes. However, from each node position, *target points* can be freely chosen (i.e. there is no fixed isocentre). As travelling to a new node position requires a considerable amount of time while targeting a new target point can be done almost instantaneously, the number of node positions should be as small as possible. Van de Water *et al* (2011a,b) generated samples of candidate beams and used the multi-criteria optimizer from iCycle (Breedveld *et al* 2009a, chapter 5 in this thesis), *including* all 117 node positions and 12 cone sizes at once. Then, beams that fell below a certain *MU* level were removed. Also and an additional 5% of the beams with the least contribution were removed. This iterative procedure was repeated until the plan quality degraded. The iterative procedure was part of a larger loop where new candidate beams were added and node positions were removed (based on their contribution to the plan), repeated until the desired number of node positions was reached.

For proton therapy, the large dimensionality originates from the required multiple energy levels and dense proton spot grid, as dose deposition of the Bragg-peak is very localized (compared to photon therapy). An iterative re-sampling procedure, similar to the one used for the CyberKnife, was used to reduce the dimensionality for intensity modulated proton therapy planning (Van de Water *et al* 2012). For a fixed beam setup, ≈ 5000 spots are randomly sampled (spatially in the target, which automatically includes different energy levels). A full multi-criteria optimization was performed, and spots with a low number of *MU* were removed from the set. Additionally, 5% of the spots with the least contribution to the objectives were removed as well. Then, new spots were added

to the problem. In this loop of iterative optimization and re-sampling, plan quality strictly improved as the beams selected in the previous iteration were optimized together with newly selected spots. After several iterations, the plan quality converged, and the optimization finished. An additional result of the re-sampling is that the final number of proton spots was relatively low, resulting in a shorter treatment time.

The next step is to optimize the beam angles for proton therapy, which is currently under active research.

References

- AHMAD, R., HOOGEMAN, M.S., BONDAR, M.L., DHAWTAL, V., QUINT, S., DE PREE, I., MENS, J.W. & HEIJMEN, B.J.M. (2011). Increasing treatment accuracy for cervical cancer patients using correlations between bladder filling changes and cervix-uterus displacements; proof of principle. *Radiother. Oncol.*, **98**, 340–346, [📄](#). 146
- ALBER, M. & NÜSSLIN, F. (2001). Optimization of intensity modulated radiotherapy under constraints for static and dynamic MLC delivery. *Phys. Med. Biol.*, **46**, 3229–3239, [📄](#). 153
- ALBER, M. & REEMTSEN, R. (2007). Intensity modulated radiotherapy treatment planning by use of a barrier-penalty multiplier method. *Optim. Methods Softw.*, **22**, 391–411, [📄](#). 47, 64, 91, 104, 116, 150
- ALBER, M., BIRKNER, M. & NÜSSLIN, F. (2002a). Tools for the analysis of dose optimization: II. sensitivity analysis. *Phys. Med. Biol.*, **47**, N265–N270, [📄](#). 51, 149
- ALBER, M., MEEDT, G. & NÜSSLIN, F. (2002b). On the degeneracy of the IMRT optimization problem. *Med. Phys.*, **29**, 2584–2589, [📄](#). 22, 150
- ALEMAN, D.M., KUMAR, A., AHUNJA, R.K., ROMEIJN, H.E. & DEMPSEY, J. (2008). Neighborhood search approaches to beam orientation optimization in intensity modulated radiation therapy treatment planning. *J. Glob. Optim.*, **42**, 587–607, [📄](#). 61
- ALEMAN, D.M., ROMEIJN, H.E. & DEMPSEY, J.F. (2009). A response surface approach to beam orientation optimization in intensity modulated radiation therapy treatment planning. *INFORMS J. Comput.*, **21**, 62–76, [📄](#). 61, 113
- ALEMAN, D.M., GLASER, D., ROMEIJN, H.E. & DEMPSEY, J.F. (2010). Interior point algorithms: guaranteed optimality for fluence map optimization in IMRT. *Phys. Med. Biol.*, **55**, 5467–5482, [📄](#). 149
- ALUWINI, S., VAN ROOIJ, P., HOOGEMAN, M., BANGMA, C., KIRKELS, W.J., INCROCCI, L., & KOLKMAN-DEURLOO, I.K. (2010). Cyberknife stereotactic radiotherapy as monotherapy for low- to intermediate-stage prostate cancer: early experience, feasibility and tolerance. *J. Endourol.*, **24**, 865–869, [📄](#). 113

- ANDERS, L.C., STIELER, F., SIEBENLIST, K., SCHÄFER, J., LOHR, F. & WENZ, F. (2012). Performance of an atlas-based autosegmentation software for delineation of target volumes for radiotherapy of breast and anorectal cancer. *Radiother. Oncol.*, **102**, 68–73, [↗](#). 144
- ANDERSON, E., BAI, Z., ANDD S BLACKFORD, C.B., DEMMEL, J., DONGARRA, J., CROZ, J.D., GREENBAUM, A., HAMMARLING, S., MCKENNY, A. & SORENSEN, D. (1999). *LAPACK Users' Guide*. Philadelphia, PA: Society for Industrial and Applied Mathematics, [↗](#). 15, 149
- ARCANGELI, G., FOWLER, J., GOMELLINI, S., ARCANGELI, S., SARACINO, B., PETRONGARI, M., BENASSI, M. & STRIGARI, L. (2011). Acute and late toxicity in a randomized trial of conventional versus hypofractionated three-dimensional conformal radiotherapy for prostate cancer. *Int. J. Radiat. Oncol. Biol. Phys.*, **79**, 1013–21, [↗](#). 113
- AZIZI SULTAN, A.S. & KÜFER, K.H. (2006). A dynamic algorithm for beam orientations in multicriteria IMRT planning. *Berichte des Fraunhofer ITWM*, **101**, [↗](#). 61, 80, 81
- BAATAR, D., HAMACHER, H.W., EHRGOTT, M. & WOEGINGER, G.J. (2005). Decomposition of integer matrices and multileaf collimator sequencing. *Discrete Appl. Math.*, **152**, 6–34, [↗](#). 153
- BEDFORD, J.L. & WEBB, S. (2006). Constrained segment shapes in direct-aperture optimization for step-and-shoot IMRT. *Med. Phys.*, **33**, 944–958, [↗](#). 153
- BENSON, H.Y. & SHANNO, D.F. (2007). Interior-point methods for nonconvex nonlinear programming: regularization and warmstarts. *Comput. Optim. Appl.*, **40**, 143–189, [↗](#). 68, 148
- BERTSEKAS, D.P. (1995). *Nonlinear Programming*. Belmont: Athena Scientific. 51
- BLOMGREN, H., LAX, I., NASLUND, I. & SVANSTROM, R. (1995). Stereotactic high dose fraction radiation therapy of extracranial tumours using an accelerator. *Acta Oncol.*, **34**, 861–870, [↗](#). 113
- BONDAR, M.L., HOOGEMAN, M.S., OSORIO, E.M.V. & HEIJMEN, B.J.M. (2010). A symmetric nonrigid registration method to handle large organ deformations in cervical cancer patients. *Med. Phys.*, **37**, 3760–3772, [↗](#). 141
- BONDAR, M.L., HOOGEMAN, M.S., MENS, J.W., DHAWTAL, V., DE PREE, I., AHMAD, R., QUINT, S. & HEIJMEN, B.J.M. (2011). Towards an individualized target motion management for IMRT of cervical cancer based on accurate prediction of the cervix-uterus shape and position. *Radiother. Oncol.*, **99**, 240–245, [↗](#). 146
- BONDAR, M.L., HEIJMEN, B.J.M. & HOOGEMAN, M.S. (2012). Fast and robust automated segmentation of the cervix-uterus structure in CT-images driven by patient-

- specific motion-models. *Med. Phys.*, **39**, 3881, [↗](#). 144
- BORTFELD, T., BURKELBACH, J., BOESECKE, R. & SCHLEGEL, W. (1990). Methods of image reconstruction from projections applied to conformation radiotherapy. *Phys. Med. Biol.*, **35**, 1423–1434, [↗](#). 7, 30
- BORTFELD, T., STEIN, J. & PREISER, K. (1997). Clinically relevant intensity modulation optimization using physical criteria. *Proc. XII Int. Conf. Use of Computers in Radiation Therapy (Salt Lake City, UT)*. 24, 32
- BRAHME, A. (1995). *Radiation Therapy Physics*, chap. 11 Treatment Optimization Using Physical and Radiobiological Objective Functions, 209–246. Berlin: Springer-Verlag, editor Alfred R. Smith. 7, 30
- BREEDVELD, S., STORCHI, P.R.M., KEIJZER, M. & HEIJMEN, B.J.M. (2006). Fast, multiple optimizations of quadratic dose objective functions in IMRT. *Phys. Med. Biol.*, **51**, 3569–3579, [↗](#). 21, 29, 31, 32, 47, 153
- BREEDVELD, S., STORCHI, P.R.M., KEIJZER, M., HEEMINK, A.W. & HEIJMEN, B.J.M. (2007a). A novel approach to multi-criteria inverse planning for IMRT. *Phys. Med. Biol.*, **52**, 6339–6353, [↗](#). 47, 48, 49, 53, 61, 63, 88, 89, 101, 104, 108, 114
- BREEDVELD, S., STORCHI, P.R.M., KEIJZER, M. & HEIJMEN, B.J.M. (2007b). *Automated adaption of voxel-dependent importance factors in inverse planning*, vol. 1, 232–236. Proc. XV Int. Conf. Use of Computers in Radiation Therapy (Toronto, Canada). 32
- BREEDVELD, S., STORCHI, P. & HEIJMEN, B. (2009a). The equivalence of multi-criteria methods for radiotherapy plan optimization. *Phys. Med. Biol.*, **54**, 7199–7209, [↗](#). 60, 61, 63, 65, 66, 81, 88, 89, 101, 104, 117, 129, 137, 149, 154
- BREEDVELD, S., STORCHI, P. & HEIJMEN, B. (2009b). Multi-criteria beam angle IMRT optimization with iCycle. *Radiother. Oncol.*, **92**, S204, [↗](#). 152
- BREEDVELD, S., STORCHI, P., VOET, P. & HEIJMEN, B. (2012). iCycle: Integrated, multicriterial beam angle, and profile optimization for generation of coplanar and non-coplanar IMRT plans. *Med. Phys.*, **39**, 951–963, [↗](#). 88, 89, 101, 102, 103, 104, 108, 113, 114, 116, 129, 131, 137, 141
- BRENNER, D. & HALL, E. (1999). Fractionation and protraction for radiotherapy of prostate carcinoma. *Int. J. Radiat. Oncol. Biol. Phys.*, **43**, 1095–101, [↗](#). 113
- BUETTNER, F., GULLIFORD, S., WEBB, S. & PARTRIDGE, M. (2010). Using a parameterized representation of the 3D dose distribution to predict radiation-induced toxicities. *Proc. XVI Int. Conf. Use of Computers in Radiation Therapy (Amsterdam, The Netherlands)*. 146

- BYRD, R.H., LU, P., NOCEDAL, J. & ZHU, C. (1995). A limited memory algorithm for bound constrained optimization. *SIAM J. Sci. Comput.*, **16**, 1190–1208, [↗](#). 153
- CAMPADELLI, P., CASIRAGHI, E. & PRATISSOLI, S. (2010). Performance evaluation of automatic anatomy segmentation algorithm on repeat or four-dimensional computed tomography images using deformable image registration method. *Artif. Intell. Med.*, **50**, 3–11, [↗](#). 142
- CARLSSON, F. & FORSGREN, A. (2006). Iterative regularization in intensity-modulated radiation therapy optimization. *Med. Phys.*, **33**, 225–234, [↗](#). 11
- CHANKONG, V. & HAIMES, Y.Y. (1983a). *Multiobjective Decision Making Theory and Methodology*. New York: Elsevier Science. 51
- CHANKONG, V. & HAIMES, Y.Y. (1983b). Optimization-based methods for multiobjective decision making: an overview. *Large Scale Syst.*, **5**, 1–33. [47](#), [51](#), [57](#)
- CHO, P.S. & PHILLIPS, M.H. (2001). Reduction of computational dimensionality in inverse radiotherapy planning using sparse matrix operations. *Phys. Med. Biol.*, **46**, N117–N125, [↗](#). [7](#), [9](#)
- CLARK, V., CHEN, Y., APTE, A., MICHALSKI, J. & DEASY, J. (2010). Prioritized prescription IMRT optimization: A comparison with pinnacle planning results. *Proc. XVI Int. Conf. Use of Computers in Radiation Therapy (Amsterdam, The Netherlands)*. [61](#)
- COTRUTZ, C. & XING, L. (2002). Using voxel-based importance factors for interactive dvh-based dose optimization. *Phys. Med. Biol.*, **47**, 1659–1669, [↗](#). [7](#), [21](#), [30](#), [32](#), [44](#)
- COTRUTZ, C. & XING, L. (2003). IMRT dose shaping with regionally variable penalty scheme. *Med. Phys.*, **30**, 544–551, [↗](#). [30](#)
- COTRUTZ, C., LAHANAS, M., KAPPAS, C. & BALTAS, D. (2001). A multiobjective gradient-based dose optimization algorithm for external beam conformal radiotherapy. *Phys. Med. Biol.*, **46**, 2161–2175, [↗](#). [29](#)
- CRAFT, D. & BORTFELD, T. (2008). How many plans are needed in an IMRT multiobjective plan database? *Phys. Med. Biol.*, **53**, 2785–2796, [↗](#). [47](#), [48](#), [61](#), [131](#), [144](#)
- CRAFT, D. & MONZ, M. (2010). Simultaneous navigation of multiple Pareto surfaces, with an application to multicriteria IMRT planning with multiple beam angle configurations. *Med. Phys.*, **37**, 736–741, [↗](#). [61](#), [80](#)
- CRAFT, D., SÜSS, P. & BORTFELD, T. (2007). The tradeoff between treatment plan quality and required number of monitor units in intensity-modulated radiotherapy. *Int. J. Radiat. Oncol. Biol. Phys.*, **67**, 1596–1605, [↗](#). [154](#)
- CRAFT, D.L., HALABI, T.F. & BORTFELD, T.R. (2005). Exploration of tradeoffs in

- intensity-modulated radiotherapy. *Phys. Med. Biol.*, **50**, 5857–5868, [↗](#). 29, 43
- CRAFT, D.L., HALABI, T.F., SHIH, H.A. & BORTFELD, T.R. (2006). Approximating convex Pareto surfaces in multiobjective radiotherapy planning. *Med. Phys.*, **33**, 3399–3407, [↗](#). 29, 43
- CRAFT, D.L., HONG, T.S., SHIH, H.A. & BORTFELD, T.R. (2012). Improved planning time and plan quality through multicriteria optimization for intensity-modulated radiotherapy. *Int. J. Radiat. Oncol. Biol. Phys.*, e83–e90, [↗](#). 97, 109
- DAS, S.K., CULLIP, T., TRACTON, G., CHANG, S., MARKS, L., ANSCHER, M. & ROSENMAN, J. (2003). Beam orientation selection for intensity-modulated radiation therapy based on target equivalent uniform dose maximization. *Int. J. Radiat. Oncol. Biol. Phys.*, **55**, 215–224, [↗](#). 61, 72
- DAS, S.K., BELL, M., LAWRENCE, B.M. & ROSENMAN, J.G. (2004). A preliminary study of the role of modulated electron beams in intensity modulated radiotherapy, using automated beam orientation and modality selection. *Int. J. Radiat. Oncol. Biol. Phys.*, **59**, 602–617, [↗](#). 82
- DAWSON, L.A., ECCLES, C. & CRAIG, T. (2006). Individualized image guided iso-NTCP based liver cancer SBRT. *Acta Oncol.*, **45**, 856–864, [↗](#). 135
- DEASY, J.O. (1997). Multiple local minima in radiotherapy optimization problems with dose-volume constraints. *Med. Phys.*, **24**, 1157–1161, [↗](#). 149
- DEMANES, D., RODRIGUEZ, R., SCHOUR, L., BRANDT, D. & ALTIERI, G. (2005). High-dose-rate intensity-modulated brachytherapy with external beam radiotherapy for prostate cancer: California endocurietherapy's 10-year results. *Int. J. Radiat. Oncol. Biol. Phys.*, **61**, 1306–16, [↗](#). 113
- DIJKEMA, T., RAAIJMAKERS, C.P.J., TEN HAKEN, R.K., ROESINK, J.M., BRAAM, P.M., HOUWELING, A.C., MOERLAND, M.A., EISBRUCH, A. & TERHAARD, C.H.J. (2010). Parotid gland function after radiotherapy: the combined Michigan and Utrecht experience. *Int. J. Radiat. Oncol. Biol. Phys.*, **78**, 449–453, [↗](#). 88, 92, 103
- DJAJAPUTRA, D., WU, Q., WU, Y. & MOHAN, R. (2003). Algorithm and performance of a clinical IMRT beam-angle optimization system. *Phys. Med. Biol.*, **48**, 3191–3212, [↗](#). 87
- DUFF, I., ERISMAN, A.M. & REID, J.K. (1986). *Direct Methods for Sparse Matrices*. Oxford: Clarendon. 10
- DUTCH CANCER SOCIETY (2011). Aantal nieuwe kankerpatiënten per jaar stijgt met 40% naar 123.000. [↗](#), [Online; published 6-September-2011]. 145
- EASLEY, D. & KLEINBERG, J. (2008). *Networks*, 71. Cornell Store Press. 146

- ECCLES, C.L., DAWSON, L.A., MOSELEY, J.L. & BROCK, K.K. (2011). Interfraction liver shape variability and impact on gtv position during liver stereotactic radiotherapy using abdominal compression. *Int. J. Radiat. Oncol. Biol. Phys.*, **80**, 938–946, [↗](#). 141
- EHRGOTT, M., HOLDER, A. & REESE, J. (2008). Beam selection in radiotherapy design. *Linear Algebr. Appl.*, **428**, 1272–1312, [↗](#). 61
- FORSGREN, A., GILL, P.E. & WRIGHT, M.H. (2002). Interior methods for nonlinear optimization. *SIAM Rev.*, **44**, 525–597, [↗](#). 52
- FOWLER, J., CHAPPELL, R. & RITTER, M. (2001). Is alpha/beta for prostate tumors really low? *Int. J. Radiat. Oncol. Biol. Phys.*, **50**, 1021–1031, [↗](#). 113
- FREEMAN, D. & KING, C. (2011). Stereotactic body radiotherapy for low-risk prostate cancer: five-year outcomes. *Radiother. Oncol.*, **6**, 3, [↗](#). 113
- FREEMAN, D.E., FRIEDLAND, J.L. & MASTERTON-MCGARY, M.E. (2010). Stereotactic radiosurgery for low-intermediate risk prostate cancer: An emerging treatment approach. *Am. J. Clin. Oncol.*, **33**, 208, [↗](#). 113
- FREIMAN, M., COOPER, O., LISCHINSKI, D. & JOSKOWICZ, L. (2011). Liver tumors segmentation from CTA images using voxels classification and affinity constraint propagation. *Int. J. Comput. Assist. Radiol. Surg.*, **6**, 247–255, [↗](#). 142
- FULLER, D., MARDIROSSIAN, G., WONG, D. & MCKELLAR, H. (2011). Prospective evaluation of CyberKnife stereotactic body radiotherapy for low- and intermediate-risk prostate cancer: Emulating HDR brachytherapy dose distribution. 113
- FULLER, D.B., NAITOH, J., LEE, C., HARDY, S. & JIN, H. (2008). Virtual HDR CyberKnife treatment for localized prostatic carcinoma: dosimetry comparison with HDR brachytherapy and preliminary clinical observations. *Int. J. Radiat. Oncol. Biol. Phys.*, **70**, 1588–1597, [↗](#). 113
- GOLUB, G.H. & VAN LOAN, C.F. (1989). *Matrix Computations*. Baltimore MD: Johns Hopkins University Press. 11
- GONDZIO, J. (1996). Multiple centrality corrections in a primal-dual method for linear programming. *Comput. Optim. Appl.*, **6**, 137–157, [↗](#). 148
- GONDZIO, J. (2012). Matrix-free interior-point method. *Comput. Optim. Appl.*, **51**, 457–480, [↗](#). 153
- GONDZIO, J. & GROTHEY, A. (2008). A new unblocking technique to warmstart interior point methods based on sensitivity analysis. *SIAM J. Optim.*, **19**, 1184–1210, [↗](#). 148
- GRANAT, J. & MAKOWSKI, M. (2000). Interactive specification and analysis of aspiration-based preferences. *Eur. J. Oper. Res.*, **122**, 469–485, [↗](#). 152
- GRILLS, I., MARTINEZ, A., HOLLANDER, M., HUANG, R., GOLDMAN, K., CHEN, P. &

- GUSTAFSON, G. (2004). High dose rate brachytherapy as prostate cancer monotherapy reduces toxicity compared to low dose rate palladium seeds. *J. Urol.*, **171**, 1098–104, [↗](#). 113
- GU, X., PAN, H., LIANG, Y., RICHARD CASTILLO AND, D.Y., CHOI, D., CASTILLO, E., MAJUMDAR, A., GUERRERO, T. & JIANG, S.B. (2010). Implementation and evaluation of various demons deformable image registration algorithms on a gpu. *Phys. Med. Biol.*, **55**, 207–220, [↗](#). 144
- GUNAWARDENA, A.D.A., D'SOUZA, W.D., GOADRICH, L.D., MEYER, R.R., SORENSEN, K.J., NAQVI, S.A. & SHI, L. (2006). A difference-matrix metaheuristic for intensity map segmentation in step-and-shoot IMRT delivery. *Phys. Med. Biol.*, **51**, 2517–2536, [↗](#). 153
- GUSTAVSON, F.G. (1978). Two fast algorithms for sparse matrices: multiplication and permuted transposition. *ACM Trans. Math. Soft.*, **4**, 250–269, [↗](#). 10, 15, 149
- HAIMES, Y.Y., LASDON, L.S. & WISMER, D.A. (1971). On a bicriterion formulation of the problems of integrated system identification and system optimization. *IEEE Trans. Syst. Man Cybern.*, **1**, 296–297, [↗](#). 43, 47, 49
- HALABI, T., CRAFT, D. & BORTFELD, T. (2006). Dose-volume objectives in multi-criteria optimization. *Phys. Med. Biol.*, **51**, 3809–3818, [↗](#). 29, 36, 43, 150
- HEIJMEN, B.J.M., DE BOER, J.C.J., STROOM, J.C. & LEVENDAG, P.C. (2003). Geometrical uncertainties and inverse treatment planning for IMRT: an integrated approach instead of using planning margins. *Int. J. Radiat. Oncol. Biol. Phys.*, **57**, S235, [↗](#). 7
- HOFFMANN, A.L., SIEM, A.Y.D., DEN HERTOOG, D., KAANDERS, J.H.A.M. & HUIZENGA, H. (2006). Derivative-free generation and interpolation of convex Pareto optimal IMRT plans. *Phys. Med. Biol.*, **51**, 6349–6369, [↗](#). 29, 43, 44
- HOFFMANN, A.L., DEN HERTOOG, D., SIEM, A.Y.D., KAANDERS, J.H.A.M. & HUIZENGA, H. (2008). Convex reformulation of biologically based multi-criteria intensity-modulated radiation therapy optimization including fractionation effects. *Phys. Med. Biol.*, **53**, 6345–6362, [↗](#). 47
- HOLDSWORTH, C., STEWART, R.D., KIM, M., LIAO, J. & PHILLIPS, M.H. (2011). Investigation of effective decision criteria for multiobjective optimization in IMRT. *Med. Phys.*, **38**, 2964–2947, [↗](#). 144
- HOUWELING, A.C., PHILIPPENS, M.E., DIJKEMA, T., ROESINK, J.M., TERHAARD, C.H., SCHILSTRA, C., HAKEN, R.K.T., EISBRUCH, A. & RAAIJMAKERS, C.P. (2010). A comparison of dose-response models for the parotid gland in a large group of head-and-neck cancer patients. *Int. J. Radiat. Oncol. Biol. Phys.*, **76**, 1259–1265,

[↗](#). 145

- ICRU REPORT 83 (2010). Prescribing, Recording, and Reporting Photon-Beam Intensity-Modulated Radiation Therapy (IMRT). vol. 10, Oxford University Press, Avenel, NJ, [↗](#). 118
- JABBARI, S., WEINBERG, V., KAPREALIAN, T., HSU, I., MA, L., CHUANG, C., DESCOVICH, M., SHIAO, S., SHINOHARA, K., ROACH, M. & GOTTSCHALK, A. (2012). Stereotactic body radiotherapy as monotherapy or post-external beam radiotherapy boost for prostate cancer: technique, early toxicity, and PSA response. *Int. J. Radiat. Oncol. Biol. Phys.*, **82**, 228–34, [↗](#). 113
- JEE, K.W., MCSHAN, D.L. & FRAASS, B.A. (2007). Lexicographic ordering: intuitive multicriteria optimization for IMRT. *Phys. Med. Biol.*, **52**, 1845–1861, [↗](#). 30, 43, 47, 49, 61
- JERAJ, R., KEALL, P.J. & SIEBERS, J.V. (2002). The effect of dose calculation accuracy on inverse treatment planning. *Phys. Med. Biol.*, 301–407, [↗](#). 131
- JIN, R., MIN, Z., SONG, E., LIU, H., & YE, Y. (2010). A novel fluence map optimization model incorporating leaf sequencing constraints. *Phys. Med. Biol.*, **55**, 1243–1264, [↗](#). 153
- KATZ, A. & SANTORO, M. (2009). Cyberknife radiosurgery for early carcinoma of the prostate: A three year experience. *Int. J. Radiat. Oncol. Biol. Phys.*, **75**, S312–S313, [↗](#). 113
- KAVANAGH, B.D., MCGARRY, R.C. & TIMMERMAN, R.D. (2006). Extracranial radiosurgery (stereotactic body radiation therapy) for oligometastases. *Semin. Radiat. Oncol.*, **16**, 77–84, [↗](#). 135
- KILBY, W., DOOLEY, J.R., KUDUVALLI, G., SAYEH, S. & MAURER, J., C. R. (2010). The cyberknife robotic radiosurgery system in 2010. *Technol. Cancer Res. Treat.*, **9**, 433–452, [↗](#). 113
- KING, C. & FOWLER, J. (2001). A simple analytic derivation suggests that prostate cancer alpha/beta ratio is low. *Int. J. Radiat. Oncol. Biol. Phys.*, **51**, 213–214, [↗](#). 113
- KING, C., LEHMANN, J., ADLER, J. & HAI, J. (2003). Cyberknife radiotherapy for localized prostate cancer: rationale and technical feasibility. *Technol. Cancer Res. Treat.*, **2**, 25–30, [↗](#). 113
- KING, C., BROOKS, J., GILL, H. & PRESTI, J.J. (2011). Long-term outcomes from a prospective trial of stereotactic body radiotherapy for low-risk prostate cancer. *Int. J. Radiat. Oncol. Biol. Phys.*, **82**, 877–82, [↗](#). 113
- KOLATA, G. (1990). What if they closed 42d street and nobody noticed? New York

- Times, [↗](#), [published 25-December-1990]. [146](#)
- KÜFER, K.H., MONZ, M., SCHERRER, A., SÜSS, P., ALONSO, F., AZIZI SULTAN, A.S., BORTFELD, T., CRAFT, D. & THIEKE, C. (2005). Multicriteria optimization in intensity modulated radiotherapy planning. *Berichte des Fraunhofer ITWM*, **77**, [↗](#). [29](#), [44](#)
- LAHANAS, M., SCHREIBMANN, E. & BALTAS, D. (2003). Multiobjective inverse planning for intensity modulated radiotherapy with constraint-free gradient-based optimization algorithms. *Phys. Med. Biol.*, **48**, 2843–2871, [↗](#). [29](#)
- LEE, E.K., FOX, T. & CROCKER, I. (2006). Simultaneous beam geometry and intensity map optimization in intensity-modulated radiation therapy. *Int. J. Radiat. Oncol. Biol. Phys.*, **64**, 1325–1337, [↗](#). [61](#)
- LEINDERS, S.M., BREEDVELD, S., ROMERO, A.M., SCHAART, D., SEPPENWOOLDE, Y. & HEIJMEN, B. (2013). Adaptive liver SBRT: can automated daily plan re-optimization prevent dose delivery degradation caused by anatomy deformation? *Int. J. Radiat. Oncol. Biol. Phys.*, **87**, 1016–1021, [↗](#). [152](#)
- LEVENDAG, P.C., TEGUH, D.N., VOET, P., VAN DER EST, H., NOEVER, I., DE KRUIJF, W.J.M., KOLKMAN-DEURLOO, I.K., PREVOST, J.B., POLL, J., SCHMITZ, P.I.M. & HEIJMEN, B.J.M. (2007). Dysphagia disorders in patients with cancer of the oropharynx are significantly affected by the radiation therapy dose to the superior and middle constrictor muscle: A dose-effect relationship. *Radiother. Oncol.*, **85**, 64–73, [↗](#). [101](#)
- LI, X.A., LIU, F., TAI, A., AHUNBAY, E., CHEN, G., KELLY, T., LAWTON, C. & ERICKSON, B. (2011). Development of an online adaptive solution to account for inter- and intra-fractional variations. *Radiother. Oncol.*, **100**, 370–374, [↗](#). [135](#)
- LI, Y., YAO, D., YAO, J. & CHAN, W. (2005). A particle swarm optimization algorithm for beam angle selection in intensity-modulated radiotherapy planning. *Phys. Med. Biol.*, **50**, 3491–3514, [↗](#). [61](#)
- LIU, F., ERICKSON, B., PENG, C. & LI, X.A. (2012). Characterization and management of interfractional anatomic changes for pancreatic cancer radiotherapy. *Int. J. Radiat. Oncol. Biol. Phys.*, **83**, e423–e429, [↗](#). [135](#)
- LLACER, J., DEASY, J.O., BORTFELD, T.R., SOLBERG, T.D. & PROMBERGER, C. (2003). Absence of multiple local minima effects in intensity modulated optimization with dose-volume constraints. *Phys. Med. Biol.*, **48**, 183–210, [↗](#). [150](#)
- MAGMA (2011). Matrix Algebra on GPU and Multicore Architectures. Innovative Computer Laboratory, University of Tennessee, [↗](#). [152](#)
- MANGASARIAN, O.L. (1969). *Nonlinear Programming*. New York: McGraw-Hill. [51](#)

- MATUSZAK, M.M., LARSEN, E.W., JEE, K.W., MCSHAN, D.L. & FRAASS, B.A. (2008). Adaptive diffusion smoothing: A diffusion-based method to reduce IMRT field complexity. *Med. Phys.*, **35**, 1532–1546, [↗](#). 153
- MCDONALD, J.H. (2009). *Handbook of Biological Statistics*, 198–201. Sparky House, Baltimore, MD, 2nd edn. 92
- MEEDT, G., ALBER, M. & NÜSSLIN, F. (2003). Non-coplanar beam direction optimization for intensity-modulated radiotherapy. *Phys. Med. Biol.*, **48**, 2999–3019, [↗](#). 61, 87
- MEHROTRA, S. (1992). On the implementation of a primal-dual interior point method. *SIAM J. Optim.*, **2**, 575–601, [↗](#). 148
- MEN, C., ROMELIJN, E., TAŞKIN, C. & DEMPSEY, J. (2007). An exact approach to direct aperture optimization in IMRT treatment planning. *Phys. Med. Biol.*, **52**, 7333–7352, [↗](#). 153
- MEN, C., JIA, X. & JIANG, S. (2010). GPU-based ultra-fast direct aperture optimization for online adaptive radiation therapy. *Phys. Med. Biol.*, **55**, 4309–4320, [↗](#). 153
- MÉNDEZ ROMERO, A., WUNDERINK, W., HUSSAIN, S.M., DE POOTER, J.A., HEIJMEN, B.J.M., NOWAK, P.C.J.M., NUYTENS, J.J., BRANDWIJK, R.P., VERHOEF, C., IJZERMANS, J.N.M. & LEVENDAG, P.C. (2006). Stereotactic body radiation therapy for primary and metastatic liver tumors: A single institution phase i-ii study. *Acta Oncol.*, **45**, 831–837, [↗](#). 135
- MÉNDEZ ROMERO, A., ZINKSTOK, R.T., WUNDERINK, W., VAN OS, R.M., JOOSTEN, H., SEPPENWOOLDE, Y., NOWAK, P.J., BRANDWIJK, R.P., VERHOEF, C., IJZERMANS, J.N., LEVENDAG, P.C. & HEIJMEN, B.J.M. (2009). Stereotactic body radiation therapy for liver tumors: impact of daily setup corrections and day-to-day anatomic variations on dose in target and organs at risk. *Int. J. Radiat. Oncol. Biol. Phys.*, **75**, 1201–1208, [↗](#). 135, 137
- MICHALSKI, J., GAY, H., JACKSON, A., TUCKER, S. & DEASY, J. (2010). Radiation dose-volume effects in radiation-induced rectal injury. *Int. J. Radiat. Oncol. Biol. Phys.*, **76**, S123–S129, [↗](#). 118, 130
- MIETTINEN, K. (1999). *Nonlinear multiobjective optimization*. Boston: Kluwer Academic Publishers. 50, 51, 57, 143
- MIRALBELL, R., ROBERTS, S., ZUBIZARRETA, E. & HENDRY, J. (2012). Dose-fractionation sensitivity of prostate cancer deduced from radiotherapy outcomes of 5,969 patients in seven international institutional datasets: $\alpha/\beta=1.4$ (0.9–2.2) Gy. *Int. J. Radiat. Oncol. Biol. Phys.*, **82**, e17–e24, [↗](#). 113
- MONZ, M., KÜFER, K.H., BORTFELD, T.R. & THIEKE, C. (2008). Pareto navigation -

- algorithmic foundation of interactive multi-criteria IMRT planning. *Phys. Med. Biol.*, **53**, 985–998, [↗](#). [47](#), [48](#), [61](#), [131](#), [144](#)
- MOORE, K.L., BRAME, R.S., LOW, D.A. & MUTIC, S. (2012). Quantitative metrics for assessing plan quality. *Semin. Radiat. Oncol.*, **22**, 62–69, [↗](#). [144](#)
- MURAI, T., SHIBAMOTO, Y., BABA, F., HASHIZUME, C., MORI, Y., AYAKAWA, S., KAWAI, T., TAKEMOTO, S., SUGIE, C. & OGINO, H. (2012). Progression of non-small-cell lung cancer during the interval before stereotactic body radiotherapy. **82**, 463–467, [↗](#). [145](#)
- MURDOCH-KINCH, C.A., KIM, H.M., VINEBERG, K.A., SHIP, J.A. & EISBRUCH, A. (2008). Dose-effect relationships for the submandibular salivary glands and implications for their sparing by intensity modulated radiotherapy. *Int. J. Radiat. Oncol. Biol. Phys.*, **72**, 373–382, [↗](#). [88](#), [92](#), [103](#)
- NOCEDAL, J. & WRIGHT, S. (2000). *Numerical optimization*. Springer. [148](#)
- NORKUS, D., MILLER, A., KURTINAITIS, J., HAVERKAMP, U., POPOV, S., PROTT, F. & VALUCKAS, K. (2009). A randomized trial comparing hypofractionated and conventionally fractionated three-dimensional external-beam radiotherapy for localized prostate adenocarcinoma : a report on acute toxicity. *Strahlenther. Onkol.*, **185**, 715–21, [↗](#). [113](#)
- NUTTING, C.M., ROWBOTTOM, C.G., COSGROVE, V.P., HENK, J.M., DEARNALEY, D.P., ROBINSON, M.H., CONWAY, J. & WEBB, S. (2001). Optimisation of radiotherapy for carcinoma of the parotid gland: a comparison of conventional, three dimensional conformal, and intensity-modulated techniques. *Radiother. Oncol.*, **60**, 163–172, [↗](#). [87](#)
- OGRYCZAK, W. & KOZLOWSKI, B. (2011). Reference point method with importance weighted ordered partial achievements. *Top*, **19**, 380–401, [↗](#). [152](#)
- OSBORNE, M.J. (2003). *An Introduction to Game Theory*. Oxford University Press. [145](#)
- PAGÈSA, A., GONDZIO, J. & NABONAA, N. (2009). Warmstarting for interior point methods applied to the long-term power planning problem. *Eur. J. Oper. Res.*, **197**, 112–125, [↗](#). [148](#)
- PETIT, S.F., WU, B., KAZHDAN, M., DEKKER, A., SIMARI, P., KUMAR, R., TAYLOR, R., HERMAN, J.M. & MCNUTT, T. (2012). Increased organ sparing using shape-based treatment plan optimization for intensity modulated radiation therapy of pancreatic adenocarcinoma. *Radiother. Oncol.*, **102**, 38–44, [↗](#). [147](#)
- PISSANETSKY, S. (1984). *Sparse Matrix Technology*. London: Academic. [10](#)
- POLLACK, A., HANLON, A., HORWITZ, E., FEIGENBERG, S., KONSKI, A., MOVSAS,

- B., GREENBERG, R., UZZO, R., MA, C., MCNEELEY, S., BUYYOUNOUSKI, M. & PRICE, R.J. (2006). Dosimetry and preliminary acute toxicity in the first 100 men treated for prostate cancer on a randomized hypofractionation dose escalation trial. *Int. J. Radiat. Oncol. Biol. Phys.*, **64**, 518–526, [↗](#). 113
- VAN DER POOL, A.E., MÉNDEZ ROMERO, A., WUNDERINK, W., HEIJMEN, B.J.M., LEVENDAG, P.C., VERHOEF, C. & IJZERMANS, J.N. (2009). Stereotactic body radiation therapy for colorectal liver metastases. *Br. J. Surg.*, **97**, 377–382, [↗](#). 135
- DE POOTER, J.A., MÉNDEZ ROMERO, A., JANSEN, W., STORCHI, P., WOUDESTRA, E., LEVENDAG, P. & HEIJMEN, B. (2006). Computer optimization of noncoplanar beam setups improves stereotactic treatment of liver tumors. *Int. J. Radiat. Oncol. Biol. Phys.*, **66**, 913–922, [↗](#). 88
- DE POOTER, J.A., WUNDERINK, W., MÉNDEZ ROMERO, A., STORCHI, P.R.M. & HEIJMEN, B.J.M. (2007). Ptv dose prescription strategies for SBRT of metastatic liver tumours. *Radiother. Oncol.*, **85**, 260–266, [↗](#). 77, 83
- DE POOTER, J.A., MÉNDEZ ROMERO, A., WUNDERINK, W., STORCHI, P.R.M. & HEIJMEN, B.J.M. (2008). Automated non-coplanar beam direction optimization improves IMRT in SBRT of liver metastasis. *Radiother. Oncol.*, **88**, 376–381, [↗](#). 61, 83, 87, 88, 113
- POTREBKO, P.S., MCCURDY, B.M.C., BUTLER, J.B. & EL-GUBTAN, A.S. (2008). Improving intensity-modulated radiation therapy using the anatomic beam orientation optimization algorithm. *Med. Phys.*, **35**, 2170–2179, [↗](#). 61
- PUGACHEV, A. & XING, L. (2001). Computer-assisted selection of coplanar beam orientations in intensity-modulated radiation therapy. *Phys. Med. Biol.*, **46**, 2467–2476, [↗](#). 61, 113
- ROMEIJN, H.E., AHUJA, R.K., DEMPSEY, J.F., KUMAR, A. & LI, J.G. (2003). A novel linear programming approach to fluence map optimization for intensity modulated radiation therapy treatment planning. *Phys. Med. Biol.*, **48**, 3521–3542, [↗](#). 150
- ROMEIJN, H.E., DEMPSEY, J.F. & LI, J.G. (2004). A unifying framework for multi-criteria fluence map optimization models. *Phys. Med. Biol.*, **49**, 1991–2013, [↗](#). 47
- ROMEIJN, H.E., AHUJA, R.K., DEMPSEY, J.F. & KUMAR, A. (2005). A column generation approach to radiation therapy treatment planning using aperture modulation. *SIAM J. Optim.*, **15**, 838–862, [↗](#). 154
- ROSSI, L. (2012). *Prostate cancer dose optimization with a robotic CyberKnife X-ray unit extended with a dynamic multi-leaf collimator*. Master's thesis, Alma Mater Studiorum - Università di Bologna. 153
- ROSSI, L., BREEDVELD, S., HEIJMEN, B.J.M., VOET, P.W.J., LANCONELLI, N. &

- ALUWINI, S. (2012). On the beam direction search space in computerized non-coplanar beam angle optimization for IMRT - prostate SBRT. *Phys. Med. Biol.*, **57**, 5441–5458, [↗](#). 141
- ROWBOTTOM, C.G., OLDHAM, M. & WEBB, S. (1999). Constrained customization of non-coplanar beam orientations in radiotherapy of brain tumours. *Phys. Med. Biol.*, **44**, 383–399, [↗](#). 61
- RULE, W., TIMMERMAN, R., TONG, L., ABDULRAHMAN, R., MEYER, J., BOIKE, T., SCHWARZ, R.E., WEATHERALL, P. & CHINSOO CHO, L. (2011). Phase I dose-escalation study of stereotactic body radiotherapy in patients with hepatic metastases. *Ann. Surg. Oncol.*, **18**, 1081–1087, [↗](#). 135
- RUOTSALAINEN, H., MIETTINEN, K., PALMGREN, J.E. & LAHTINEN, T. (2010). Interactive multiobjective optimization for anatomy-based three-dimensional HDR brachytherapy. *Phys. Med. Biol.*, **55**, 4703–4719, [↗](#). 61
- SALARI, E., MEN, C. & ROMELJN, H.E. (2011). Accounting for the tongue-and-groove effect using a robust direct aperture optimization approach. *Med. Phys.*, **38**, 1266–1279, [↗](#). 153
- VAN SANTVOORT, J.P.C. & HEIJMEN, B.J.M. (1996). Dynamic multileaf collimation without ‘tongue-and-groove’ underdosage effects. *Phys. Med. Biol.*, **41**, 2091–2105, [↗](#). 118, 153
- SCHERRER, A., KÜFER, K.H., BORTFELD, T., MONZ, M. & ALONSO, F. (2005). IMRT planning on adaptive volume structures - a decisive reduction in computational complexity. *Phys. Med. Biol.*, **50**, 2033–2053, [↗](#). 30
- SCHREIBMANN, E., LAHANAS, M., XING, L. & BALTAS, D. (2004). Multiobjective evolutionary optimization of the number of beams, their orientations and weights for intensity-modulated radiation therapy. *Phys. Med. Biol.*, **49**, 747–770, [↗](#). 61, 80
- SHANNO, D.F. & VANDERBEI, R.J. (2000). Interior-point methods for nonconvex non-linear programming: orderings and higher-order methods. *Math. Program. Ser. B*, **87**, 303–316, [↗](#). 68, 148
- SHEPARD, D.M., EARL, M.A., LI, X.A., NAQVI, S. & YU, C. (2002). Direct aperture optimization: A turnkey solution for step-and-shoot IMRT. *Med. Phys.*, **29**, 1007–1018, [↗](#). 153
- SHOU, Z., YANG, Y., COTRUTZ, C., LEVY, D. & XING, L. (2005). Quantitation of the *a priori* dosimetric capabilities of spatial points in inverse planning and its significant implication in defining IMRT solution space. *Phys. Med. Biol.*, **50**, 1469–1482, [↗](#). 30
- SIMS, R., ISAMBERT, A., GRÉGOIRE, V., BIDAULT, F., FRESCO, L., SAGE, J., MILLS, J., BOURHIS, J., LEFKOPOULOS, D., COMMOWICK, O., BENKEBIL, M. & MA-

- LANDAIN, G. (2009). A pre-clinical assessment of an atlas-based automatic segmentation tool for the head and neck. *Radiother. Oncol.*, **93**, 474–478, [↗](#). 142
- SONNEVELD, P. & VAN GIJZEN, M.B. (2008). IDR(s): a family of simple and fast algorithms for solving large nonsymmetric linear systems. *SIAM J. Sci. Comput.*, **31**, 1035–1062, [↗](#). 153
- SPIROU, S.V. & CHUI, C.S. (1998). A gradient inverse planning algorithm with dose-volume constraints. *Med. Phys.*, **25**, 321–233, [↗](#). 7, 30
- STORCHI, P.R.M. & WOUDESTRA, E. (1996). Calculation of the absorbed dose distribution due to irregularly shaped photon beams using pencil beam kernels derived from basic beam data. *Phys. Med. Biol.*, **41**, 637–656, [↗](#). 8, 36, 68, 118
- STRASSEN, V. (1969). Gaussian elimination is not optimal. *Numer. Math.*, **13**, 354–356, [↗](#). 152
- SÜSS, P., KÜFER, K.H. & THIEKE, C. (2007). Improved stratification algorithms for step-and-shoot MLC delivery in intensity-modulated radiation therapy. *Phys. Med. Biol.*, **52**, 6039–6051, [↗](#). 153
- TEGUH, D.N., LEVENDAG, P.C., VOET, P.W.J., AL-MAMGANI, A., HAN, X., WOLF, T.K., HIBBARD, L.S., NOWAK, P., AKHIAT, H., DIRKX, M.L.P., HEIJMEN, B.J.M. & HOOGEMAN, M.S. (2011). Clinical validation of atlas-based auto-segmentation of multiple target volumes and normal tissue (swallowing/mastication) structures in the head and neck. *Int. J. Radiat. Oncol. Biol. Phys.*, **81**, 950–957, [↗](#). 101, 142
- TEICHERT, K., SÜSS, P., SERNA, J.I., MONZ, M., KÜFER, K.H. & THIEKE, C. (2011). Comparative analysis of pareto surfaces in multi-criteria IMRT planning. *Phys. Med. Biol.*, **56**, 3669–3684, [↗](#). 109, 144
- THIEKE, C., NILL, S., OELFKE, U. & BORTFELD, T. (2002). Acceleration of intensity-modulated radiotherapy dose calculation by importance sampling of the calculation matrices. *Med. Phys.*, **29**, 676–681, [↗](#). 7
- THIEKE, C., KÜFER, K.H., MONZ, M., SCHERRER, A., ALONSO, F., OELFKE, U., HUBER, P.E., DEBUS, J. & BORTFELD, T. (2007). A new concept for interactive radiotherapy planning with multicriteria optimization: First clinical evaluation. *Radiother. Oncol.*, **85**, 292–298, [↗](#). 97, 109, 131, 144
- TOWNSEND, N., HUTH, B., DING, W., GARBER, B., MOOREVILLE, M., ARRIGO, S., LAMOND, J. & BRADY, L. (2010). Acute toxicity after cyberknife-delivered hypofractionated radiotherapy for treatment of prostate cancer. *Am. J. Clin. Oncol.*, **34**, 6–10, [↗](#). 113
- VANDERBEI, R.J. (1999). LOQO: an interior point code for quadratic programming. *Optim. Methods Softw.*, **11**, 451–484, [↗](#). 148

- VANDERBEI, R.J. & SHANNO, D.F. (1999). An interior point algorithm for nonconvex nonlinear programming. *Comput. Optim. Appl.*, **13**, 231–252, [↗](#). 148
- VÁSQUEZ OSORIO, E.M., HOOGEMAN, M.S., BONDAR, M.L., LEVENDAG, P.C. & HEIJMEN, B.J.M. (2009). A novel flexible framework with automatic feature correspondence optimization for nonrigid registration in radiotherapy. *Med. Phys.*, **36**, 2848–2859, [↗](#). 141, 146
- VÁSQUEZ OSORIO, E.M., HOOGEMAN, M.S., TEGUH, D.N., AL-MAMGANI, A., KOLKMAN-DEURLOO, I.K.K., BONDAR, M.L., LEVENDAG, P.C. & HEIJMEN, B.J.M. (2011). Three-dimensional dose addition of external beam radiotherapy and brachytherapy for oropharyngeal patients using nonrigid registration. *Int. J. Radiat. Oncol. Biol. Phys.*, **15**, 1268–1277, [↗](#). 141
- VELEC, M., MOSELEY, J.L., CRAIG, T., DAWSON, L.A. & BROCK, K.K. (2012). Accumulated dose in liver stereotactic body radiotherapy: Positioning, breathing, and deformation effects. *Int. J. Radiat. Oncol. Biol. Phys.*, **83**, 1132–1140, [↗](#). 135, 141
- VOET, P., BREEDVELD, S., DIRKX, M., LEVENDAG, P. & HEIJMEN, B. (2012). Integrated multi-criterial optimization of beam angles and intensity profiles for coplanar and non-coplanar head and neck IMRT and implications for VMAT. *Med. Phys.*, **39**, 4858–4865, [↗](#). 64, 82, 101, 104, 108, 113, 116, 132
- VOET, P., DIRKX, M., BREEDVELD, S., FRANSEN, D., LEVENDAG, P. & HEIJMEN, B. (2013). Towards fully automated multi-criterial plan generation: a prospective clinical study. *Int. J. Radiat. Oncol. Biol. Phys.*, **85**, 866–872, [↗](#). 97, 132, 141
- VOGLIS, C. & LAGARIS, I.E. (2004). BOXCQP: an algorithm for bound constrained convex quadratic problems. *In Proc. 1st IC-SCCE Conf.*, [↗](#). 7, 10, 22
- WANG, H., GARDEN, A.S., ZHANG, L., WEI, X., AHAMAD, A., KUBAN, D.A., KOMAKI, R., O'DANIEL, J., ZHANG, Y., MOHAN, R. & DONG, L. (2008). Performance evaluation of automatic anatomy segmentation algorithm on repeat or four-dimensional computed tomography images using deformable image registration method. *Int. J. Radiat. Oncol. Biol. Phys.*, **72**, 210–219, [↗](#). 142
- WANG, X., ZHANG, X., DONG, L., LIU, H., WU, Q. & MOHAN, R. (2004). Development of methods for beam angle optimization for IMRT using an accelerated exhaustive search strategy. *Int. J. Radiat. Oncol. Biol. Phys.*, **64**, 301–320, [↗](#). 61
- WANG, X., ZHANG, X., DONG, L., LIU, H., GILLIN, M., AHAMAD, A., ANG, K. & MOHAN, R. (2005). Effectiveness of noncoplanar IMRT planning using a parallelized multiresolution beam angle optimization method for paranasal sinus carcinoma. *Int. J. Radiat. Oncol. Biol. Phys.*, **63**, 594–601, [↗](#). 87
- VAN DE WATER, S., HOOGEMAN, M.S., BREEDVELD, S. & HEIJMEN, B.J.M. (2011a).

- Shortening treatment time in robotic radiosurgery using a novel node reduction technique. *Med. Phys.*, **38**, 1397–1405, [↗](#). [113](#), [119](#), [154](#)
- VAN DE WATER, S., HOOGEMAN, M.S., BREEDVELD, S., NUYTENS, J.J.M.E., SCHAART, D.R. & HEIJMEN, B.J.M. (2011b). Variable circular collimator in robotic radiosurgery: A time-efficient alternative to a mini-multileaf collimator? *Int. J. Radiat. Oncol. Biol. Phys.*, **81**, 863–870, [↗](#). [154](#)
- VAN DE WATER, S., KRAAN, A., BREEDVELD, S., TEGUH, D., MADDEN, T., KOOY, H., HEIJMEN, B. & HOOGEMAN, M. (2012). Improved multi-criteria optimization for intensity modulated proton therapy using iterative resampling of randomly placed pencil-beams. *Med. Phys.*, **39**, 3981, [↗](#). [154](#)
- WEBB, S., CONVERY, D.J. & EVANS, P.M. (1998). Inverse planning with constraints to generate smoothed intensity-modulated beams. *Phys. Med. Biol.*, **43**, 2785–2794, [↗](#). [8](#)
- WILKENS, J.J., ALALY, J.R., ZAKARIAN, K., THORSTAD, W.L. & DEASY, J.O. (2007). IMRT treatment planning based on prioritizing prescription goals. *Phys. Med. Biol.*, **52**, 1675–1692, [↗](#). [30](#), [47](#), [49](#)
- WOUDSTRA, E. & HEIJMEN, B.J.M. (2003). Automated beam angle and weight selection in radiotherapy treatment planning applied to pancreas tumors. *Int. J. Radiat. Oncol. Biol. Phys.*, **56**, 878–888, [↗](#). [83](#)
- WOUDSTRA, E. & STORCHI, P.R.M. (2000). Constrained treatment planning using sequential beam selection. *Phys. Med. Biol.*, **45**, 2133–2149, [↗](#). [61](#), [83](#), [87](#), [113](#)
- WOUDSTRA, E., HEIJMEN, B.J.M. & STORCHI, P.R.M. (2005). Automated selection of beam orientations and segmented intensity-modulated radiotherapy (IMRT) for treatment of oesophagus tumors. *Radiother. Oncol.*, **77**, 254–261, [↗](#). [83](#)
- WOUDSTRA, E., HEIJMEN, B.J.M. & STORCHI, P.R.M. (2008). A comparison of an algorithm for automated sequential beam orientation selection (Cycle) with simulated annealing. *Phys. Med. Biol.*, **53**, 2003–2018, [↗](#). [83](#)
- WRIGHT, S.J. (1997). *Primal-dual interior-point methods*. Philadelphia: SIAM publishers. [51](#), [148](#)
- WU, C., OLIVERA, G.H., JERAJ, R., KELLER, H. & MACKIE, T.R. (2003). Treatment plan modification using voxel-based weighting factors/dose prescription. *Phys. Med. Biol.*, **48**, 2479–2491, [↗](#). [7](#), [30](#), [149](#)
- WU, Q. & MOHAN, R. (2000). Algorithms and functionality of an intensity modulated radiotherapy optimization system. *Med. Phys.*, **27**, 701–711, [↗](#). [7](#), [30](#)
- WU, Q.J., THONGPHIEW, D., WANG, Z., CHANKONG, V. & YIN, F. (2008). The

- impact of respiratory motion and treatment technique on stereotactic body radiation therapy for liver cancer. *Med. Phys.*, **35**, 1440–1451, [↗](#). 141
- WULF, J., GUCKENBERGER, M., HAEDINGER, U., OPPITZ, U., MUELLER, G., BAIER, K. & FLENTJE, M. (2006). Stereotactic radiotherapy of primary liver cancer and hepatic metastases. **45**, 838–847, [↗](#). 135
- WUNDERINK, W., MÉNDEZ ROMERO, A., DE BOER, J.C.J., BRANDWIJK, R., LEVENDAG, P. & HEIJMEN, B. (2004). Evaluation of the positional accuracy in stereotactic radiotherapy for liver tumors using a stereotactic body frame. *Radiother. Oncol.*, **73**, S390–S391, [↗](#). 135
- WUNDERINK, W., MÉNDEZ ROMERO, A., VASQUEZ OSORIO, E., DE BOER, J., BRANDWIJK, R., LEVENDAG, P. & HEIJMEN, B. (2006). Target coverage in image-guided hypofractionated radiotherapy of liver tumours. *Radiother. Oncol.*, **81**, S230, [↗](#). 135
- WUNDERINK, W., MÉNDEZ ROMERO, A., VASQUEZ OSORIO, E.M., DE BOER, H.C.J., BRANDWIJK, R., LEVENDAG, P.C. & HEIJMEN, B.J.M. (2007). Target coverage in image-guided stereotactic body radiotherapy of liver tumors. *Int. J. Radiat. Oncol. Biol. Phys.*, **68**, 282–290, [↗](#). 135
- WUNDERINK, W., MÉNDEZ ROMERO, A., DE KRUIJF, W., DE BOER, H.C.J., LEVENDAG, P.C. & HEIJMEN, B.J.M. (2008). Reduction of respiratory liver tumor motion by abdominal compression in stereotactic body frame, analyzed by tracking fiducial markers implanted in liver. *Int. J. Radiat. Oncol. Biol. Phys.*, **71**, 907–915, [↗](#). 141
- XIA, P., YU, N., SUN, X. & VERHEY, L.J. (2005). Investigation of using a power function as a cost function in inverse planning optimization. *Med. Phys.*, **32**, 920–927, [↗](#). 47
- YANG, D. & MOORE, K.L. (2012). Automated radiotherapy treatment plan integrity verification. *Med. Phys.*, **39**, 1542–1551, [↗](#). 146
- YANG, Y. & XING, L. (2004). Inverse treatment planning with adaptively evolving voxel-dependent penalty scheme. *Med. Phys.*, **31**, 2839–2844, [↗](#). 7, 30, 44, 47
- YEOH, E., BOTTEN, R., BUTTERS, J., DI MATTEO, A., HOLLOWAY, R. & FOWLER, J. (2011). Hypofractionated versus conventionally fractionated radiotherapy for prostate carcinoma: Final results of phase iii randomized trial. *Int. J. Radiat. Oncol. Biol. Phys.*, **81**, 1271–1278, [↗](#). 113
- YILDIRIM, E.A. & WRIGHT, S.J. (2002). Warm-start strategies in interior-point methods for linear programming. *SIAM J. Optim.*, **12**, 782–810, [↗](#). 148
- ZHANG, T., CHI, Y., MELDOLESI, E. & D, Y. (2007). Automatic delineation of on-line head-and-neck computed tomography images: toward on-line adaptive radiotherapy.

- Int. J. Radiat. Oncol. Biol. Phys.*, **68**, 522–530, [DOI](#). 142
- ZHANG, X., LI, X., QUAN, E.M., PAN, X. & LI, Y. (2011). A methodology for automatic intensity-modulated radiation treatment planning for lung cancer. *Phys. Med. Biol.*, **56**, 3873–3893, [DOI](#). 109
- ZHAO, B., JOINER, M.C., ORTON, C.G. & BURMEISTER, J. (2010). SABER: A new software tool for radiotherapy treatment plan evaluation. *Med. Phys.*, **37**, 5586–5592, [DOI](#). 146
- ZHU, L., LEE, L., MA, Y., YE, Y., MAZZEO, R. & XING, L. (2008). Using total-variation regularization for intensity modulated radiation therapy inverse planning with field-specific numbers of segments. *Phys. Med. Biol.*, **53**, 6653–6672, [DOI](#). 153
- ZINCHENKO, Y., CRAIG, T., KELLER, H., TERLAKY, T. & SHARPE, M. (2008). Controlling the dose distribution with gEUD-type constraints within the convex radiotherapy optimization framework. *Phys. Med. Biol.*, **53**, 3231–3250, [DOI](#). 150

List of publications

Journal Articles

1. Breedveld, S., Storchi, P.R.M., Keijzer, M. & Heijmen, B.J.M. **2006** Fast, multiple optimizations of quadratic dose objective functions in IMRT *Physics in Medicine and Biology*, **51**, 3569-3579 [↗](#)
2. Breedveld, S., Storchi, P.R.M., Keijzer, M., Heemink, A.W. & Heijmen, B.J.M. **2007** A novel approach to multi-criteria inverse planning for IMRT *Physics in Medicine and Biology*, **52**, 6339-6353 [↗](#)
3. Breedveld, S., Storchi, P.R.M. & Heijmen, B.J.M. **2009** The equivalence of multi-criteria methods for radiotherapy plan optimization *Physics in Medicine and Biology*, **54**, 7199-7209 [↗](#)
4. Van de Water S., Hoogeman M.S., Breedveld S. & Heijmen B.J.M. **2011** Shortening treatment time in robotic radiosurgery using a novel node reduction technique *Medical Physics*, **38**, 1397-1405 [↗](#)
5. Van de Water S., Hoogeman M.S., Breedveld S., Nuyttens J.J.M.E., Schaart D.R. & Heijmen B.J.M. **2011** Variable circular collimator in robotic radiosurgery: a time-efficient alternative to a mini-multileaf collimator? *International Journal of Radiation Oncology*Biology*Physics*, **81**, 863-870 [↗](#)
6. Osman S.O.S., Astreinidou E., de Boer H.C., Keskin-Cambay F., Breedveld S., Voet P.W.J., Al-Mamgani A., Heijmen B.J.M. & Levendag P.C. **2012** IMRT for image-guided single vocal cord irradiation *International Journal of Radiation Oncology*Biology*Physics*, **82**, 989-997 [↗](#)
7. Breedveld S., Storchi P.R.M., Voet P.W.J. & Heijmen B.J.M. **2012** iCycle: Integrated, multicriterial beam angle, and profile optimization for generation of coplanar and noncoplanar IMRT plans *Medical Physics*, **39**, 951-963 [↗](#)

8. Voet P.W.J., Breedveld S., Dirx M.L.P., Levendag P.C. & Heijmen B.J.M. **2012** Integrated multicriterial optimization of beam angles and intensity profiles for coplanar and noncoplanar head and neck IMRT and implications for VMAT *Medical Physics*, **39**, 4858-4865 [↗](#)
9. Voet P.W.J., Dirx M.L.P., Breedveld S., Fransen D., Levendag P.C. & Heijmen B.J.M. **2013** Toward fully automated multicriterial plan Generation: a prospective clinical study *International Journal of Radiation Oncology*Biophysics*Physics*, **85**, 866-872 [↗](#)
10. Rossi L., Breedveld S., Heijmen B.J.M., Voet P.W.J., Lanconelli N. & Aluwini S. **2012** On the beam direction search space in computerized non-coplanar beam angle optimization for IMRT – prostate SBRT *Physics in Medicine and Biology*, **57**, 5441-5458 [↗](#)

Oral Presentations at International Conferences

1. Breedveld, S., Storchi, P.R.M., Keijzer, M. & Heijmen, B.J.M. **2007** Automated adaption of voxel-dependent importance factors in inverse planning *Proceedings of the XVth International Conference on the Use of Computers in Radiation Therapy (Toronto, Canada)*, **1**, 232-236 (ICCR)
2. Heijmen, B.J.M., Breedveld, S. Storchi, P.R.M. & Keijzer, M. **2007** A fully automatic multi-criteria algorithm for optimizing constraints for IMRT *Radiotherapy and Oncology*, **84**, S30 (ESTRO) [↗](#)
3. Van de Water, S., Hoogeman, M.S., Breedveld, S., Nuyttens, J.J.M.E. & Heijmen, B.J.M. **2009** A Variable Circular Collimator: A time-efficient alternative for a multi-leaf collimator in robotic radiosurgery? *Radiotherapy and Oncology*, **92**, S115 (ESTRO) [↗](#)
4. Breedveld, S., Storchi, P.R.M., Luiza, M.L., Vásquez Osorio, E.M., Hoogeman, M.S. & Heijmen, B.J.M. **2010** A fast and accurate automated method for online re-planning in adaptive radiotherapy *Proceedings of the XVIth International Conference on the Use of Computers in Radiation Therapy (Amsterdam, The Netherlands)* (ICCR)
5. Van de Water, S., Hoogeman, M.S., Breedveld, S. & Heijmen, B.J.M. **2010** Shortening treatment time in robotic radiosurgery by novel node reduction techniques *Medical Physics*, **37**, 3421 (AAPM) [↗](#)
6. Breedveld, S., Voet, P.W.J., Storchi, P.R.M. & Heijmen, B.J.M. **2011** Automating treatment planning using the multi-level wish-list and its application to fast online

- re-planning *Proceedings of the 21st International Conference on Multiple Criteria Decision Making (MCDM)* [↗](#)
7. Voet, P.W.J., Breedveld, S., Dirkx, M.L.P. & Heijmen, B.J.M. **2011** Fully integrated computerized optimization of beam angles and fluences in (non)-coplanar IMRT and implications for VMAT *Radiotherapy and Oncology*, **99**, S126-S127 (*ESTRO*) [↗](#)
 8. Leinders, S., Seppenwoolde, Y., Breedveld, S., Vásquez Osorio, E.M., Méndez Romero, A. & Heijmen, B.J.M. **2011** Adaptive liver SBRT: daily re-planning to compensate for non-rigid anatomy changes improves dose distributions *Radiotherapy and Oncology*, **99**, S218 (*ESTRO*) [↗](#)
 9. Voet, P.W.J., Dirkx, M.L.P., Breedveld, S., Fransen, D., Levendag, P.C. & Heijmen, B.J.M. **2012** Towards fully automated multi-criterial plan generation: a prospective clinical study *Radiotherapy and Oncology*, **103**, S219 (*ESTRO*) [↗](#)
 10. Van de Water, S., Kraan, A.C., Breedveld, S., Teguh, D., Madden, T., Kooy, H., Heijmen, B.J.M. & Hoogeman, M.S. **2012** Improved multi-criteria optimization for intensity modulated proton therapy using iterative resampling of randomly placed pencil-beams *Medical Physics*, **39**, 3981 (*AAPM*) [↗](#)

Poster Presentations at International Conferences

1. Breedveld, S., Storchi, P.R.M. & Heijmen, B.J.M. **2005** A robust and fast algorithm for IMRT optimization with dose-volume constraints *Radiotherapy and Oncology*, **76**, S169 (*ESTRO*) [↗](#)
2. Heijmen, B.J.M., Breedveld, S. & Storchi, P.R.M. **2009** Multi-criteria beam angle IMRT optimization with iCycle *Radiotherapy and Oncology*, **92**, S204 (*ESTRO*) [↗](#)
3. Heijmen, B.J.M., Van de Water, S., Breedveld, S., Nuyttens, J.J.M.E. & Hoogeman, M.S. **2009** A Variable Circular Collimator: A time-efficient alternative for a multi-leaf collimator in robotic radiosurgery? *International Journal of Radiation Oncology*Biography*Physics*, **75**, S674-S675 (*ASTRO*) [↗](#)
4. Breedveld, S., Storchi, P.R.M., Bondar, M.L., Vásquez Osorio, E.M., Hoogeman, M.S. & Heijmen, B.J.M. **2010** Fast on-line plan adjustment for adaptive radiotherapy evaluated for prostate and cervical cancer *International Journal of Radiation Oncology*Biography*Physics*, **78**, S744-S745 (*ASTRO*) [↗](#)
5. Heijmen, B.J.M., Bin Kassim, I., Breedveld, S., Voet, P.W.J., Woudstra, E. & Méndez Romero, A. **2011** Computer optimized non-coplanar beam arrangements

- in intensity-modulated liver SBRT versus VMAT and coplanar IMRT *Radiotherapy and Oncology*, **99**, S502 (*ESTRO*) [↗](#)
6. Dirx, M.L.P., Voet, P.W.J., Breedveld, S. & Heijmen, B.J.M. **2011** Fully integrated computerized beam angle optimization for coplanar and non-coplanar IMRT treatments of head and neck-cancer patients and implications for VMAT *Medical Physics*, **38**, 3672 (*AAPM*) [↗](#)
 7. Leinders, S., Seppenwoolde, Y., Breedveld, S., Vásquez Osorio, E.M., Méndez Romero, A. & Heijmen, B.J.M. **2011** Adaptive liver SBRT: daily re-planning to compensate for non-rigid anatomy changes improves dose distributions *Medical Physics*, **38**, 3634 (*AAPM*) [↗](#)
 8. Wang, Y., Incrocci, L., Zolnay, A., Joosten, H., Breedveld, S., McNutt, T., Heijmen, B.J.M. & Petit, S.F. **2012** A novel software tool to guide dosimetrists to efficiently generate high quality prostate IMRT treatment plans *Radiotherapy and Oncology*, **103**, S139 (*ESTRO*) [↗](#)
 9. Heijmen, B.J.M., Rossi, L., Breedveld, S., Voet, P.W.J., Lanconelli, N. & Aluwini, S. **2012** On the extend of the beam direction search space in computerized non-coplanar beam angle optimization for IMRT *Radiotherapy and Oncology*, **103**, S360 (*ESTRO*) [↗](#)
 10. Voet, P.W.J., Dirx, M.L.P., Breedveld, S., Fransen, D., Levendag, P.C. & Heijmen, B.J.M. **2012** Towards Fully Automated multi-criterial plan generation: a prospective clinical study *Medical Physics*, **39**, 3848 (*AAPM*) [↗](#)
 11. Voet, P.W.J., Rossi, L., Breedveld, S., Aluwini, S. & Heijmen, B.J.M. **2012** Plan quality in computerized non-coplanar IMRT beam angle optimization is highly dependent on the extent of the beam direction search space *Medical Physics*, **39**, 3855 (*AAPM*) [↗](#)

Summary

When a patient is diagnosed with cancer and the choice of treatment is radiation therapy, a treatment plan has to be designed which is intended to effectively destroy the tumour while sparing surrounding healthy tissues as much as possible. In current clinical practice, plans are generated using an iterative trial-and-error procedure, called *forward* planning. Each iteration consists of a selection of plan parameters, such as gantry angles, and of weighting factors for the objective functions by a dosimetrist, followed by a computer optimization to establish remaining parameters. With forward planning, the final dose distribution will generally depend on the skills and available time of the involved dosimetrist and physician. Moreover, the iterative process may be labour-intensive, taking up to several days for an individual patient. In this thesis, we have developed and investigated algorithms for treatment plan optimization aiming at full automation (i.e. avoidance of human interaction), inclusion of optimization of beam angles (both coplanar and non-coplanar arrangements), multi-criteria optimization resulting in Pareto-optimal plans for beam profiles, and clinically feasible calculation times. The investigations in chapters 2-5 have led to development of iCycle (chapters 6-10), an optimization algorithm with all these features incorporated.

In chapter 2 a solver for inverse treatment planning is presented. Inverse treatment planning for intensity modulated radiotherapy may include time consuming, multiple minimizations of an objective function. In this chapter, methods are presented to speed up the process of (repeated) minimization of the well-known quadratic dose objective function, extended with a smoothing term that ensures generation of clinically acceptable beam profiles. In between two subsequent optimizations, the voxel-dependent importance factors of the quadratic terms will generally be adjusted, based on an intermediate plan evaluation. The objective function has been written canonical matrix-vector format, facilitating the use of a recently published, fast quadratic minimization algorithm, instead of commonly applied gradient based methods. This format also reduces the calculation time in between subsequent minimizations, related to adjustment of the voxel-dependent importance factors. Sparse matrices are used to limit the required amount of computer memory. For three patients comparisons have been made with a gradient method, where

mean speed improvements of up to a factor of 37 have been achieved.

Chapter 3 describes how to adapt voxel-dependent importance factors for quadratic objective functions, to generate dose distributions that satisfy given constraints. In the quadratic objective function, the OAR are weighted against each other and the PTV. In clinical practice, volume-wide weighting factors are generally adapted manually with the above described forward planning procedure. Voxel-dependent importance factors increase the flexibility for generating optimal plans. A two-step algorithm is introduced that automatically adapts these voxel-dependent importance factors for dose-volume and maximum-dose constraints. The constraints are divided into different sets with different priorities. This allows meeting important constraints prior to meeting less important constraints.

This method is further expanded in chapter 4 for multi-criteria optimization. Optimizing solely on one objective or on a sum of *a priori* weighted objectives may result in inferior treatment plans. Manually adjusting weights or constraints in a trial-and-error procedure is time-consuming. In this chapter we introduce a novel multi-criteria optimization approach to automatically optimize treatment constraints (dose-volume and maximum-dose). The algorithm tries to meet these constraints as well as possible, but in case of conflict it relaxes lower priority constraints so that higher priority constraints can be met. Afterwards, all constraints are tightened, starting with the highest priority constraints. Applied constraint priority lists (a predecessor of the *wish-list*, see below) can be used as class solutions for patients with similar tumour types. The presented algorithm does iteratively apply an underlying algorithm for beam profile optimization, as described in chapters 2 and 3.

To overcome the limitations of the algorithms described in previous chapters, in chapter 5 the 2-phase ϵ -constraint (*2pec*) algorithm is introduced and compared to the weighted-sum multi-criteria optimization. *2pec* is a novel method for fully automated multi-criteria optimization of beam profiles for a pre-selected set of beam directions, based on a wish-list with constraints and prioritized objectives. Priorities are ordinal parameters used for relative importance ranking of the objectives. The higher an objective priority is, the higher the probability that the corresponding goal for the objective will be met. Beam profile optimization with *2pec* results in Pareto-optimal treatment plans. Weighted-sum optimization and *2pec* are uniquely related to each other. It is demonstrated that it is possible to switch from the (constrained) *2pec* method to the weighted-sum method by using the Lagrange multipliers from the constrained optimization problem, and vice versa by setting the appropriate constraints. In general, the theory presented in this chapter can be useful in cases where a new situation is slightly different from the original situation, as e.g. in automated treatment planning, where changes to the automated plan have to be made. An example is given where the planner is not

satisfied with the result from the *2pec* and wishes to decrease the dose in a structure. By using the Lagrange multipliers, a weighted-sum optimization problem is constructed, which generates a Pareto-optimal solution in the neighbourhood of the original plan, fulfilling the new treatment objectives.

iCycle, our novel algorithm for integrated, multi-criteria optimization of beam angles and IMRT profiles is described in chapter 6. Again, optimization is based on a *wish-list* (chapter 5), containing hard constraints and objectives with ascribed priorities. Beam directions are selected from an input set of candidate directions. Input sets can be restricted, e.g. to allow only generation of coplanar plans, or to avoid collisions between patient/couch and the gantry in a non-coplanar setup. Obtaining clinically feasible calculation times was an important design criteriom for development of iCycle. This could be realized by sequentially adding beams to the treatment plan in an iterative procedure. Each iteration loop starts with selection of the optimal direction to be added. Then the *2pec* method (chapter 5) is used to generate a Pareto-optimal IMRT plan for the (fixed) beam setup that includes all so far selected directions. To select the next direction, each not yet selected candidate direction is temporarily added to the plan and an optimization problem, derived from the Lagrangian obtained from the just performed optimization for establishing the Pareto-optimal plan, is solved. For each patient, a single 1-beam, 2-beam, 3-beam, etc. Pareto-optimal plan is generated until addition of beams does no longer result in significant plan quality improvement. Plan generation with iCycle is fully automated and steered by the wish-list. Fine-tuning of the wish-list is of utmost importance for generation of optimal plans. This is done in close collaboration between dosimetrists and physicians in an iterative trial-and-error process, generating plans for a small group of patients to gradually improve the quality of the wish-list. Performance and characteristics of iCycle are demonstrated by generating plans for a maxillary sinus case, a cervical cancer patient, and a liver patient treated with SBRT. Plans generated with beam angle optimization did better meet the clinical goals than equi-angular or manually selected configurations. For the maxillary sinus and liver cases, significant improvements for non-coplanar setups were seen. The cervix case showed that also in IMRT with coplanar setups, beam angle optimization with iCycle may improve plan quality. Computation times for coplanar plans were around 1-2 hours and for non-coplanar plans 4-7 hours, depending on the number of beams and the complexity of the problem.

In chapter 7, iCycle is used to investigate the dependence of salivary gland sparing in head-and-neck patients on applied beam numbers and directions, and to study the impact of optimized nonzero couch angles on the quality of VMAT plans. For 20 patients, five IMRT plans, based on one wish-list, are compared: i), ii) 7- and 9-beam equi-angular coplanar plans (iCycle_{7equi}, iCycle_{9equi}), iii), iv) 9-beam plans with opti-

mized coplanar and non-coplanar beam orientations ($iCycle_{\text{copl}}$, $iCycle_{\text{noncopl}}$) and v) a 9-beam coplanar plan with optimized gantry angles and one optimized couch rotation ($iCycle_{\text{couch}}$). VMAT plans without and with this optimized couch rotation were evaluated. $iCycle_{\text{noncopl}}$ resulted in the best salivary gland sparing, but $iCycle_{\text{couch}}$ yielded similar results for 18 patients. For $iCycle_{7\text{equi}}$, submandibular gland NTCP values were on average 5% higher. $iCycle_{9\text{equi}}$ performed better than $iCycle_{7\text{equi}}$. $iCycle_{\text{copl}}$ showed further improvement. Application of the optimized couch angle from also improved NTCP values in VMAT plans. In conclusion, $iCycle$ allows objective comparison of competing planning strategies. Integrated optimization of beam profiles and angles can significantly improve normal tissue sparing, where $iCycle_{\text{noncopl}}$ showed the best results.

The next step was to evaluate $iCycle$ for daily treatment planning, which was done in a prospective clinical study (chapter 8). Plans automatically generated with $iCycle$ were compared to plans generated manually by dosimetrists with the standard forward planning procedure using the clinical treatment planning system. For 20 randomly selected head-and-neck cancer patients with various tumour locations (of whom 13 received sequential boost treatments) we offered the treating physician the choice between an automatically generated $iCycle$ plan and a manually optimized plan following standard clinical procedures. While $iCycle$ used a fixed wish-list with hard constraints and prioritised objectives, the dosimetrists manually selected the beam configuration and fine-tuned the constraints and objectives for each IMRT plan. Dosimetrists were not informed in advance whether or not a competing $iCycle$ plan was made. The two plans were simultaneously presented to the physician, who then selected the plan to be used for treatment. In 32/33 plan comparisons the physician selected the $iCycle$ plan for treatment. This highly consistent preference for automatically generated plans was mainly caused by improved sparing for the large majority of critical structures. With $iCycle$, the NTCPs for parotid and submandibular glands were reduced by $2.4\% \pm 4.9\%$ (maximum: 18%, $p = 0.001$) and $6.5\% \pm 8.3\%$ (maximum: 27%, $p = 0.005$), respectively. The reduction in mean oral cavity dose was $2.8 Gy \pm 2.8 Gy$ (maximum: 8.1 Gy, $p = 0.005$). For swallowing muscles, oesophagus and larynx, the mean dose reduction was $3.3 Gy \pm 1.1 Gy$ (maximum: 9.2 Gy, $p < 0.001$). In addition, for 15 of the 20 patients, the target coverage was improved as well. So, in 97% of cases, the automatically generated plan was selected for treatment because of superior quality. Apart from improved plan quality, automatic plan generation is economically attractive because of reduced workload.

In chapter 9, the impact of the (non-coplanar) beam direction search space (i.e. the set of candidate beam directions that may be selected for generating an optimal plan) on plan quality was assessed. For a group of 10 prostate cancer patients, optimal IMRT plans were made for Stereotactic Body Radiation Therapy (SBRT), mimicking High Dose Rate (HDR) brachytherapy dosimetry. Plans were generated for 5 different beam direction

input sets, a coplanar set and four non-coplanar sets. For coplanar (CP) treatments, the search space consisted of 72 orientations (5° separations). The non-coplanar CK-space contained all directions available in the robotic CyberKnife treatment unit. The fully non-coplanar (F-NCP) set facilitated the highest possible degree of freedom in selecting optimal directions. CK⁺ and CK⁺⁺ were subsets of F-NCP to investigate some aspects of the CK-space. For each input set, plans were generated with up to 30 selected beam directions. Generated plans were clinically acceptable, according to an assessment of our clinicians. Convergence in plan quality occurred only after around 20 included beams. For individual patients, variations in PTV dose delivery between the 5 generated plans were minimal, as aimed for (average spread in $V_{95\%}$: 0.4%). This allowed plan comparisons based on organ at risk (OAR) doses, with the rectum considered most important. Plans generated with the non-coplanar search spaces had improved OAR sparing compared to the CP search space, especially for the rectum. OAR sparing was best with F-NCP, with reductions in rectum D_{Mean} , $V_{40\text{Gy}}$, $V_{60\text{Gy}}$ and $D_{2\%}$ compared to CP of 25%, 35%, 37%, and 8%, respectively. Reduced rectum sparing with the CK search space compared to F-NCP could be largely compensated by expanding CK with beams with relatively large direction components along the superior-inferior axis (CK⁺⁺). Addition of posterior beams (CK⁺⁺ \rightarrow F-NCP) did not lead to further improvements in OAR sparing. Plans with 25 beams performed clearly better than 11-beam plans. For coplanar plans, an increase from 11 to 25 involved beams resulted in reductions in rectum D_{Mean} , $V_{40\text{Gy}}$, $V_{60\text{Gy}}$ and $D_{2\%}$ of 39%, 57%, 64%, and 13%, respectively.

In chapter 10, iCycle was used to investigate how dose distributions for liver Stereotactic Body Radiation Therapy (SBRT) can be improved by automated, daily plan re-optimization to account for anatomy deformations, compared to set-up corrections only. For 12 tumours, three different strategies for dose delivery were simulated. In the first strategy, CT-scans made before each treatment fraction were used only for patient re-positioning prior to dose delivery for correction of detected tumour set-up errors. In the adaptive second and third strategies, in addition to the isocentre shift, IMRT beam profiles were re-optimized, or both intensity profiles and beam orientations were re-optimized, respectively. All optimizations were performed with iCycle. In six of 12 cases, violations of organs at risk (OAR; heart, stomach, kidney) constraints of 1 – 6 Gy in single fractions occurred in case of tumour re-positioning only. With the adaptive strategies these could be avoided (< 1 Gy). For one case, this needed adaptation by slightly underdosing the PTV. For two cases with restricted tumour dose in the planning phase to avoid OAR constraint violations, fraction doses could be increased by 1 and 2 Gy due to more favourable anatomy. Daily re-optimization of both beam profiles and beam angles (third strategy) performed slightly better than re-optimization of profiles only, but the latter required only some minutes computation time while full re-optimization

took a few hours. This simulation study demonstrated that re-planning based on daily acquired CT-scans can improve liver SBRT dose delivery.

Samenvatting

Wanneer bestralingstherapie is gekozen als behandeling voor kanker, dient er een bestralingsplan te worden gemaakt. Het doel van bestralingstherapie is om de tumor voldoende te bestralen, zodat deze verdwijnt, maar daarnaast het gezonde weefsel zoveel mogelijk spaart. In de huidige klinische praktijk worden de bestralingsplannen handmatig gemaakt, via een herhaaldelijk trial-and-error proces (voorwaarts plannen). De parameters, zoals bundelhoeken, gewichtsfactoren, dosimetrische doelen e.d. worden handmatig ingesteld, waarna de computer een optimalisatie doet om de resterende parameters te bepalen en de dosis te berekenen. Indien deze dosis niet voldoet aan de wensen van de planner, worden de parameters aangepast en nogmaals geoptimaliseerd. Met deze voorwaartse planmethode hangt de kwaliteit van het uiteindelijke plan erg af van de kundigheid van de planner en de beschikbare tijd. Voor complexe sites kan dit voor een individuele patiënt zelfs enkele dagen in beslag nemen. In dit proefschrift presenteer ik mijn onderzoek naar de ontwikkeling en validatie van een volledig geautomatiseerde planning. Het algoritme optimaliseert zowel bundelhoeken (coplanair als niet-coplanair) als intensiteit gemoduleerde fluentieprofielen, in een multi-criteria setting wat resulteert in Pareto optimale plannen. De rekentijden zijn klinisch acceptabel. De voorgaande onderzoeken (hoofdstukken 2-5) hebben geleid tot de ontwikkeling van iCycle (hoofdstukken 6-10), een algoritme dat al deze elementen omvat.

In hoofdstuk 2 wordt er een nieuwe solver geïntroduceerd. Bij het maken van een IMRT (Intensity Modulated Radiation Therapy) plan wordt vaak gebruik gemaakt van een kwadratische doelfunctie die herhaaldelijk wordt geoptimaliseerd. Dit kost veel tijd, en in dit hoofdstuk worden methoden gepresenteerd om de snelheid voor het herhaaldelijk minimaliseren van de kwadratische doelfunctie te verbeteren. Deze functie bevat ook een smoothing term die ervoor zorgt dat het resultaat een realiseerbaar plan oplevert. Tussen twee opeenvolgende optimalisaties worden de voxel-afhankelijke gewichtsfactoren aangepast, op basis van een tussentijdse planevaluatie. De doelfunctie is omgeschreven in een canonieke matrix-vector vorm, waardoor het mogelijk is gebruik te maken van een recent gepubliceerde oplosmethode voor kwadratische minimalisatie, in plaats van gebruikelijke gradiëntmethoden. Deze vorm vermindert ook de rekentijd bij opeenvolgende

minimalisaties ten gevolge van het aanpassen van de voxel-afhankelijke factoren. Om het geheugengebruik beperkt te houden worden ijle matrices gebruikt. Voor drie patiënten is er een vergelijking gemaakt met een gradiënten methode, waarbij onze nieuwe methode tot 37 keer sneller was.

Hoofdstuk 3 beschrijft een methode hoe de voxel-afhankelijke gewichten aangepast kunnen worden om de gewenste dosisverdeling te krijgen. Dit wordt bereikt door het herhaaldelijk optimaliseren van de kwadratische doelfunctie, waarbij de tumor en de risico-organen gewogen worden. In de hedendaagse klinische praktijk worden de gewichtsfactoren handmatig aangepast, wat uitmondt in een langdurig proefondervindelijk proces (waarbij het nooit duidelijk is hoe goed het uiteindelijke plan is). Deze gewichtsfactoren werken voor een geheel volume. De werking kan sterk worden verbeterd door gewichten aan individuele voxels toe te kennen, zodat er op lokaal niveau gestuurd kan worden. In dit hoofdstuk wordt een twee-staps algoritme geïntroduceerd dat automatisch de voxel-afhankelijke gewichtsfactoren aanpast op basis van vooraf ingestelde dosis-volume- en maximum-dosis constraints. De constraints zijn ingedeeld in verschillende categorieën met verschillende prioriteiten. Hiermee wordt getracht om aan de belangrijkste constraints te voldoen voordat er gewerkt wordt aan minder belangrijke constraints. De uiteindelijke dosisverdelingen zijn erg conform.

Deze methode wordt verder uitgebreid in hoofdstuk 4 voor multi-criteria optimalisatie. Het optimaliseren van één objective of een gewogen opsomming van verschillende objectives kan resulteren in inferieure bestralingsplannen. In dit hoofdstuk introduceren we een nieuwe vorm van multi-criteria optimalisatie waarmee automatisch aan constraints (zoals dosis-volume en maximum-dosis) wordt voldaan. Het algoritme tracht zo goed mogelijk hieraan te voldoen, maar wanneer deze conflicterend zijn krijgen de constraints met hogere prioriteit voorrang op de lagere. Daarna worden alle constraints iteratief verlaagd (of verhoogd voor een PTV (Planning Target Volume, de tumor)), te beginnen met de hoogste prioriteiten. Een dergelijke geprioriteerde lijst met constraints (een voorloper van de *wish-list*) kan worden gebruikt als generieke lijst voor een groep patiënten. Het hier geïntroduceerde algoritme is geïntegreerd in het eerder beschreven algoritme voor fluentie-optimalisatie (hoofdstukken 2 en 3).

In hoofdstuk 5 wordt de multi-criteria optimalisatie methode die in hoofdstuk 4 is geïntroduceerd verder gegeneraliseerd, en uitgezet tegen de gewogen-som multi-criteria methode. Ook is er een nieuwe optimizer gebruikt. In de gewogen-som methode worden verschillende objectives gewogen en opgesomd. In de geconstraineerde optimalisatiemethode (vergelijkbaar met die in hoofdstuk 4), zijn de doelstellingen (objectives) voor het behandelplan *a priori* gedefinieerd in een *wish-list*, en het doel is om een plan te vinden dat hieraan zo goed mogelijk voldoet, dan wel beter is. De geconstraineerde optimalisatie methode die wordt gebruikt in dit hoofdstuk, de $2pec$ (2-fase ϵ -constraint) methode is

gebaseerd op de ϵ -constraint methode, die resulteert in Pareto-optimale oplossingen. Beide benaderingen hebben een unieke relatie tot elkaar. In dit hoofdstuk laten we zien dat een gewogen-som resultaat omgeschreven kan worden naar een geconstraïnd probleem, en vice versa, het resultaat van de $2pec$ methode naar een gewogen-som functie omgeschreven kan worden met behulp van de Lagrangiaan. Praktijk toepassingen worden behandeld, bijvoorbeeld wanneer de planner niet tevreden is met het resultaat van de $2pec$ methode en de dosis in een structuur wil verlagen. Met behulp van de Lagrange multipliers wordt een gewogen-som probleem gedefinieerd, welk een Pareto-optimale oplossing genereert in de nabijheid van het oorspronkelijke plan, maar wel voldoet aan de nieuwe doelstellingen.

iCycle, ons algoritme voor het optimaliseren van bestralingshoeken (bundelhoeken), wordt beschreven in hoofdstuk 6. Dit is een nieuw algoritme voor een geïntegreerde, multi-criteria optimalisatie van de bundelhoeken en IMRT profielen. Een multi-criteria planoptimalisatie met iCycle is gebaseerd op het concept van de *wish-list* (hoofdstuk 5). De lijst bestaat uit een geprioriteerde lijst met objectives (doelstellingen) en constraints. Hoe hoger de prioriteit, hoe groter de kans dat de desbetreffende doelstelling zal worden gehaald. Bundelrichtingen worden gekozen uit een vooraf gegenereerde lijst van richtingen. De richtingen in deze lijst kunnen coplanair zijn of niet-coplanair. Richtingen waarbij de gantry mogelijk de patiënt/tafel raakt zijn uitgezonderd. Een belangrijke doelstelling in het ontwikkelen van iCycle waren klinisch haalbare rekentijden. Dit kan worden gerealiseerd door iteratief bundels aan een plan toe te voegen. Elke iteratie begint met de selectie van de optimale richting, en wordt vervolgens toegevoegd aan de lijst met actieve bundels. Vervolgens wordt één Pareto-optimaal IMRT plan gegenereerd voor de actieve bundelconfiguratie, met het algoritme uit hoofdstuk 5. Voor de volgende bundelselectie wordt elke nog niet geselecteerde richting tijdelijk toegevoegd aan de actieve set, en wordt een optimalisatieprobleem opgelost, gebaseerd op de Lagrangiaan uit de vorige $2pec$ multi-criteria optimalisatie. Voor elke patiënt wordt een Pareto-optimaal 1-bundelplan, 2-bundelplan, 3-bundelplan, etc. gegenereerd totdat het toevoegen van meer bundels niet langer resulteert in een significante verbetering van het bestralingsplan. Het genereren van plannen met iCycle is volledig geautomatiseerd. De werking van iCycle wordt gedemonstreerd voor een patiënt met een hoofd-hals tumor, een patiënt met baarmoederhalskanker en een patiënt met leverkanker. Plannen waarvoor de bundelhoeken zijn geoptimaliseerd voldoen beter aan de klinische doelstellingen dan equidistante of handmatig gekozen hoeken. Voor de hoofd-hals patiënt en de lever patiënt werden aanzienlijke verbeteringen voor niet-coplanaire opstellingen gezien. Voor de baarmoederhals patiënt bleek dat ook met coplanaire opstellingen de plannen verbeterd zijn door bundelhoek-optimalisatie met iCycle. Rekentijden voor coplanaire plannen waren in de orde van 1-2 uur en voor niet-coplanaire plannen 4-7 uur, afhankelijk van het aantal bundels en

de complexiteit. Er kan worden geconcludeerd dat geïntegreerde IMRT en bundelhoek-optimalisatie met iCycle tot aanzienlijke verbeteringen leiden in de plankwaliteit. Als gevolg van het automatiseren is de werklust minimaal.

Of iCycle in staat is om klinische plannen te produceren is onderzocht in hoofdstuk 7. In dit hoofdstuk wordt gekeken naar speekselklier sparing voor hoofd-hals patiënten. Er is ook onderzocht of VMAT (Volumetric Modulated Arc Therapy) plannen verbeterd kunnen worden door de tafelhoek te optimaliseren. iCycle is gebruikt voor het automatisch genereren van multi-criteria IMRT plannen met geoptimaliseerde bundelhoeken en is vergeleken met plannen waarbij de bundels equidistant gekozen zijn. Voor 20 patiënten zijn vijf verschillende IMRT plannen vergeleken, op basis van één enkele wish-list: i), ii) 7 - en 9-bundel equidistante coplanaire plannen (iCycle_{7equi}, iCycle_{9equi}), iii), iv) 9-bundel plannen met geoptimaliseerde coplanaire en niet-coplanaire bundelhoeken (iCycle_{copl}, iCycle_{noncopl}) en v), een 9-bundel coplanair plan met geoptimaliseerde bundelhoeken en tafelrotatie (iCycle_{couch}). De VMAT plannen zijn geëvalueerd met en zonder deze geoptimaliseerde tafelrotatie. iCycle_{noncopl} resulteerde in de beste sparing voor de speekselklier, maar iCycle_{couch} leverde vergelijkbare resultaten op voor 18 patiënten. Voor iCycle_{7equi} waren de NTCP (Normal Tissue Complication Probability) waarden voor de kleine speekselklier gemiddeld 5% hoger. iCycle_{9equi} presteerde beter dan iCycle_{7equi}, waarbij iCycle_{copl} een verdere verbetering liet zien. Een geoptimaliseerde tafelhoek van iCycle_{couch} liet ook verbeterde NTCP waarden zien voor VMAT plannen. iCycle maakt het mogelijk om een objectieve vergelijking te maken van verschillende planningsstrategieën. De geïntegreerde optimalisatie van de IMRT profielen en bundelhoeken leidt tot een aanzienlijke verbetering in de sparing van gezond weefsel, waarbij de beste resultaten met iCycle_{noncopl} behaald worden.

Om te beoordelen of iCycle geschikt is voor de dagelijkse klinische planning is er een prospectieve studie gestart (hoofdstuk 8). Hiervoor zijn er voor 20 willekeurige hoofd-hals patiënten (waarvan er 13 een sequentiële boost kregen) twee plannen gemaakt: een iCycle plan, en een handmatig plan, gemaakt volgens de huidige klinische procedures, waarbij de laborant zelf de bundelhoeken en objectives moet bepalen. De laborant werd niet van tevoren geïnformeerd of er ook een iCycle plan zou worden gemaakt. Het iCycle plan is berekend volgens één enkele wish-list, en het resultaat is in het klinische planningsstelsel gereconstrueerd. De behandelend arts kreeg (blind) beide plannen voorgelegd. Voor de groep patiënten hebben we verschillen in dosiscoverage voor het PTV en het sparen van kritieke weefsels bekeken. In 32 van de 33 plannen heeft de arts het iCycle plan gekozen voor de behandeling. Deze zeer consistente voorkeur voor de automatisch gegenereerde plannen werd vooral veroorzaakt door een betere sparing voor het merendeel van de kritieke organen. Met iCycle zijn de NTCP's voor de grote en kleine speekselklieren verminderd met respectievelijk $2,4\% \pm 4,9\%$ (maximum: 18%, $p = 0,001$) en $6,5\% \pm$

8,3% (maximum: 27%, $p = 0,005$). De daling van de gemiddelde dosis in de mondholte was $2,8 \text{ Gy} \pm 2,8 \text{ Gy}$ (maximum: $8,1 \text{ Gy}$, $p = 0,005$). Voor de slikspieren, slokdarm en strottenhoofd was de gemiddelde verlaging van de dosis $3,3 \text{ Gy} \pm 1,1 \text{ Gy}$ (maximum: $9,2 \text{ Gy}$, $p < 0,001$). Verder is voor 15 van de 20 patiënten de dosiscoverage van de tumor ook verbeterd. Dus in 97% van de gevallen is het automatisch gegenereerde plan gekozen voor de behandeling vanwege de superieure kwaliteit. Naast de verbeterde kwaliteit van de plannen is automatisch plannen ook economisch aantrekkelijk vanwege verminderde werkdruk.

In hoofdstuk 9 wordt de impact onderzocht van verschillende sets (niet-coplanaire) bundelrichtingen. Voor een groep van 10 patiënten met prostaatkanker zijn IMRT plannen gemaakt voor Stereotactische Body RadioTherapie (SBRT) waarbij High Dose Rate (HDR) brachytherapie dosimetrie is nagebootst. De plannen zijn gegenereerd voor 5 verschillende bundelrichting zoekruimten: een coplanaire set en vier niet-coplanaire. De coplanaire (CP) zoekruimte bestaat uit 72 oriëntaties (5° afstand). De niet-coplanaire CK-zoekruimte bevat alle standaardrichtingen van de CyberKnife. De volledig niet-coplanaire (F-NCP) zoekruimte biedt de meeste vrijheidsgraden aan. CK^+ en CK^{++} zijn een deelverzameling van de F-NCP om een aantal aspecten van de CK-zoekruimte te onderzoeken. Voor elke set zijn plannen gegenereerd met maximaal 30 bundels. De gegenereerde plannen waren klinisch relevant. De plankwaliteit convergeerde na ongeveer 20 bundels. Voor de individuele patiënten waren de variaties in PTV dosis tussen de 5 gegenereerde plannen minimaal, zoals was nagestreefd (gemiddelde spreiding $V_{95\%}$: 0,4%). Hierdoor konden plannen worden vergeleken op basis van dosis in risico-organen, waarbij het rectum het meest belangrijk was. Plannen gegenereerd met de niet-coplanaire zoekruimte hadden een betere sparing ten opzichte van de CP zoekruimte, vooral voor het rectum. Sparing was het beste met de F-NCP zoekruimte: in vergelijking met de CP zoekruimte waren de reducties in de rectum D_{Mean} , $V_{40\text{Gy}}$, $V_{60\text{Gy}}$ en $D_{2\%}$ van respectievelijk 25%, 35%, 37% en 8%. Verminderde rectum sparing met de CK zoekruimte in vergelijking tot de F-NCP zoekruimte zou grotendeels gecompenseerd kunnen worden door de CK zoekruimte uit te breiden met bundels langs de superieure-inferieure as (CK^{++}). Het toevoegen van posterieure bundels ($CK^{++} \rightarrow$ F-NCP) leidde niet tot een verdere verbetering in het sparen van de risico-organen. Plannen met 25 bundels deden het duidelijk beter dan plannen met 11 bundels. Voor coplanaire plannen leidden meerdere bundels (van 11 naar 25) in een vermindering van de dosis in het rectum van de D_{Mean} , $V_{40\text{Gy}}$, $V_{60\text{Gy}}$ en $D_{2\%}$ met respectievelijk 39%, 57%, 64% en 13%.

In het laatste hoofdstuk, hoofdstuk 10, is iCycle gebruikt om te onderzoeken hoe dosisverdelingen voor Stereotactische Body Radiation Therapy (SBRT) van de lever verbeterd kunnen worden door automatische, dagelijkse heroptimalisatie van plannen om rekening te houden met anatomische vervormingen, in vergelijking met herpositioner-

ing alleen. Er zijn plannen gemaakt voor 12 tumoren en drie verschillende strategieën. In de eerste strategie werden de CT-scans voor elke behandel-fractie alleen gebruikt voor herpositionering voorafgaande aan de bestraling. In de tweede en derde adaptieve strategie is naast het herpositioneren van het isocentrum ook opnieuw fluentie (IMRT) geoptimaliseerd, of zowel fluentie als bundelhoekoptimalisatie. Alle optimalisaties zijn uitgevoerd met iCycle. Voor herpositionering alleen kregen de risico-organen (hart, maag, nieren) in 6 van de 12 gevallen 1 tot 6 *Gy* meer dan toegestaan. Met de adaptieve strategieën kon dit worden vermeden (tot < 1 *Gy*). Voor één geval leidde dit tot een lichte onderdosering in het PTV. Echter, voor twee andere gevallen waar eerst een beperkte tumor dosis was gepland, kon de fractie-dosering worden verhoogd met 1 en 2 *Gy* vanwege een gunstigere anatomie. Dagelijkse heroptimalisatie van zowel de fluentie inclusief bundelhoeken (derde strategie) leidde tot iets betere plannen, maar vereist een paar uur rekentijd, terwijl heroptimalisatie van fluentie alleen slechts enkele minuten rekentijd kost. Deze studie toont aan dat herplannen op basis van de dagelijkse CT-scans de fractiedosis sterk verbetert.

Acknowledgements

Successful research is never done alone. During the years, many people have contributed, and became friends rather than colleagues. Special thanks go to:

Ben Heijmen, my promoter, for guiding me through the wild field of radiation therapy, and always valuing my ideas on the directions of the research. With your support, I was able to start something from scratch, and by that creating something new. As soon as the development of iCycle gave reasonable results, you saw the potential, which led to a rapid development towards clinical use.

Pascal Storchi, for supervising me. Through the many discussions I learned how to apply mathematics to real world problems, and helped me many times by solving my inverse-mathematical problems (solve a problem first, then find the reason why it works, and construct a solid proof).

Peter Voet, from the beginning you understood my ideas and urge to change the current practice of treatment planning. Ever since, you have been my “oracle” for every question I had about clinical relevance of new ideas. You were the first to embrace iCycle in a clinical setting, and due to continuous feedback on all aspects, iCycle quickly matured. But I also greatly enjoy our conversations on other matters, like coffee and tea.

Evert Woudstra, for answering many questions, and transferring knowledge and experience on beam angle optimization with Cycle, so I did not have to re-invent both wheels to iCycle.

Linda Rossi, it was a pleasure to work with you, with your challenging project for me and iCycle. I am also fortunate to have experienced the Italian way of life.

Sarah Osman, my roommate for all our years. It was a pleasure having you nearby, and share our experiences on life.

Eliana Vásquez Osorio, you have been working at our department for as long as I do, and I enjoy all the conversations we had about work, life, the universe and everything.

Steven van de Water, you were the first to use my source code, also for beam angle optimization. Your fundamentally different approach leads to interesting discussions and insights, forcing me to keep an open mind.

Dennie Fransen and Anne Gangsaas, who have been the first using iCycle in daily

clinical practice. In the beginning, iCycle was not always easy to use, but was quickly streamlined thanks to your support and feed-back.

Students who did an internship at our department: Astrid Kloosterman, Kris Manios, Piet van Everdingen, Suzanne Leinders and Alex Sangers. You have all actively participated in the research which eventually led to iCycle. The majority of your contributions are still essential parts of the current version.



PhD Portfolio

Summary of PhD training and teaching

Name PhD student:	PhD period:
Sebastiaan Breedveld	2006 - 2012
Erasmus MC Department:	Promoter:
Radiation Oncology	Prof.dr. B.J.M. Heijmen
Research School:	Supervisor:
Molecular Medicine	Dr.ir. P.R.M. Storchi

1. PhD training	Year
General courses	
Scientific Writing in English for Publication - writing to be read Erasmus MC, Rotterdam, The Netherlands	2009
GPU Programming for Medical Physics and Medical Imaging UCSD, San Diego, CA, USA	2010
Oral and poster presentations at international conferences	
XVth International Conference on the Use of Computers in Radiation Therapy ICCR, Toronto, Canada	2007
XVIth International Conference on the Use of Computers in Radiation Therapy ICCR, Amsterdam, The Netherlands	2010
ASTRO 52nd Annual Meeting ASTRO, San Diego, CA, USA	2010
21st International Conference on Multiple Criteria Decision Making <i>as an invited speaker</i> MCDM, Jyväskylä, Finland	2011
Selected other presentations	
Kring voor Radiotherapeutische en Klinische Fysica Eindhoven, The Netherlands	2007
Decanen en Docentendag EWI, TU Delft Leiden, The Netherlands	2007
Kring voor Radiotherapeutische en Klinische Fysica Amsterdam, The Netherlands	2010
Workshop Recent Developments in the Solution of Indefinite Systems Eindhoven, The Netherlands	2012

Other

Peer reviewed 13 papers for 5 journals

Administrating High Performance Computing cluster

2. Teaching	Year
Internal presentations	
Journal club: Inverse planning without margins for respiratory tumour motion	2006
Journal club: Higher mathematics in Radiotherapy I. Numerical Linear Algebra	2006
Journal club: Higher mathematics in Radiotherapy II. Multi-criteria Optimization	2007
Students TU Delft: Optimization of Treatment Plans in Radiotherapy	2007
Journal club: Optimization for Rapid Arc and VMAT	2008
Refereeravond: Multi-criteria optimalisatie	2008
Refereeravond: A fast and accurate automated method for online re-planning in adaptive radiotherapy	2010
Journal club: Direct Aperture Optimization: What it is, the challenges and the solutions	2011
Journal club: Plan optimization in TomoTherapy	2012
Supervising students	
K. Manios, Student Bachelor of Science at <i>Amsterdam University of Applied Science</i>	2006
A.P. van Everdingen, Student Master of Science at <i>Delft, University of Technology (internship)</i>	2007
A. Sangers, Student Master of Science at <i>Delft, University of Technology (internship)</i>	2011
L. Rossi, Student Master of Science at <i>Alma Mater Studiorum - Università di Bologna</i>	2011

3. Distinctions and awards	Year
Article <i>Fast, multiple optimizations of quadratic dose objective functions in IMRT</i> selected for inclusion in IOPselect	2006
U.S. Patent 8,144,833 <i>Planning for adaptive radiotherapy</i>	2010

Curriculum Vitae

Sebastiaan Breedveld was born on August 2nd 1980 in Rotterdam, The Netherlands. After finishing high school at the Libanon Lyceum, Rotterdam, he continued at Delft, University of Technology following the study Applied Mathematics in 1998.

Having the desire applying mathematics to health-care, Sebastiaan did his internship for his master thesis at the Department of Radiation Oncology, Erasmus Medical Center, Rotterdam, on the subject of radiation therapy treatment planning. He graduated in 2005.

After a few months of freelance work in line of the master thesis, and a sabbatical of several months, Sebastiaan started his Ph.D. research in 2006 at the ErasmusMC which should eventually lead to a beam angle optimization algorithm for intensity modulated radiation therapy. Under the supervision of Ben Heijmen and Pascal Storchi, this goal, and more, was attained, leading to this thesis.

Since 2005 he lives together with Berry van Oers in 's-Hertogenbosch, The Netherlands. In the next years, they became the proud parents of Nicolai (2006), Skanne (2007) and Ingmar (2009).

Currently, Sebastiaan continues his research on improving treatment planning at the department.

Currently, for each radiotherapy patient a treatment plan is generated by a team of specialists with the help of a dedicated software application, called treatment planning system (TPS). This is a time-consuming and labour intensive process, while the final result may be suboptimal for individual patients. The problem to be solved is highly complex and there is no guarantee that the input of the team will lead the TPS towards generation of a plan that is (close to) optimality, accounting for the patient's unique anatomy, tumour size and shape, etc. This concerns the team's choices on the number of treatment beams and their directions, but also a priori choices on the mathematical treatment objectives and constraints applied into the TPS, that are often 'optimized' in the trial-and-error planning process.

In this thesis, novel algorithms for automated plan generation (no human interference) are developed, leading to the iCycle algorithm and its evaluation and application in treatment planning studies. With iCycle, intensity modulated radiotherapy (IMRT) treatment plans are generated fully automatically, including selection of beam angles. Evidence is provided that iCycle plans are superior to the current clinical plans. Due to the automation, iCycle can be used for objective comparison of treatment strategies, e.g. to study the value of non-coplanar beam setups compared to coplanar, or evaluate treatment strategies.

Sebastiaan Breedveld obtained a master in Applied Mathematics at the Delft University of Technology. The research for his master thesis on radiation therapy treatment planning was done at the Department of Radiation Oncology of the Erasmus Medical Center in Rotterdam. Here he also did the PhD research described in this thesis.



Stellingen behorende bij het proefschrift
Towards Automated Treatment Planning in Radiotherapy
Sebastiaan Breedveld, 13 maart 2013

1. IMRT plannen met een niet-coplanaire bundelopzet zijn in het algemeen kwalitatief beter dan plannen met een coplanaire bundelopzet, wanneer beide automatisch zijn geoptimaliseerd met een algoritme voor gecombineerde bundelhoekoptimalisatie en IMRT. (dit proefschrift)
2. Het automatisch genereren van kwalitatief hoogstaande IMRT plannen met geoptimaliseerde bundelrichtingen kan binnen klinisch aanvaardbare rekestijden. (dit proefschrift)
3. Het gebrek aan algoritmen voor geautomatiseerde en gecombineerde IMRT en hoekoptimalisatie heeft goed vergelijkend onderzoek tussen snelle coplanaire technieken (inclusief VMAT) en niet-coplanaire technieken ernstig belemmerd. (dit proefschrift)
4. Geautomatiseerd plannen maakt het mogelijk om meer criteria te beschouwen in de optimalisatie (zoals het reduceren van dosis in de slikspiers) zonder de belangrijkste criteria te compromitteren, en zonder de werklust te verhogen. (dit proefschrift)
5. Zelfs met beperkte grootte van de niet-coplanaire zoekruimte (b.v. voor de CyberKnife) is het nog zo dat plannen met niet-coplanaire bundelrichtingen het veel beter kunnen doen dan plannen met slechts coplanaire bundelrichtingen. (dit proefschrift)
6. In tegenstelling tot vlees, is het niet aan te raden groente te eten die gelopen heeft.
7. Een product aanprijzen als “dermatologisch getest” is niet dermate logisch, aangezien het niets zegt over de uitkomst van de test. (Vervolgens wordt zo'n product “als beste getest”.)
8. Het teruglezen van oude schetsen voor de aanpak van een probleem kan tot vernieuwende ideeën en inzichten leiden, aangezien je in het begin nog geen tunnelvisie had, maar jaren later wel veel inzicht en ervaring rijker bent.
9. Beginnende onderzoekers zouden zoveel mogelijk gemotiveerd moeten worden zich elke dag ten minste 1 uur in te lezen in vakliteratuur. Dit is niet alleen goed om kennis op te doen en inzicht te krijgen in de stand van zaken in het vakgebied, de kans is ook groter dat dit een gewoonte wordt.
10. “Een idee dat is uitgewerkt en uitgevoerd is belangrijker dan een idee dat slechts bestaat als idee.” (Buddha)
11. Vertaling: “Het keuzeaxioma leert ons om één element uit elke verzameling te selecteren – en terecht te stellen als voorbeeld voor de anderen.”
Onderschrift: “Mijn wiskundeleraar was een groot voorstander van bewijs door intimidatie.”
(xkcd.com)

